Advancing Shoreline Oil Spill Response with Eco-friendly Functional Nanomaterials

Rengyu Yue

A Thesis

In the Department of

Building, Civil and Environmental Engineering

Presented in Partial Fulfillment of the Requirements

For the Degree of

Doctor of Philosophy (Civil Engineering)

at Concordia University

Montréal, Québec, Canada

November 2023

CONCORDIA UNIVERSITY
SCHOOL OF GRADUATE STUDIES

This is to certify that the thesis prepared

By Rengyu Yue

Entitled Advancing Shoreline Oil Spill Response with Eco-friendly Functional Nanomaterials

and submitted in partial fulfillment of the requirements for the degree of

DOCTOR OF PHILOSOPHY (Civil Engineering)

complies with the regulations of the University and meets the accepted standards with respect to originality and quality.

Signed by the final examining committee:

_____ Chair
Dr. René Witte

_____ External Examiner
Dr. Ying Zheng

_____ Examiner
Dr. Catherine Mulligan

_____ Examiner
Dr. Zhi Chen

_____ Examiner
Dr. Sana Jahanshahi Anbuhi

_____ Thesis Supervisor
Dr. Chunjiang An, Dr. Zhibin Ye

Approved by

_____
Dr. S. Samuel Li, Department Chair

December 2023

_____
Dr. Mourad Debbabi, Dean

ABSTRACT

Advancing Shoreline Oil Spill Response with Eco-friendly Functional Nanomaterials

Rengyu Yue, Ph.D.

Concordia University, 2023

Marine oil spills can cause serious environmental damage. When the spilled oil reaches the coast, it can result in negative implications for the coastal ecosystems. Coastal oil cleanup operations are often expensive and time-consuming. Surface washing can be used following an oil spill to enhance the removal of stranded oil from coastal surfaces. Surface washing agents (SWAs) are typically applied directly on stranded oils and oil is then flushed with ambient water to remove the oil and direct it to a controlled area for physical recovery. However, there is still a gap between the available SWAs and the increasing application need. Many SWAs have been produced for the treatment of oiled shorelines. Although the toxicity of some SWAs is moderate, they can still have a potentially adverse impact on the shoreline environment after application. Moreover, the effluents after washing can be further recovered through appropriate disposal to avoid secondary pollution.

This thesis presents the development of multiple environmentally friendly surface washing fluids that demonstrate commendable performance, reusability, and remarkable stimuli-responsiveness. The efficacy of these washing fluids was meticulously assessed under various environmental conditions. To gauge their impact on selected species, biotoxicity experiments and modeling were conducted. Molecular dynamic and thermodynamic modeling was utilized to unveil the intricate mechanism of oil removal. Additionally, post-treatment methods were explored to curtail potential secondary pollution stemming from washing sludge. Notably, the stimuli-responsive nature of these washing fluids played a pivotal role in generating clean supernatants with minimal turbidity

and oil content. In a bid to harness water motion for both physical and chemical actions, a piezocatalytic washing fluid was also conceived. This innovative fluid demonstrated the capability to degrade oil into low molecular-weight hydrocarbons. Overall, this thesis holds immense value in significantly benefiting shoreline oil spill response by enriching cleanup techniques, reducing environmental impact, and enhancing cost-efficiency. Moreover, this thesis contributes to enhancing oil spill preparedness and response capacity and safeguarding valuable coastal regions.

ACKNOWLEDGMENT

"All human wisdom is contained in these two words: Wait and hope."

In turning the ideas into this thesis, I am most grateful to my supervisors, Dr. Chunjiang An and Dr. Zhibin Ye, for their warm hospitality, stimulating environment, endless drive, and insightful feedback on the ideas presented here. It's wonderful to write under the guidance of masters at the craft! I'm grateful that they each undertook repeated readings of the umpteenth draft with fresh eyes and ever-wise suggestions. Of course, any and all remaining errors are solely my own.

I also want to thank the International Tuition Award of Excellence and Doctoral Graduate Fellowships from Concordia University and the Chinese Government Award for Outstanding Self-financed Students Abroad.

I am thrilled and grateful for the support from collaborators especially Dr. Kenneth Lee, Dr. Baiyu Zhang, Dr. Yiqi Cao, Dr. Xixi Li, Dr. Xiujuan Chen, Dr. Peng Zhang, Sichen Gao, and laboratory technicians Hong Guan, Luc Demers from Concordia University and Dr. Lihong Shang, and David Liu from McGill University. I extend my sincere gratitude to Dr. Peter Grütter and Sean Chen from the Department of Physics at McGill University for their invaluable assistance in the characterization process. They carried this project forward at every stage, and without their excellent support, the thesis simply could not have been written.

I'm doubly blessed to have the support and skills of my colleagues, especially Shuyan Wan, Zhikun Chen, Dr. Zheng Wang, Zhaonian Qu, Dr. Xudong Liu, Jalal Rahmatinejad, Dr. Qi Feng, Huifang Bi, and Bahareh Raisi.

I’m grateful to my thesis committee members, Dr. Ying Zheng, Dr. Catherine Mulligan, Dr. Zhi Chen, and Dr. Sana Jahanshahi Anbuhi, for their constructive suggestions and insightful comments.

I would like to thank Kobe Bryant for showing me that there is no such thing as magic but only hard work. Thank you for 20 years you gave me the game all you had, and I am eternally grateful.

Significantly, this thesis has been a family undertaking, with love, understanding, and counsel. Moreover, my girlfriend, Dr. Bingjie Meng, is an indispensable partner in every aspect of my work and life. Thank goodness for her wisdom and infinite patience.

TABLE OF CONTENT

LIST OF FIGURES

LIST OF TABLES

LIST OF ABBREVIATIONS

SFT	Surface tension
IFT	Interfacial tension
NS	Nanoclay/sodium alginate
SA	Sodium alginate
NaCl	Sodium chloride
SDS	Sodium dodecyl sulfate
HA	Humic acid sodium salt
$CaCl_2$	calcium chloride
UP	Ultrapure
CA	Calcium alginate
ANOVA	Analysis of variance
NaCas	Sodium caseinate
SWA	Surface washing agents
MD	Molecular simulation
SOD	Superoxide dismutase
PDB	Protein data bank
COD	Chemical oxygen demand
TOC	Total organic carbon
WCA	Water contact angle
OCA	Oil contact angle
H_2SO_4	Sulfuric acid
HCl	Hydrochloric acid

NH_4Cl	Ammonium chloride
KH_2PO_4	Monopotassium phosphate
$Na_2MoO_4 \cdot 2H_2O$	Sodium molybdate dihydrate
CH_4N_2S	Thiourea
p-BQ	P-benzoquinone
TBA	*Tert*-butanol
TEOA	Triethanolamine
L-his	L-histidine
DMPO	5,5-dimethyl-1-pyrroline-n-oxide
TEMP	2,2,6,6-tetramethyl-4-piperidinol

CHAPTER 1 INTRODUCTION

1.1 Background

Oil pollution has emerged as a significant environmental concern within the petroleum industry. The yearly discharge of crude oil and its derivatives into marine environments is estimated to range from 1.7 to 8.8 million tonnes (Chen et al., 2020a). This predominantly stems from natural seepage, offshore drilling and production, and transportation losses. Marine accidents amplify this issue, as spilled oil frequently reaches coastlines. Canada has by far the longest coastline of any country in the world. Coastal oiling not only brings about environmental harm but also triggers socioeconomic repercussions, disrupting activities like subsistence, commercial operations, and recreation. Stranded oil often undergoes weathering, and emulsification, rendering its removal complex. Cleanup operations on shores are arduous and costly, with up to 80-90% of major spill cleanup expenses allocated to coastal areas. While some coastal remediation approaches, including the physical removal of oiled substances and the use of chemical countermeasures, have been explored, the ever-increasing threat of marine oil spills highlights a gap in effective solutions, particularly in Canada. Strategies to address oil contamination on coasts must strike a balance between environmental impact and benefit, as aggressive cleanup operations can exacerbate adverse effects.

Surface washing stands as a viable approach post an oil spill incident, facilitating the efficient removal of stranded oil from coastal surfaces. Surface Washing Agents (SWAs) are typically administered directly onto the oiled areas, followed by flushing with ambient water, thereby relocating the oil to a controlled space for physical recovery. Given the localized application of SWAs, their administration can range from manual usage via hand-held or backpack sprayers to larger-scale implementation using vehicle-mounted or vessel-mounted sprayers.

In-situ washing of oiled sediments can also be orchestrated through the utilization of tanks or reaction chambers, where oiled sediments are washed using a suitable agent. Clean sediments are subsequently separated and returned to the shoreline, while the used washing solution is collected and appropriately treated to prevent secondary pollution. The cleanup of oiled pebbles and cobbles using a concrete mixed truck or purpose-built facility in situ has been proved in previous practices.

SWAs emerge as a potentially effective and well-received alternative to more aggressive techniques. However, the current scenario reveals a gap between the growing application demand, particularly in the context of Canadian coastal environments, and the available range of SWAs. Presently, only Nalco's Corexit 9580 holds approval by Environment and Climate Change Canada as a surface-washing agent. In contrast, the U.S. Environmental Protection Agency (EPA) has endorsed over 70 agents. Closing this gap becomes pertinent in addressing the requirements of Canadian coastal environments. To enhance public acceptance, it is imperative to prioritize the advancement of SWAs that are not only efficient but also possess attributes like biodegradability, low toxicity, and origin from renewable biomass resources. Adopting this approach not only aligns with environmental consciousness but also underscores the importance of sustainability.

1.2 Research objectives

The primary goal of this thesis is to engineer environmentally friendly surface washing fluids with the capacity to effectively address shoreline oil spills. Addressing shoreline treatment is a multifaceted endeavor, entailing intricate intersections of social, economic, environmental, technical, and political dimensions. The proposed project will integrate SWA development

characterization, oil removal assessment, process optimization, mechanism study, and biotoxicity analysis. In detail, the thesis involves the following objectives: (1) Preparation of green nanomaterial-based washing fluids; (2) Assessment of characteristics of green washing nanofluids.; (3) Assessment of green nanofluids for enhanced oil removal; and (4)Process optimization for green nanofluid-aided coastal cleanup.

1.3 Thesis outline

Chapter 1 serves as a succinct introduction, outlining the background and research objectives of this thesis.

Chapter 2 is a comprehensive review that summarizes recent advances using such green materials for oil spill treatment, namely, oil/water filtration, oil sorption, and surface washing. The preparation methods, wettability characteristics, oil removal performance, and stability of green biomass-derived materials were introduced. The perspectives for future challenges and prospects of green materials in oil spill response are also proposed.

Chapter 3 develops a novel and dual-responsive nanoclay/sodium alginate (NS) washing fluid and systematically evaluates its application potential in an oiled shoreline cleanup. Compared to the commercial surfactants, the NS composite exhibited satisfactory removal efficiencies for treating oily sand. Green materials-stabilized Pickering emulsion can potentially be used for oil/water separation. The NS washing agent displayed excellent pH- and Ca^{2+}- responsiveness, generating transparent supernatants with low oil concentration and turbidity.

Chapter 4 proposes an innovative green surface washing method based on sodium caseinate (NaCas) for the cleanup of oiled sand that is removed from the shoreline and treated by washing ex-situ. A comprehensive performance evaluation, biotoxicity analysis, and molecular dynamic simulation were conducted to explore the washing process. Notably, the washing effluent displayed good pH responsiveness, generating a super-clean supernatant. Moreover, biotoxicity tests proved that the presence of NaCas could relieve the toxicity caused by oil droplets. The molecular dynamic simulation further revealed that NaCas could break the oil layer on the sand surface and move the oil droplets away from the sand.

Chapter 5 designs an innovative, environmentally benign, recyclable, and magnetically mediated surface washing fluid based on water-dispersible magnetite nanoparticles and investigated for the cleanup of oiled beach sand. Thermodynamic modeling was applied to theoretically elucidate the mechanism and the results were in alignment with the experimental findings. The magnetic fluid had a relatively low operation cost and good reusability for a number of multiple cycles. In terms of other operational limitations, it was noted that washing performance declined as clay (kaolinite) concentrations and salinity values increased.

Chapter 6 introduces a cheap food-grade sodium caseinate (NaCas) as a pH-responsive washing fluid in the remediation of phenanthrene (PHE) affected peat moss. The effects of environmental factors on the removal of PHE were systematically investigated. Due to the pH-responsive property of NaCas, the turbidity, total organic carbon (TOC), and chemical oxygen demand (COD) of the washing effluent were remarkably reduced by simply adjusting the solution acidity. Significantly, the toxicity modeling proved that NaCas can reduce the binding energy between PHE and

superoxide dismutase (SOD) of the selected marine organism, and thus relieve the toxicity of PHE to the organisms.

Chapter 7 deploys the innocuous, widely available, and biodegradable sodium caseinate (NaCas) to capture oil pollutants from oily wastewater. Oil droplets can be effectively and rapidly captured by NaCas and subsequently removed after pH-triggered separation, producing a clean supernatant with low turbidity. Biotoxicity experiments proved that NaCas can fully offset the inhibitory effect of oil on the photosynthesis of algae and thus promote algae growth. Two post-treatment methods, namely thermal treatment, and biodegradation, can be used for the post-treatment of NaCas/oil precipitation residues.

Chapter 8 presents piezoelectric MoS_2 as a surface washing fluid to decontaminate oiled sands physically and chemically. The MoS_2 displayed single- and few-layer structures, which were conducive to piezocatalysis. The addition of MoS_2 could decrease the interfacial tension, thereby facilitating oil removal. The oil removal efficiency varied in different environmental conditions. Quenching experiments with different scavengers and electron paramagnetic resonance (EPR) spectra showed the existence of reactive oxygen species (ROSs) including $^1O_2$, $\bullet O_2^-$, and •OH. Notably, results indicated that high molecular-weight hydrocarbons were degraded into lower molecular-weight ones, indicating the existence of chemical oxidation pathways in oil removal.

Chapter 9 lists the contributions and significance, as well as some outlooks for future research.

CHAPTER 2 LITERATURE REVIEW [‡]

2.1 Problem statement

Intensive energy production and consumption are associated with many oil spill accidents which can result in environmental pollution and other socio-economic impacts. (Djellabi et al., 2021; Yue et al., 2020). The total volume of oil released to the environment from tanker spills in 2020 was approximately 1,000 tonnes. Although oils naturally attenuate (i.e., through biodegradation, evaporation, and other processes) after a spill, oil trapped on the shoreline may persist and impair the functions of the coastal ecosystem according to oil types and environmental conditions (An et al., 2017; Chen et al., 2020a). Therefore, to minimize the adverse impact on the environment, oils floating on the surface of the sea and reaching the shoreline should be removed as quickly as possible.

Oil/water separation (namely, oil/water filtration and oil sorption) and surface washing strategies have been adopted to remove oil from both water and shorelines (Gupta et al., 2017). In particular, special wettable materials with significantly opposite affinities for water and oil are considered candidates for selective oil/water filtration and sorption (Afzal et al., 2019). Generally, two types of wettable materials are suitable for oil/water separation applications, hydrophilic/oleophobic materials, and hydrophobic/oleophilic materials. Theoretically, the surface chemistry and structure can affect the wetting behavior of materials (Akmanova et al., 2021; Ma et al., 2016). Materials with special surface structures can have superhydrophilic and superoleophilic properties. Surface

[‡] This work has been published as R. Yue, C. An, Z. Ye, E. Owens, E. Taylor, S. Zhao. Green biomass-derived materials for oil spill response: Recent advancements and future perspectives. Current Opinion in Chemical Engineering, 2022, 36: 100767.

washing agents (SWAs), typically consisting of solvents and surfactants, are promising materials for oiled shoreline treatment. Currently, over 50 SWAs have been licensed for oil spill response.

Figure 2.1 Types of green materials applied in oil spill cleanup.

Recently, green biomass-derived materials have attracted tremendous interest from researchers since they are low-cost, non-toxic, widely available, and environmentally friendly. According to the currently developed approaches, green materials used for oil treatment can be generally classified into three major types (Figure 2.1). The literature review comprehensively summarizes recent advances using such green materials for oil spill treatment, namely, oil/water filtration, oil sorption, and surface washing. We also discuss the opportunities for developing more advanced, effective, and stable green materials for oil spill control.

2.2 Use of green biomass-derived materials for oil treatment

2.2.1 Oil/water filtration

Filtration materials for oil/water filtration need to be superhydrophilic and underwater superoleophobic, allowing water to permeate while repelling the other fluid from passing through (Liu et al., 2020; Ma et al., 2016). Polymeric membranes, such as polyvinylidene fluoride membranes and polyethersulfone membranes, have been widely employed for treating oiled wastewater (Li et al., 2021a). Due to the lipophilic nature of most polymers, complicated and costly modification processes involving blending and surface coating with hydrophilic components are often required to enhance membranes' hydrophilicity and oil resistance, considerably inhibiting their widespread application (Figure 2.2) (Li et al., 2021a). Chitin is a component of shrimp shells and has abundant hydrophilic hydroxyl and acetylamino groups, making it good performance for oil removal (Table 2.1). Yan et al. (Yan et al., 2018) fabricated a chitin nanofiber membrane (CNM) using a vacuum filtration method. The as-prepared CNM exhibited both superhydrophilic and underwater oleophobic properties, with a water contact angle (WCA) of 0° and an underwater oil contact angle of 168°. Importantly, the CNM membrane displayed high separation efficiency (> 95%) and high water flux (> 1500 L m^{-2} h^{-1}).

Table 2.1 Chitin-, chitosan- and cellulose-based oil/water separation

Material	Fabrication	Oil rejection (%)	Flux (L m^{-2} h^{-1})	Refs.
Chitin nanofiber	Vacuum filtration	> 95	> 1500	(Yan et al., 2018)

Chitin/graphene oxide	Vacuum filtration	> 97.5	109.2	(Ou et al., 2019)
Chitin	Electrospinning	99.1	> 151.1	(Gopi et al., 2018)
Cellulose/chitin nanocrystals	Vacuum filtration	> 99.9	> 33.3	(Yagoub et al., 2019)
Chitosan/sodium alginate	Cross-linking	> 99	> 680	(Zhou et al., 2019)
Polydopamine/chitosan	Dip-coating	> 99	15100-30000	(Wang et al., 2020b)
Chitosan/cellulose	Freeze-dried	> 98.6	12960	(Zhang et al., 2018a)
Cellulose/chitosan/TiO_2	Cross-linking	99.4%	Not given	(Yu et al., 2019a)
Tunicate cellulose nanocrystals	Cross-linking	> 98	> 238.3	(Huang et al., 2019)
Cellulose nanofiber	Freeze-dried	99.8	360	(Sun et al., 2017)

Chitosan is commercially produced via the deacetylation of chitins and is also a promising candidate for oil/water separation membrane fabrication (Table 1) due to its non-toxicity and superhydrophilicity. However, the drawbacks of a pure chitosan film include poor mechanical strength, brittleness, and weak acid resistance. Crosslinking chitosan with other polymers is an effective option to overcome these limitations. For example, Wang et al. (Wang et al., 2020b) prepared a polydopamine/chitosan (PDA/chitosan) membrane via dip-coating. The as-prepared superhydrophilic and underwater superoleophobic PDA/chitosan membrane exhibited outstanding oil rejection (> 99%) and very high water flux (> 15000 L m^{-2} h^{-1}). Importantly, the membrane maintained superwetting behavior against acid/salt/basic erosion. Moreover, Yu et al. (Yu et al., 2019a) found that adding inorganic TiO_2 nanoparticles could enhance the mechanical property of chitosan membranes. It is also challenging to work with chitosan membranes because it is difficult to prepare a homogenous polyelectrolyte complex for membrane fabrication since positively charged chitosan can rapidly link with negatively charged polymers through strong electrostatic interactions (Liang et al., 2018). To address this obstacle, Zhou et al. (Zhou et al., 2019) designed a homogeneous polyelectrolyte complex by dissolving chitosan and sodium alginate (ALG) in an alkaline solvent. The CS/ALG membrane demonstrated low oil adhesion, salt resistance, and superior self-cleaning when soaked in water. Notably, the membrane exhibited higher rejection (> 99%) and flux (> 680 L m^{-2} h^{-1}) for crude oil/water separation.

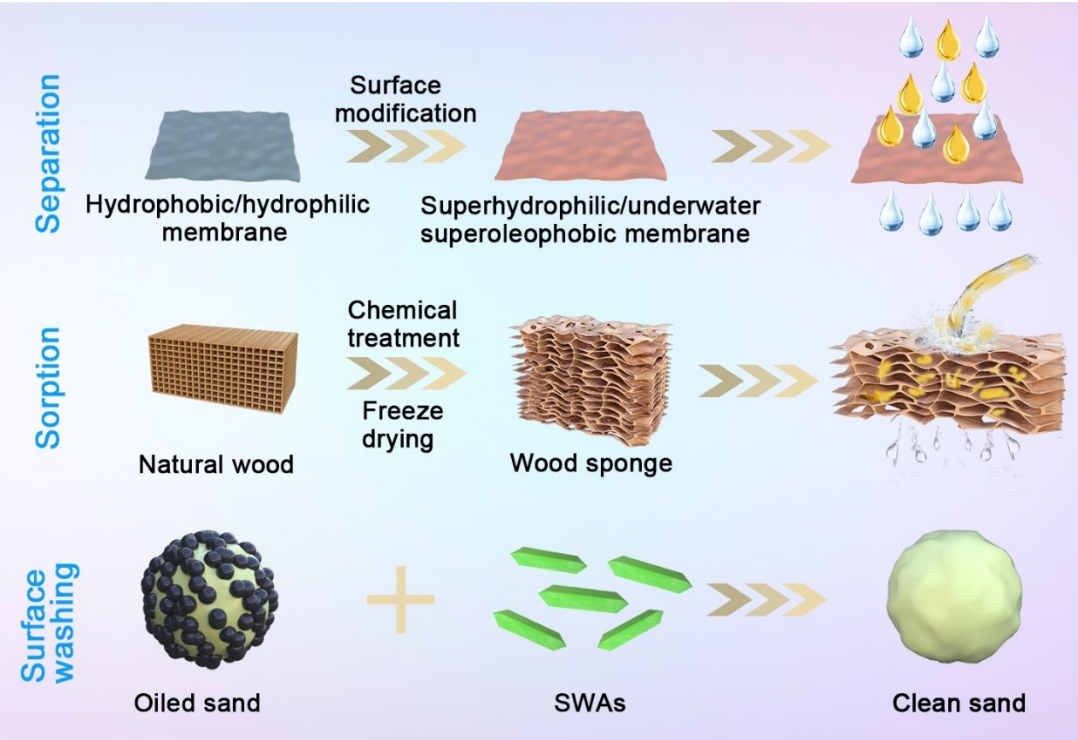

Figure 2.2 Illustration of the oil/water separation, oil sorption, and surface washing.

Cellulose is an essential structural component of the primary cell wall of green plants and is the most abundant bio-based organic compound on earth (Yin et al., 2021b). Similar to chitin and chitosan, cellulose is both hydrophilic and oleophobic because of its abundance of hydroxyl groups; thus, cellulose shows considerable potential for the development of cellulose-based membranes for oil removal (Table 1). Huang et al. (Huang et al., 2019) subjected a membrane of superhydrophilic tunicate cellulose nanocrystals to a physical coating method and a chemical cross-linking method. The as-prepared filters, prepared by either coating or cross-linking, could effectively separate oil from oil/water emulsions and showed excellent stability in and tolerability to harsh environments and UV irradiation. A cellulose nanofiber (CNF) aerogel membrane was fabricated and reported by Sun et al. (Sun et al., 2017). The introduction of sulfonic groups could inhibit the self-

aggregation of NF and increase the polarity of the as-prepared NF aerogels, which endowed the aerogel membranes with superhydrophilicity and underwater superoleophobicity.

2.2.2 Oil sorption

Sorbents for oil/water separation can selectively adsorb/absorb oil or water onto their surface and into their inner porous structure but repel the other components when immersed in an oil/water mixture (Ma et al., 2016). Due to their low cost and environmentally friendly properties, chitin-, chitosan-, and cellulose-based sorbents have been applied in oil/water sorption as summarized in Table 2. For instance, Elanchezhiyan et al. (Elanchezhiyan and Meenakshi, 2016) synthesized metal-modified CS powdered adsorbents, which exhibited high oil removal efficiency (82%). However, metal leaching and adsorbent recovery are two main obstacles to utilizing metal-modified CS-powered adsorbents for oil adsorption, as these issues would result in secondary pollution for freshwater. When CS was integrated with magnetic Fe_3O_4, composite adsorbents could easily be separated from treated water using a magnet (Soares et al., 2017).

Recently, increasing attention has been given to three-dimensional (3D) porous absorbents (Table 2.2), such as aerogel, hydrogel, and sponges, due to their low density, high porosity, and high surface area (Sun et al., 2020). Interestingly, unlike hydrophilic membranes for oil/water separation, 3D absorbents for oil removal were hydrophobic and oleophilic. For instance, Gu et al. (Gu et al., 2020a) prepared a hydrophobic and magnetic nanocellulose/oleic acid/Fe_3O_4 (NCA/OA/ Fe_3O_4) aerogel with a low density and a high absorption ability of 68.06 g/g. WCAs demonstrated that the presence of oleic acid (OA) and Fe_3O_4 improved the hydrophobicity of the composite aerogel. Moreover, Phanthong et al. (Phanthong et al., 2018) applied a freeze-drying method to prepare a

hydrophobic nanocellulose (NC) sponge. After surface modification, the composite absorbent had a high WCA of 160° and could absorb almost 100% of oil spilled on the water surface. The simple fabrication methods and high hydrophobicity of these green 3D absorbents make them promising materials for selective oil/water separation.

Table 2.2 Different sorbents for oil sorption

Sorbents	Type	Sorption capacity (g/g)	Refs.
Lanthanum modified chitin	Particle	Not given	(Elanchezhiyan and Meenakshi, 2016)
Chitosan/Fe_3O_4/silica	Particle	Not given	(Soares et al., 2017)
Chitosan	Aerogel	41.97	(Li et al., 2016)
Nanocellulose/oleic acid/Fe_3O_4	Aerogel	68.06	(Gu et al., 2020a)
Cellulose nanofiber/chitosan	Aerogel	82-253	(Zhang et al., 2021a)
Nanocellulose	Sponge	25-55	(Phanthong et al., 2018)

Eichhornia crassipes	Foam	49.97-140.9	(Sun et al., 2020)
Carbon	Aerogel	80-161	(Li et al., 2017)
Biomass carbon/SiO_2/MnO_2	Aerogel	60-120	(Yuan et al., 2018)
Chitosan	Aerogel	63	(Yi et al., 2020)
Balsa wood	Sponge	41	(Guan et al., 2018)
Balsa wood	Sponge	7.28	(Chao et al., 2020b)

Benefitting from their intrinsic hydrophobicity, carbon-based 3D porous architectures have also shown great potential in oil/water separation, including graphene (Zhao et al., 2019b), carbon nanotube (Muñoz-Sandoval et al., 2017), and MXene (Wang et al., 2019c). However, their expensive precursors and complicated fabrication processes have constrained their wide application in oil spill response. As a result, it is important to explore sustainable carbon-based absorbents with biodegradability, cheap precursors, and time-saving preparation routes. Recent research has shifted to focus on other classes of green nanomaterial of biomass. For example, Sun et al. (Sun et al., 2020) fabricated an oleophilic biomass foam through calcination of Eichhornia crassipes (CEC). The composite 3D absorbents possessed high porosity, low density, and ultrahigh absorption capacity. Furthermore, Li et al. (Li et al., 2017) used the pyrolysis of cellulose aerogels to synthesize a conductive carbon aerogel with an ultralow density, high compressibility, and high

absorbency. Importantly, the as-prepared absorbents exhibited superior fire-retardant properties after the combustion of oil and maintained high absorption capacity after 10 absorption-combustion cycles. However, the extraction of cellulose from plant cells involves chemical and mechanical treatments because of strong hydrogen bonding; furthermore, the assembly of cellulose aerogel is intricate (Lavoine and Bergström, 2017), which hampers the large-scale application of such bottom-up strategies. More significantly, the majority of the aerogels suffer from low mechanical robustness, thereby leading to vulnerable reusability after multiple squeezing-absorption cycles (Karatum et al., 2016).

As a reproducible material, wood is a class of 3D layer hollow fiber supports involving porous and hierarchical structures (Berglund and Burgert, 2018). By chemically removing the lignin-hemicellulose matrix in the cell walls, highly elastic and porous wood sponges can be generated (Song et al., 2018) (Figure 2.2). Such a top-down method is time-saving and scalable and indicates a promising avenue for developing high-quality 3D absorbents directly from wood. For instance, Guan et al. (Guan et al., 2018) applied an effective top-down strategy to synthesize highly porous, mechanically flexible, and hydrophobic wood sponges directly from balsa wood. The resultant sponge exhibited superior mechanical elasticity, low density, and hydrophobic/oleophilic features, giving the wood sponge an oil absorption capacity as high as 41 g/g and high stability after 10 absorption-release cycles. The cycled filtration tests demonstrated that the sponge could effectively filtrate the oil phase but reject water, achieving both oil/water separation and oil collection. However, these 3D absorbents are less effective in removing highly viscous oils (Ge et al., 2017). To address this concern, Chao et al. (Chao et al., 2020b) fabricated a wood/reduced graphene oxide (RGO) absorbent for high-viscosity oil removal. Due to the excellent photothermal conversion of RGO, a thermogenesis process could rapidly increase the temperature to 80 ℃, at which point the

viscosity of crude oil decreased remarkably, and thus the composite absorbent exhibited superior oleophilic and hydrophobic properties. While at room temperature, no oil-wetting behavior was observed, owing to the high oil viscosity.

2.2.3 Surface washing for oiled shoreline

SWAs are a class of materials that can facilitate stranded oil removal from shorelines by altering the rheological properties of the oil/water interface (Chen et al., 2020a; Chen et al., 2021c) (Figure 2). For instance, Bi et al. (Bi et al., 2020) investigated the impact of environmental factors on oil removal from sand using a commercial COREXIT EC9580A (Corexit 9580A) SWA. Temperature and humic acid concentration significantly affected oil removal efficiency. Chen et al. (Chen et al., 2021c) have demonstrated the good performance of green cellulose nanocrystal (CNC) for oiled shoreline cleanup. At the standard reference level, the CNC fluid could remove more than 70% of oil from the surface of the sand. Thermodynamic modeling further confirmed that the addition of CNC would enhance the oil/water miscibility, and biotoxicity tests suggested that CNC can reduce the oil toxicity to green algae. In addition, Chen et al. (Chen et al., 2021b) designed a chitosan/rhamnolipid (CS/RL) complex for oiled sand surface washing. It was found that the addition of CS can reduce the surface tension of the RL solution, thereby boosting the cleaning performance of the complex.

2.3 Research gap and limitations

In summary, emerging green materials offer significant opportunities for developing membranes, sorbents, and SWAs at low costs and with low environmental impacts for the treatment of oily wastewater and oiled shorelines. In spite of significant progress achieved in the past few years,

research on the use of green materials for oil spill response still needs to be further investigated. To advance development and research, the following issues should be addressed:

(1) Developing more effective and sustainable eco-friendly materials

Although nano-chitin and nano-cellulose have low toxicity and have excelled at oil removal, the fabrication processes are complicated and time-consuming. Therefore, designing environmentally friendly, biodegradable, and renewable biomass materials should be prioritized. Applying food-grade substances is a promising alternative. For example, protein nanoparticles can be obtained through a simple anti-solvent precipitation method (Feng and Lee, 2016). Conversely, given the abundant functional groups of green materials, there is considerable room to further optimize their performance. To achieve this goal, surface modifications such as polymerization, electrostatic interaction, and cross-linking can be used. However, the toxicity to organisms of treated materials should be evaluated as well.

(2) Functionalizing eco-friendly materials for oil spill response

Traditional oil/water separations are based mostly on physical processes; not only does this cause the membranes and sorbents fouling during oil removal but the separated oil may also cause secondary oiling of the environment. Integrating physical separation and chemical oxidation is an innovative approach that can improve both the flux of membranes and the sorption capacities of sorbents. Consequently, it is desirable to design green, reactive, and self-cleaning membranes and sorbents for oil/water separation.

Moreover, surface washing processes result in many oil droplets in the washing effluent emulsions, which could cause secondary water pollution and increase capital and operating costs if not treated

properly. Therefore, future research may focus on identifying demulsification methods to separate oil from washing effluents. To address this issue, stimuli-responsive green SWAs for oil removal can be designed. By altering external stimuli, such as pH, temperature, and salinity, the surface properties of the SWAs would undergo some physical or chemical transformation, in turn, influencing the wettability and dispersibility of the SWAs. Importantly, supernatants need to be quantitatively analyzed to evaluate the demulsification performance of the washing effluents, including residual oil concentration, turbidity, and total organic carbon.

(3) Modeling of oil removal and separation processes

Environmental modeling can be used to further analyze environmental processes (Le et al., 2020; Shrestha and Wang, 2020b). Although many experimental studies have been conducted, the modeling of oil removal and separation processes is still lacking. Molecular dynamics simulations can be further used to analyze the interfacial activity of oil/liquid interfaces, which can help understand the mechanism of emulsification and separation of oil droplets. In addition, thermodynamic modeling can be performed to analyze some characteristics such as miscibility under different conditions. In the field application of SWAs, oil, and washing effluent may transport on shorelines. Numerical simulation can be used to quantitatively describe the distribution and transport of oil and washing effluent in the subsurface, thereby characterizing and predicting the cleanup performance and its impact on the shoreline environment. The uncertainty analysis of complex contaminant transport is also of great significance in this process.

(4) Coupling with other technologies for pre - or post-treatment of oil spill response

Each technology, i.e., separation, sorption, and surface washing, is barely able to completely resolve oil spill problems. Oil spill treatments are comprehensive processes that involve various

remediation procedures. Some pre - or post-treatment methods can be used to improve the overall treatment performance. For example, advanced oxidation processes (AOPs), such as Fenton, peroxymonosulfate, and photocatalysis (Yue et al., 2021b; Yue and Rahaman, 2021b), can be used for pre - or post-treatment to improve oil removal. In addition, when developing coupled approaches for a shoreline response, both the overall treatment efficiency and socio-economic impacts should be considered.

(5) Evaluating oil removal performance in practical application

From the practical application perspective, manufacturing costs and mass production capacity are the most important aspects of large-scale application and cannot be ignored, incentivizing the exploration of easier-to-use techniques to promote the industrial application of green materials. Additionally, most studies of oil removal materials have occurred in the laboratory and under simulated environmental conditions. Once oil spill accidents occur, the oil needs to be removed from various oil/seawater mixtures that consist of different components, e.g., salinity and humic acid substances; therefore, it remains unknown whether green material will perform well in these real-world conditions. As a result, materials should be evaluated more extensively under practical conditions that involve more complex factors, such as multi-component mixtures, mechanical turbulence, and viscous oils. It is also expected to design and scale up these techniques for practical applications on-site.

CHAPTER 3 CLEANUP OF OILED SHORELINES USING A DUAL RESPONSIVE NANOCLAY/SODIUM ALGINATE SURFACE WASHING FLUID ‡

3.1 Background

Oil spills may disturb ecosystems, devastate the sustainable development of energy systems, and endanger public health (via respiratory damage, liver damage, and cancer risk) (Cai et al., 2019; Wang et al., 2021c; Yue et al., 2020). Millions of tonnes of oil and petroleum products have been discharged into oceans over the last five decades (ITOPF, 2017; Yue and Rahaman, 2021a). Once released into the marine environment, a certain amount of oil can reach the shoreline via waves, wind, tides, and currents (Elmobarak and Almomani, 2021a; Geng et al., 2020; Wang et al., 2021b). This oil is increasingly recalcitrant as it undergoes weathering through biodegradation, photo-oxidation, and evaporation (Jin et al., 2021; Owens et al., 2016).

Various strategies, such as physical removal and biodegradation, have been adopted to mitigate oil contamination on the shoreline (Lee, 2000; Sun et al., 2019; Yue et al., 2021b). Although the biodegradation method is environment-friendly, wide application for shoreline cleanup has been limited by its low oil removal efficiency and unstable performance (Boufadel et al., 2019; Owens et al., 2016; Shang et al., 2020). The use of surface washing agents (SWAs) has proven to be a suitable alternative to facilitate oil decontamination by influencing the rheological properties or interactions at the oil/water interface (Bi et al., 2020; Chen et al., 2021c). Some commercial SWAs (e.g. Corexit 9580 and Cytosol) have been considered for oil removal (U.S.EPA, 2021). SWAs with

‡ This work has been published as R. Yue, C. An, Z. Ye, H. Bi, Z. Chen, X. Liu, X. Zhang, K. Lee. A dual responsive nanoclay/sodium alginate surface washing agent for effective shoreline cleanup. Environmental Research, 2022, 205: 112531.

high oil removal efficiency, low temperature and pressure requirements for flushing water, and minor impacts to shorelines are advantageous (Chen et al., 2020a). The reported SWAs often consist of surfactants and solvents, which have toxic effects on organisms and human health (Barron et al., 2020; Chen et al., 2019). Therefore, the development of novel SWAs that are non-toxic, effective, and economical is imperative. The post-washing effluent is also a concern, as it could cause secondary pollution if not treated properly. Previous studies have mainly focused on the oil-washing performance of SWAs (Bonal et al., 2018; Kim et al., 2019; Offiong et al., 2021), while the subsequent separation processes of washing effluents were either complicated or neglected, thereby limiting their feasibility in practical applications. Consequently, a straightforward and time-saving method to separate oil from washing effluent after the application of SWAs must also be designed.

Pickering emulsion refers to an oil/water emulsion that is stabilized by solid particles (Aveyard et al., 2003; Binks et al., 2008). It has attracted increased attention from researchers due to its enhanced emulsion stability, low cost, and easy operation compared to traditional surfactants (Low et al., 2020; Tang et al., 2015a). Montmorillonite (MMT), which is environmentally benign, economical, and has good dispersibility, has proven to be an ideal candidate for Pickering emulsion formation (Machado et al., 2019; Wang et al., 2021a). Modifying MMT with surfactants is one approach to preparing an MMT-based Pickering emulsion. For instance, Zhang et al. (2014b) used an in-situ method to prepare cetyltrimethylammonium bromide (CTAB)/MMT composite, which can stabilize oil/water emulsion. Dong et al. (2014) synthesized bis(2-hydroxyethyl)oleylamine-modified MMT particles, which hindered the coalescence of oil droplets at a low concentration of 0.1 w/v%. However, some chemicals used in these methods are costly and toxic, making large-scale practical applications difficult.

Sodium alginate (SA) is the sodium salt form of alginic acid and gum, which is mainly extracted from brown algae. It has good biocompatibility and is suitable for the stabilization of MMT-based Pickering emulsion. Tang et al. (2021) prepared chitosan/SA composites through electrostatic interaction and found that the presence of SA increased the Pickering emulsion stability. Wang et al. (2020a) demonstrated that the addition of SA could co-stabilize the MMT-based Pickering emulsion for up to three months, while MMT and SA systems were both unstable within 48 h. Additionally, SA is a polyelectrolyte and its rheological property is pH-responsive. Hence, the presence of SA can aid precipitation in acidic conditions (pH<4), which can contribute to the recovery of SWAs and oil in washing effluent.

In this study, we developed a novel and dual-responsive nanoclay/sodium alginate (NS) washing fluid and systematically evaluated its application potential in an oiled shoreline cleanup. Characterizations were performed to verify the interaction between nanoclay and SA. Batch experiments were conducted to investigate oil removal performance under various conditions, and factorial design analysis was used to assess how different factors affected removal efficiency. Additionally, the washing effluents were effectively separated based on the dual pH and Ca^{2+} responsive properties of SA. The residual oil content and turbidity of supernatants were also determined. Moreover, the removal efficiency of the NS fluid was compared to commercial surfactants to assess its potential as an SWA for shoreline cleanup.

3.2 Materials and methods

3.2.1 Materials

Shell Rotella T4 diesel engine oil (15W40) was used as the representative oil in this study and its properties are detailed in Table 3.1. Standard washed and thermally treated sand (30 – 40 mesh) was purchased from Millipore (Oakville, Canada). Sodium alginate (SA), nanoclay (montmorillonite clay), sodium chloride (NaCl), Tween 80, Tween 20, sodium dodecyl sulfate (SDS), Triton X-100 (TX-100), humic acid sodium salt (HA), calcium chloride ($CaCl_2$), and n-hexane were purchased from Millipore Sigma (Oakville, Canada). Ultrapure (UP) water (18 MΩ) was produced by a Milli-Q ultrapure water purification system (MilliporeSigma, USA)

Table 3.1 Characteristics of the engine oil.

Properties	**Value**
Density at 15 °C	0.878 g/mL
Kinematic Viscosity at 40 °C	118 mm^2/s
Viscosity index	133
Sulfated ash	1%
Total base number	10.1 mg KOH/g
Flashpoint	234 °C
Pour point	-36 °C

3.2.2 Preparation of oiled sand

The engine oil was weathered at 20 ℃ for 7 days before use. The oil-contaminated sand had a concentration of 5 g oil/ kg sand; it was prepared by adding 5 g of engine oil to 1 kg of sand. Next,

the engine oil was dissolved with hexane and the mixture was sonicated and agitated for 10 min. The hexane was then evaporated under a fume hood at 20 ℃ for 48 h. The as-prepared oiled sand was sealed for future use.

3.2.3 Preparation of nanoclay/sodium alginate surface washing agent

A certain amount of nanoclay (400, 600, 800, and 1000 mg/L) was mixed with SA solution at different concentrations (0.05, 0.1, 0.2, and 0.5 wt%). The mixture was dispersed in a sonicator for 15 min, and then magnetically stirred for 30 min to form a homogeneous dispersion. A series of NS washing agents were prepared.

3.2.4 Sand-washing procedure and factorial design analysis

For this process, 1 g of oiled sand and 15 mL of washing agent were added to each vial (20 mL). All washing experiments were conducted using a shaker (New Brunswick Innova 42R Incubator Shaker, USA) at 300 rpm at 20 ℃ for 24 h. The liquid washing agent was removed after the washing process, and any washing agent that had potentially adsorbed by the sand was removed with UP water. Subsequently, the wetted sand was dried at 50℃ overnight to ensure that the DI water did not impact the following extraction step. The residual oil from the sand surface was extracted by adding 15 mL of hexane into the vials, which were shaken for 24 h. The extracted oil concentration was determined using a UV-Vis spectrophotometer (Agilent Cary 3500, USA) at a wavelength of 284 nm. The oil washing efficiency was calculated by the equation: $R = 1 - (Oil_R/Oil_T)$, where Oil_R and Oil_T refer to the amount of residual oil after washing and the total amount of oil on the sand before washing, respectively.

The single and interactive effects of different factors were assessed by applying a two-level factorial design analysis (He et al., 2018; Li et al., 2020). Four environmental factors, namely temperature, oil content, salinity, and HA were tested at two levels. A 2^4 factorial design analysis was used for this study and detailed information is provided in Tables 3.2 and 3.3.

Table 3.2 High and low levels for the 2^4 factorial design.

Factor	Temperature A (℃)	Oil content B (g oil/ kg sand)	Salinity C (wt%)	HA D (mg/L)
High level (+1)	20	10	3.5	20
Low level (-1)	10	5	0	0

Table 3.3 Coded levels and corresponding values for factorial design matrix.

Number	**Coded levels**				**A**	**B**	**C**	**D**
	A	B	C	D	Temperature (℃)	Oil content (g oil/ kg sand)	Salinity (wt%)	HA (mg/L)
1	-1	-1	-1	-1	10	5	0	0
2	-1	-1	-1	1	10	5	0	20
3	-1	-1	1	-1	10	5	3.5	0
4	-1	-1	1	1	10	5	3.5	20
5	-1	1	-1	-1	10	10	0	0
6	-1	1	-1	1	10	10	0	20
7	-1	1	1	-1	10	10	3.5	0

8	-1	1	1	1	10	10	3.5	20
9	1	-1	-1	-1	20	5	0	0
10	1	-1	-1	1	20	5	0	20
11	1	-1	1	-1	20	5	3.5	0
12	1	-1	1	1	20	5	3.5	20
13	1	1	-1	-1	20	10	0	0
14	1	1	-1	1	20	10	0	20
15	1	1	1	-1	20	10	3.5	0
16	1	1	1	1	20	10	3.5	20

To demonstrate the oil removal performance of NS washing agents, nonionic surfactants (Tween 20, Tween 80, and TX-100) and an anionic surfactant (SDS) were selected as commercial surfactants for the washing experiments. The cationic surfactants were not considered in this study due to their limited effectiveness in oil washing, which resulted in strong adsorption by sand (Chu, 2003). The surfactant properties are given in Table 3.4.

Table 3.4 Properties of selected surfactants

Surfactants	Chemical nomenclature	Molecular weight	Critical micelle concentration (CMC)
SDS	Sodium dodecyl sulfate	288	2.3 g/L
Triton X-100	4-(1,1,3,3-Tetramethylbutyl)phenyl-polyethylene glycol	625	0.2 g/L
Tween-20	Polyoxyethylene (20) sorbitan monolaurate	1228	73.7 mg/L
Tween-80	Polyoxyethylene (80) sorbitan monooleate	1310	15.7 mg/L

3.2.5 Separation and recovery of washing effluents

Washing effluents can be separated and recovered by the following two methods. (1) The rheological property of SA is related to the pH of the solution and precipitates when the pH is less than 4 (Tang et al., 2015a). After oil washing, the pH of the washing effluent was adjusted to 1.5 by adding a certain volume of HCl acid (1 mM), after which the NS composite formed precipitates and was recovered by removing the supernatant. (2) SA can react with Ca^{2+} ions to form calcium alginate (CA), which is insoluble in water. In this study, the washing effluent was added to the $CaCl_2$ solution, and small CA hydrogel beads were generated which subsequently precipitated at the bottom of a beaker.

3.2.6 Analytical and characterization methods

All batch experiments were conducted three times and the mean values were used for data analysis. The experiment design and results analysis were carried out using Minitab (Minitab, LLC., USA). Additionally, the statistical significance of the results ($p < 0.05$) was determined through a one-way analysis of variance (ANOVA) (He et al., 2018). The attenuated total reflection-Fourier transform infrared (ATR-FTIR) result was obtained using a Thermo Scientific Nicolet 6700 FTIR spectrometer (USA). X-ray diffraction (XRD) analysis was performed using an X-ray diffractometer (BRUKER D8 Discover, USA). A zeta potential test was performed using a Zetasizer (MALVERN, USA). Surface tension and interfacial tension measurements were recorded using a force tensiometer (KRUSS K100, Germany). The surface tension (SFT) measurement was conducted by immersing and withdrawing a platinum plate into the sample; the interfacial tension (IFT) was measured following the operation instructions from the KRUSS company. Microscope images were obtained with a fluorescence microscope system (ESC-350, ACCU-SCOPE, USA). Turbidity tests were performed using a turbidity meter (ORION AQ3010, THERMO SCIENTIFIC, Canada). Thermogravimetric curves were obtained using a TGA instrument (Q50, TAINSTRUMENTS, USA). Viscosity tests were performed using a viscosity meter (AMETEK, BROOKFIELD, Canada).

3.3. Results and discussion

3.3.1 Characterizations of nanoclay/sodium alginate

The ATR-FTIR characterization was applied to investigate the interaction between nanoclay and SA. As depicted in Figure 3.1a, in the spectrum of SA, two peaks at 1600 and 1408 cm^{-1} corresponded to symmetric and asymmetric carboxylate groups, respectively, and the peak at 3252

cm^{-1} was assigned to the -OH stretching vibration (Wang et al., 2020a). The spectrum of nanoclay exhibited three characteristic peaks, namely 3613 (Si-OH), 3386 (-OH symmetric stretching), and 1635 cm^{-1} (hydroxyl bending) (Etcheverry et al., 2017). Notably, the NS composite displayed peaks of both SA and nanoclay, confirming the two had successfully been combined. Additionally, the peaks of hydroxyl groups of both SA (3252 cm^{-1}) and nanoclay (3386 cm^{-1}) shifted to 3397 cm^{-1} in the NS spectrum, which indicates the existence of hydrogen bonds between SA and nanoclay (Barreca et al., 2014; Hosseini et al., 2013; Wang et al., 2020a).

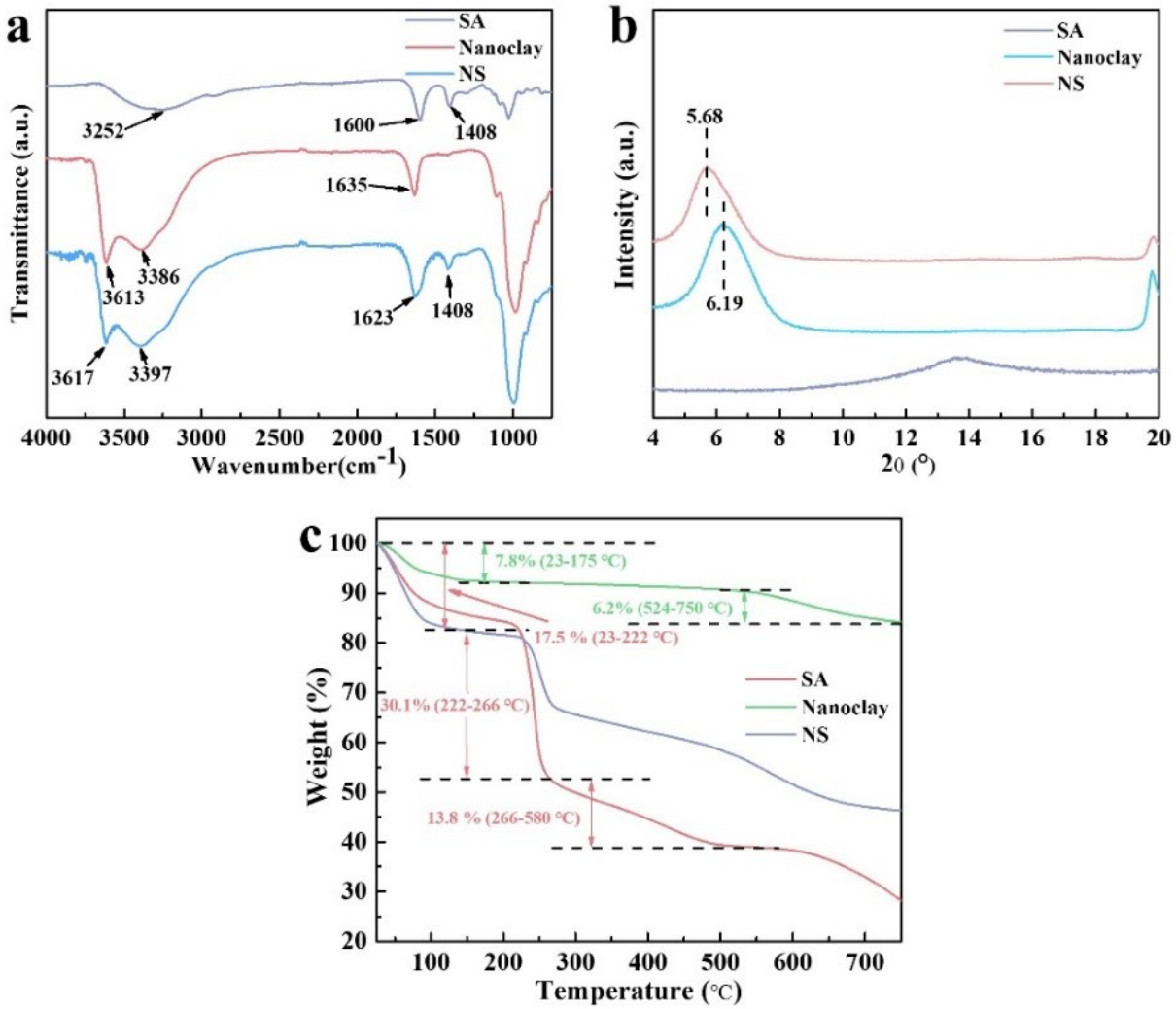

Figure 3.1 ATR-FTIR spectrum (a) XRD patterns (b) and TGA curves (c) of SA, nanoclay, and NS.

XRD patterns (Figure 3.1b) show that the diffraction peak shifted from 6.19° to 5.68° with the addition of SA, demonstrating that the interlayer distance of nanoclay increased from 1.42 to 1.55 nm. This observation may imply that SA was intercalated into the nanoclay interlayer spacing. Figure 3.1c shows the results of the TGA measurement of nanoclay, SA, and NS composite. Weight loss of 7.8% of nanoclay at 23–175 ℃ was attributed to water loss from both surface and crystal structure, while another mass loss of 6.2% at 534–750 ℃ was attributed to dihydroxylation (Santos et al., 2018). Approximately 17.5% of SA mass was lost in the range of 23–222 ℃, possibly due to water evaporation. The main skeleton and structure of SA decomposed between 222 and 266 ℃, leading to 30.1% of weight loss (Abbasi et al., 2020). SA decomposition began at 266 ℃ and the total weight loss reached approximately 72%. Notably, the TGA curve of the NS composite displayed the weight loss behavior of both nanoclay and SA, indicating that the two substances had combined.

3.3.2 Effect of sodium alginate and nanoclay concentrations

To determine the optimal SA and nanoclay content, a series of experiments with gradient variation of SA and nanoclay was conducted. Figure 3.2a shows the oil removal efficiencies of the different NS washing agents. Apparently, the enhancement in SA and nanoclay concentrations had positive effects on oil removal. For instance, when fixing the SA concentration 0.2 wt%, the removal efficiency increased gradually from 62.3% to 72.3% as enhancing nanoclay concentration from 400 to 800 mg/L. However, the further increase in nanoclay concentration from 800 to 1000 mg/L only led to a slight improvement of 1.0% in oil removal efficiency. There are three possible reasons to explain why nanoclay enhanced the oil removal: (1) organic materials combined with nanoclay

via Van der Waals forces, thus entering the space between the neighboring sheets of the nanoclay structure (Stevenson, 1994); (2) the swelling property of nanoclay in the aqueous environment can enlarge its interlayer space, thereby adsorbing more organic matter (Churchman et al., 2006); and (3) the oil–nanoclay interaction results in the formation of oil-particle aggregates (OPAs), which can enhance the dispersion of oil droplets, thus hindering the mutual effect between oil droplets and sand surface.

Conversely, with a fixed nanoclay concentration of 800 mg/L, the oil decontamination efficiency climbed stepwise from 63.1% to 72.7% as SA concentration escalated from 0.05 to 0.5 wt%. This may be because the addition of SA improved the viscoelasticity and stability of the NS Pickering emulsion. Wang et al. (2020a) found that SA usage may improve the storage stability of montmorillonite (MMT)-based Pickering emulsion. The MMT/SA-stabilized Pickering emulsion exhibited outstanding stability at higher SA concentrations (0.1 to 1.0 wt%), of which the viscoelasticity and absolute value of Zeta potential increased gradually with increasing SA content. Moreover, the presence of SA decreased the surface and interfacial tensions of the NS washing agents (Figure 3.2b), because SA could promote the diffusion of nanoclay particles from bulk to interface (Jiang et al., 2021). The reduced surface and interfacial tensions were conducive to the formation of oil/water emulsion.

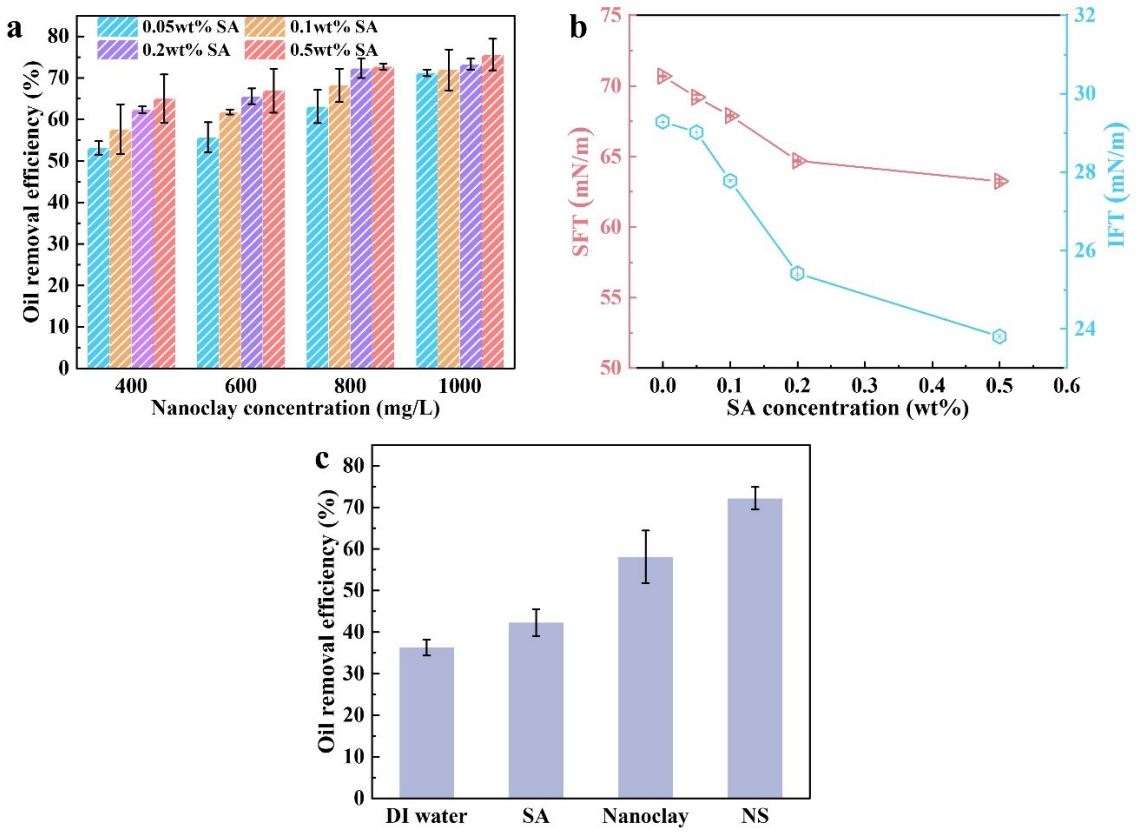

Figure 3.2 (a) oil removal efficiencies of different NS fluids, (b) SFT and IFT of NS composites with different SA concentrations (the concentration of nanoclay was 800 mg/L), and (c) the oil removal efficiency of different washing fluids.

In this study, an NS washing agent containing 800 mg/L of nanoclay and 0.2 wt% of SA was used to systemically explore oil removal performance under different experimental conditions. Figure 3.2c depicts the oil removal efficiency of different washing agents. SA solution (0.2 wt%) had a slightly higher oil removal efficiency (51.1%) than UP water (36.3%). Additionally, 58.1% of the oil was effectively washed by using a nanoclay washing agent (800 mg/L). With the help of SA, the NS composite had excellent washing performance, exhibiting the highest removal performance (72.2 %) of the four washing agents.

3.3.3 Effect of salinity

The salinity of the ocean is approximately 3.5 wt%, although this value is lower in the nearshore area where freshwater discharges from rivers (Cao et al., 2020b; Zhai et al., 2020). The effect of salinity on the NS washing fluid performance is illustrated in Figure 3.3a. Salinity was found to positively impact oil removal efficiencies, which increased to 80.2% and 80% at low salinities of 0.1 wt% and 0.3 wt%, respectively. However, the NS fluid washing performance declined and became stable with high salinities: 75.8%, 74.1%, 76.3%, 76.8%, and 75.5% of the oil was removed as salinity increased from 0.5 wt% to 4.0 wt%. These findings demonstrate that the NS washing agent has a high potential for shoreline cleanup in a saline environment.

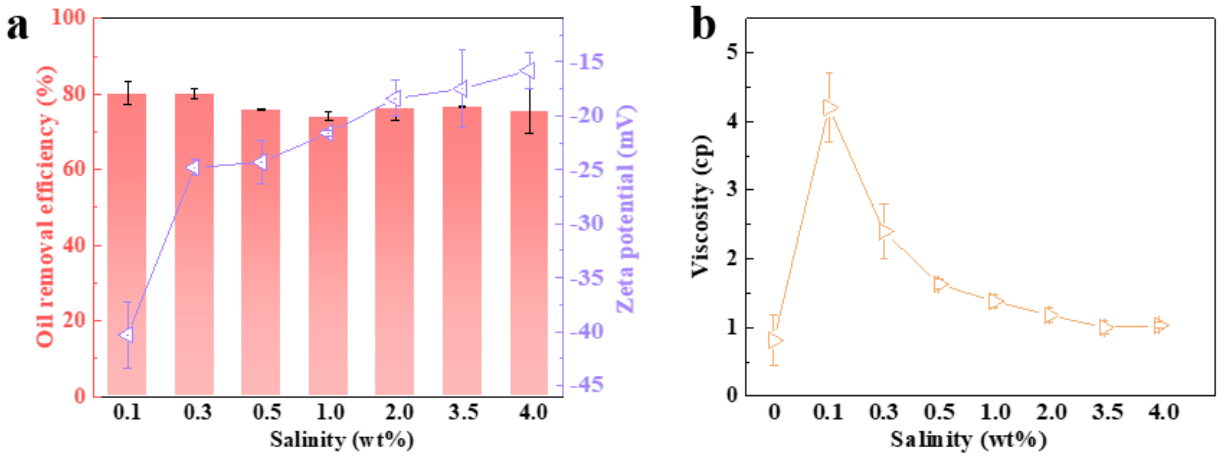

Figure 3.3 Effect of salinity on (a) oil removal of NS washing agent and its corresponding Zeta potential and (b) viscosity.

One explanation for the oil removal enhancement in salty water is that the positively charged ions, including Na^{+} and Ca^{2+}, may compress the double layer of NS composite and decrease its absolute value of zeta potential (Figure 3.3a), thus leading to aggregation of the NS washing fluid (Molnes et al., 2016; Zhong et al., 2012). This may promote OPA formation, which accelerates the

detachment of oil contaminants from the sand surface (Le Floch et al., 2002). On the other hand, Le Floch et al. (2002) demonstrated that salinity was beneficial to OPA formation, with over 75% of OPAs formed in saline water but only about 10% formed in DI water. Furthermore, salinity may enhance the stability of the Pickering emulsion. Dong et al. (2014) found that in synthetic seawater, high salinity drove clay particles from the brine phase to the oil/water interface, promoting the approach of clay to the surfaces of oil droplets, thus stabilizing the clay-based Pickering emulsion.

The diminished oil washing performance at high salinity (≥ 0.5 wt%) can be attributed to variations in the interaction between nanoclay particles and oil droplets. With a salinity between 0.1 wt% and 0.3 wt%, the nanoclay particles tended to aggregate and form 3D networks into which oil droplets could be easily incorporated (Yu et al., 2021). This was conducive to the stabilization of Pickering emulsion. At higher salinities (≥ 0.5 wt%), due to the reduced surface charge of the nanoclay particles (Figure 3.3a), nanoclay were more likely to gather through face-to-face interaction, allowing stable nanoclay clusters to form. In this case, the amount of nanoclay capable of forming strong clay droplet networks declined, thereby destabilizing the Pickering emulsion (Yu et al., 2021).

The viscosity of the washing agent under different salinities also influenced the oil removal efficiency. At low salinities of 0.1 wt% and 0.3 wt%, the viscosity of the washing fluid increased significantly to 4.2 and 2.4 cp (Figure 3.3b), respectively, because the 3D nanoclay networks restricted the motion of clay particles. The enhanced fluid viscosity stabilized the Pickering emulsion and thus improved the oil removal performance (Wang et al., 2020a). However, at higher salinities, nanoclay particles interconnected to create a loose nanoclay network, which caused both viscosity and oil removal efficiency to decline (Yu et al., 2021).

3.3.4 Effect of temperature

The average temperature of the shoreline in North America varies from 5–25 ℃ (Dethier et al., 2012). The impact of temperature on oil washing efficiency was investigated and the results are shown in Figure 3.4. Oil removal efficiency increased moderately from 62.3% at 5 ℃ to 72.2% at 20 ℃. As the temperature rose, the oil viscosity decreased, improving hydrocarbon solubility and mobility. Further, decreased viscosity can reduce the interaction forces between sand and oil, thereby promoting the detachment of oil from sand and emulsion formation. Additionally, increasing the temperature decreased the zeta potential of silica, the main component of sand, and increased its negative charge (Chen et al., 2021c; Vahabisani et al., 2021). This resulted in higher repulsive forces between oil and sand, hindering the re-attachment of the removed oil.

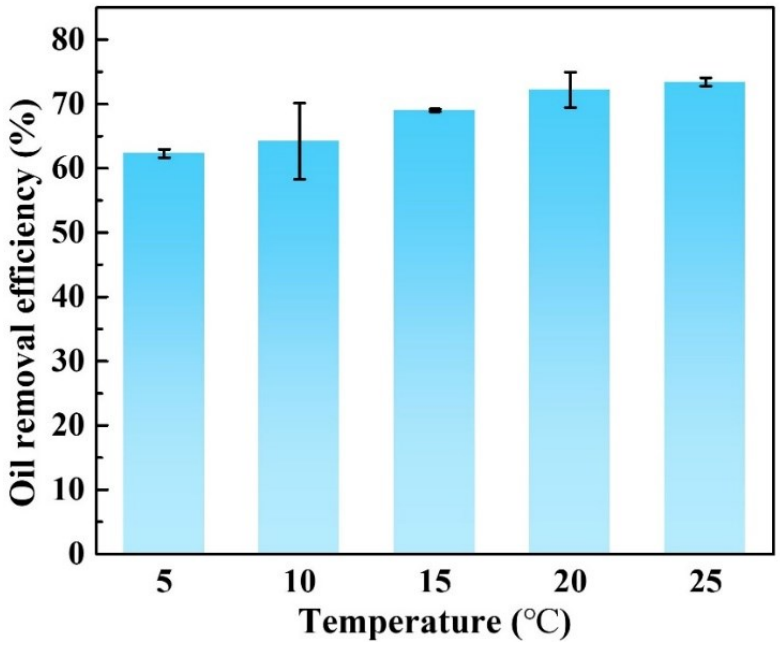

Figure 3.4 Effect of temperature on oil removal of NS washing agent.

Additionally, it was found that a further temperature increase from 20 to 25 ℃ only caused a slight rise in oil removal efficiency, from 72.2% to 73.4%. Sørensen et al. (2014) investigated the interaction between oil droplets and sediments under different conditions. They found that the absorption ability of the sediment towards oil was the highest at a low temperature of 5 ℃, while it decreased and remained stable at 10, 15, and 25 ℃. Overall, the positive effect of temperature on oil removal can be attributed to the changes in viscosity, dissolution, and emulsion.

3.3.5 Effect of humic acid

A product of dead organism biodegradation, HA is widespread in the natural environment and can affect the transportation behavior of contaminants (Yue et al., 2021a; Zhao et al., 2019a). The impact of HA on oil removal efficiency was explored in this work and the results are plotted in Figure 3.5. It was concluded that more oil contaminants were released from the sand surface when HA was present in the flush water. Oil removal efficiency increased from 75.4% to 80.5% when the HA content increased from 1 to 10 mg/L. However, this positive effect was less obvious at higher HA concentrations (≥ 20 mg/L). A previous study demonstrated that HA enhanced the solubility of hydrophobic organic contaminants (HOCs) (Cho et al., 2002). Additionally, HA may be adsorbed on both oil droplets in the oil/water emulsion and on the sand surface, increasing their negative charge. Therefore, the re-attachment behavior of oil on the sand surface was inhibited because of the enhanced repulsive forces between oil and sand (Cai et al., 2017; Pitois et al., 2008).

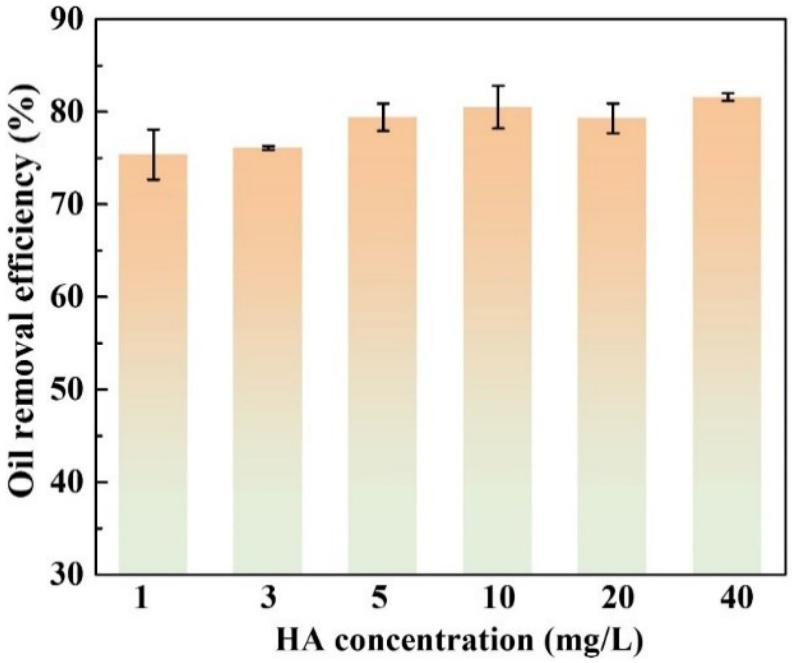

Figure 3.5 Effect of HA on oil removal of NS washing agent.

3.3.6 Effect of oil concentration and comparison with surfactants

Coastal sand is contaminated to varying degrees following an oil spill. Therefore, it is necessary to explore the performance of the NS washing agent at different concentrations of oil-contaminated sand. As shown in Figure 3.6a, oil washing efficiency decreased stepwise from 83.7% to 66.1% with increasing oil concentration from 0.2 to 1 g /1 kg. Importantly, the NS washing agent still exhibited high removal performance (66.1%) at the high oil concentration of 10 g/ 1 kg, indicating that the NS washing agent used in this study is a promising SWA for shoreline cleanup.

The oil removal performance of the NS washing agent was also compared with different surfactants. As shown in Figure 3.6b, SDS had the greatest decontamination efficiency of the four surfactants, releasing 73.4% and 85.2% of oil from the sand surface at the CMC and 2CMC concentrations, respectively. The other three nonionic surfactants displayed relatively low washing performances

and the removal efficiencies of Tween80, Tween20, and TX100 were 55.4% (71.3%), 54.5% (70.6%), and 59.8% (71.6%), respectively. The NS washing agents were able to remove approximately 72.2% of attached oil, performing comparably to commercially available surfactants. Nanoclay and SA are non-toxic and have low environmental impacts because the former is a natural mineral and the latter is a natural gelling agent derived from the cell walls of brown algae. According to our previous study (Bi et al., 2021c), toxicity may be more important than cost when considering a suitable washing option. Once an oil spill occurs, oil pollution must be controlled as soon as possible, while related costs may not be a priority for consideration. In summary, our results support the potential application of NS washing agents for shoreline cleanup.

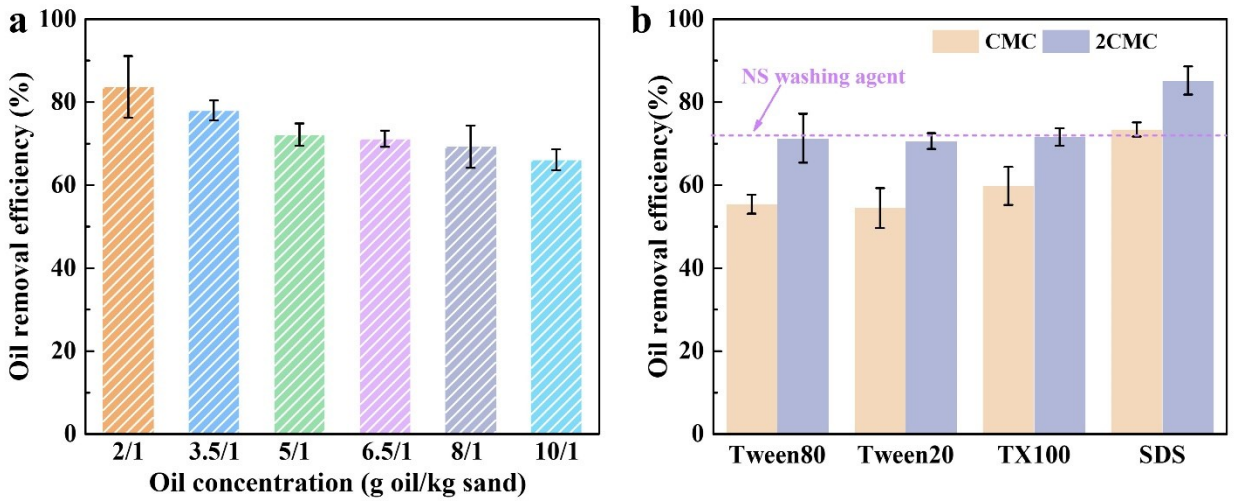

Figure 3.6 (a) Effect of oil concentration on the removal efficiency and (b) comparison of removal efficiency of the NS washing agent with commercial surfactants.

3.3.7 Factorial design analysis of conditions affecting the NS washing performance

As mentioned above, it was concluded that the oil removal efficiency of the NS washing fluid was affected by temperature, oil concentration, salinity, and HA content. Aside from the influence of each factor, interactions between these factors may also affect washing performance. In this study,

a full factorial design analysis was employed to analyze the effects of these factors. According to the principle of hierarchical effects, a system is usually dominated by main effects and lower-order interactions, while higher-order interactions may be less important (Chen et al., 2020b; Shen et al., 2017). As a result, only individual factor and two-factor interactions were considered in this factorial design analysis. The results of the factorial design analysis and its corresponding ANOVA are shown in Figure 3.7. The oil removal efficiency can be calculated by the following polynomial equation: Oil removal efficiency = 0.6195 + 0.00928 A - 0.1170B - 0.0263 C + 0.00153 D - 0.00172 AB + 0.001539 AC + 0.000172 AD + 0.0191 BC - 0.00681 CD + 0.000520 CD. The R-squared and adjusted R-squared of the regression model were 0.8459 and 0.8762, respectively. Moreover, the lack-of-fit of the p-value was 0.960, indicating a very good model fit. According to the Pareto chart (Figure 3.7a), the significant factors were temperature (A), oil content (B), salinity(C), and the two interactions of BD and AC.

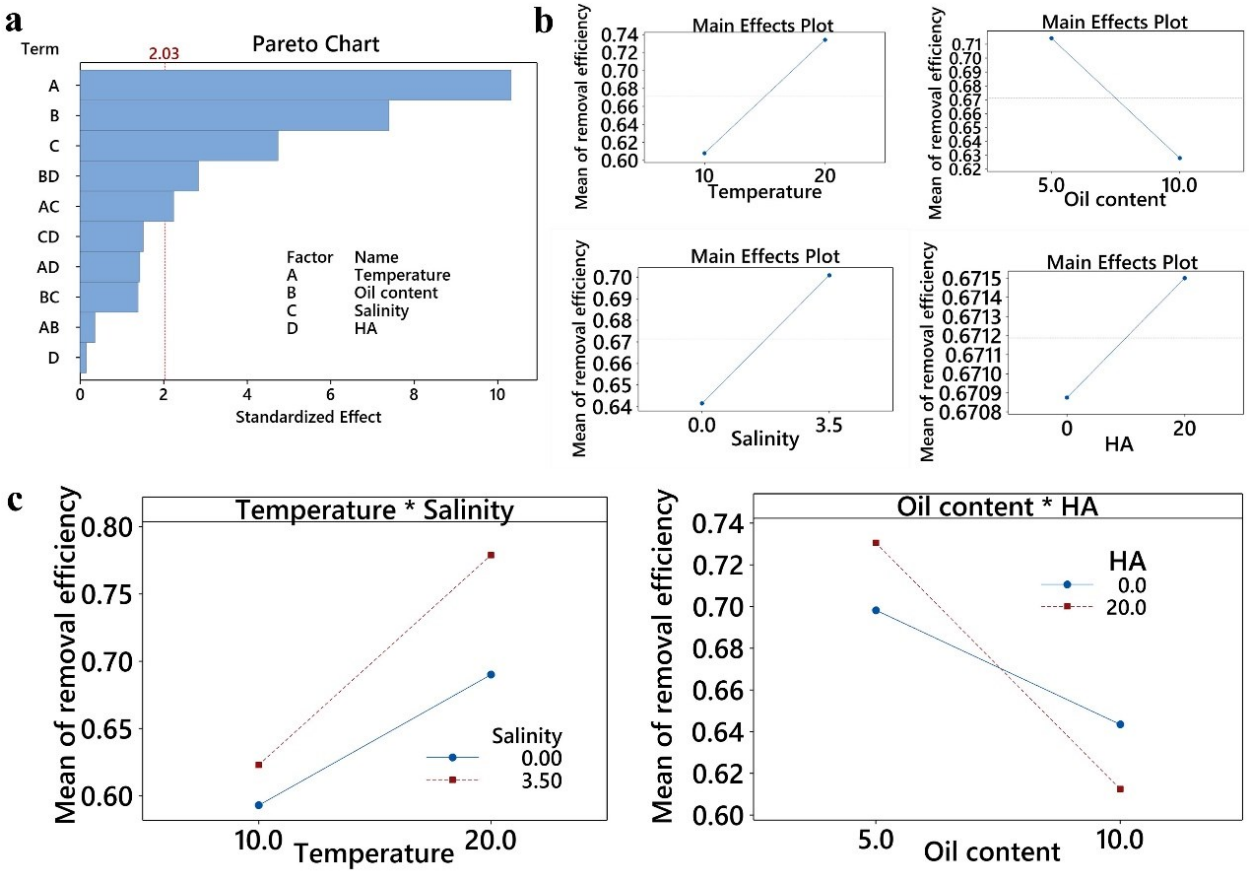

Figure 3.7 Result of factorial design analysis for oil removal efficiency: (a) Pareto chart, (b) main effect plots connecting the response mean at each factor level with a line, and (c) interaction plots.

The temperature had the most prominent effect on the oil removal efficiency of the NS fluid. Due to differences in solar radiation, the ocean surface temperature varies greatly in different regions, latitudes, and seasons. The seawater temperature can exceed 30 ℃ for an entire year in equatorial regions and can be as low as -2 ℃ in polar regions (Observations, 2020; Shrestha and Wang, 2020a). Based on NASA data, the average long-term global temperature is 16.1 ℃ (Observations, 2020). Therefore, 10 and 20 ℃ were chosen as the low and high levels of temperature in this study. The removal efficiencies were 60.8% and 73.2% at the low and high levels, respectively (Figure 3.7b).

Oil content is another important parameter that affects the washing removal efficiency of NS fluid. Lighter oils are prone to evaporation and degradation; therefore, a small amount of these oils is deposited on banks and shorelines. With exposure to sunlight and waves, the heavier oils are likely to form dense, sticky substances that are difficult to remove from sand and rocks. In this work, two oil concentrations, 5 and 10 g/ kg, were applied as the low and high levels, respectively. Although the removal efficiency decreased from 71.4% (low level) to 62.5% (high level) (Figure 3.7b), the NS fluid still exhibited good washing performance at the higher oil content.

Salinity was also a factor that remarkably influenced oil removal efficiency. The removal efficiencies were 64.1% at the low level and 69.8% at the high level (Figure 3.7b). The average salinity of seawater, 3.5 wt%, may vary in offshore areas because of freshwater discharge from runoff and estuaries (Yu et al., 2020). The findings demonstrated that the NS composite was more suitable for use in marine environments than in freshwater. Importantly, seawater can be used directly to prepare NS washing agents, thereby reducing the demand for freshwater and facilitating on-site application. Additionally, the oil removal efficiencies were 67.0% and 67.2% at HA concentrations of 0 (low level) and 20 mg/L (high level), respectively (Figure 3.7b). The main impact of the HA on the oil removal efficiency was insignificant based on the factorial design analysis ($p > 0.05$), which also proved the potential applicability of NS-based fluid for shoreline cleanup in the marine environment with HA.

The interactive effects of two factors were further analyzed, and the results are displayed in Figure 3.7c. The remarkable interactive effects were AC (temperature and salinity) and BD (oil content and HA), according to the ANOVA ($p < 0.05$). For the interaction between A and C, although salinity enhanced the oil removal efficiency at low and high temperatures, its positive effect was

more significant at 20 ℃. This can be attributed to the fact that OPA forms more easily in seawater at high temperatures than at low ones (Henry et al., 2020). There was also a significant interaction between oil content (B) and HA (D). At the high HA content, the negative effect of higher oil content was more noticeable.

3.3.8 Dual responsive separation of oil and washing fluid

To avoid secondary water pollution, the oil must be separated from washing effluents. As shown in Figures 3.8a and b, the washing effluent was turbid and precipitated slowly after 12 h in the absence of either acid or Ca^{2+}. However, the addition of HCl facilitated demulsification because SA became hydrophobic in the acid condition (Figure 3.8c). Therefore, the oil droplets wrapped by the NS composite were able to be separated. Further, when the washing effluent was added to the $CaCl_2$ solution, SA reacted with Ca^{2+} to form small calcium alginate hydrogel beads, which quickly precipitated at the bottom (Figure 3.8d).

To further evaluate the separation performance, the residual oil concentration and turbidity of the supernatant were detected (Figure 3.8f). The oil concentration and turbidity of the washing effluent were 241 mg/L and 460.6 NTU, respectively. After 12 h of settlement, 185.0 mg/L of oil droplets remained in the supernatants, in which turbidity was as high as 48.2 NTU. However, in the pH-responsive method, the oil concentration and turbidity were 110.0 mg/L and 0.143 NTU, respectively. Additionally, acid effluent surface charge decreased significantly (Figure 3.8e), facilitating the demulsification and subsequent separation of oil droplets. Notably, the Ca^{2+}-responsive approach exhibited distinct advantages; only 15.0 mg/L of oil and 0.02 NTU of turbidity were detected.

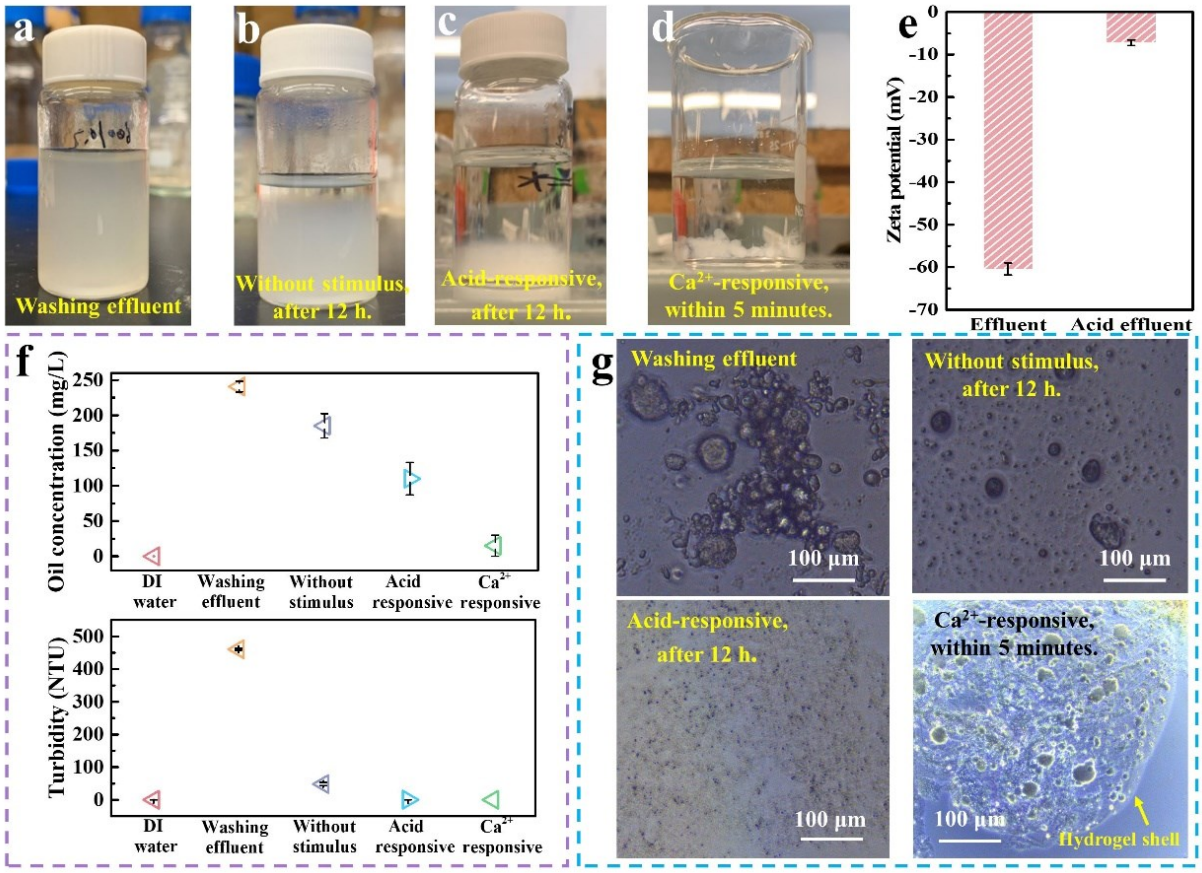

Figure 3.8 (a–d) Photographs of different washing effluents with and without responsive NS, (e) Zeta potential of effluent with and without acid, (f) oil concentration and turbidity of different responsive supernatants, (g) microscopy images of oil droplets of effluent and responsive precipitates.

The microscopic images of oil droplets from effluents and precipitates were also recorded to explore variations in the oil morphology. As shown in Figure 3.8g, oil droplets from both initial effluent and stimulus-free effluent (after 12 h of settlement) displayed similar particle sizes (top images). With the addition of acid, the oil droplets in the sediments were split into smaller droplets (bottom left). Interestingly, a prominent change in the precipitate morphology was observed in the Ca^{2+}-responsive effluent (Figure 3.8g, bottom right). The oil droplets and OPAs were packaged in

CA hydrogel shells and formed capsule-like structures. These capsule-like structures may effectively inhibit oil leakage to supernatants, yielding a super-clean supernatant with low oil content and turbidity. This dual responsiveness made the treatment of washing effluent more sustainable and efficient than many other washing strategies without effluent separation.

3.4. Summary

This study was the first to report a novel dual-responsive and environment-friendly NS washing agent that can effectively decontaminate oiled sand. The main findings include: (1) The characterization results demonstrated that SA combined with nanoclay via hydrogen bonds, and was inserted into the interlayer spacing of nanoclay. (2) The optimal concentrations of nanoclay and SA of the NS washing agent were 800 mg/L and 0.2 wt%, respectively. (3) The factorial design analysis showed that three single factors (temperature, oil concentration, and salinity), and two interactive effects (temperature/salinity; and oil concentration/HA) displayed significant effects on the oil removal efficiency of the NS washing fluid. (4) Compared with the commercial surfactants, the NS composite exhibited satisfactory removal efficiencies for treating oily sand. (5) After demulsifying the washing effluent via pH- and Ca^{2+}-responsive strategies, the oil concentration and turbidity of the supernatants decreased remarkably compared to the initial washing effluent, which can reduce the risk of secondary water pollution. In conclusion, the NS washing agent is a promising alternative for shoreline cleanup because of its low toxicity, low cost, great washing performance, and easy separation. Further study can also be conducted to find additional green options to clean up oiled shorelines.

CHAPTER 4 CLEANUP OF OILED SHORELINES USING A PH-RESPONSIVE PHOSPHOPROTEIN SURFACE WASHING FLUID ‡

4.1 Background

Oil spills occur when liquid petroleum hydrocarbons are released into the environment, particularly within marine ecosystems, as a result of various human activities (Hua et al., 2007; Wang et al., 2021c; Yue et al., 2022g; Yue et al., 2020). In 2020, the total amount of oil released into the environment from tanker spills was approximately 1,000 metric tons. When oil spills transpire, wind, waves, tides, and currents can cause oil to reach and become stranded on shorelines, which may affect the ecosystem and endanger public health (D'Ugo et al., 2021; Wang et al., 2005; Wang et al., 2021b). Oil spill clean-up and recovery are difficult and are impacted by various factors, including the type of spill, ocean temperature (which affects evaporation and biodegradation), and the types of shorelines and beaches (Chen et al., 2019; Ma et al., 2021b; Zhu et al., 2021).

Surface washing agents (SWAs) are used to accelerate oil detachment from oiled sand surfaces by changing the interactions of the oil/water interface (Chen et al., 2020a; Chen et al., 2021c; Yue et al., 2022a). Although there are several commercially available SWAs (Fingas, 2002), they have seen limited use due to a lack of suitable guidelines and concerns about their potentially harmful effects. The development of cost-effective and non-toxic SWAs is an effective and environmentally friendly strategy for dealing with oily shores. In addition, it is expected oil droplets can be further removed from washing effluent in order to minimize the potential for secondary pollution. A

‡ This work has been published as A pH-responsive phosphoprotein surface washing fluid for cleaning oiled shoreline: Performance evaluation, biotoxicity analysis, and molecular dynamic simulation. Chemical Engineering Journal, 2022, 437: 135336.

strategy is to make washing effluent stimuli-responsive to external conditions, such as acidity, temperature, illumination, and chemical agents (Chen et al., 2021b). Among different responsive options, a pH-responsive operation is one of the simplest and easiest stimulus-response approaches to implement (Yang et al., 2013a).

A stable emulsion is usually formed in the presence of a stabilizer, such as a chemical surfactant or solid particles (Xiao et al., 2016). Pickering emulsions refer to emulsions that are stabilized by solid particles. These solutions have attracted enormous research attention, as they enable cheaper and more facile recovery than traditional surfactants. To date, food-grade materials, such as polysaccharides and proteins, have been applied in Pickering emulsion systems due to their many advantages over inorganic particles (Bi et al., 2021a; Xiao et al., 2016). These advantages include: (1) raw materials such as cellulose and chitin are cheap and easily available particles that can be produced on a large scale without environmental impact; (2) the organic and soft properties of these edible materials are susceptible to physical or chemical modifications, which enable the functionalization of the emulsion interface; (3) they enable the formation of a robust and elastic interface that is believed to enhance the resistance to emulsion droplet coalescence; and (4) they are acceptable for human consumption due to their digestible nature and low risk of toxicity. A responsive interface triggered by external stimuli is highly promising in the development of multifunctional Pickering emulsions. Many food-grade polymers, including starch, chitin, and nanocellulose, have been studied in efforts to construct responsive Pickering emulsions (Tang et al., 2015a). Nonetheless, their practical application has been critically inhibited by their low synthesis yields, complicated and tedious modification processes, and the related use of toxic modifiers. In lieu of these issues, this research seeks to find a green alternative that has a responsive nature.

Casein is primarily composed of αs_1- and αs_2-caseins, β-casein, and κ-casein (β- and κ-caseins have both hydrophilic and oleophilic groups), which then undergo α-helix and β-folding to form the spatial structure of casein. Sodium caseinate (NaCas) is the sodium salt of casein and is the main protein in bovine milk. NaCas contains various essential amino acids and trace elements required by the human body and is not only used as a nutritional supplement for various food products but as a mineral trace element for the human body. NaCas is also a safe and harmless thickener and emulsion stabilizer. For instance, Perugini et al. (2018) prepared a food oil/water nanoemulsion stabilized by NaCas and Tween 20. Xu et al. (2020) explored the impact of inulin and konjac glucomannan on the stability, rheological properties, and microstructure of NaCas stabilized oil/water emulsion. Significantly, NaCas is an amphoteric electrolyte and can form precipitates at the isoelectric point, which has the potential to facilitate the separation of protein and oil from washing effluent after surface washing. Research is yet to be undertaken to investigate the potential feasibility of using NaCas for oiled shoreline cleanup. In addition, the environmental conditions of oiled shorelines may vary a lot and it is required to well assess the washing performance impacted by complicated conditions.

In this study, we have comprehensively explored the innovative use of NaCas fluid to treat oiled sand that is removed from the shoreline and treated by washing ex-situ. Batch experiments were conducted to evaluate washing performance at different conditions, and various factors affecting the washing performance of the NaCas fluid were studied through factorial analysis. A comparison of NaCas and surfactants in terms of washing performance was also undertaken. Biotoxicity analysis was further performed to investigate the oil toxicity in the presence of this washing fluid.

In addition, molecular dynamic (MD) simulation was performed to unveil the mechanisms of NaCas-assisted oil removal.

4.2 Materials and methods

4.2.1 Materials

Shell Rotella T4 diesel engine oil (15W40) was used as the representative oil in this study. Standard washed and thermally treated sand (30–40 mesh), NaCas, NaCl, hydrochloric acid (HCl), sodium hydroxide (NaOH), Tween 80, Tween 20, SDS, TX-100, and n-hexane were purchased from Millipore Sigma (Oakville, Canada). Heavy crude oil and light crude oil were obtained from Cold Lake oil in Alberta, Canada, and the Hibernia oil field in Newfoundland, Canada, respectively. Ultrapure (UP) water (18 MΩ) was produced by a Milli-Q ultrapure water purification system (MilliporeSigma, USA).

4.2.2 Preparation of oiled sand

The engine oil was weathered at 20 ℃ for 7 days before use. The oiled sand (5 g oil/1 kg sand) was prepared by dropping the engine oil on the sand and then adding n-hexane to dissolve the oil. Subsequently, the sand/oil/hexane mixture was sonicated and agitated for 10 minutes. Finally, the oiled sand was obtained by evaporating the hexane in a fume hood at 20 ℃ for 48 h.

4.2.3 Sand washing experiments and factorial design

All washing experiments were conducted in a shaker (Innova 42R Incubator Shaker, USA) at 300 rpm and 20 ℃ for 24 h. Typically, 1 g of oiled sand was added to the vial, followed by 15 mL of NaCas washing fluid (concentrations: 0.02, 0.05, 0.1, 0.2, 0.5, and 1.0 wt% in deionized (DI) water).

After surface washing, the sand was lightly washed with DI water to remove NaCas that had potentially been adsorbed on the sand. Subsequently, the sand was dried at 60 ℃ to completely remove DI water. Then, 15 mL of n-hexane was added to extract the residual oil from the sand surface at 300 rpm for 24 h. The extracted oil concentration was measured using a UV-Vis spectrophotometer (Agilent Cary 3500, USA) at a wavelength of 284 nm. The oil washing efficiency was calculated using the equation, $R = 1-(Oil_R/Oil_T)$, where Oil_R and Oil_T refer to the concentration of the residual oil after washing and the initial concentration of oil on the sand before washing, respectively. This testing method has been used for the evaluation of washing agents (Bi et al., 2021b; Chen et al., 2021c; Yue et al., 2022a) and it can also be used for interlaboratory comparison.

A two-level factorial design was used to evaluate the impacts of the single and interactive effects of experimental factors (Bi et al., 2020). Four factors, namely temperature, pH, salinity, and NaCas concentration, were tested at two levels. A 2^4 factorial design was used in the current work and the detailed information about the factorial design is shown in Tables 4.1 and 4.2.

Table 4.1 High and low levels for the 2^4 factorial design.

Factor	**Temperature (℃)**	**pH**	**Salinity (wt%)**	**NaCas concentration (wt%)**
High level (+1)	20	9	3.5	0.5
Low level (-1)	10	6	0	0.1

Table 4.2 Coded levels and corresponding values for factorial design matrix.

Number	**Coded levels**				**A**	**B**	**C**	**D**
	A	B	C	D	Temperature (°C)	pH	Salinity (wt%)	NaCas concentration (wt%)
1	-1	-1	-1	-1	10	6	0	0.1
2	-1	-1	-1	1	10	6	0	0.5
3	-1	-1	1	-1	10	6	3.5	0.1
4	-1	-1	1	1	10	6	3.5	0.5
5	-1	1	-1	-1	10	9	0	0.1
6	-1	1	-1	1	10	9	0	0.5
7	-1	1	1	-1	10	9	3.5	0.1
8	-1	1	1	1	10	9	3.5	0.5
9	1	-1	-1	-1	20	6	0	0.1
10	1	-1	-1	1	20	6	0	0.5
11	1	-1	1	-1	20	6	3.5	0.1
12	1	-1	1	1	20	6	3.5	0.5
13	1	1	-1	-1	20	9	0	0.1
14	1	1	-1	1	20	9	0	0.5
15	1	1	1	-1	20	9	3.5	0.1
16	1	1	1	1	20	9	3.5	0.5

4.2.4 Biotoxicity test

The green algae *Chlamydomonas reinhardtii* (CPCC 243) was chosen as the testing species to analyze biotoxicity since they are the main food source for various plankton and plays a critical role in the food chain (Naselli Flores and Barone, 2009). The algae were cultivated in Bold's Basal Medium (BBM) under a 12 h light/12 h dark cycle at 23 ℃ for 4 days (Yin et al., 2021a). The algae were exposed to 3% oil for 72 hours. In addition, a control group with only algae was evaluated. For comparison, the toxicity of co-existing NaCas (0.1 wt%) was investigated at 72 h (with DI water for the control group). The cell density, chlorophyll, reactive oxygen species (ROSs), cell size (forward scatter [FSC]), and cell content (side scatter [SSC]) were measured using a flow cytometer (BD, Accuri C6 Plus, Canada).

4.2.5 Molecular dynamic simulation

Modeling can be used to further analyze environmental processes and develop response strategies (Hong et al., 2021; La and Chai, 2021; Yoo et al., 2021). The homology modeling and docking of the NaCas structures were reported in previous studies (Cao et al., 2020a; Sun et al., 2021). MD simulation and subsequent analysis were conducted using a large-scale atomic/molecular massively parallel simulator (LAMMPS) software in the present study. Silica was selected as a typical mineral component in the sand formation, and a methylated surface with a dimension of 161.6 × 49.13 × 30 $Å^3$ was applied to feature the oil wettability. (Morris et al., 2016). An oil droplet was simulated as a mixture of 250 n-octane molecules attached to the silica surface, which was merged in a water box of 161.6 × 49.13 × 105 $Å^3$ in size (Morris et al., 2016). The energy of the system was minimized by using 5000 steps of the conjugate gradient algorithm. Subsequently, the equilibration of the

system was calculated in the isothermal-isobaric (NPT) ensemble in a 100 ps MD simulation at 298 K and 1 bar. The production run for the protein system equilibration was conducted for 10 ns.

4.2.6 Analytical and characterization methods

The zeta potential test was performed using a Zetasizer (Malvern, USA). Surface tension (SFT) and interfacial tension (IFT) measurements were recorded using the force tensiometer (KRUSS K100, Germany) and spinning drop tensiometer (KRUSS, Germany). Turbidity tests were performed using a turbidity meter (ORION AQ3010, Thermo Scientific, Canada). Fourier transform infrared (FTIR) spectra were obtained through an INVENIO S FTIR spectrometer (Bruker, Germany). The FTIR mapping images were captured at the Canadian Light Source in Saskatoon, Canada. All batch experiments were conducted in triplicate, and the mean values were used for the data analysis. The experimental design and result analysis were carried out using Minitab (Minitab, LLC., USA). In addition, the statistical significance of the results ($p < 0.05$) was determined through a one-way analysis of variance (ANOVA) (He et al., 2018).

4.3. Results and discussion

4.3.1 Effect of sodium caseinate concentrations

The oil removal performances of washing fluid with different NaCas concentrations are plotted in Figure 4.1a. When compared to the UP water, the NaCas washing fluid exhibited almost doubled oil washing efficiency (> 61.0%). The oil removal efficiency increased from 61.0% to 66.8% with the increase of NaCas content from 0.02 to 0.1 wt%. Figures 4.1b and c demonstrate that at low concentrations (< 0.2 wt%), the addition of NaCas significantly decreased both SFT and IFT of the NaCas/engine oil interface due to the amphiphilic property of NaCas. Reduced SFT and IFT are

conducive to oil-water miscibility, which facilitates oil diffusion and leads to a higher oil removal performance. Moreover, the reduction in both SFT and IFT can decrease the size of oil droplets, in turn boosting their motion to NaCas fluid (Liang et al., 2019). Liang et al. (2019) reported that oil droplets were prone to be split into small fragments at a low IFT interface as the coherent energy of the droplets decreased, promoting the detachment of the oil droplets.

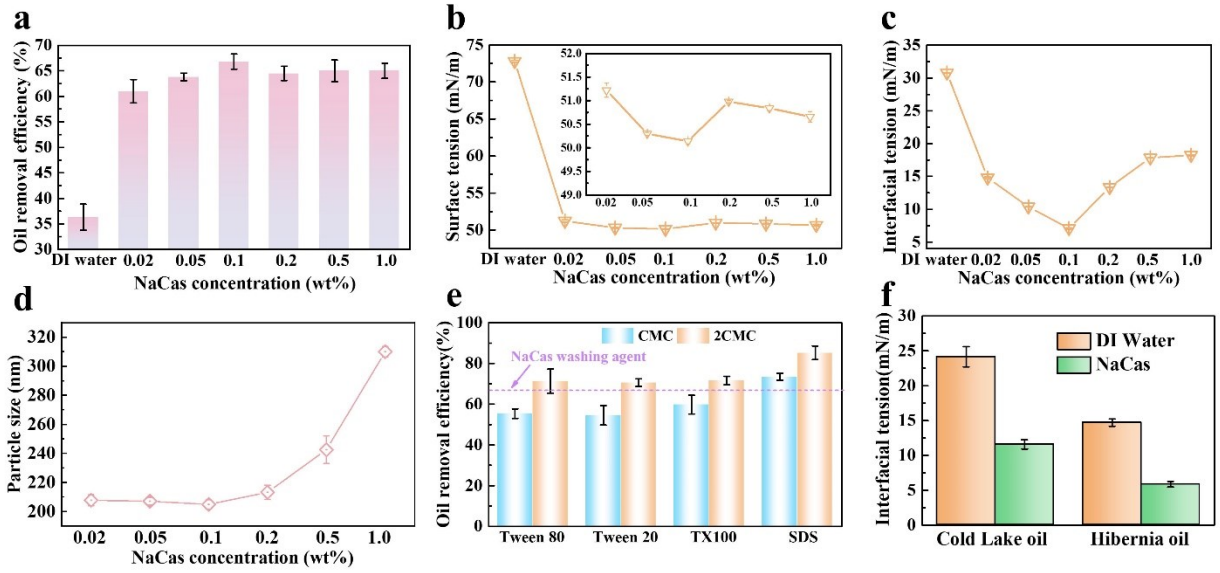

Figure. 4.1 (a) Oil removal efficiencies of washing fluids with different NaCas concentrations, (b) SFTs, (c) IFTs of NaCas/engine oil, (d) particle size distribution of the NaCas fluid at different concentrations, (e) comparison of removal efficiency of NaCas fluid and commercial surfactants, and (f) IFTs of different fluid/oil interfaces.

At higher concentrations (> 0.2 wt%), the NaCas fluid became less effective for oiled sand cleanup, washing around 64% of oil from the sand surface. The increased surface and interfacial tensions at high NaCas concentrations could be due to the reduced β-casein amount at the oil/water interface (Srinivasan, 1998). The increased particle size may also explain the affected oil removal. As illustrated in Figure 4.1d, the particle size of NaCas increased stepwise with increasing

concentrations of NaCas. Smaller particle sizes have faster adsorption kinetics and are more conducive to the formation of effective particle build-up at the oil-water interface. In other words, smaller particles are more likely to facilitate the production of stable Pickering emulsions (Wu and Ma, 2016), which may enhance the efficiency of oil removal.

In the subsequent experiments, the optimum concentration of 0.1 wt% NaCas was used for oiled sand cleanup. Figure. 4.1e compares the washing performances of the NaCas fluid and some commercial surfactants. All the selected surfactants were employed at their critical micelle concentration (CMC) and double CMC (2CMC), respectively. In the comparison with the anionic surfactant (SDS), three nonionic surfactants (Tween 80, Tween 20, and TX100) displayed relatively low oil removal efficiencies due to their adsorption on the sand. Notably, the results demonstrated that the NaCas fluid displayed a comparable washing performance relative to the surfactants. Moreover, the decreased IFTs of NaCas/crude oil (Figure 4.1f) further proved the surface-active property of NaCas. These indicated that it is feasible to use NaCas-assisted washing fluid as a viable alternative in oil spill responses for practical applications.

In addition, FTIR was applied to demonstrate the washing effectiveness of the NaCas fluid (Figure 4.2). The characteristic peaks at 2954, 2923, and 2853 cm^{-1} corresponded to aliphatic C-H stretching in oil (Figure 4.2a). (Ancheyta, 2016). The washed sand exhibited lower peak intensities than the oiled sand, indicating the detachment of oil from the sand surface. FTIR mapping was performed to further analyze the spatial oil content on the sand surface. As depicted in Figures 4.2b and c, the striped bright areas and blue areas represent more and less oil accumulation, respectively, suggesting that the oil was not uniformly distributed on the sand surface. After surface washing, the peak intensity weakened remarkably, demonstrating the detachment of oil from the sand surface.

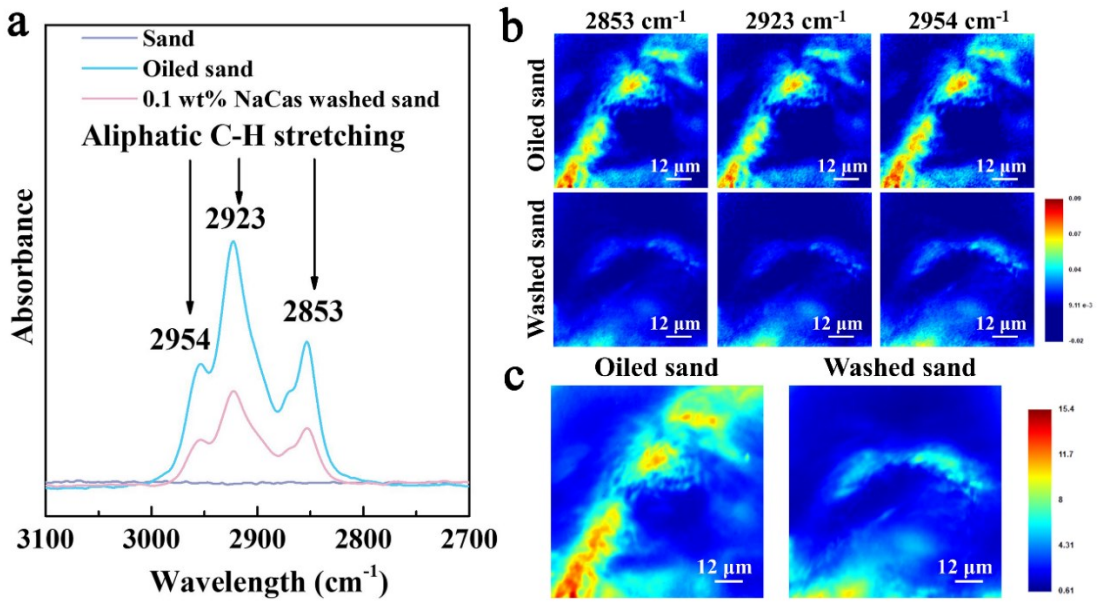

Figure 4.2 (a) FTIR spectra of clean sand, oiled sand, and NaCas-washed sand; FTIR mapping of (b) three individual peaks and (c) 2800-3000 cm^{-1} of the oiled sand and washed sand.

4.3.2 Effect of temperature

Temperature can affect oil behavior by altering its viscosity, and the temperature range of the coastline is often at 5 to 25 ℃ (Chen et al., 2022b; Dethier et al., 2012). Figure. 4.3a displays the impacts of temperature on the oil washing efficiency of the NaCas fluid. According to the results, the washing performance improved from 43.8% to 66.8% as the washing temperature increased from 5 to 20 ℃. The improved temperature may have decreased both the SFT and IFT of the NaCas fluid (Figure. 4.3b). This is because the higher temperature affected the mutual solubility of the solvent, the adsorption kinetics of NaCas molecules, and the distribution of NaCas between oil and water, influencing SFT and IFT (Corpuz et al., 2019). The increased temperature may have shortened the time needed to reach the IFT equilibrium (Ye et al., 2008). Similar to surfactants, NaCas is an amphiphilic material containing both hydrophilic and lipophilic groups (Xi et al., 2020). Ye et al. (Ye et al., 2008) studied the effects of temperature on IFT between crude oil and surfactants.

Their results demonstrated that increased temperature considerably decreased both IFT and its equilibrium time. This trend can facilitate the release of oil from the sand surface as a result.

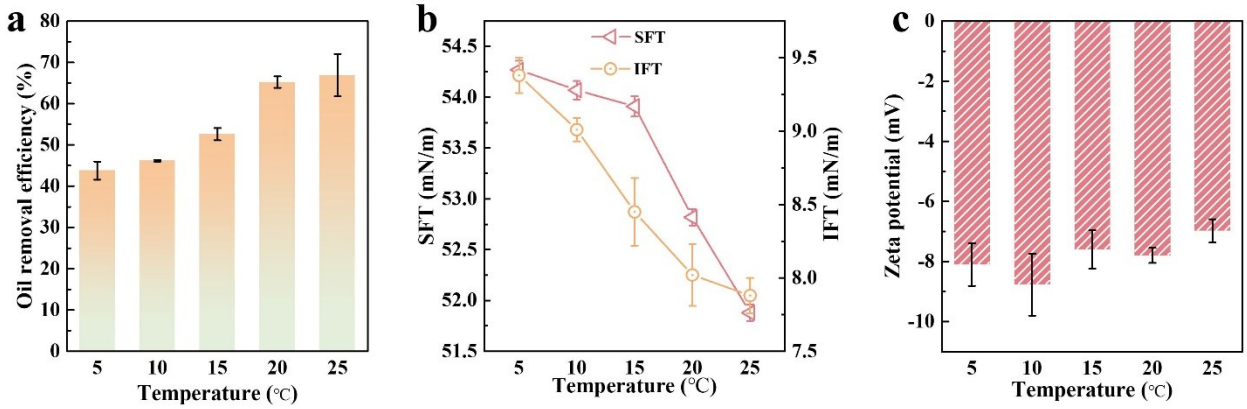

Figure 4.3 Effects of temperature on (a) oil removal efficiency, (b) SFT and IFT, and (c) Zeta potential of NaCas fluid/oil mixture.

In addition, the increased fluid temperature may reduce the viscosity of the oil/NaCas mixture during the washing process, promoting the release of the attached oil and the stabilization of the Pickering emulsions. Temperature can also change the behavior of the oil that adheres to the sand surface by altering oil viscosity (Stoffyn-Egli and Lee, 2002). Oil with a low viscosity is prone to be broken into small droplets, weakening the interactions between the oil and sand surfaces. Studies have shown that the silica surface is more negatively charged at higher temperatures (Dai and Chung, 1995). Figure 4.3c confirms that the surface charges of the NaCas/oil mixture at the temperature gradient were stable. Therefore, the enhanced surface charge may have hindered the reattachment of oil on the sand surface by increasing the repulsive forces between the silica and NaCas/oil emulsion.

4.3.3 Effect of salinity

The salinity in the shoreline areas may vary spatially and temporally (Chen et al., 2021c). Figure 4.4a shows the influence of salinity on the washing performance of the NaCas fluid. While the oil removal efficiency declined moderately to 57.1% with the addition of 0.1 wt% salinity, it recovered gradually and reached efficiency levels as high as 69.5% at a salinity of 3.5 wt%. Srinivasan et al. (Srinivasan et al., 2000) reported that the concentration of NaCas (1 wt%) attached to an oil droplet surface declined with the addition of 0 to 20 mM of NaCl and increased at higher NaCl concentrations (> 40 mM). Additionally, in an emulsion made with 3% NaCas, the surface concentration of NaCas on the oil droplet surface decreased as the content of NaCl increased from 0 to 1000 mM. The reduced surface concentration of NaCas fluid is unfavorable for the formation of a stable Pickering emulsion, which may reduce the washing performance of the NaCas fluid.

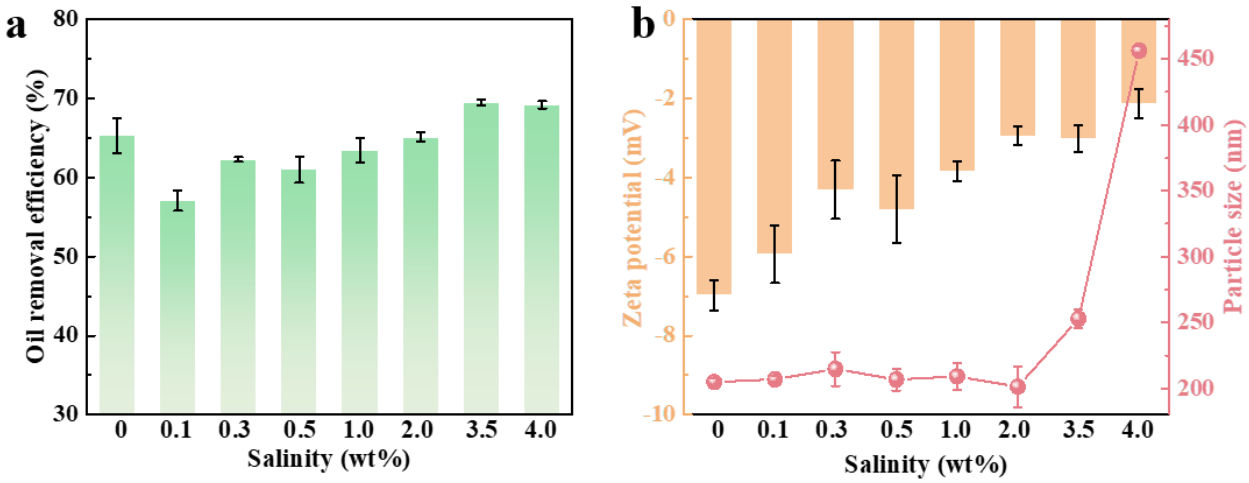

Figure 4.4 Effects of salinity on (a) oil removal efficiency and (b) particle size of NaCas (red line) and Zeta potential of the washing effluent (orange columns).

The increased oil release at high salinity levels was associated with the formation of oil particle aggregates (OPAs). As illustrated in Figure 4.4b, high ionic strength can compress the electric

double layer of a NaCas/oil emulsion to form OPAs, promoting the release of attached oils (Le Floch et al., 2002). In the present research, the particle sizes of NaCas were less than 500 nm at different salinities (Figure 4.4b), which may have improved the generation of stable OPAs. In a recent study by Yu et al. (Yu et al., 2019b) on the mechanisms of OPA formation, the results demonstrated that small particles of less than 100 μm in size can generate stable OPAs.

4.3.4 Effect of pH and pH-responsive separation

The typical pH range of seawater is 7.5 – 8.4, while the pH of coastal areas can vary due to the input surface water from land estuaries (Roy and Tim, 2012). Figure 4.5 plots the effect of pH on the washing performance of the NaCas fluid. The oil removal efficiencies of the NaCas fluid were 68.8% and 67.1% at pH levels of 6 and 7, respectively. Under alkalic conditions (pH = 8 and 9), the washing efficiency decreased to approximately 50%. The size of the micelles in the NaCas fluid grew with increasing pH values (Figure. 4.5a). Furthermore, because the surface charge of the individual NaCas molecules was more negative when the pH shifted from acid to alkaline, the structure of the NaCas micelles became looser due to enhanced electrostatic repulsion, rendering the increased micelle size (Liu and Guo, 2008). As demonstrated in Figures 4.5a and b, the particle size, SFT, and IFT of the NaCas fluid increased as pH increased, leading to an unstable Pickering emulsion and low oil-water miscibility. This could be because NaCas-based emulsions are more stable under acidic conditions (Farshchi et al., 2013). In a previous study, Farshchi et al. (2013) observed that NaCas-stabilized oil/water emulsion was stable at pH levels of 6.0 and 6.5, as the adsorbed protein molecules frequently formed a stable gel network.

Protein is an amphoteric electrolyte. At the isoelectric point, proteins are the most unstable electrolyte because they do not repel each other of the same charge and are prone to combining rapidly into larger aggregates through electrostatic gravity. This causes them to precipitate out. NaCas had an isoelectric point of roughly 4.4. When the acidity of the washing effluent was adjusted to be close to 4.4, the NaCas became insoluble casein and rapidly precipitated from the emulsion, generating a super-clean supernatant with a turbidity of 0.08 NTU and an oil concentration of 20.0 mg/L (Figures. 4.5c and d). In contrast, the washing effluent remained turbid after 12 h of settlement without any stimulus while with 170.0 mg/L of oil pollutants. In addition, microscopy images showed that there were only a few oil droplets remained in the pH-responsive supernatant.

NaCas is an intrinsically disordered protein with an open conformation. Individual casein molecules are highly amphiphilic copolymers with a high proportion of non-polar C-terminal structural domains (Portnaya et al., 2006). Under acidic or alkaline conditions, the protonation and deprotonation of the phosphoserine groups inside the protein structure can switch the hydrophilicity/hydrophobicity of NaCas, enabling NaCas-stabilized emulsions to cycle between reversible emulsification/demulsification (Xi et al., 2020). Significantly, most proteins have a remarkably well-organized secondary structure and close tertiary structure, with oleophilic chains usually inside the entire structure (De Kruif et al., 2012; Wang et al., 2019d). This makes it difficult to rapidly construct and destroy emulsions that are stabilized by these compact proteins. It is also worth noting that casein has an open construction and no tertiary structure.

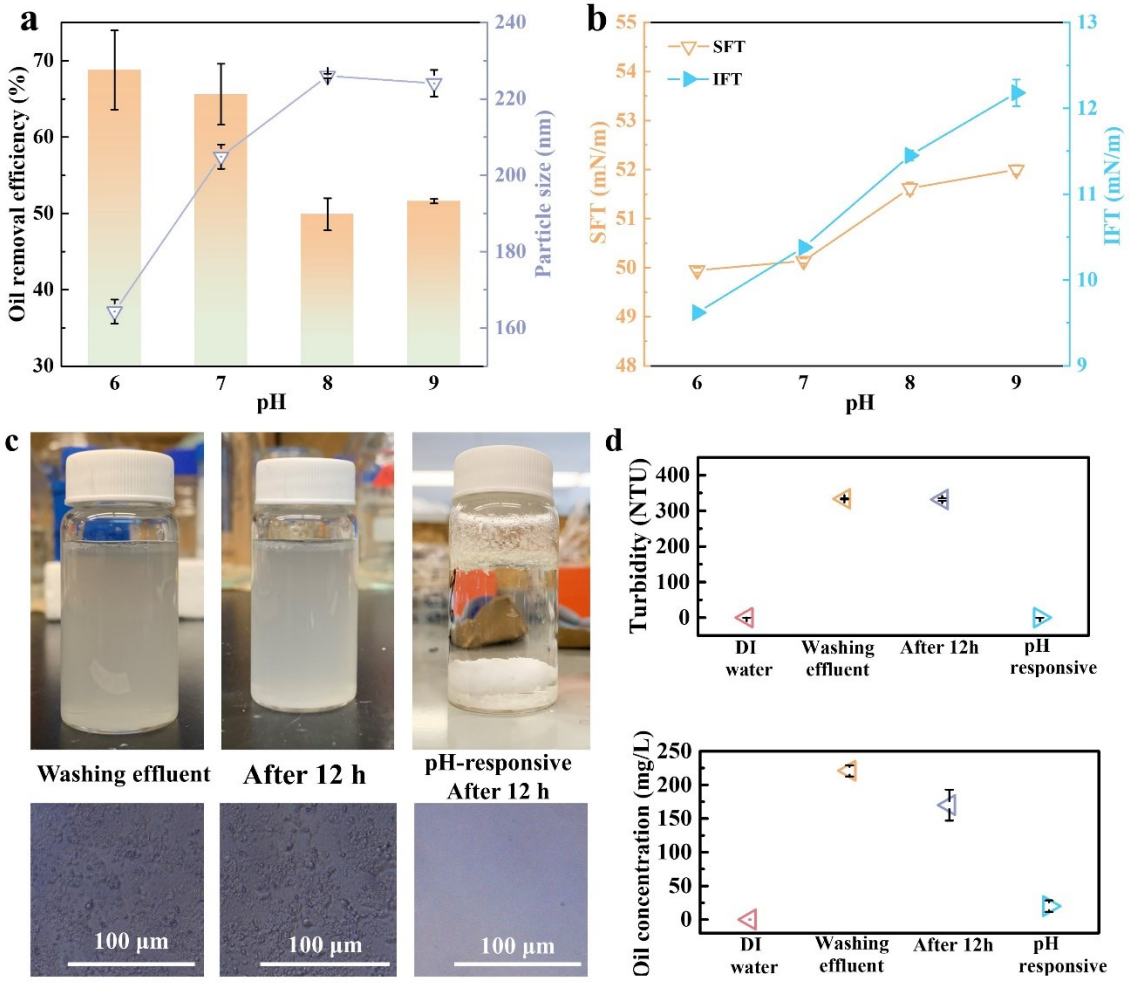

Figure 4.5 (a) Effects of pH on the oil removal efficiency and particle size, (b) SFT and IFT of NaCas fluids at different pH values, (c) photographs and microscopy images of washing effluents at different conditions, and (d) turbidity and residual oil concentrations of the effluents at different conditions.

The feature of pH responsiveness made the pretreatment of washing wastewater more efficient and applicable, compared with the methods without effluent separation or those requiring the assistance of CO_2 or N_2 (Bonal et al., 2018; Kim et al., 2019; Xu et al., 2018b). The experimental findings of this study proved that oil contaminants can be easily separated from washing effluent after tuning acidity and thus NaCas fluid has a strong potential for practical applications. For the

implementation of this approach, the oiled sand can be excavated, and washing can be conducted ex-situ within certain mixing reactors. After washing, the produced washing fluid can be readily treated through this proposed pH-responsive separation.

4.3.5 Factorial analysis of conditions affecting the washing performance of sodium caseinate

As demonstrated above, the NaCas washing performance was affected by temperature, pH, salinity, and fluid concentration. The interactions between these factors may have also affected the washing ability of the NaCas fluid. The principle of hierarchical effects suggests that while a system is usually composed of its primary effects and lower-order interactions, higher-order interactions can be ignored (Shen et al., 2017; Wen et al., 2021). Therefore, the factorial analysis only considered individual factors and two-factor interactions. The results of the factorial analysis and ANOVA are depicted in Figure 4.6. As a function of the four factors, the oil removal efficiency can be expressed by the following equation: mean of oil removal efficiency = 0.7135 + 0.01296 A - 0.07260 B + 0.0072 C - 0.063 D + 0.001194 AB + 0.000843 AC + 0.00292 AD - 0.00305 BC - 0.0060BD + 0.0144 CD. Moreover, the p-value of the model was 0.219, confirming its suitability ($p > 0.05$). The significant individual factors included temperature (A), pH (B), NaCas concentration (D), and the interactions of AB, BC, and AC (C: salinity).

The temperature was found to be the most significant factor affecting the washing performance of NaCas (Figure 4.6a), with the oil removal efficiency increasing from 35.9% at 5 ℃ to 60.2% at 25 ℃. This indicated that an increased temperature was beneficial to the enhancement of washing efficiency. The positive impacts of temperature could be explained by the reduced SFT, IFT, and mixture viscosity. In sum, NaCas washing fluid can present better oil removal efficiency at a

suitably high temperature. Nonetheless, an excessive increase in temperature may be detrimental to cleaning performance on oiled shorelines because higher temperatures can change the properties of proteins and cause them to coagulate, which is irreversible and prevents proteins from being restored to their original structures. High temperatures may also adversely affect plankton, vegetation, and creatures along the coastline (Holloway, 1991).

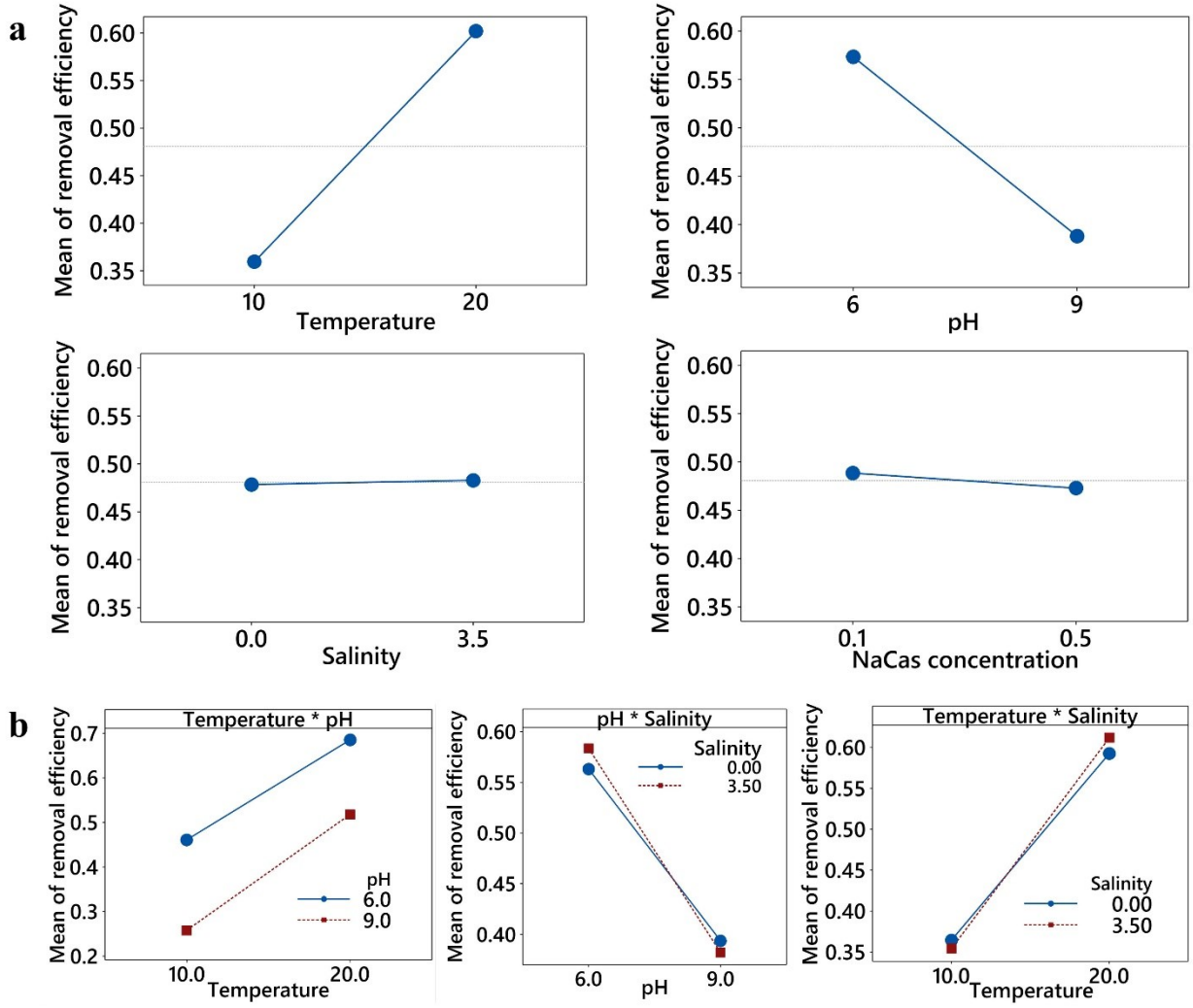

Figure 4.6 Factorial analysis of oil removal efficiency: (a) main effect plots, and (b) interaction plots.

The fluid acidity was another parameter that significantly affected the washing performance of NaCas (Figure 4.6a), with the oil removal efficiency decreasing from 57.3% to 38.8% upon the increase in pH from 6.0 to 8.0. This suggests that neutral or weak acid fluid could be good for washing oil from oily sand. Notably, acidification may lead to reduced shell production in shellfish and other aquatic organisms with calcium carbonate shells and present several other physiological challenges for marine organisms as well. The effective concentration of NaCas in oil washing was a critical parameter for assessing its feasibility for wholescale practical applications (Figure 4.6a). Concentrations of 0.1 wt% and 0.5 wt% were chosen as the low and high levels of NaCas in the test of its effects on the washing performance. The observation of a slightly decreased washing efficiency from 48.85% to 47.28% upon the increase of NaCas concentration from 0.1 to 0.5 wt% demonstrated that NaCas was effective for oil removal at relatively low concentrations. According to the factorial analysis (Figure 4.6a), salinity was an insignificant factor ($p > 0.05$) that led to the removal of 47.8% and 48.1% of oils from the sand surface at low and high levels, respectively. The results suggested that NaCas could be more effective for oil removal in salty water than in freshwater environments. Marine water could also be used to prepare such washing fluids on site.

4.3.6 Biotoxicity analysis

The biotoxic effect of the cleanup process is an important consideration for decision-making (Cai et al., 2019; Cao et al., 2020b; Yue et al., 2021b). The present study investigated the biotoxicity of oil to algae in the presence of NaCas. Cell density is a common indicator for evaluating aquatic toxicity at the community level (Gao et al., 2020; Xin et al., 2021). Figure 4.7a shows the population of algae under different growth conditions. The control group was free of oil and NaCas,

and only green algae were included in the culture medium. While oil significantly inhibited algae growth ($p < 0.05$), the addition of NaCas relieved these adverse impacts ($p < 0.05$).

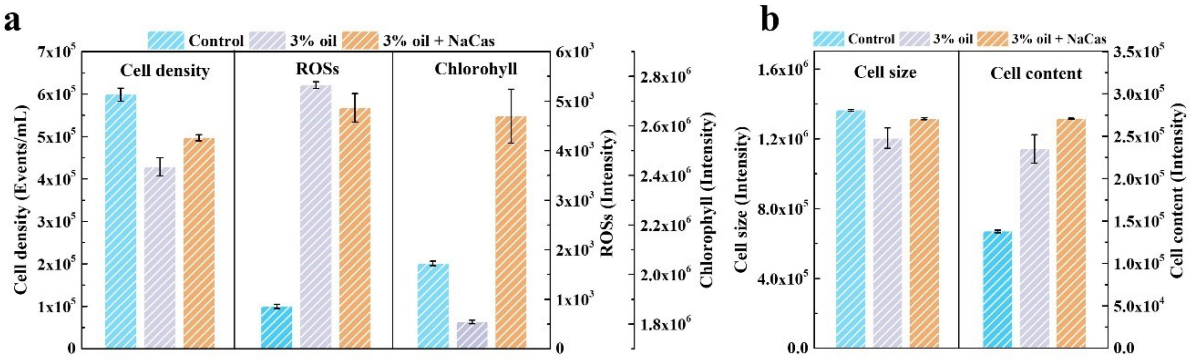

Figure 4.7 (a) Cell density, ROSs, and Chlorophyll, and (b) cell size and cell content of algae under different conditions.

From a biological point of view, ROSs are a natural byproduct of normal oxygen metabolism and play a pivotal role in cell signaling and homeostasis. However, high concentrations of ROSs can be harmful and lead to oxidative damage. ROSs can react with biological macromolecules — deactivating or altering them — cause organelle dysfunction, alter cell structure, and result in mutagenesis. Figure 4.7a shows the ROSs intensities of the algae under different conditions. When compared to the control group, the ROSs intensity enhanced significantly ($p < 0.05$) with the presence of oil pollutants. This may be because the oil droplets changed the environmental pressure, disrupting the cellular homeostasis of the algae and stimulating the production of ROSs (Gao et al., 2020; Gomes et al., 2017). Nonetheless, in the presence of NaCas which can mitigate oxidative damage to algae cells, the generation of ROSs was restrained. Chlorophyll is another important parameter for assessing algae biomass. As illustrated in Figure 4.7a, the presence of oil droplets significantly led to the decreased chlorophyll content at 72 h ($p < 0.05$). A possible explanation for this is that oil layers that form around algae cells can retard the diffusion of gases (Ramadass et al.,

2015). The addition of NaCas also significantly enhanced chlorophyll production ($p < 0.05$). NaCas can strengthen chlorophyll stability in the aqueous system by inhibiting the storage decomposition and light degradation of chlorophyll (He et al., 2019).

Figure 4.7b shows the variations in the cell size and content of the algae. The cell growth was restrained after exposure to oil pollutants ($p < 0.05$). This was due to cellular aging caused by ROSs and the weakened photosynthesis of the alga cells. NaCas did not significantly affect cell growth. The cell content of algae increased in oil-containing BBM, indicating the high complexity of the algae cells. Higher levels of complexity indicated changes in cellular ultrastructure and severe damage to organelles (Cai et al., 2016a). In the current study, NaCas exhibited an insignificant effect on cell complexity ($p > 0.05$). The above-mentioned results demonstrate that the introduction of NaCas can relieve the oil toxicity to algae.

4.3.7 Molecular dynamic simulation of oil behaviors

To further unveil the mechanisms of oil removal, MD simulation was applied to investigate the movement of oil in the water and NaCas fluid systems, respectively. In both systems, oil molecules spread onto the sand surface to form an oil layer at the initial stage (0 ns). In the water system (Figure 4.8a), the oil droplets accumulated tightly on the sand surface to form an oil layer, which remained on the surface until 10 ns. In addition, a few oil droplets were detached from the sand surface. However, in the presence of NaCas, the oil layer became loose and was split into small fragments, resulting in a visible crack and the transport of more oil droplets to the liquid phase (Figure. 4.8b). This observation indicated that more oil droplets were released from the sand surface.

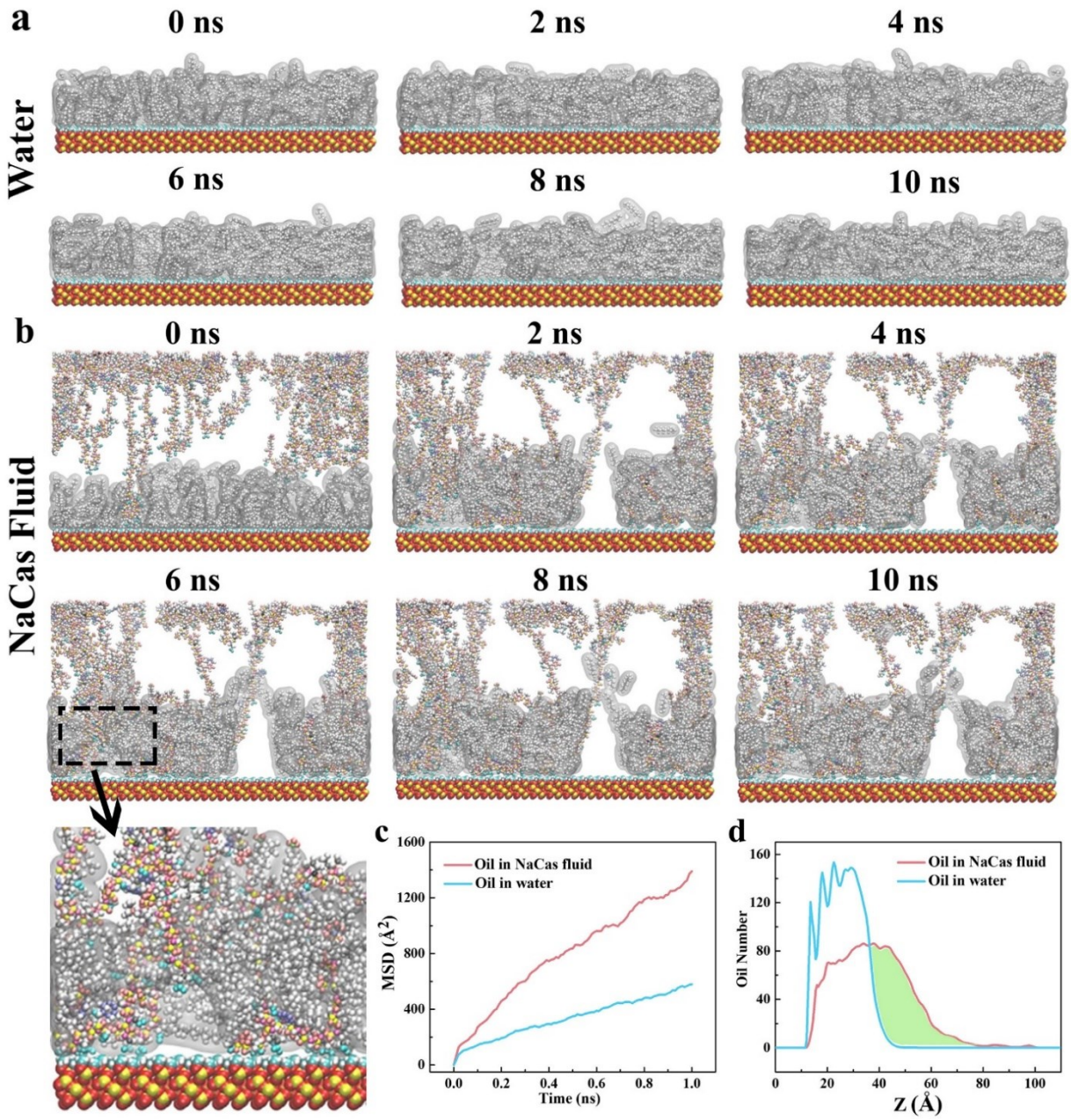

Figure 4.8 Oil movement in (a) water and (b) NaCas fluid; (c) MSD curves and (d) oil distribution in the water and NaCas fluid, respectively.

With its amphiphilic property, the hydrophobic ends of NaCas molecules entered into the oil layer and encapsulated the oil droplets, strengthening the interaction of the oil and water phases and enhancing the interfacial activity of the oil/liquid interface. Because the higher interfacial activity

indicated high emulsion capability, more oil droplets were desorbed from the sand surface during the surface washing process. Moreover, the weakened interaction between the oil encapsulated by the NaCas molecules and the sand surface may contribute to the release of the oil, which promoted the detachment of oil from the sand surface. Liang et al. (Liang et al., 2019) studied the oil transport behavior at the silica/liquid interface in an MD simulation system. These findings showed that modified nanoparticles capable of reducing the IFT were able to impair the adsorption of oil pollutants to the silica surface and accelerate their release.

To quantitatively illustrate the oil motion behavior, the mean squared displacement (MSD) and oil distributions of the water and NaCas systems are plotted in Figures 4.8c and d. MSD is a measure of the deviation of the position of a particle relative to a reference position over time. It is also the most common approach for measuring the spatial extent of random motion (Michalet, 2010; Ramil et al., 2020). The oil molecules in the NaCas fluid exhibited higher MSD values than those in the water (Figure 4.8c), demonstrating that oil droplets diffused more rapidly in the NaCas environment than in the water environment. Moreover, oil distribution curves confirmed that more oil droplets moved to areas away from the sand surface in the NaCas fluid (Figure 4.8d, green area), which implied the desorption of oil from the sand surface. These simulation findings are in alignment with experimental results and that can help further reveal the mechanisms of good oil removal efficiency of NaCas washing fluid.

4.4 Summary

In the present study, an innovative green surface washing method based on food-grade NaCas was proposed for oiled shoreline cleanup. A comprehensive performance evaluation, biotoxicity

analysis, and molecular dynamic simulation were conducted to explore the washing process. The addition of NaCas was able to decrease both SFT and IFT, resulting in high oil removal efficiency. While the washing efficiency was enhanced with the increase of NaCas concentration at the low-concentration range, it showed a trend of decrease at higher concentrations. In addition, the NaCas fluid showed a high washing performance under acidic and neutral conditions, but with a deteriorated ability in alkaline environments. The temperature and high salinity facilitated oil detachment from the sand. The factorial analysis demonstrated that three individual factors (temperature, pH, and NaCas concentration) and three interactive effects (temperature/salinity, temperature/pH, and salinity/pH) significantly impacted the washing performance of NaCas fluid. Notably, the washing effluent displayed good pH responsiveness, generating a super-clean supernatant with low turbidity and oil concentration. Moreover, biotoxicity tests proved that the presence of NaCas could reduce the toxicity caused by oil droplets by enhancing the chlorophyll concentration and decreasing the ROSs content, respectively. The MD simulation further revealed that NaCas could break the oil layer on the sand surface and move the oil droplets away from the sand. In conclusion, NaCas fluid is a promising candidate for oiled shoreline cleanup due to its low cost, good biocompatibility, pH responsiveness, and high oil removal efficiency.

CHAPTER 5 CLEANUP OF OILED SHORELINES USING A MAGNETIC-MEDIATED WASHING FLUID ‡

5.1 Background

Oil spills impacting beaches are a challenge because beaches are frequently high amenity sites (ie., in many cases, frequently used recreational spots) and sensitive ecosystems for flora and fauna (e.g. clam beds, nesting areas for sea birds, etc) that are also expensive to clean (Lee et al., 2020; Wang et al., 2021c; Yue et al., 2020). In addition, spills of oil on coastal shorelines may pose a long-time threat to regional economies, and public health (D'Ugo et al., 2021; Wang et al., 2005; Wang et al., 2021b). Accordingly, effective techniques for cleaning oiled shoreline environments are urgently needed.

In-situ or *ex-situ* surface washing methods can effectively remove the oil from the affected shoreline (Chen et al., 2021b; Yue et al., 2022a). Surface washing agents (SWAs) traditionally consist of solvents and surfactants that enhance hydrocarbon removal by improving oil miscibility (Chen et al., 2020a). However, the application of SWAs itself may pose certain environmental risks, and this is an important consideration when dealing with oil spill cleanup (Bi et al., 2021c). In this regard, detrimental environmental impacts of oil spill cleanup efforts in shoreline environments can be avoided through the design of less toxic surface washing materials. Moreover, to minimize secondary treatment costs as a part of this process, a simple and effective approach to separate the washing materials and hydrocarbons from the washing effluent is essential. In this regard, most of

‡ This work has been published as R. Yue, C. An, Z Ye. X. Chen, K. Lee, K. Zhang, S. Wan, Z. Qu. Exploring the characteristics, performance, and mechanisms of a magnetic-mediated washing fluid for the cleanup of oiled beach sand. Journal of Hazardous Materials. 2022, 438: 129447.

the washing fluids currently in use can only be used once, which increases the operational cost and reduces the practicality of these techniques. These considerations underscore the need for a washing fluid that maintains good stability and reusability after use in surface washing.

Magnetic nanoparticles have garnered considerable attention owing to their distinct features and crucial applicability in biology and biomedicine (Shasha and Krishnan, 2021; Zamani Kouhpanji et al., 2021; Zhu et al., 2018). In particular, magnetite (Fe_3O_4) nanoparticles have been intensively applied in bio-separation (Kim et al., 2018), drug delivery (Asgari et al., 2021), and pollution treatment (Jiang et al., 2019; Lin et al., 2021; Shan et al., 2021) due to their good biocompatibility, stability, environmental benignity (Babincova et al., 2000), and superparamagnetic property. Recently, hydrophobic magnetite nanoparticles have been employed to collect crude oil from water and have displayed good oil uptake performance, where the adsorbent can be readily recovered by applying a magnet (Debs et al., 2019). However, while the strong interaction at the hydrophobic-hydrophobic interface promotes oil capture, the poor dispersibility of these particles in water inhibits their application in surface washing. To address this, hydrophilicity modifications with hydroxyl, SiO_2, and polyvinylpyrrolidone have been proposed to enhance the stability of magnetite dispersion (Elmobarak and Almomani, 2021b; Mirshahghassemi et al., 2019). Ge et al. (2007) synthesized water-dispersible magnetite crystals with controlled diameters. However, the poly(acrylic acid) linked to the crystals is not biodegradable and biocompatible, and thus its application is limited.

Sodium citrate is a food-grade material that is extensively used in the food and medicine industries, while citric acid is an intermediate of the citric acid cycle in the human body (Springsteen et al., 2018). The carboxyl groups on sodium citrate have a strong coordination affinity with Fe^{3+} ions.

That would facilitate the surface functionalization of the magnetite nanoparticles with citric groups and prevent them from accumulating into large clusters (Liu et al., 2009). In the study described herein, we employed a facile solvothermal method to synthesize magnetite nanoparticles with low toxicity, excellent water dispersibility, stability, and magnetic responsiveness. The morphology, crystal structure, and surface chemical groups of the magnetite nanoparticles were characterized. The surface washing performance of the magnetite fluid under different conditions was investigated, and the mechanisms of the surface washing were explored. Thermodynamic modeling was also applied to further reveal the mechanism of oil removal. Furthermore, the reusability, economic feasibility, and post-treatment of the magnetite fluid were evaluated as discussed herein.

5.2 Materials and methods

5.2.1 Materials

The oil used in this study was standard engine oil (Shell Rotella T4 15W40). Standard sand, iron chloride hexahydrate ($FeCl_3 \cdot 6H_2O$), ethylene glycol, kaolinite, sodium citrate dihydrate, sodium acetate anhydrous, NaCl, n-hexane, and ethanol were sourced from Sigma Aldrich (Oakville, Canada). Ultrapure (UP) water was produced by a Milli-Q ultrapure water purification system (MilliporeSigma, USA).

5.2.2 Synthesis of water-dispersible magnetite

The magnetite nanoparticles were synthesized by using a modified solvothermal approach (Liu et al., 2009). 1.625 g of $FeCl_3 \cdot 6H_2O$ and 0.650 g of sodium citrate dihydrate were dissolved in 30 mL of ethylene glycol under vigorous agitation at room temperature (solution A). 3 g of anhydrous sodium acetate was dissolved in 10 mL of ethylene glycol under vigorous agitation at room

temperature (solution B). Then, solution B was added dropwise into solution A under agitation for 5 min at room temperature. Subsequently, the mixture was poured into a 100 mL Teflon-sealed autoclave and heated at 200 ℃ for 9 h. After cooling to the ambient temperature, the obtained products were washed with ethanol and UP water three times.

5.2.3 Preparation of oiled sand

Oiled sand (oil content: 5 g of oil per 1 kg of sand) was prepared by mixing the engine oil with clean sand. Specifically, n-hexane containing the engine oil was mixed with the clean sand under agitation to make the engine oil uniformly distributed. The as-prepared oiled sand was achieved once n-hexane had completely evaporated at room temperature.

5.2.4 Sand washing experiments

Vials each containing 1 g of oiled sand and 15 mL of magnetite washing fluid (dispersed in UP water) were placed in a shaker (Innova 42R Incubator Shaker, USA) at 300 rpm and 20 ℃ for 24 h. After pouring out the washing fluid, UP water was gently added to rinse the sand to remove the residual washing fluid, followed by drying the sand at 60 ℃ overnight. Then, the vials containing 15 mL of n-hexane and 1 g of washed sand were shaken at 300 rpm for 24 h to extract the remaining oil. The oil removal efficiency was calculated by determining the oil concentration using an Agilent Cary UV-Vis spectrophotometer (3500, USA) at a wavelength of 284 nm. This testing method, it should be noted, has been widely applied for surface washing (Chen et al., 2021c; Yue et al., 2022a) and it is also suitable for interlaboratory comparison. After magnetite recovery, the residual oil concentration in the washing effluent was also extracted using n-hexane at 300 rpm for 24 h and was measured using the UV-Vis spectrophotometer.

5.2.5 Analytical and characterization methods

The zeta potential and average particle size tests were performed using a Zetasizer (Malvern, USA) and a particle size analyzer (LISST-200X, USA). Interfacial tension (IFT) results were recorded using a KRUSS force tensiometer (K100, Germany). Transmission electron microscopy (TEM) images were obtained using a Thermo Scientific Talos F200X G2 S/TEM. Furthermore, the surface morphology of the magnetite nanoparticles was recorded on a scanning electron microscope (SEM, Hitachi S–3400N). X-ray photoelectron spectroscopy (XPS) characterization was performed using a Thermo Scientific K-Alpha spectroscopy, and X-ray diffraction (XRD) measurements were conducted on a Bruker D4 X-ray diffractometer. Attenuated total reflectance Fourier transform infrared (ATR-FTIR) spectra were measured using an FTIR spectrometer (INVENIO, Bruker, USA). X-ray fluorescence (XRF) and FTIR mappings (Pixel size 3.3 × 3.3 μm) were undertaken at the VESPERS (07B2-1) and a 01B1-01 (MidIR) beamlines, respectively, of the Canadian Light Source. Water contact angles (WCAs) and oil contact angles (OCAs) were obtained using a CA instrument (AST Product, USA), and thermogravimetric analysis (TGA, Q500, USA) was applied to investigate the weight loss behavior of the materials under study. Magnetic field strengths at different horizontal distances were determined by putting a Gauss meter (MF-30K AC/DC, LATNEX, Canada) at a given distance.

5.2.6 Thermodynamic modeling

Modeling is an extensively used technique to elucidate environmental processes and design remediation approaches (Wen et al., 2021; Yoo et al., 2021). In this study, the oil-water miscibility in the magnetite fluid was explored using a thermodynamic model.

From the perspective of thermodynamics, a miscible blend is usually indicated from a negative or zero free energy of mixing ($\Delta G \le 0$) but a positive second derivative ΔG with respect to composition ($\frac{\partial^2 \Delta G}{\partial \phi^2}$) (McGlashan, 2007). The Flory–Huggins theory has been one of the most commonly-accepted theoretical models which are applicable for solvent/polymer–solvent mixtures in various chemical processes, particularly, for the chain-like alkanes and water (Flory, 1942; Huggins, 1942) following the equation below,

$$\Delta G = \chi_{12} RT \phi_1 \phi_2 + RT(n_1 \ln \phi_1 + n_2 \ln \phi_2) \quad (1)$$

where χ_{12} is the Flory–Huggins interaction parameter, R is the universal gas constant, T is system temperature, n_1, and n_2 are respective molecule numbers of components 1 and 2 on the molecular basis, ϕ_1 and ϕ_2 are the respective molar concentrations of the components 1 and 2. However, the conventional Flory–Huggins theory may not be capable of properly handling the additions of nanoclay. Recently, a modified thermodynamic model was developed to predict the thermodynamic miscibility of the oil–water system with additions of surfactant-decorated nanoparticles (Zhang et al., 2018b). Based on the previous study, the free energy of mixing for the system here is presented as follows,

$$\Delta G = \Delta G_{\text{flu}} + \Delta G_{\text{np}} \quad (2)$$

where ΔG_{flu} is the free energy from the interactions between the water and nanoparticles and ΔG_{np} is the free energy contributed by the nanoparticles. The free energy between the oil and pure water is assumed to be negligible here since, with the additions of nanoparticles, the water phase is modified while the oil phase has almost no change and its effect is thus very small. In this case, Eq. 2 could be rearranged and presented to be,

$$\Delta G_{\mathrm{m}} = \frac{\phi}{v_{\mathrm{p}}}(1-\phi)p(\frac{r_{\mathrm{NP}}}{r_0})\frac{3r_{NP}^2}{2\sqrt{v_1 v_2}r_0^2} + \chi_{\mathrm{flu}}\phi(\frac{r_0}{r_{\mathrm{NP}}})(1-\phi) + \frac{\phi}{v_{\mathrm{p}}}[\ln\phi + p(\frac{r_{\mathrm{NP}}}{r_0})\frac{4\phi-3\phi^2}{(1-\phi)^2}] \quad (3)$$

where ϕ is the weight fraction of nanoparticles, r_{NP} is the radius of a single nanoparticle, r_0 is the monomer radius, v_{Np} is the volume of a single nanoparticle, χ_{flu} and is the Flory–Huggins interaction parameter between the water and nanoparticles. It should be noted that the nanoparticle is assumed to be a spherical hydrophilic particle and the model is restricted to pure water (without salinity change) in this study. More details could be found elsewhere (Zhang et al., 2018b), which could be checked if interested and won't be duplicated here.

5.3 Results and discussion

5.3.1 Characterization and magnetic properties of magnetite

The ATR-FTIR spectrum of the magnetite is shown in Figure 5.1a. As can be seen, the bands at 3400 and 1068 cm^{-1} corresponded to the C–H vibration and O–H vibration, respectively (Liu et al., 2009). In addition, the bands at 1582 and 1384 cm^{-1} were associated with the carboxyl groups (Divandari et al., 2019), while a typical band of the Fe–O stretching was visible at 570 cm^{-1} (Liu et al., 2009). The XRD pattern of the magnetite (Figure 5.1b) exhibited all the characteristic peaks of (220), (311), (400), (422), (511), and (440) (Deng et al., 2008). However, XRD characterization was not sufficient to verify the magnetite, since it exhibits a similar pattern to γ-Fe_2O_3 (Liu et al., 2016). Therefore, the XPS measurement provided additional evidence for the characterization. As depicted in Figure 5.1c, peaks at 710.7 and 724.3 eV were observed corresponding to the Fe $2p_{3/2}$ and Fe $2p_{1/2}$, respectively. Moreover, two sets of peaks were detected corresponding to Fe^{3+} (712.1 and 726.4 eV) and Fe^{2+} (710.4 and 724.1 eV) (Huang et al., 2016; Zhang et al., 2020), confirming the successful synthesis of the magnetite. Meanwhile, the three characteristic peaks at 530.0, 531.5,

and 533.0 eV in the high-resolution O1s spectrum (Figure 5.1d) indicated the presence of Fe–O, C(O)OH, and C–O, respectively (Sordello et al., 2014). Owing to the hydrophilic carboxyl groups and strong negative surface charge (−33.7 ± 0.79 mV, Figure 5.2a), the magnetite nanoparticles were easily and uniformly dispersed in UP water (Figure 5.2b). Moreover, when a permanent magnet (1200 Gauss) was applied, the magnetite nanoparticles were magnetically separated. Notably, it was found that the nanoparticles could be re-dispersed easily by lightly shaking the mixture after withdrawing the magnet. In addition, it was observed that the strong magnetic attraction force between the magnet and magnetite can uplift a centrifugation tube (50 mL in capacity, Figure 5.2c).

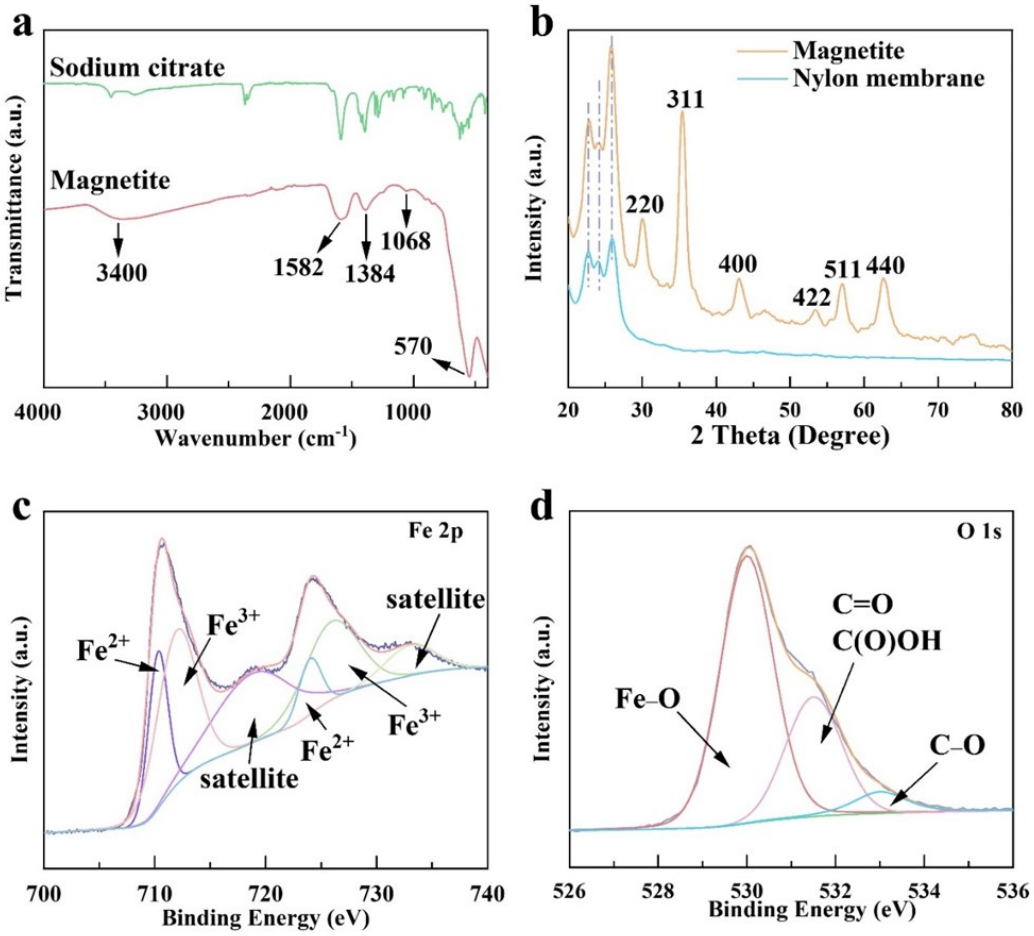

Figure 5.1 (a) ATR-FTIR spectra, (b) XRD patterns, and (c, d) XPS spectra of the magnetite. The XRD characterization was conducted by vacuum filtrating magnetite dispersion onto a Nylon membrane.

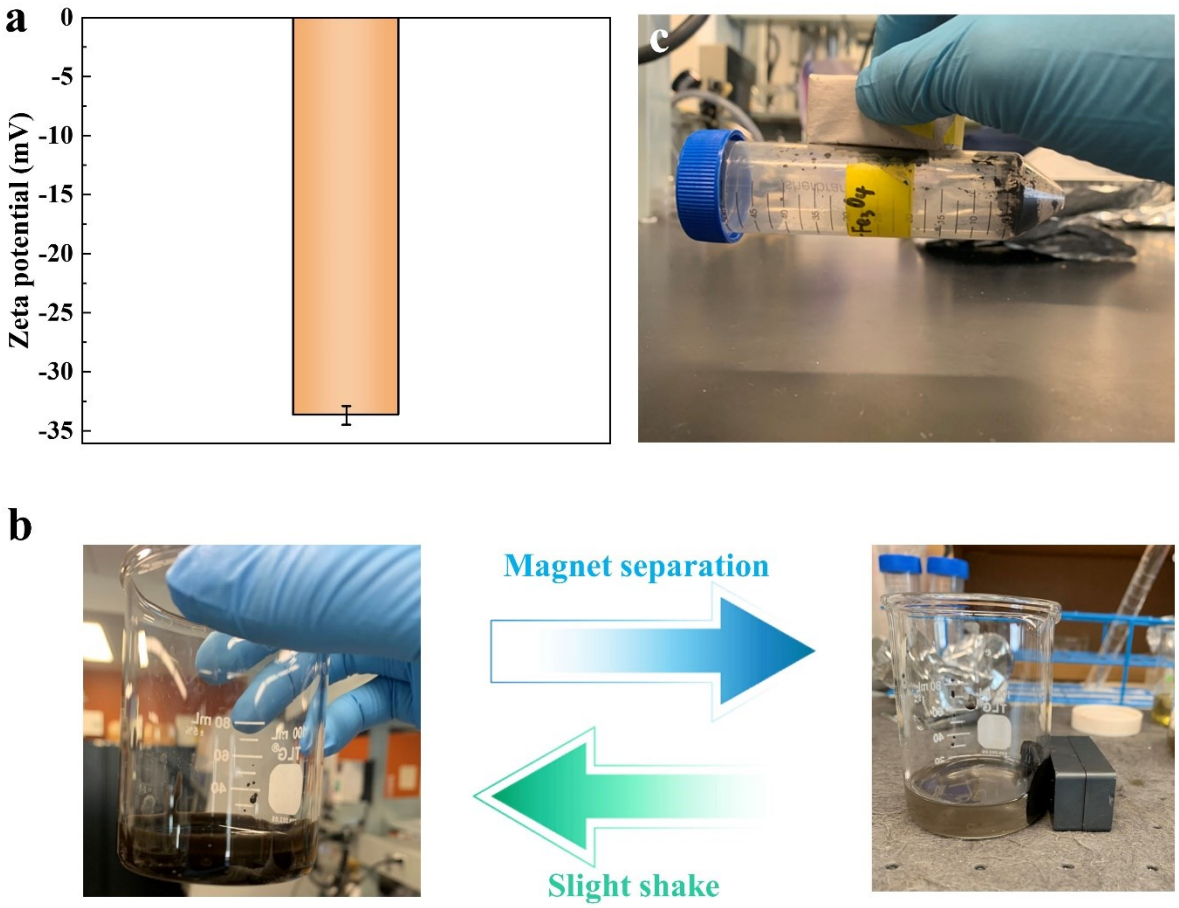

Figure 5.2 (a) Zeta potential of magnetite nanoparticles, (b) photographs of magnetite dispersion in UP water, and (c) photograph of magnetite.

The TEM images (Figures 5.3a and b) show that the magnetite nanoparticles dispersed uniformly and had a nearly spherical shape, with an average diameter of around 250 nm as revealed by the particle size distribution (inset of Figure 5.3a). The elemental mapping (Figures 5.3c–2f) suggested

that carbon elements were uniformly distributed on the nanoparticles' surface, indicating the presence of carboxyl groups.

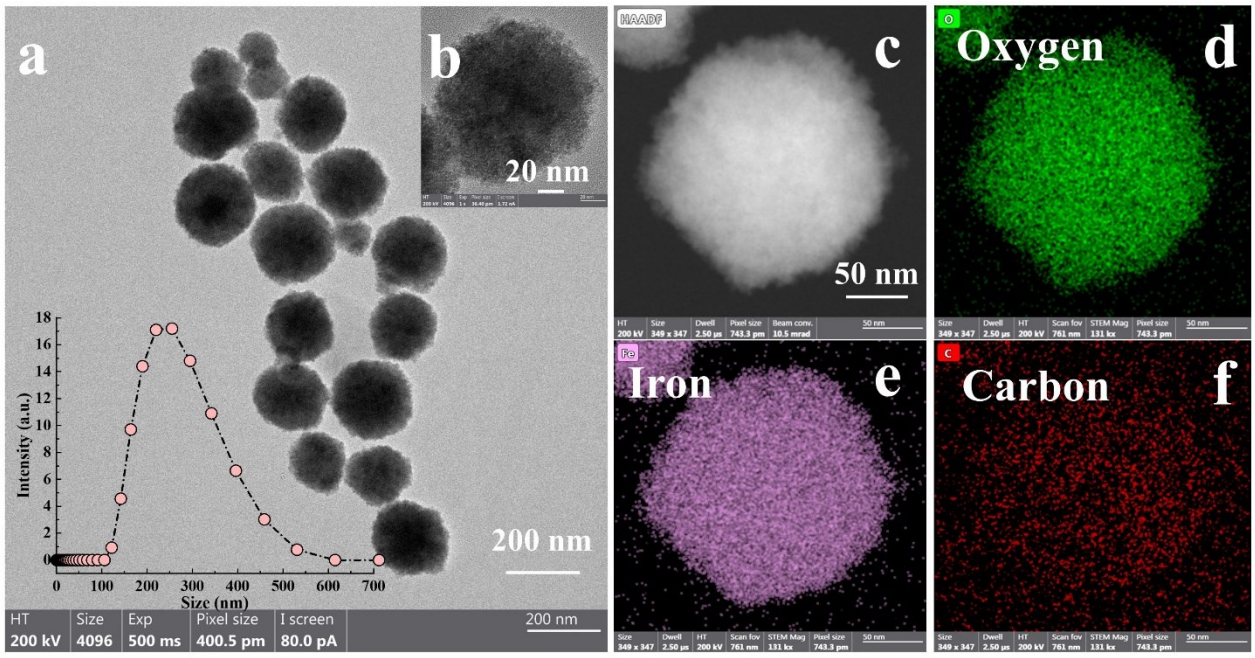

Figure 5.3 (a, b) TEM images of magnetite nanoparticles, the particle size distribution of magnetite nanoparticles (inset of Figure 5.3a), and (c–f) elemental distributions of magnetite nanoparticles.

5.3.2 Effect of magnetite concentration on oil removal

The effect of the magnetite concentration on the washing performance was investigated, and it was found that the magnetite concentration had a positive contribution to the fluid washing performance. The washing effectiveness increased from 61.4% to 70.2% with the increase of the magnetite fluid concentration from 0.02 to 1.0 g/L (Figure 5.4a). The high concentration of the magnetite fluid reduced the IFT of the fluid-oil interface (Figure. 5.4b), possibly attributable to the presence of carboxyl groups on the magnetite surface. It should be noted that engine oil is a complex mixture of chemicals consisting of 90% base oil and 10% additives, where the former comprises linear

alkanes, branched alkanes, and one- to six-ring cyclic alkanes (Manheim et al., 2019). Sayed et al. (2019) found that the addition of carboxylic acid decreased the IFT of the n-decane/water system.

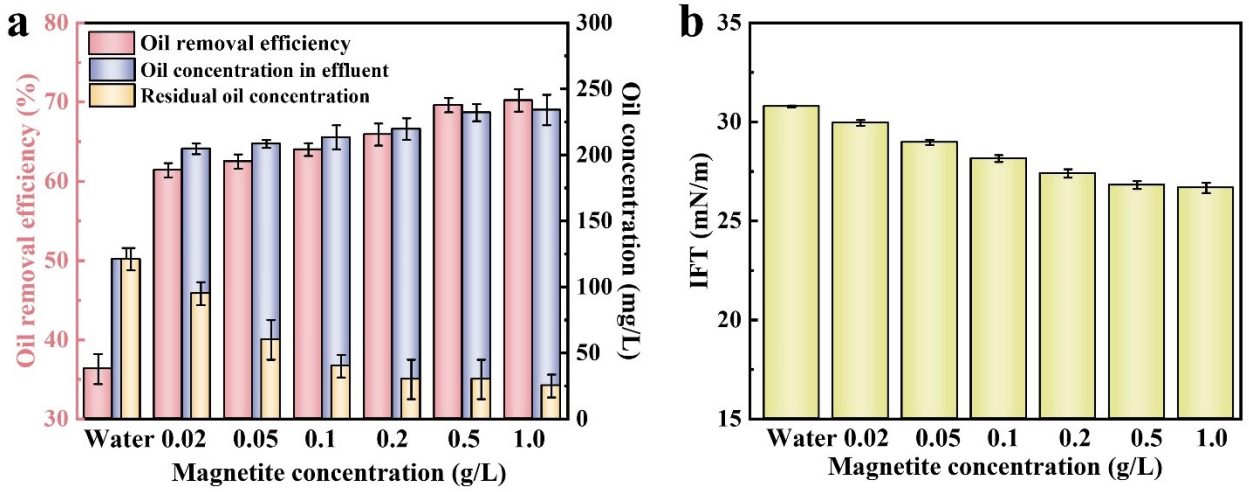

Figure 5.4 (a) Effect of magnetite concentration on washing performance and residual oil concentration after magnetite recovery, and (b) IFT of different magnetite fluids.

Many conventional approaches have been applied in oil removal from the water body, i.e. membrane separation and chemical oxidation. However, some toxic chemicals were involved in surface modification in membrane fabrication (Rezaeian et al., 2020; Yang et al., 2021). The peroxymonosulfate used in chemical oxidation is capable of generating toxic hydrogen sulfide (Dong et al., 2021). Due to the outer citric acid layer, the magnetite has good biocompatibility and low cytotoxicity (Liu et al., 2009). Thus, the water-dispersible magnetite nanoparticles hold great potential for oily wastewater treatment.

5.3.3 Effect of kaolinite on oil removal

The environmental processes can be impacted by various factors (Hong et al., 2019; La and Chai, 2021; Sundar et al., 2021; Wang et al., 2022c; Wen et al., 2021). Clay minerals are ubiquitous in

both nearshore areas and shorelines. Because of its high adsorption capacity, high cation exchange capacity, and large surface area, clay can be a significant factor in contaminant transport in aqueous solutions (Zhao et al., 2014). Natural seawater containing various components can be used for the *ex-situ* washing process after oil spills. As depicted in Figure 5.5a, oil removal efficiency decreased from 65.9% to 52.6% with the increasing kaolinite concentration. During surface washing, kaolinite was adsorbed on the magnetite surface, as shown in the ATR-FTIR spectra (Figure 5.5b), where the unique bands of kaolinite appeared in the used magnetite spectrum. Since kaolinite had no surface-active property (Figure 5.5c), the kaolinite/magnetite mixture had a higher IFT compared to the magnetite fluid (Figure 5.5a), making the mixture less conducive to oil detachment from the sand surface. In addition, with kaolinite increased, the surface charge of the magnetite decreased gradually, which led to an increase in average particle size (Figure 5.5d). The possible mechanisms underlying the effect of surface charge and average particle size on the oil removal are further discussed in detail in Section 5.3.7.

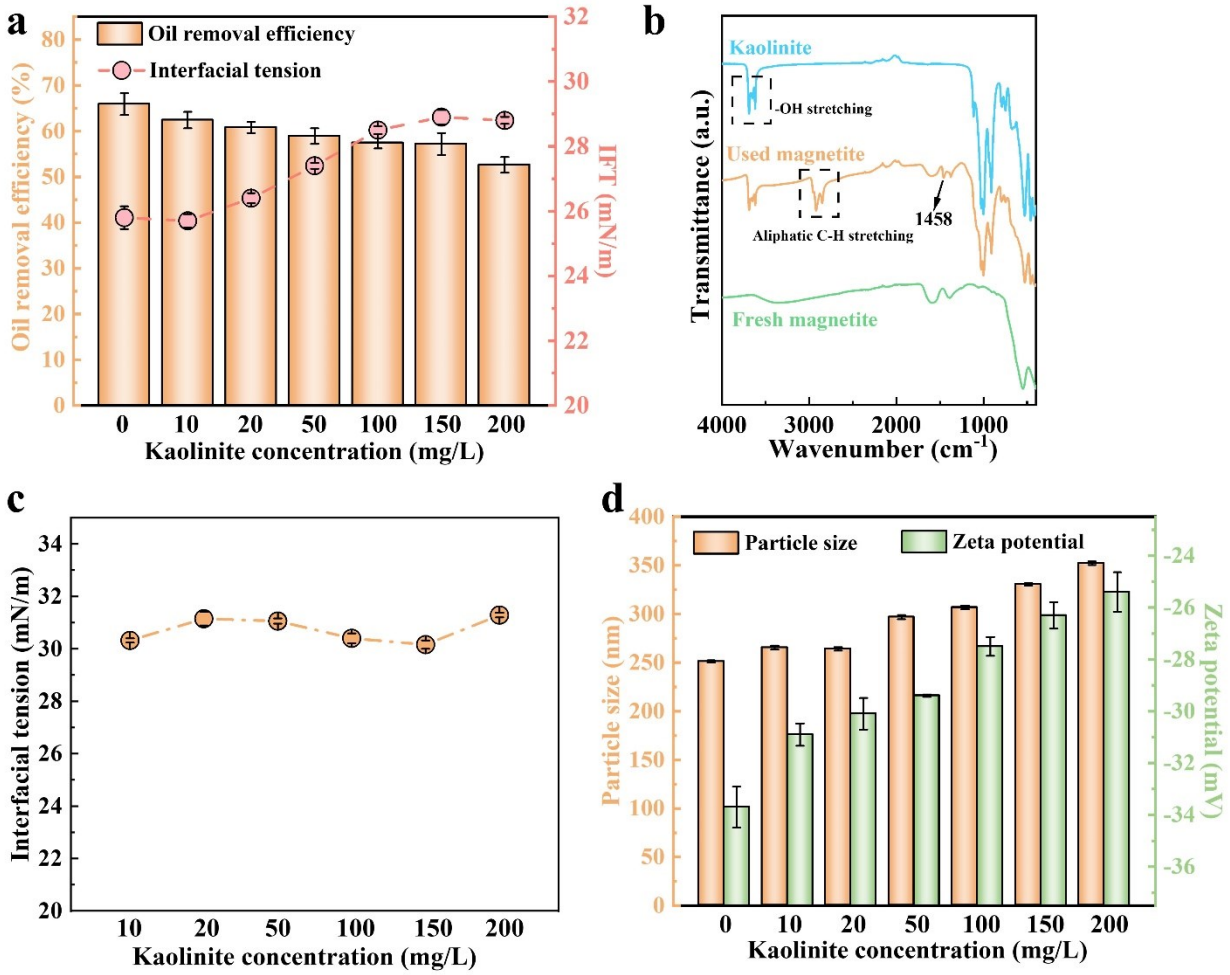

Figure 5.5 Effect of kaolinite on (a) washing performance and IFT, (b) ATR-FTIR spectra of fresh magnetite, used magnetite and kaolinite. The ATR-FTIR bands of the used magnetite at 2850–3000 cm^{-1} (2854, 2924, and 2954) and 1458 cm^{-1} were assigned to the aliphatic C–H stretching and C–H bend or scissoring of hydrocarbons, respectively (LiBreTests; Liu et al., 2021b), (c) interfacial tension of kaolinite at different concentrations, and (d) average particle size and zeta potential of the magnetite fluid.

5.3.4 Effect of salinity on oil removal

While the salinity of seawater is approximately 3.5 wt%, this value can vary over a wide range in estuarine areas. Thus, as part of our study, washing performance was also investigated over a range of salinity values. Despite the higher IFT, better washing ability was observed at low salinity (0.1 wt%), as evidenced by the increased oil removal efficiency (Figure 5.6a). This may be due to the fact that Na^+ accelerated the desorption of polar components in the oil, resulting in the sand surface having more water-wetness (Ding and Gao, 2021).

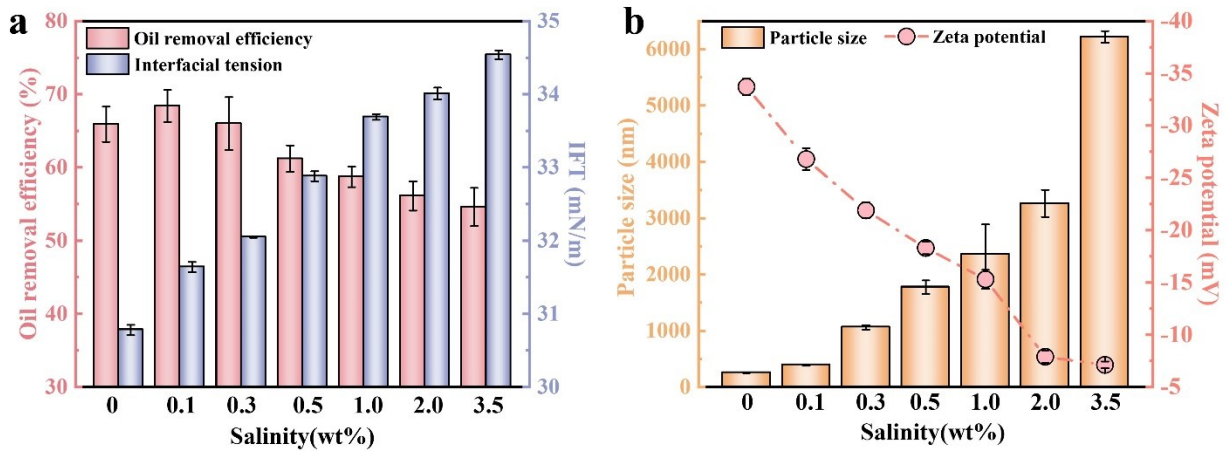

Figure 5.6 Effect of salinity on (a) the washing performance and IFT, and (b) average particle size and zeta potential of the magnetite fluid.

On the other hand, the oil removal efficiency decreased stepwise to 54.6% as a result of doping a high amount of NaCl content (> 0.3 wt%). This may be attributable to the increased IFT at higher salinity levels (Figure 5.6a). A study by Moeini et al. (2014) revealed that, at the water-oil interface, water-salt hydrogen bonds are destroyed at high salinity (> 200,000 ppm), thereby creating a high-energy medium for ion migration. Accordingly, the salt ions on the interface could be transported to the fluid phase, thus leading to a negative surface excess concentration of the salt ions and a higher IFT. The zeta potential and average particle size of the magnetite fluid were further evaluated

to explain the detrimental effect caused by the high salinity. The surface charge decreased remarkably with the addition of NaCl (Figure 5.6b), giving rise to the aggregation of the magnetite nanoparticles. As depicted in Figure 5,5b, the average particle size of the fluid increased sharply from 251 to 6,170 nm at high ionic strengths. The increased size might reduce the number of magnetite nanoparticles at oil-water interfaces and thus decrease washing performance.

5.3.5 Effect of magnetic field strength on oil separation

Although the oil pollutants are effectively released from the sand surface, the remaining washing effluent containing high concentrations of hydrocarbon and magnetite can cause environmental problems if discharged directly. As such, further treatment of the washing effluent after washing should be carried out to minimize the risk of secondary pollution. Owing to the adsorption of oil on the magnetite, a magnetic field can be applied to potentially collect both magnetite and oil droplets. The oil separation efficiency under different magnetization strengths was thus explored. As plotted in Figure 5.7a, due to the weak magnetic strength, the oil harvesting ability of the magnetite diminished at long distances (Figure 5.7b), thereby resulting in high residual oil content in the washing effluent. In addition, the experimental findings suggested that prolonging the magnetic response time promoted the oil capture from the effluent; this was due to the fact more magnetite nanoparticles can be magnetically recovered over an extended magnetic suction period.

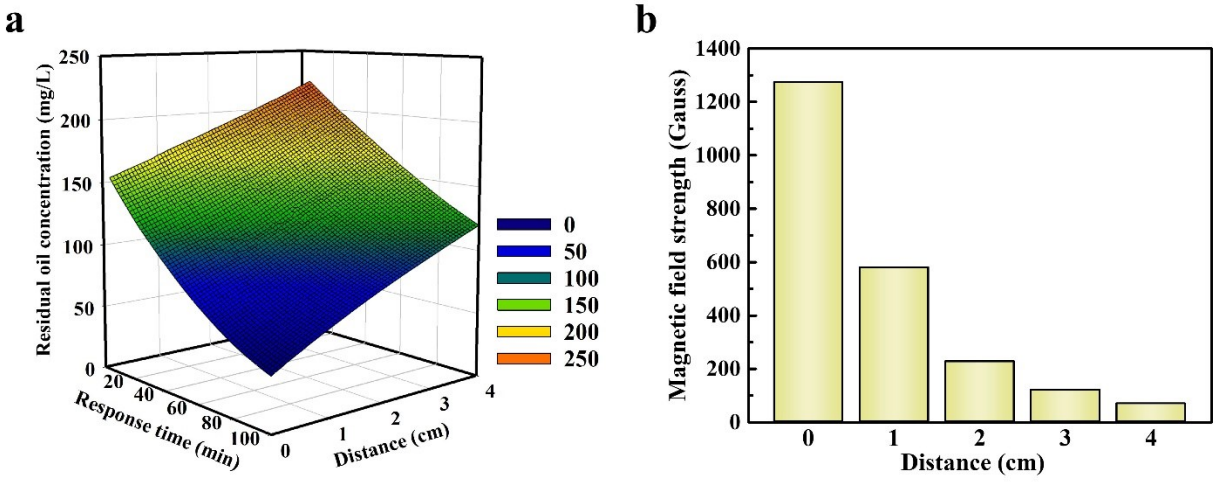

Figure 5.7 (a) Residual oil concentrations in the washing effluent under different conditions, and (b) magnetic field strength at different distances.

5.3.6 Thermodynamic modeling

Fluid miscibility is a critical state in the homogenization of two liquids and can affect the interface mass transfer of two liquids (Babamiri et al., 2021; Zhang et al., 2018b). As a result, the investigation of oil-fluid miscibility in terms of thermodynamics can help reveal the mechanism of oil removal. Herein, the thermodynamic theory was employed to evaluate the oil-fluid miscibility by adding the water-dispersible magnetite nanoparticles under various concentrations and temperatures. As calculated in Figure 5.8a, the free energy for mixing the liquid phase and oil decreased sharply by adding the magnetite up to a certain value (which was around 0.2 g/L in this study), which proved the enhanced miscibility of the oil-fluid system. After that, further addition of magnetite exerted slightly adverse impacts on the miscibility. It can be concluded that the concentration of the magnetite fluid within a certain range promoted the washing performance. Moreover, the temperature can affect the miscibility of the oil-fluid system, but not so strongly as the concentration. The high temperature was beneficial to the oil-fluid miscibility by reducing the

free energy. The modeling observations were in accordance with the experimental findings (Figure 5.8b) and theoretically elucidated the effect of fluid concentration and washing temperature on oil removal.

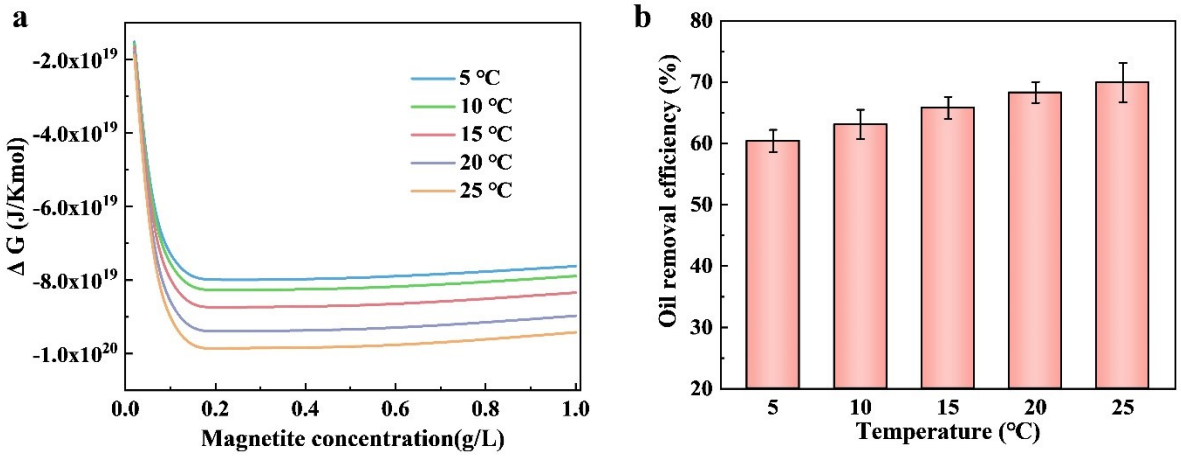

Figure 5.8 (a) Free energy of mixing magnetite fluid with oil at different concentrations and temperatures and (b) effect of temperature on oil removal.

5.3.7 Mechanisms underlying surface washing with magnetite nanoparticles

As discussed above, the magnetite fluid exhibited varying properties (i.e., IFT, average particle size, and surface charge) under different experimental conditions. Based on these observations, four mechanisms were proposed to likely affect surface washing performance.

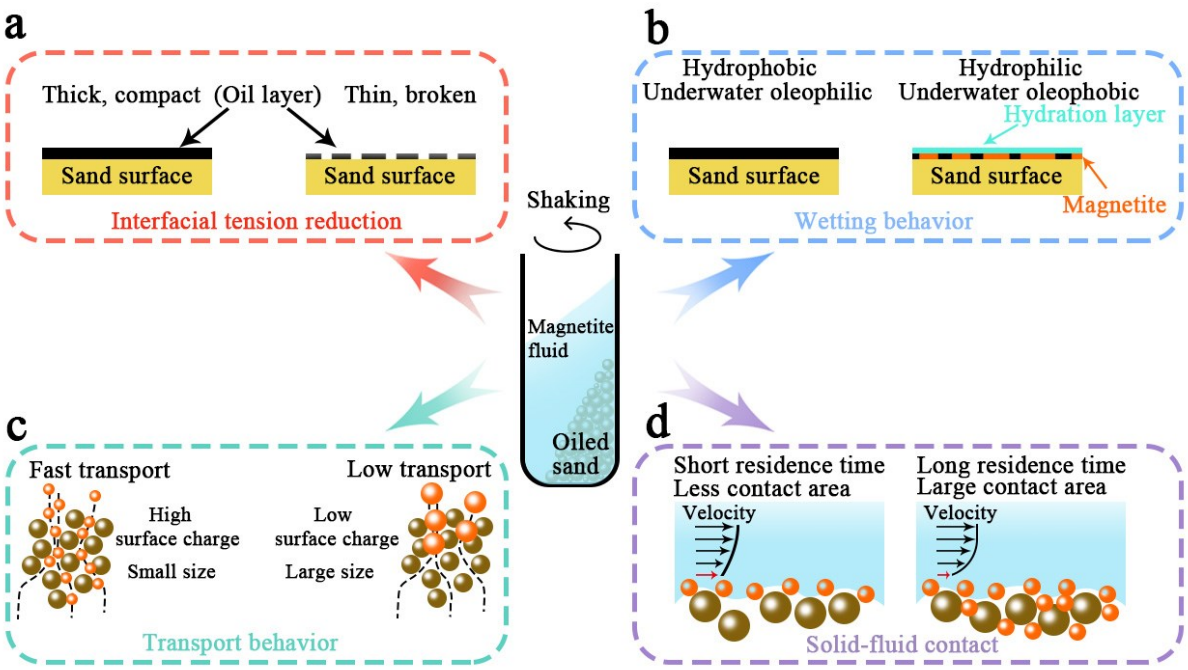

Figure 5.9 Graphical illustration of proposed mechanisms of (a) IFT reduction, (b) wetting behavior, (c) transport behavior, and (d) solid-fluid contact.

(1) IFT reduction

The first mechanism is related to the IFT variation, which plays a crucial role in oil motion behavior at the oil-fluid interface (Figure 5.9a). Molecular simulations from our previous research (Yue et al., 2022e) revealed that, at a low IFT interface, oil layers were prone to be broken down and oil droplets diffused rapidly to areas far from the sand surface. A simulation study by Liang et al. (2019) indicated that the interaction energy between oil and silica and the coherent energy of oil droplets can be impaired as a result of the addition of surface-active materials, which facilitated the oil detachment. The thermodynamic analysis, meanwhile, demonstrated that the free energy for oil-water mixing was less in a low-IFT system. Hence, the addition of kaolinite and NaCl inhibited the oil removal by augmenting the fluid IFT.

(2) Wetting behavior alternation

While the first mechanism has to do with rapid diffusion at the oil-water interface, the second mechanism concerns how the wetting property affects the oil-fouling behavior on the sand surface (Figure. 5.9b). Wettability plays a key role in oil recovery (Ding and Gao, 2021). Wettable materials with opposite attraction to water and oil are the ideal candidates for selective oil removal (Yue et al., 2022g). In this regard, to obtain information on the sand surface wetting properties that directly correlate to oil fouling behavior, CAs, and underwater CAs were measured. As depicted in Figure 5.10a, the clean sand was found to have a superhydrophilic surface on which no stable WCA was observed. In comparison, the oiled sand showed a hydrophobic and underwater oleophilic surface with a high WCA of 124.6° ± 2.0° and a low underwater OCA of 55.0° ± 2.5°, respectively (Figure 5.10b, d). It has been noted that surfaces of this nature have a firm affinity force to hydrophobic materials owing to the strong hydrophobic-hydrophobic interaction (Wang and Lin, 2017). Notably, the washed sand had a hydrophilic (83.3° ± 2.0°) and underwater oleophobic (118.6° ± 3.0°) surface after surface washing (Figure 5.10c, e). It should be noted that wetting a water-loving surface underwater for an oil droplet requires the destruction of a hydration layer on the sand surface, which is energetically infeasible because of the relatively high hydrogen bonding energy. The studies by Divandari et al. (2019) and Izadi et al. (2019) proved that wettability alteration caused by magnetite adsorption could result in enhanced oil recovery.

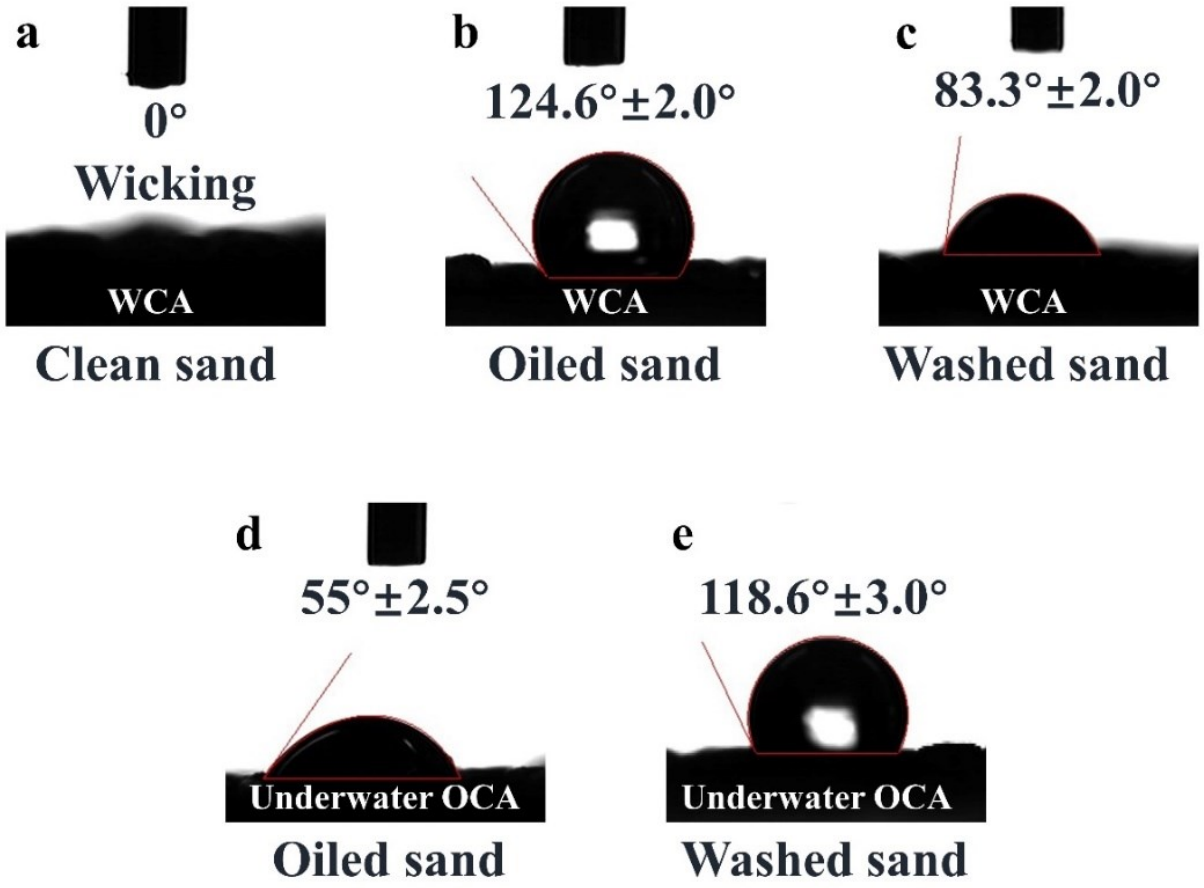

Figure 5.10 WCA of (a) clean sand, (b) oiled sand, and (c) washed sand. Underwater OCA of (d) oiled sand and (e) washed sand. Wicking means that the sand surface was wetted by a testing liquid immediately, and no stable CA images could be captured (Huang et al., 2017).

To further explore the mechanism of wetting alternation, the surface morphologies of different sands were investigated in detail. The clean sand was found to have a smooth and clean surface containing carbon elements (21.81% of atomic weight) and trace amounts of iron elements (0.19% of atomic weight, Figure 5.11a–c). However, the oiled sand was found to have a rough surface after oil fouling, with many oil droplets adhering to its surface (Figure 5.11d). The elemental mapping demonstrated that the carbon content had increased markedly to 85.98% of atomic weight (Figure

5.11e), suggesting the presence of hydrocarbons, but with negligible iron content (Figure 5.11f). The oil covering improved hydrophobicity and underwater oleophilicity. The rough sand surface led to hydrophobicity as well, because the increased area between the liquid and solid gave rise to high interfacial energy, which, in turn, increased the CA (Nosonovsky and Bhushan, 2006). Almost no oil droplets were observed on the washed sand surface (Figure 5.11g). Significantly, the SEM and elemental line scan images (Figure 5.11h, i) show that magnetite nanoparticles had been adsorbed on the washed sand surface. Moreover, the Fe–O band (570 cm^{-1}) was detected on the spectrum of the washed sand (Figure 5.12a). The dynamic WCA results (Figure 5.12d) confirmed the superhydrophilic property of the magnetite nanoparticles, with WCA decreasing rapidly to 0° within one second. In other words, the formation of magnetite layers converted the sand surface from oil-loving to oil-hating, and this prevented the oil droplets from attaching to the sand surface. In addition, the peak intensity of hydrocarbon weakened considerably (Figure 5.12b, c), signifying the removal of oil from the sand surface.

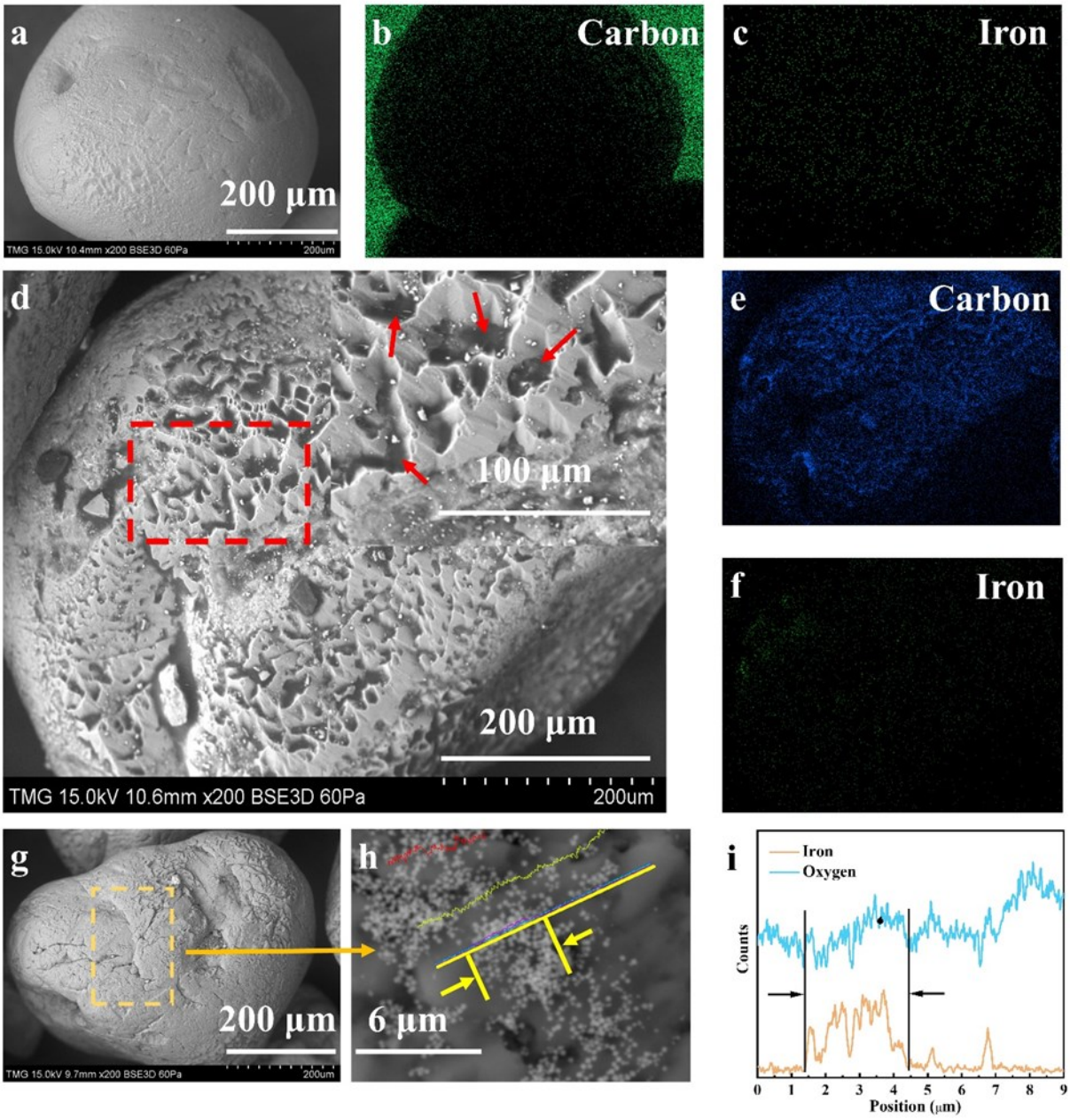

Figure 5.11 SEM images and elemental mappings of (a–c) clean sand, (d–f) oiled sand, and (g–i) washed sand.

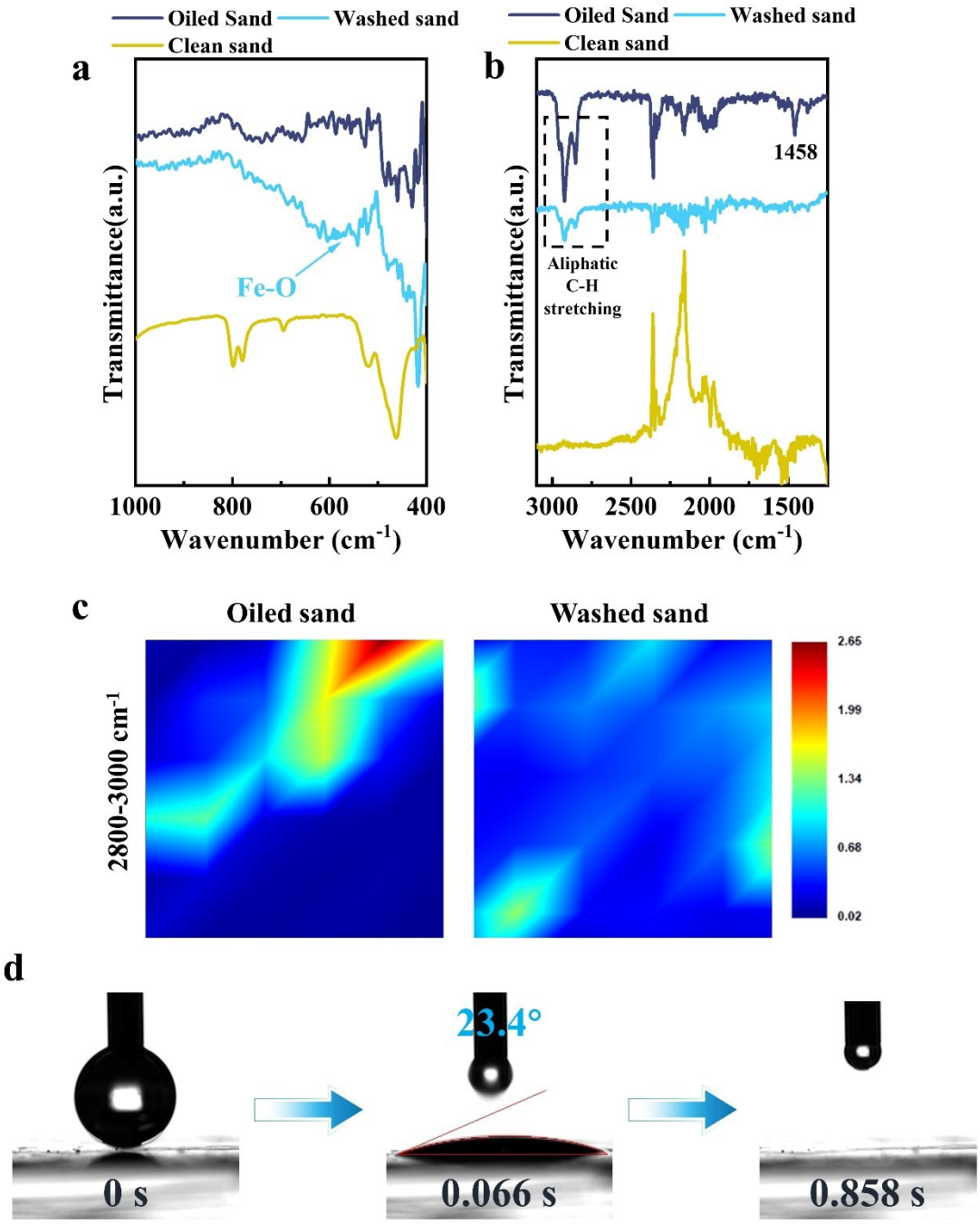

Figure 5.12 (a, b) ATR-FTIR spectra, (c) FTIR mapping of different sands, and (d) dynamic WCA of magnetite nanoparticles.

The elemental distribution on sands was characterized by XRF as well. The energy peak at about 6400 eV (Figure 5.13a) corresponded to the characteristic peak of Fe *Kα* (Chen et al., 2022a). Compared to the clean and oiled sands, the Fe X-ray emission intensity of the washed sand was found to be considerably higher. Moreover, as revealed by the Fe distributions on sands (Figure 5.13b–d), much more Fe was observed on the washed sand surface, indicating the presence of magnetite nanoparticles.

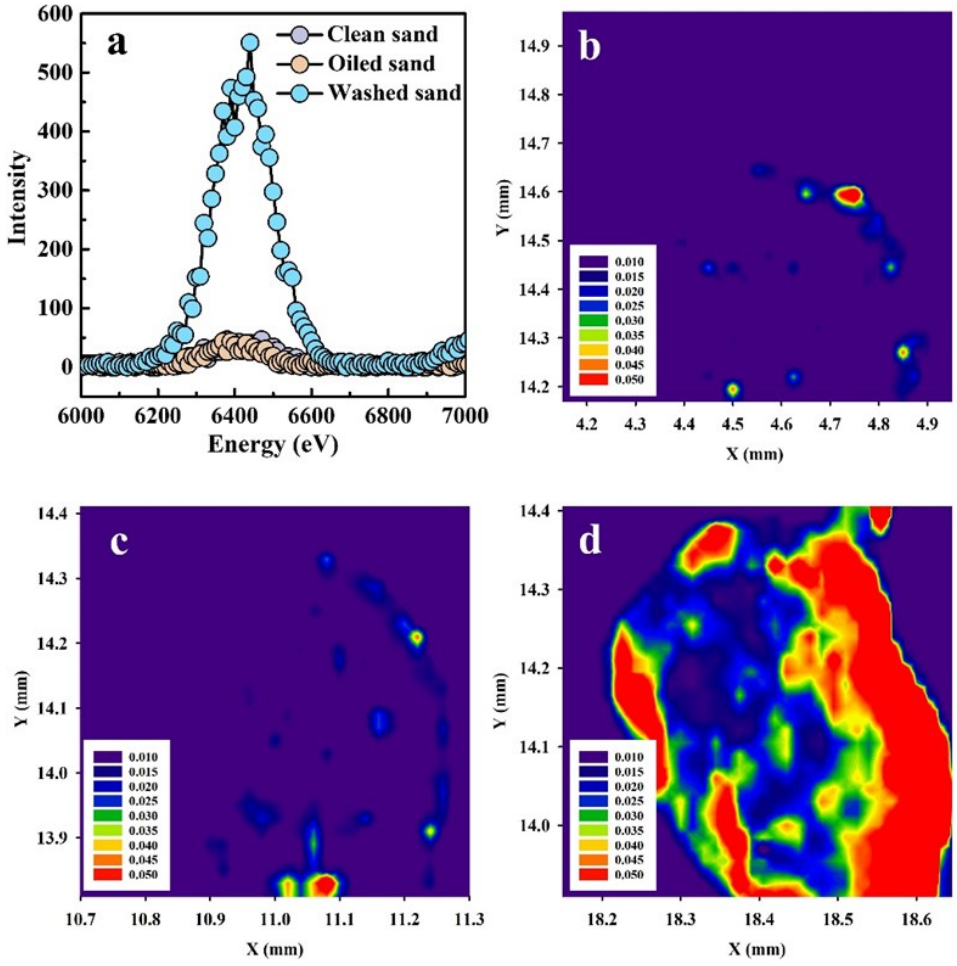

Figure 5.13 XRF spectra (a) and XRF mappings of Fe on (b) clean sand, (c) oiled sand, and (d) washed sand.

(3) Transport behavior

During the washing process, the sand tended to pile up against the vial wall. The upper layer of sand was observed to be more susceptible to the flush from the magnetite fluid than the bottom layer. Therefore, cleaning the bottom layer of sand is likely to be a key factor in improving the overall washing performance. With this practice in place, transport of the magnetite from top to bottom may affect the washing performance (Figure 5.9c). Another consideration is that nanosized particles will more easily pass through porous media than those of micro or macro size (Izadi et al., 2019). In addition, the transport of particles in a porous sand medium may be affected by the interaction between the two (i.e., the particles and the porous sand medium). To be specific, the significantly reduced surface charge diminished the repulsion between the fluid and the sand, thereby promoting the adsorption of the magnetite on the sand in the upper layer, and implying that less magnetite will reach the sand in the bottom layer. A recent work by Tong et al. (2020) has suggested that, compared to the control experiments, fewer plastic particles of large size and low surface charge can pass through a quartz column because of the enhanced adsorption between the particles and the quartz sand at high ionic strength. With increasing kaolinite and ionic strength in the fluid, the increased particle size and decreased surface charge of the magnetite nanoparticles impeded their effective transport to the lower layers of the oiled sand, thereby inhibiting the release of oil from the surface of the sands at lower layers.

(4) Solid-fluid contact

It is widely acknowledged that an air layer is present at an oleophilic surface-water interface (Chao et al., 2020a; Luo et al., 2010). The existence of such a surface-bounded air layer on the hydrophobic oiled sand surface was evidenced by the relatively reflective appearance of the submerged oiled sand (Figure 5.14), attributable to the different refractive indices between water

and air (Kavalenka et al., 2015; Nguyen et al., 2012). Based on the presence of the air layer, a fourth mechanism–i.e., solid-fluid contact–was identified (Figure 5.9d).

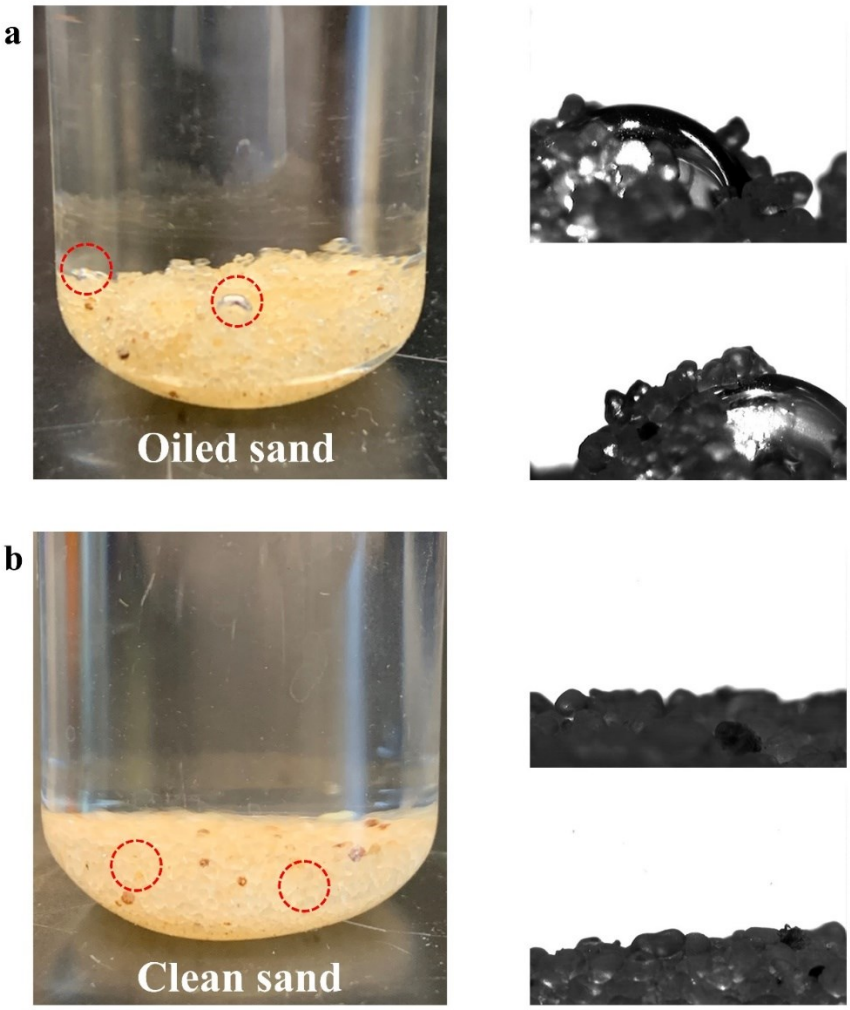

Figure 5.14 Photographic images of submerged oiled sand (a) and clean sand (b).

It should be noted that, at the initial surface washing stage, the hydrophobicity of the oiled sand surface can reduce the contact area at the fluid-oil interface. The air layer between the hydrophobic sand surface and the magnetite fluid adjacent to it is effective in decreasing the drag to flow, owing to the slip boundary effect (McHale et al., 2010), and this shortened the residence time of the magnetite on the sand surface. This aspect can reduce the overall adhesive interaction between the

magnetite nanoparticles and the oiled sand. In addition, the local flow velocity is almost zero at a solid-water interface in nonslip boundary theory, while the flow velocity is considered to be positive at a slip boundary (Kavalenka et al., 2015). The higher flow rate on a non-permeable and hydrophobic surface led to significantly reduced residence time for the interaction between particles and surface. For a permeable porous structure, the impact of the local residence time was found to be even more significant. As the washing process proceeded, the air layer would be damaged or even disappear when the sand surface became hydrophilic. The strong affinity at the hydrophilic sand-fluid interface enhanced the contact area and prolonged the residence time caused by the intrusion of the washing fluid into the porous structure of the oiled sands, thereby strengthening the interaction between the magnetite and the sand surface. Based on this theory, Su et al. (2019) also proposed the solid-water contact mechanism to explain the membrane fouling behavior.

5.3.8 Reusability, material cost analysis, and waste calcination

Besides the good washing capacity, it is also expected the surface washing fluid can be used repeatedly. The magnetite nanoparticles were separated and re-dispersed directly in fresh UP water after each cycle without removing the containing oils. In the present study, the magnetite fluid maintained good performance after 5 repetitions. The magnetic separation ability of the magnetite for oil droplets weakened gradually with the repeated cycles (Figure 5.15a), due to the reduced adsorption sites on the magnetite nanoparticles. It could also be attributed to the reduced magnetite content caused by either the adsorption on the sand surface or the formation of oil-particle aggregates.

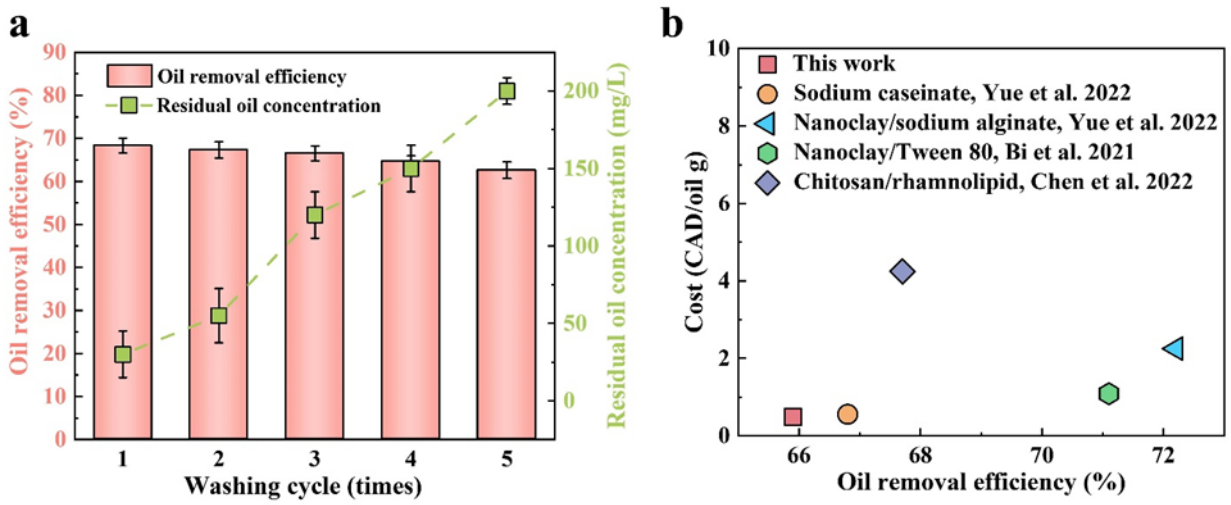

Figure 5.15 (a) reusability of the magnetite fluid and residual oil concentration, and (b) economic analysis of the magnetite fluid.

Material costs are not a negligible factor when it comes to assessing the practicability of a given washing fluid. The chemical costs of surface washing were compared, as shown in Figure 5.15b. The prices of the chemicals used in those studies are given in Table 5.1. It can be seen that the chemical cost of the magnetite fluid per gram of oil removed was the lowest among the surface washing fluids being compared. However, it should be noted this evaluation example could be affected by agent costs in different suppliers and countries. Moreover, the material cost is not the only consideration when dealing with an oil spill. Biotoxicity, effectiveness, and washing performance are also critical.

Table 5.1 Price of chemicals.

Chemicals	Price (CAD/g)
$FeCl_3 \cdot 6H_2O$	0.888

Sodium acetate anhydrous	0.185
Sodium citrate	0.093
Ethylene glycol	0.056
Sodium caseinate	0.1268
Nanoclay	0.194
Sodium alginate (SA)	0.193
Tween 80	0.128
Chitosan	1.168
Rhamnolipid	3.64

The chemical prices (Canadian dollars, CAD) were obtained from Sigma Aldrich (Oakville, Canada).

Despite the effective oil removal ability and good reusability of the magnetite, the post-treatment of the oil on the magnetite is a matter of concern. In this regard, controlled burning has been used in oil spill response (Cai et al., 2016b; Merlin et al., 2021; Wang et al., 2022d). In the present study, the used magnetite nanoparticles underwent calcination to remove the oil from their surface. As observed in Figure 5.16a, the unique ATR-FTIR bands of the oil and carboxyl groups disappeared after thermal treatment at 500 ℃, indicating the complete elimination of adsorbed oil pollutants and carboxyl groups. The weight-loss behavior of the used magnetite, meanwhile, was explored using TGA measurements (Figure 5.16b). Both fresh and used magnetites exhibited the same weight-loss curves at temperatures below 200 ℃, owing to the water evaporation. However, a prominent difference in TGA curves was observed when the temperature exceeded 200 ℃. For the fresh magnetite, the weight loss at such high temperatures was attributable to the removal of carboxyl groups whereas, in the case of the used magnetite, the weight loss at temperatures higher

than 200 ℃ was attributable to the elimination of both carboxyl groups and adsorbed oil. The TGA results implied that the calcination temperature of the oiled magnetite should be over 200 ℃ to ensure effective oil removal.

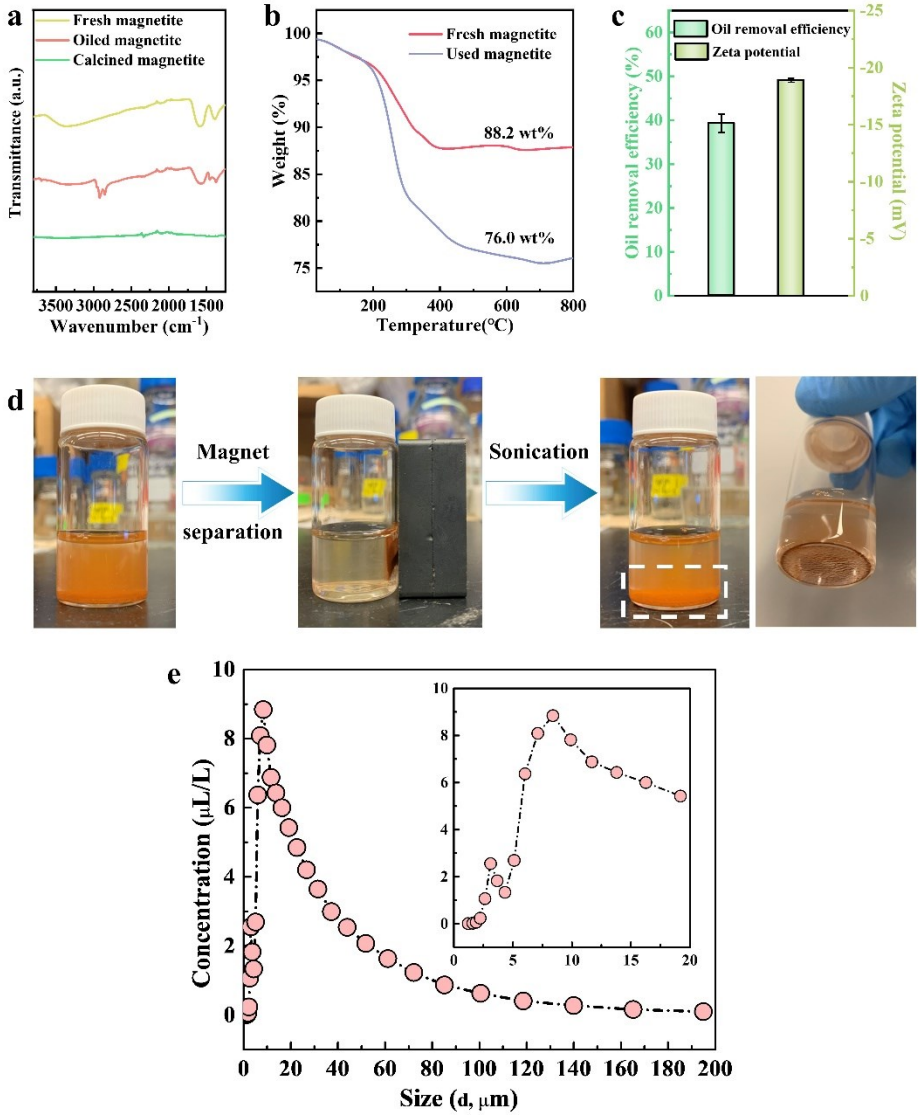

Figure 5.16 (a) ATR-FTIR spectra of different magnetite, (b) TGA curves of the fresh and used magnetites, (c) oil removal efficiency and zeta potential of the magnetite fluid after calcination, (d) photographs of the magnetite dispersion in UP water after calcination, and (e) particle size distribution of magnetite after calcination.

Because of the lack of hydrophilic carboxyl groups, the magnetite after calcination could not form a homogeneous and stable dispersion in UP water even after sonication (Figure 5.16d). After magnetic separation, the increased average particle size of the magnetite (Figure 5.16e) caused by the reduced surface charge (Figure 5.16c) gave rise to rapid precipitation after sonication. Furthermore, the poor stability of the fluid was also detrimental to its washing performance (Figure 13c), with only cleaning 39.8% of the oil from the sand surface. These findings demonstrate that, although calcination is a promising method for post-treatment of oil, this failed to maintain the good performance of the magnetite fluid. Such residues after calcination can be disposed of in the landfill.

5.4 Summary

In the present study, an innovative, low-toxic, recyclable, and magnetic-mediated surface washing fluid based on water-dispersible magnetite nanoparticles was investigated for use on sand beaches. The characterization results showed that the carboxyl-functionalized magnetite nanoparticles had a spherical morphology with a diameter of around 250 nm. Because of the superhydrophilicity, the magnetite exhibited superior water dispersibility even after gentle shaking. Apart from the effective surface washing, the magnetite nanoparticles showed a good performance of oil recovery from the washing effluent. Results suggested that IFT reduction, wetting behavior, transport behavior, and solid-fluid contact mechanisms might jointly affect the oil removal from the sand surface. Notably, thermodynamic modeling proved that the magnetite enhanced the oil-fluid miscibility and the results were in alignment with the experimental findings. The magnetic fluid was found to have a relatively low material cost and good reusability but with diminished oil separation ability after multiple runs. Moreover, the experimentation with calcination at high temperatures demonstrated

that the adsorbed oil can be completely removed, but that the loss of the carboxyl group after calcination deteriorated the washing performance of the magnetite fluid. In terms of operational limitations, high clay concentrations (kaolinite) and elevated saline conditions (above 0.3 wt%) inhibited the washing performance of the magnetic fluid. Despite these potential limitations, based on our experimental results, we believe that the proposed magnetite fluid, with a low cost, good reusability and stability, and responsiveness, warrants further investigation as a basis for the cleanup of oil-contaminated sand beaches.

CHAPTER 6 REMOVAL OF PHENANTHRENE FROM CONTAMINATED PEAT MOSS USING A PH-RESPONSIVE PHOSPHOPROTEIN WASHING FLUID ‡

6.1 Background

Oil pollution is a major environmental concern in the petroleum industry (Cai et al., 2019; Wang et al., 2020c; Yue et al., 2020). On May 29, 2020, such an industrial disaster occurred in Norilsk, Russia, where up to 17,500 tons of diesel oils were spilled into local rivers and land. In such cases, the leakage of oil into the soil causes changes in the soil's physical and chemical properties and affects the composition and structure of soil microbial communities (Yang et al., 2006; Yin et al., 2021a; Yue et al., 2022g), leading to the deterioration of the soil quality. Meanwhile, the migration and diffusion of hydrocarbon pollutants into underground aquifers pose a serious threat to the groundwater environment and human health. Therefore, the remediation of petroleum-impacted soil is of great importance.

Peat moss is a complex material characterized by its vegetative composition and is globally important in maintaining various ecosystem functions, such as hydrology, climatology, and biodiversity (CSPMA, 2022). North America is home to 32% of the Earth's peatland, most of which is located in Canada (Peatlands, 2022). Oil pollution can occur during oil extraction and transportation. The Northwest Territories (NWT) of Canada contains significant untapped oil and gas reserves, and it is estimated that the region may hold 37% of Canada's marketable light crude oil resources (Subramanian et al., 2017). In fact, the NWT has over 870 km of oil transportation

‡ This work has been published as R. Yue, C. An, Z. Ye, X Li, Q. Li; P. Zhang, Z. Qu; S. Wan. A pH-responsive phosphoprotein washing fluid for the removal of phenanthrene from contaminated peat moss in the cold region. Chemosphere, 2023, 313: 137389.

pipelines. Due to the expansion or thawing of cryosolic soils and their variable nature, these pipelines are susceptible to damage from excessive deformation, which could result in oil pollution. Because of the fragility of ecosystems in cold regions, oil contamination can cause more serious damage to such land ecosystems, given their low resilience stability. To date, peat moss decontamination by environmentally benign materials after oil spills has not been well studied. Therefore, it is of urgency to seek washing fluids for the cleanup of hydrocarbon-contaminated peat moss.

Polycyclic aromatic hydrocarbons (PAHs) are a class of components of oil (Zhao et al., 2015; Zhao et al., 2019a). The presence of PAHs may result in the contamination of soil and groundwater, which threatens human and environmental health (Yu et al., 2011; Yue et al., 2022a; Yue et al., 2022c). Surfactant-based surface washing has been identified as a viable strategy for the remediation of PAH-contaminated soil (Befkadu and Quanyuan, 2018; Chen et al., 2021a). For instance, Bai et al. (2019) demonstrated that Tween 80 with a concentration of 15 g/L and a liquid-to-soil ratio of 10:1 was effective for soil decontamination of phenanthrene (PHE). Another study by Qiu et al. (2019) found that three PAHs could be partially removed with 20 g/L of sodium dodecyl sulfate. However, many ionic and non-ionic surfactants are toxic to animals and plants, thereby bringing potential environmental risks (Mulligan et al., 2001). Recently, biosurfactants have received considerable attention in research on PAH decontamination due to their advantages of biodegradability and lower toxicity (Markande et al., 2021). Hirata et al. (2009) reported that 60% of sophorolipids were degraded within 28 days, while some anionic and non-ionic surfactants displayed little biodegradability. Although biosurfactants have a limited environmental impact, the high production cost and difficulties of in situ production are major hurdles to their large-scale use. Notably, some techniques (i.e., air stripping, membrane processes, and sorption) can be applied to

further treat the effluent from a washing process (Trellu et al., 2021; Yue and Rahaman, 2021a), but the complicated operations and high costs are not sustainable. Therefore, seeking an alternative with low toxicity, low cost, and an easy separation approach for treating washing effluent is also required.

Sodium caseinate (NaCas) is the sodium salt of casein, the main protein in milk, and it contains several essential nutrients required by the human body. In addition, NaCas has both hydrophilic and oleophilic groups, which enables it to remove hydrophobic PAHs. It is worth noting that NaCas has varied isoelectric points in different systems (Ma et al., 2009; Xi et al., 2020; Yue et al., 2022e), at which NaCas can precipitate as insoluble material. The feature of pH responsiveness made the pretreatment of washing wastewater more efficient and applicable, compared with the methods without effluent separation or those requiring the assistance of CO_2 or N_2 (Bonal et al., 2018; Kim et al., 2019). In light of these features, this study aimed to investigate the performance of NaCas washing fluid for the remediation of phenanthrene (PHE)-contaminated peat moss. The effects of different environmental factors on NaCas's effectiveness were comprehensively investigated. Factorial analysis was employed to identify the significance of individual factors and their interactions, and the pH responsiveness of the effluent was also explored. Finally, toxicity modeling was applied to analyze the effect of NaCas on the biotoxicity of PHE.

6.2 Materials and methods

6.2.1 Materials

PHE (> 98%), NaCas, NaCl, HA, sulfuric acid (H_2SO_4) methanol [high-performance liquid chromatography (HPLC) grade, > 99.9%], and acetonitrile (HPLC grade, > 99.9%) were sourced from Sigma Aldrich (Oakville, Canada). The peat moss was purchased from VWR (Canada).

6.2.2 Preparation of phenanthrene-contaminated peat moss

The peat moss was completely dried at room temperature and then passed through a 0.25 mm sieve to remove any large particles. The peat moss was then spiked with PHE dissolved in methanol and subsequently agitated for 1 h to achieve a uniform distribution of PHE. The methanol was evaporated by putting the mixture in a fume hood at room temperature. The contaminated peat moss, with a final concentration of 100 mg/kg, was obtained after evaporating the solvent.

6.2.3 Peat moss washing and factorial design

The peat moss samples (0.1 g) were vigorously shaken in sealed vials (20 mL) containing 15 mL of NaCas solution for 24 h at different conditions (temperature, NaCas concentration, salinity, and humic acid). Subsequently, the liquid and solid phases were separated by centrifugation at 4000 rpm for 20 min at room temperature (21 ± 1 °C). Preliminary experiments found that the biodegradation contribution to PHE removal was negligible. After completely decanting the upper liquid, the residual PHE adsorbed on the peat moss was ultrasonically extracted with methanol (15 mL) for 10 min (Joseph-Ezra et al., 2014). This process was repeated three times; the fourth extraction could barely desorb PHE from the peat moss. A 2^4 factorial design and one-way analysis

of variance (ANOVA) evaluating the effect of different environmental factors on PHE removal were applied by using Minitab (USA).

6.2.4 Analytical and characterization methods

The PHE concentration in the extractant was detected using HPLC (1260 infinity II, Agilent, USA) equipped with a 120 EC-C18 (column size: 4.6 × 100 mm, particle size: 2.7 μm, Agilent, USA) and a diode array detector (DAD). The mobile phase consisted of ultrapure water and acetonitrile (25:75, v/v), and its flow rate was 0.6 mL/min. The injection volume and column temperature were 20 μL and 30 ℃, respectively. The PHE removal efficiency (R) was calculated using $R = 1 - (PHE_R/PHE_T) \times 100\%$, where PHE_R and PHE_T were the residual PHE content and total PHE content on the peat moss, respectively. Surface tension (SFT) was measured using a force tensiometer (KRUSS K100, Germany). Attenuated total reflectance fourier transform infrared (ATR-FTIR) measurements were conducted using an INVENIO S FTIR spectrometer (Bruker, USA). Chemical oxygen demand (COD) was tested using a COD reactor (DRB200, HACH, Canada) and a portable spectrophotometer (DR2800, HACH, Canada). Turbidity was measured on a turbidity meter (AQ3010, Thermo Scientific, Canada). The total organic carbon (TOC) results were recorded using a TOC analyzer (TOC-L, Shimadzu, Japan). The experimental design and result analysis were performed using Minitab (Minitab, LLC, USA), and the detailed information is shown in Tables 6.1 and 6.2.

Table 6.1 High and low levels for the 2^4 factorial design.

Factor	Temperature (°C)	Humic acid (mg/L)	Salinity (wt%)	NaCas concentration (g/L)
High level (+1)	20	40	3.5	1.0
Low level (-1)	5	0	0	0.2

Table 6.2 Coded levels and corresponding values for factorial design matrix.

Number	Coded levels				A	B	C	D
	A	B	C	D	Temperature (°C)	Humic acid (mg/L)	Salinity (wt%)	NaCas concentration (g/L)
1	-1	-1	-1	-1	5	0	0	0.2
2	-1	-1	-1	1	5	0	0	1.0
3	-1	-1	1	-1	5	0	3.5	0.2
4	-1	-1	1	1	5	0	3.5	1.0
5	-1	1	-1	-1	5	40	0	0.2
6	-1	1	-1	1	5	40	0	1.0
7	-1	1	1	-1	5	40	3.5	0.2
8	-1	1	1	1	5	40	3.5	1.0
9	1	-1	-1	-1	20	0	0	0.2
10	1	-1	-1	1	20	0	0	1.0
11	1	-1	1	-1	20	0	3.5	0.2
12	1	-1	1	1	20	0	3.5	1.0

13	1	1	-1	-1	20	40	0	0.2
14	1	1	-1	1	20	40	0	1.0
15	1	1	1	-1	20	40	3.5	0.2
16	1	1	1	1	20	40	3.5	1.0

6.2.5 Separation and recovery of washing effluents

Oil and NaCas in the washing effluents can be separated by using the pH-responsive method. After washing, the pH of the washing effluent was adjusted to its isoelectric point (pH was around 4.2) by adding H_2SO_4 (0.1 M), after which the NaCas formed precipitates and was recovered by removing the supernatant.

6.2.6 Toxicity modeling analysis

The homology modeling algorithm is an accepted method for predicting the synthesis of receptor proteins based on the structure of known similar proteins when there is no existing 3D structure of the receptor protein (Gu et al., 2020b). The homology modeling of NaCas can be found in previous studies (Cao et al., 2020a; Sun et al., 2021). The amino acid residue sequence of superoxide dismutase (SOD) was first obtained at the National Center for Biotechnology Information (NCBI) in the United States. Second, the amino acid sequences of the protein-binding units were submitted separately to the SWISS-MODEL server in the Automated Protein Modeling Server provided by the Glaxo Smith Kline Center in Geneva, Switzerland, to obtain new protein structures (Li et al., 2022). As the protein structures of superoxide dismutase from *Neopyropia yezoensis*, *Mytilus edulis*, *Penaeus vannamei*, and *Oncorhynchus mykiss* were missing, homology modeling was used to obtain the corresponding SOD protein structures. The SODs of *Neopyropia yezoensis* (GenBank:

AAZ75664.1), *Mytilus edulis* (GenBank: CAE46443.1), *Penaeus vannamei* (GenBank: AVP74308.1), and *Oncorhynchus mykiss* (GenBank: ACO07816.1) were obtained from NCBI, and the SOD of *Caenorhabditis elegans* (PDB ID: 3KBF) was obtained from the Protein Data Bank (PDB) of Brookhaven National Laboratory. The plausibility of the SOD structures was evaluated using Ramachandran plots in the SWISS-MODEL online evaluation server (Carugo and Djinović-Carugo, 2013).

To simulate the ability of PHE to cause oxidative stress toxicity in marine organisms, dynamic simulations of the complex of PHE and SOD proteins were carried out using the GROMACS 5.1.4 program to characterize the toxic effects of PHE on marine organisms in terms of their binding energy. The SOD proteins from five marine organisms, namely *Neopyropia yezoensis*, *Caenorhabditis elegans*, *Mytilus edulis*, *Penaeus vannamei*, and *Oncorhynchus mykiss*, were placed in a periodic cube with a side length of 20 nm, using a GROMOS 54a7 force field and adding sodium ions as a positive charge to neutralize the system. The binding energy was calculated using the molecular mechanics/Poisson-Boltzmann surface area (MMPBSA) method (Li et al., 2021b; Pu et al., 2022). It was then necessary to sample the equilibrium trajectories of the acceptor protein (SOD) and ligand molecule (PHE) of the SOD–PHE complex and calculate the free energy of the SOD–PHE complex, SOD, and PHE, respectively. MMPBSA involves the calculation of the difference in free energy between two states, and the equation is as follows:

$$G_{bind} = G_{SOD–PHE\ complex} - G_{free\text{-}SOD} - G_{free\text{-}PHE}$$

where G_{bind}, $G_{SOD–PHE\ complex}$, $G_{free\text{-}SOD}$, and $G_{free\text{-}PHE}$ refer to the binding free energy of the system, the SOD–PHE complex, the SOD, and PHE, respectively (Gu et al., 2021).

6.3 Results and discussions

6.3.1 Effect of sodium caseinate concentration on phenanthrene removal

The PHE desorption efficiency was found to be dependent on the NaCas concentration (Figure 6.1a). The rate of PHE removal grew steadily from 27.8 to 30.2 mg/kg when the NaCas concentration increased from 0.2 to 2.0 g/L. The increased PHE removal at relatively low NaCas concentrations (0.2 to 2.0 g/L) could be due to the drop in SFT. Mobilization and solubilization are two main mechanisms for the enhanced removal of hydrophobic organic compounds (HOCs) from a porous medium (Liu et al., 2021a). The mobilization effect is such that the transportation ability of HOCs can be enhanced in a low-SFT system (Nguyen et al., 2008). The hydrophobic ends of surfactants attach to the HOCs due to the strong hydrophobic–hydrophobic interaction, while their hydrophilic ends tend to be exposed to water. As a result, the sorbed HOCs can be surrounded by surfactant monomers. In our study, the low SFT of the NaCas washing fluid was capable of enhancing the mobility of PHE, thus improving the PHE removal efficiency. In the solubilization effect, the low-SFT system increased the water solubility of HOCs. The micelles with a core(hydrophobic)-shell(hydrophilic) structure could create a number of hydrophobic nano-areas in the aqueous phase for the distribution of HOCs. β-casein is an amphiphilic part of NaCas, and the hydrophobic interactions between the β-caseins lead to self-association and the formation of β-casein micelles with hydrophobic cores and hydrophilic shells (Dauphas et al., 2005; O'Connell et al., 2003). The hydrophobic cores were able to compete for the partition of HOCs of the medium (Lowry et al., 2016), which thus promoted PHE transfer into NaCas micelles.

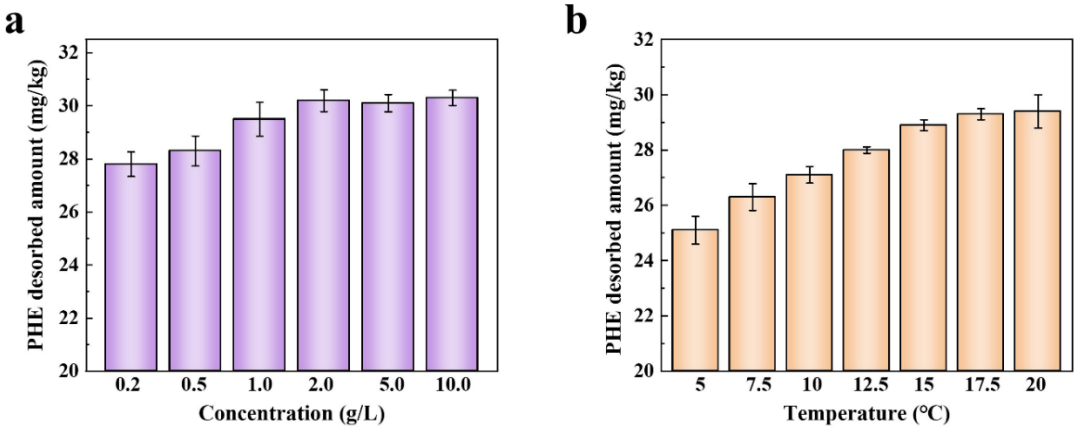

Figure 6.1 Effect of (a) NaCas concentration and (b) temperature on PHE removal.

However, PHE desorption did not experience any remarkable change with a high NaCas content in the range of 2.0 to 10 g/L. On one hand, β-casein is strong amphiphilic, as it has highly hydrophilic and polar N-terminal groups, and highly oleophilic and nonpolar C-terminal groups (Portnaya et al., 2006). Srinivasan (1998) found that the number of amphiphilic β-caseins at the NaCad-liquid interface was reduced at high NaCas concentrations, which thus increased the SFT of the NaCas fluid. On the other hand, excessive NaCas adsorption might improve the hydrophobicity of peat moss and further enhance the adsorption of PHE onto it. The effect of a high NaCas concentration on PHE removal revealed here was in alignment with the findings of a study by Urum and Pekdemir (2004), who reported that some surfactants were less effective at a high concentration (> 0.02 wt%).

6.3.2 Effect of temperature on phenanthrene removal

The average annual temperature of peatland in Canada is approximately in the range of -4 to 20 ℃. Therefore, NaCas's effectiveness in this study was evaluated at low temperatures. The effect of temperature on the washing performance of NaCas is shown in Figure 6.1b. The PHE desorption increased from 25.1 to 29.3 mg/kg with the washing temperature rising from 5 to 15 ℃. The

increase in temperature decreased the SFT of the NaCas washing fluid, which resulted in high PHE miscibility in the washing fluid and thereby accelerated the PHE desorption from the peat moss. Another explanation might be the enhanced molecular diffusion of organic compositions and the weakened van der Waals force between PHE and peat moss at high temperatures (An et al., 2011; Wang et al., 2019b). The Brownian motion of NaCas molecules and the diffusion rate of PHE were enhanced with rising temperatures. As a result, PHE molecules were incapable of forming strong bonds with the peat moss, giving rise to an enhancement in the mass transfer rate from the peat moss to the aqueous phase. Additionally, the temperature–hydrophobicity curve might explain this effect. For instance, it has been reported that the hydrophobicity of β-casein was enhanced when raising the temperature to a suitable range, owing to the increased number of available hydrophobic sites within it (O'Connell et al., 2003).

A further increase in temperature from 15 to 20 ℃ only led to a slight rise in PHE removal. It has been reported elsewhere that the solubility of β-casein in NaCas solution was higher at 2 ℃ than at 20 ℃ (Post et al., 2012). Therefore, the high temperature reduced the accessibility of β-casein for PHE removal. In a related vein, O'Connell et al. (2003) revealed that β-casein became more hydrophilic when the temperature was too high, which was a result of the aggregation of the β-caseins. Moreover, they, in this case, found that the molecular mass of β-casein more than doubled from 15 to 30 ℃. It was revealed in another study that materials with a high molecular structure often changed the micelle shape and size and thus led to the collapse of micelles and the deterioration of detergency (Urum and Pekdemir, 2004). The PHE removal tendency in this study was in line with some previous studies. Specifically, Zhang et al. (2017) investigated the effect of temperature on PHE removal, and the results demonstrated that PHE removal increased marginally when the temperature increased from 10 to 30 ℃. In another study, Bai et al. (2019) used Tween

80 to immobilize PHE from contaminated soil. However, PHE removal efficiency was found to decline when the washing temperature increased from 20 to 40 °C, which was attributable to the low solubility of the non-ionic surfactant.

6.3.3 Effect of salinity on phenanthrene removal

The PHE removal in terms of salinity is shown in Figure 6.2a. The PHE desorption mass increased stepwise to 34.6 mg/kg at low salinity (< 0.3 wt%). The positive effect of the salinity within the low range (< 0.3 wt%) can be attributed to the enhanced desorption of PHE in saline water. Wu and Sun (2010) suggested that a saline environment could significantly weaken the sorption-desorption hysteresis of PHE, thereby resulting in a much higher desorption mass than in freshwater at a given time. In addition, a study by Oh et al. (2013) found that salinity increased the desorption distribution coefficient of PHE and thus increased the PHE desorption mass.

However, the PHE desorption decreased gradually to 20.1 mg/kg with the increase of salinity when it was higher than 0.3 wt%. The high SFT at high salinity (Fig. 2a) was detrimental to the PHE removal. Moreover, when the salinity was more than 0.3 wt%, the average particle size of NaCas increased from 214.3 to 248.0 nm due to the reduced surface charge, demonstrating the aggregation of NaCas molecules (Figure 6.2a). In this case, the formation of aggregation reduced the active adsorption sites of NaCas, which deteriorated the PHE desorption efficiency.

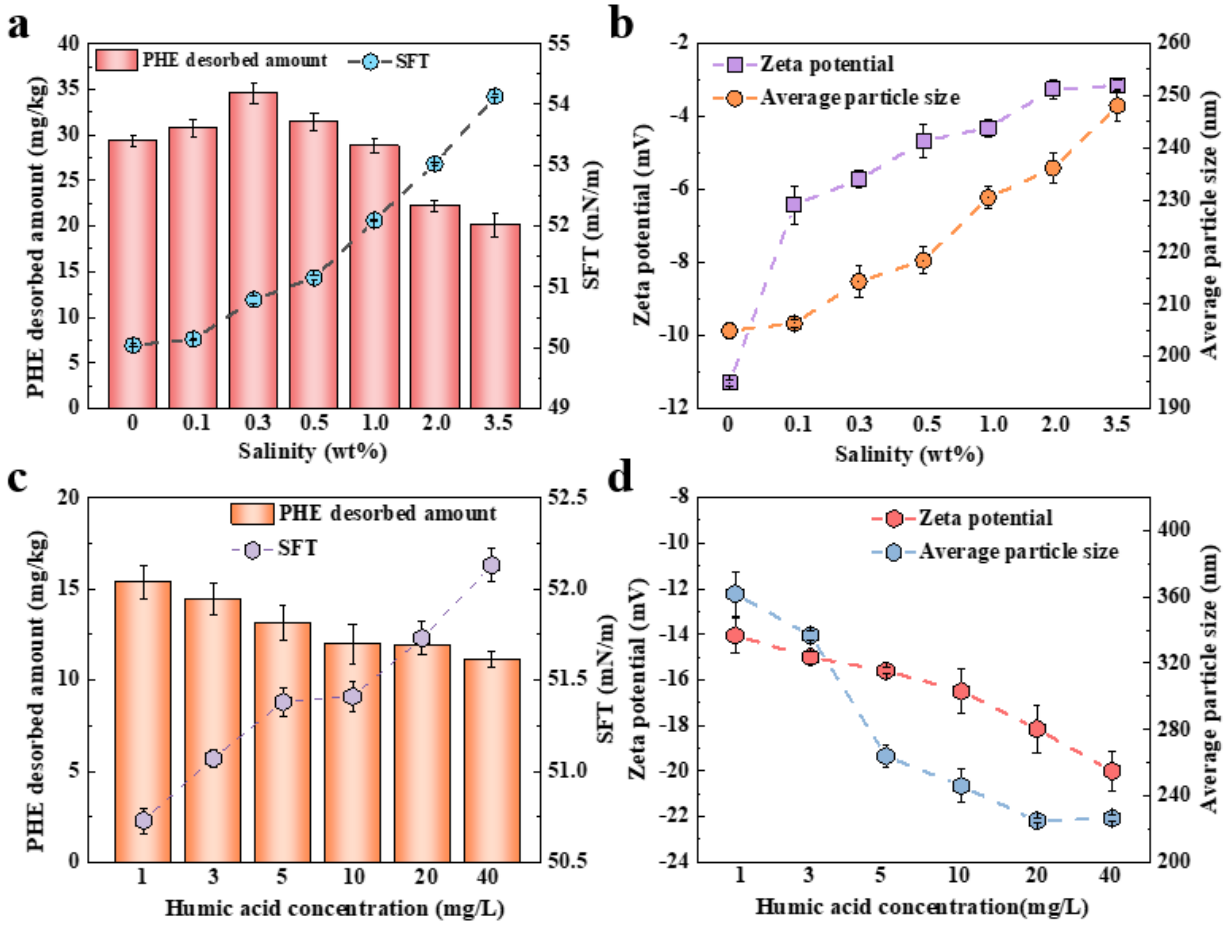

Figure 6.2 Effect of salinity on (a) PHE removal and (b) on average particle size and zeta potential of NaCas washing fluid. Effect of humic acid on (c) PHE removal and (d) on average particle size and zeta potential of NaCas washing fluid

6.3.4 Effect of humic acid on phenanthrene removal

Humic acid is abundant in peat moss (Zaccone et al., 2007), thus it is necessary to unveil the effect of humic acid on PHE removal. Humic acid sodium salt was used to represent the humic acid in seawater. Humic acid with contents of 1 to 40 mg/L was found to be detrimental to peat moss decontamination (Fig. 2b), inhibiting PHE release from 15.3 to 11.1 mg/kg. The addition of humic acid worsened the surface activity of NaCas, thereby leading to restrained PHE removal. Moreover,

the added humic acid was able to be sorbed by the peat moss. The formation of humic acid layers on peat moss can provide stronger bonding to retain PHE and thus facilitate the stabilization of PHE (Zhang et al., 2015). A study by Wen et al. (2007) investigated PHE sorption to humic acid and its fractions extracted from peat soil; the findings suggested that humic acid displayed linear and nonlinear sorption to PHE. Jones and Tiller (1999) also found that PHE was prone to binding to humic acid adsorbed on soil surfaces. Fig. S2b illustrates the variation in zeta potential and average particle size of NaCas under different humic acid contents. In the present study, the surface charge of the fluid increased gradually with humic acid content, which resulted in an enhanced repulsion force between NaCas nanoparticles, thereby giving rise to a decrease in average particle size and an increase in NaCas amount. Although more NaCas nanoparticles might bond to more PHE molecules by providing more adsorption sites, the rise in SFT and the humic acid adsorption inhibited PHE removal.

6.3.5 Factorial analysis of factors influencing phenanthrene removal

Environmental processes are simultaneously affected by various factors at the same time (La and Chai, 2021). Therefore, the interactions of the four factors discussed above in the process of PHE removal were investigated using a 2^4 full factorial design (Fig. 3), in which main effects and two-way interactions were involved. The mean of PHE removal was a function of the following four factors: = 22.66 + 0.1054*Temperature - 0.2508*Humic acid - 1.263*Salinity + 2.59*NaCas concentration - 0.00387*Temperature*Humic acid - 0.0243*Temperature*Salinity + 0.0479*Temperature*NaCas concentration + 0.02006*Humic acid*Salinity - 0.0576*Humic acid*NaCas concentration - 0.211*Salinity*NaCas concentration. The significant main effects

were humic acid, salinity, and NaCas concentration, and significant interactions were humic acid*salinity and temperature*humic acid.

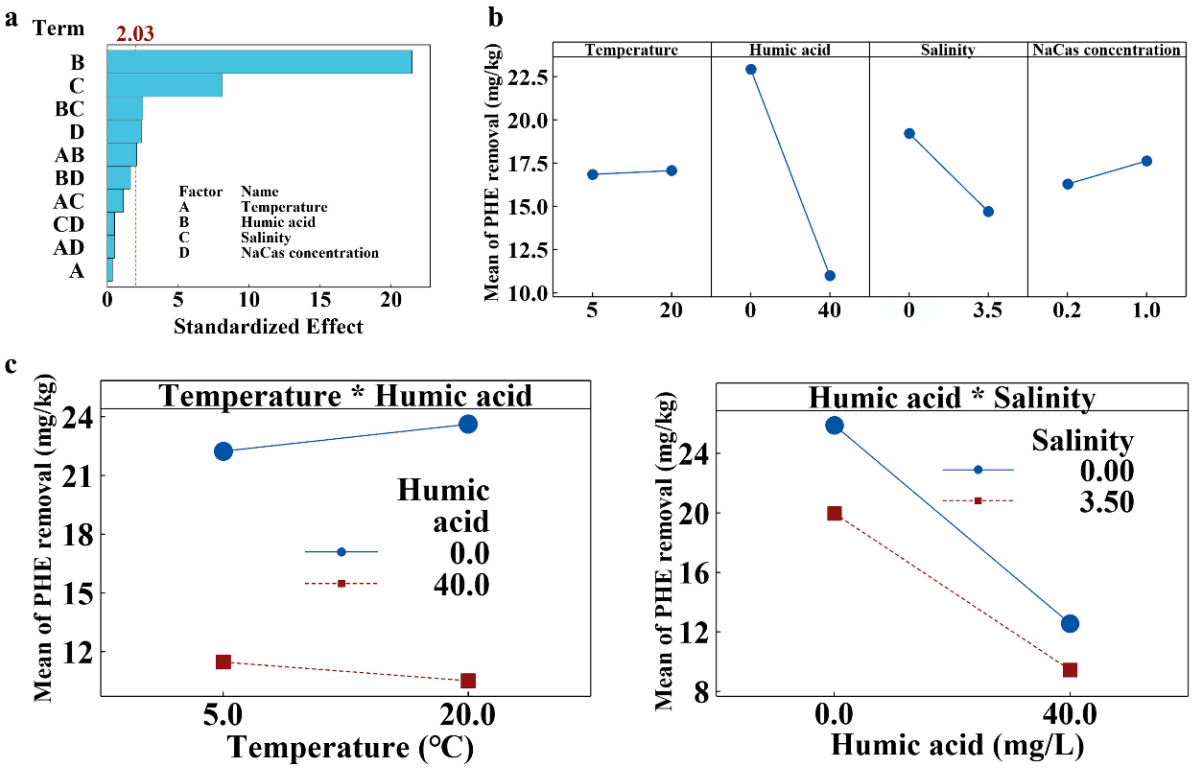

Figure 6.3 Factorial analysis of oil removal efficiency: (a) Pareto chart, (b) main effect plots, and (c) interaction plots.

Humic acid and salinity were found to be the significant factors diminishing PHE desorption. The mean PHE removal decreased from 22.9 to 10.9 mg/kg when the humic acid content increased from 0 to 40 mg/L. The NaCas washing performance was also suppressed with the addition of salinity, removing 14.6 mg/kg of PHE at a salinity of 3.5 wt%. Furthermore, the NaCas washing fluid concentration had a positive effect on peat moss remediation, which increased the mean PHE desorption to 17.6 mg/kg at a NaCas concentration of 1 g/L.

The humic acid*salinity and temperature*humic acid combinations are two significant interactions affecting PHE removal. The effect of temperature on PHE removal displayed an opposite tendency when 40 mg/L of humic acid was added. This might be because a high temperature could facilitate the interaction of humic acid adsorbed on peat moss with PHE. In addition, the negative effect of humic acid on NaCas fluid effectiveness was weakened by the coexistence of salt and humic acid.

6.3.6 Pre-treatment of washing effluent

The washing process gave rise to the production of a highly concentrated washing effluent, containing NaCas, organic matter from the peat moss, and hydrocarbons. This effluent was thus capable of causing secondary pollution if discharged directly. The feature of the pH-dependent solubility of NaCas offered a simple and attractive approach for effluent pretreatment by tuning the effluent acidity. As depicted in Figure 6.4a, the washing effluent was turbid, and there was no precipitation after 12 h. NaCas precipitated quickly when the pH of the effluent was close to the isoelectric point of NaCas. Interestingly, the color of the precipitation in the effluent changed to light brown compared to its counterpart in the pure NaCas solution (Figure 6.4a). This could be attributable to the sorption of the dissolved organic matter (DOM) that was detached from the peat moss by NaCas. The ATR-FTIR spectrum of peat moss is displayed in Figure 6.4b. The bands at 3325, 2917, 1588, and 1032 cm^{-1} were ascribed to aromatic compounds, aliphatic compounds, C=C stretching, and C-O stretching, respectively (Cocozza et al., 2003; Ramachandran et al., 2021). Characteristic bands of NaCas precipitations at 3288, 1631, and 1513 cm^{-1} (Figure 6.4b) represented O–H stretching and amine bonds, respectively (Chang et al., 2017). However, the ATR-FTIR bands of the clean peat moss were not observed in the NaCas spectrum, which may be due to the trace amount of DOM adsorbed on NaCas. Additionally, no band shift was observed in the

ATR-FTIR spectra of NaCas, which demonstrated that the interaction of NaCas and DOM might take place in the form of physical sorption. Significantly, the pH-responsive method also remarkably decreased the TOC, COD, and turbidity from 70.0 mg/L, 459.8 mg/L, and 168.5 NTU to 28.9 mg/L, 193.2 mg/L, and 27.3 NTU, respectively (Figure 6.4c).

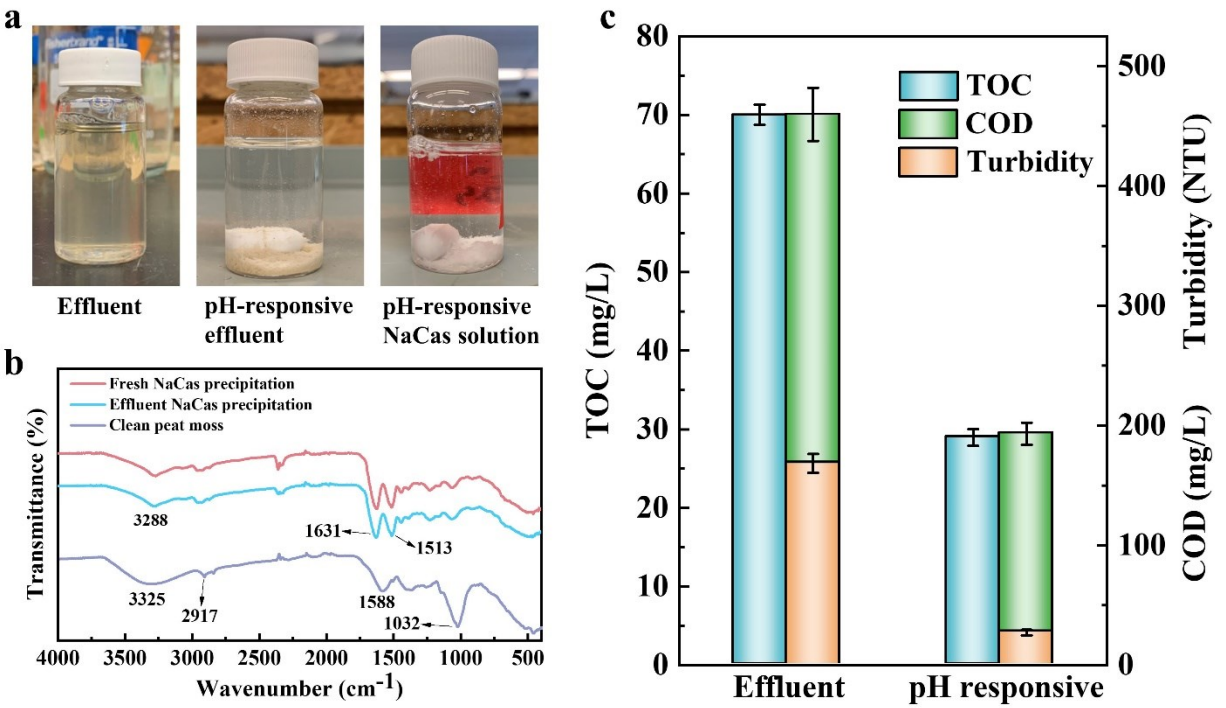

Figure 6.4 (a) Photographs of effluent before and after pH-responsive treatment, (b) ATR-FTIR spectra of NaCas precipitations and clean peat moss, and (c) TOC, COD, and turbidity of the effluents.

Various efforts have been devoted to the treatment of washing agents (Bi et al., 2021b; Chen et al., 2021b). Liquid-liquid extraction is a process of transferring target agents from wastewater to organic solvents. This process can be more time-consuming when dealing with solvent emulsions caused by surfactants. Although this approach has been practically applied in both laboratory and field settings, the high production of contaminated solvents is a real challenge for further disposal

(Trellu et al., 2021). Sorption is also a popular technology for the recovery of washing agents (Chen et al., 2021a; Zeng et al., 2020). However, sorption selectivity relies heavily on the competition process between sorbents and agents. Furthermore, the sorbents need to be regenerated by thermal treatment, which is energy-consuming and produces contaminated gas streams. Chemical oxidation, such as photocatalysis and electro-oxidation, has displayed the potential for the separation of washing agents by selectively oxidizing undesired contaminants (Bai et al., 2019; Mousset et al., 2016). Nevertheless, the effectiveness of these technologies is mainly restrained by two aspects. First, as radicals work in a nonselective pathway, oxidation competition and the inhibition of radical scavengers remarkably decrease the degradation kinetics of target contaminants (Trellu et al., 2021). Second, the micelles surrounding the target pollutants impair the oxidation effectiveness by decreasing the availability of washing agents toward radicals (Dos Santos et al., 2015). From a practical application viewpoint, there is still a long way to go in utilizing these separation strategies of a high cost and energy investment, and complicated configuration. It should also be noted that, despite the fact that some washing agents can be reused, a cost-benefit comparison between the separation cost and savings coming from the reuse of washing agents has yet to be provided.

In our study, the pH-dependent separation of NaCas simplified the pretreatment of the washing wastewater, showing the huge potential in practical hydrocarbon spill responses. The results of the separation experiments demonstrated that organic matter was removed at a remarkably high rate. From a practical point of view, contaminated peat moss can be washed ex-situ in chambers or tanks, and the washing wastewater can be pretreated through a pH-responsive strategy. Protein precipitation can be further treated in landfills and can be biodegraded by microorganisms.

6.3.7 Toxicity analysis

PHE is ubiquitous in soil, snowpack, ocean, and sediment (Marvin et al., 2021). It is prone to be enriched in organisms and can cause serious toxicity as the accumulated concentration increases, of which oxidative stress is a representative case (Zhang et al., 2014a). A study by Birben et al. (2012) showed that PAHs and their metabolites can induce reactive oxygen species (ROSs), and excessive ROSs can damage cell structures. Organisms can express antioxidant enzymes in response to excessive ROSs, reducing ROSs and mitigating cytotoxicity (Sun et al., 2006). However, PAHs in organisms exhibit an inhibitory effect on the production of antioxidant enzymes, which leads to an increase in ROSs and an amplification of oxidative stress (Bhagat et al., 2016; Zhang et al., 2021b).

NaCas might be sorbed on peat moss after washing. To investigate the effect of NaCas on PHE biotoxicity, *Caenorhabditis elegans* living in a soil environment (Félix and Braendle, 2010) were chosen as a representative. The sorbed NaCas and PHE can also get into the environment. Thus, the biotoxicity of PHE and NaCas to three aquatic species at different trophic levels, *Neopyropia yezoensis*, *Mytilus edulis*, and *Oncorhynchus mykiss*, was also analyzed. As depicted in Figure 6.5a, the SODs of *Neopyropia yezoensis*, *Mytilus edulis*, *Penaeus vannamei*, and *Oncorhynchus mykiss* were distributed in the most favored regions (95.22%, 98.68%, 93.14%, and 98.69%, respectively), additionally allowed regions (0.24%, 0.33%, 0.65%, and 0.00%, respectively), and generously allowed regions (1.44%, 1.77%, 3.07%, and 0.87%, respectively). More than 90% of the amino acid residues were distributed in the most favored regions, which proved the good quality of the constructed SOD structure (Li et al., 2022; Rose, 2019). Figures 6.5b and 6.6 display the docking and simulation images of the SOD–PHE and SOD–PHE–NaCas complexes, respectively. Figure 6.5c illustrates the binding energy of SOD–PHE in the absence and presence of NaCas, respectively.

The results revealed that the binding energy of SOD–PHE in five marine organisms decreased with the addition of NaCas, implying that NaCas can inhibit the combination of PHE and SOD and thus relieve the toxicity of PHE to organisms.

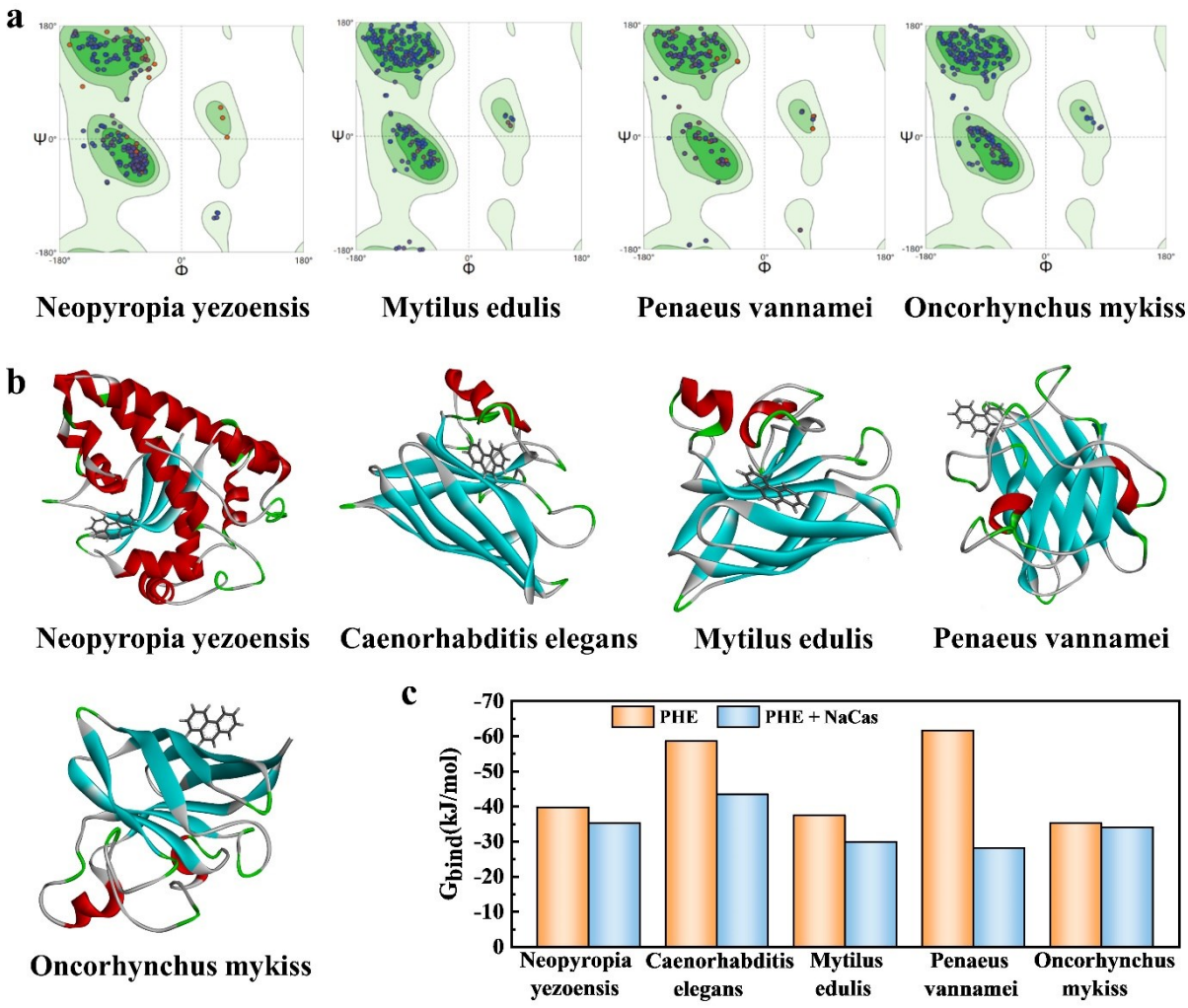

Figure 6.5 (a) Ramachandran plots of SOD of Neopyropia yezoensis, Mytilus edulis, Penaeus vannamei, and Oncorhynchus mykiss, (b) Docking images of SOD–PHE complex, and (c) binding energy of SOD–PHE complex in the absence and presence of NaCas.

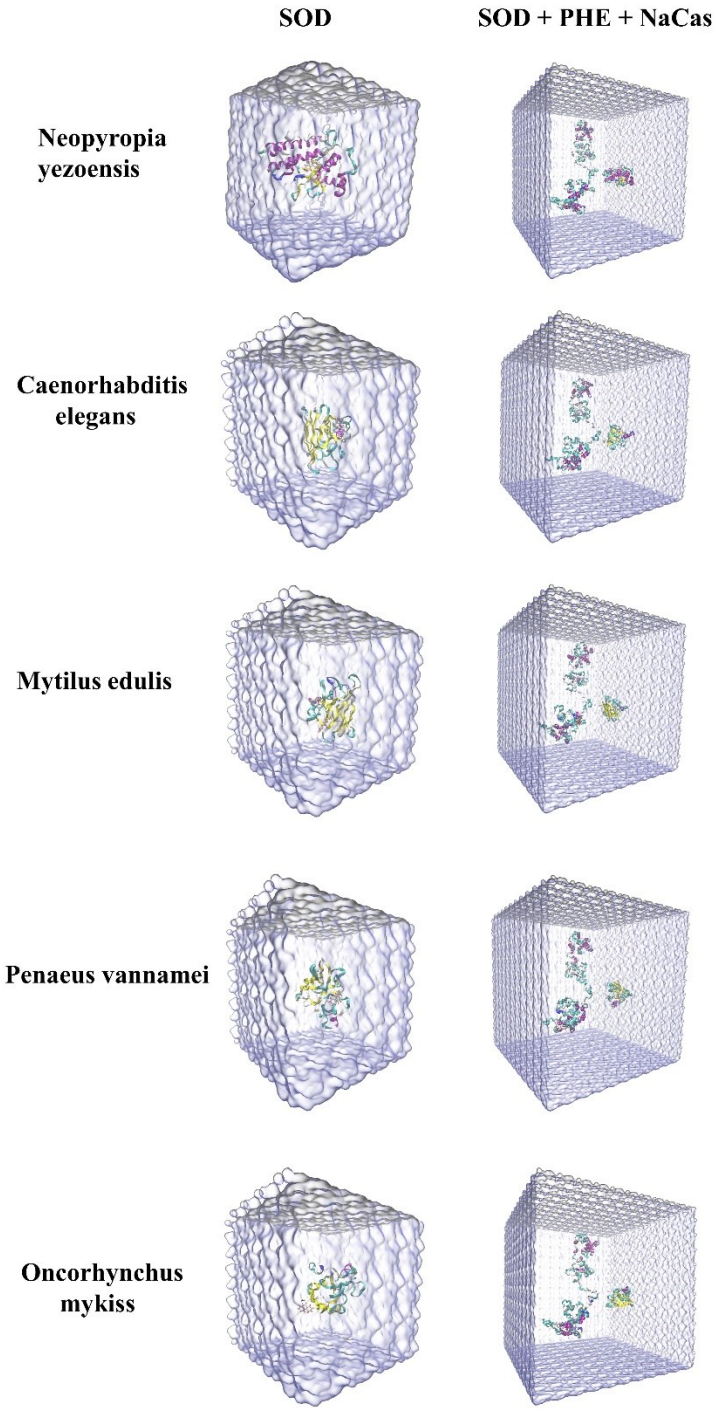

Figure 6.6 The dynamic simulation images of SOD and SOD–PHE–NaCas complex of different organisms.

6.4 Summary

Developing a washing fluid with low toxicity, cost-effectiveness, and responsive properties is crucial for mitigating hydrocarbon-contaminated peat moss. In this study, the food-grade NaCas was used as an eco-friendly washing fluid to remediate PHE-contaminated peat moss. The washing performance of NaCas was systematically investigated under different conditions. The factorial analysis demonstrated that three individual factors (humic acid, salinity, and NaCas concentration) and two interactions (humic acid*salinity and temperature*humic acid) displayed significant effects on PHE removal. Considering the small concentration of NaCas that is required for PHE desorption and the facile washing process, such a washing fluid is a very promising method for remediating contaminated peat moss. Apart from effective PHE removal, the treatment of the washing wastewater cannot be ignored. In this study, the turbidity, TOC, and COD of the washing effluent were remarkably decreased by simply adjusting the solution acidity, improving the practical application of such a washing method. Reducing biotoxicity is a priority when selecting a washing material to deal with hydrocarbon pollution. In this study, toxicity modeling results proved that NaCas could reduce the toxicity of PHE to the selected organisms. Given these advantages, NaCas-assisted washing would be a viable option for the remediation of contaminated peat moss.

CHAPTER 7 THE USE OF SODIUM CASEINATE-ASSISTED RESPONSIVE SEPARATION FOR THE TREATMENT OF OILY EFFLUENTS IN SHORELINE OIL SPILL RESPONSE ‡

7.1 Background

The dramatic success of the petroleum industry has sown the seeds of some environmental problems and created a profound challenge for the marine ecosystem. Oil spills have caused serious marine pollution, leading to threats to the well-being of billions of people and the survival of millions of species (Huang et al., 2022; Qu et al., 2022; Yue et al., 2020). Once spilled into the marine environment, oil can be dispersed in the water column through the mechanical action of waves or turbulence (Lee et al., 2016). In addition, oil slicks can reach the shoreline and attach to sands or gravels, posing a significant threat to the sensitive flora and fauna of the coastal ecosystem (Geng et al., 2020; Lee et al., 2020).

To date, various efforts have been undertaken to treat oiled shorelines. The use of washing agents has proven to be effective in removing oil from shoreline substrates. Some washing agents such as Corexit 9580 and Nalco can be applied *in situ*; the stranded oil is subsequently flushed with water and directed to a collection area where the oil is removed (ASTM, 2017; Yue et al., 2022g). "Lift-and-float" washing agents float the effluent and then redisperse the hydrocarbons into the water column. "Lift-and-disperse" washing agents act like dispersants, emulsifying and dispersing the hydrocarbon in the water column. Some SWAs are either "lift-and-float" or "lift-and-disperse,"

‡ This work has been published as R. Yue, Z. Ye, S. Gao, Y. Cao, K. Lee, C. An, Z. Qu, S. Wan. Exploring the use of sodium caseinate-assisted responsive separation for the treatment of washing effluents in shoreline oil spill response. Science of the Total Environment. 2023, 873: 162363.

depending on their concentrations in an application. In addition, some washing agents can also be used for the *ex-situ* treatment of oiled shoreline substrates. For example, Chen et al. (2021b) deployed a chitosan/rhamnolipid complex for effective oiled sand treatment. Bi et al. (2021b) synthesized a nanoclay/Tween 80 washing agent, which exhibited high washing performance. Yue et al. (2022b) designed a magnetic washing agent by fabricating carboxy-modified and water-dispersible magnetite nanoparticles. Overall, the use of washing agents can be a viable alternative for the cleanup of oiled shorelines. The constitution of washing effluents varies among spill response sites. The effluent from oiled shoreline cleanup, for example, usually contains oils, salt, organic matter, minerals, and other components that naturally exist in the ocean and coastal environment, making it different from regular oily effluent.

There are some available methods for the treatment of oil-containing wastewater. For instance, membrane separation has exhibited good performance for oil/water separation (Hu et al., 2021; Zhao et al., 2020). However, the application of this process for the treatment of a large quantity of washing effluents can be stymied by membrane fouling and complicated operation processes. An economic strategy for oily wastewater treatment is coagulation/flocculation, but it is associated with the generation of oily residues and volatile petroleum hydrocarbons (Zhao et al., 2021). Although the small oil droplets in washing effluents enable biodegradation to occur, this approach requires longer treatment time and its performance is sensitive to wastewater fluctuations (Lee et al., 2016). Given the limitations of these technologies, a novel approach with low costs and low toxicity is actively being sought.

Sodium caseinate (NaCas) is the sodium salt of casein and has been used intensively in the food industry as a thickener and emulsion stabilizer. NaCas also contains numerous amino acids and

trace elements necessary for the human body. Importantly, NaCas is biodegradable. For instance, Inglingstad et al. (2010) compared the digestion of casein from bovine and caprine by human digestive enzymes; only a few caseins were detected after 30 min. Kumura et al. (2002) reported that casein can be degraded by *Debaryomyces hansenii* 212 isolated from commercial cheese at 20 ℃ for 9 h. Our previous study has proven the great ability of the NaCas to control oil pollution in the shoreline and inland regions (Yue et al., 2022d; Yue et al., 2022f). In the present study, a new method that uses NaCas with amphiphilicity, environmental friendliness, wide availability, and pH-responsive properties is developed for the treatment of oily washing effluent. This method combines rapid oil separation and facile precipitation processes. The oil removal efficiency and effluent turbidity were evaluated under different washing effluent conditions (such as humic acid concentration and salinity), and the removal mechanism was also examined. Factorial analysis was applied to unveil the effects of individual factors and two-factor interactions. Biotoxicity was carried out to understand the mechanism of how NaCas alleviate oil toxicity to algae. Post-treatment experiments were conducted to explore the possibility of minimizing or eliminating the environmental risk of solid residues after treatment.

7.2 Materials and methods

7.2.1 Materials

Shell Rotella T4 diesel engine oil (15W40) was used as the representative oil in this study. NaCl, ammonium chloride (NH_4Cl), monopotassium phosphate (KH_2PO_4), HA, and hexane were purchased from Millipore Sigma (Oakville, Canada).

7.2.2 Oil separation experiments

Engine oil was added to ultrapure water (MilliporeSigma, USA), followed by vigorous agitation using a homogenizer (Ultra-Turrax T25, IKA, Germany) at 12,000 rpm for 30 min. Subsequently, NaCas was added to the emulsion, and the treatment process started with agitation at 300 rpm at different time points. Subsequently, NaCas was precipitated by adjusting the mixture's pH to 4.3 ± 0.1 with the addition of H_2SO_4 (0.1 mM). The treatment and precipitation processes were performed at room temperature (21 ± 1 ℃) unless otherwise specified. About 1–2 mL of supernatant was collected in glass vials, and 15 mL of hexane was added to extract the oil three times at 300 rpm and 20 ℃ for 24 h in a shaker (Innova 42R Incubator Shaker, USA). The oil concentration was measured using an ultraviolet-visible (UV–Vis) spectrophotometer (Agilent Cary 3500, USA) at a wavelength of 284 nm. The oil removal efficiency was calculated using the equation $R = 1 – (C_R/C_0)$, where C_R and C_0 are the residual and initial oil concentrations, respectively. Control experiments were performed with the same procedure but without the addition of NaCas.

7.2.3 Analytical and characterization methods

All batch experiments were conducted three times, and the mean values were used for the data analysis. Attenuated total reflection-Fourier transform infrared (ATR-FTIR) results were obtained using the Fourier transform infrared spectroscopy (FTIR, INVENIO, Bruker, USA). The zeta potential and particle size distribution tests were performed using a Zetasizer (Malvern, USA). Interfacial tension (IFT) measurements were recorded using a spinning drop tensiometer (KRÜSS, Germany). Microscope images were obtained using a fluorescence microscope system (ESC-350, Accu-Scope, USA). Turbidity tests were performed using a turbidity meter (ORION AQ3010, Thermo Scientific, Canada). Thermogravimetric curves were obtained using a TGA instrument

(Q50, TA Instruments, USA) with an argon atmosphere and a 10 °C/min ramping speed. The experimental design (Tables 7.1 and 7.2) and result analysis were carried out using Minitab (Minitab, LLC, USA). In addition, the statistical significance of the results ($p < 0.05$) was determined with a one-way analysis of variance (ANOVA).

Table 7.1 High and low levels for the 2^4 factorial design

Factor	Temperature A (°C)	Salinity B (wt%)	Humic acid C (mg/L)	NaCas content D (wt%)
High level (+1)	20	3.5	32	20
Low level (-1)	5	0	2	0

Table 7.2 Coded levels and corresponding values for factorial design matrix.

Number	Coded levels				A Temperature (°C)	B Salinity (wt%)	C Humic acid (mg/L)	D NaCas content (wt%)
	A	B	C	D				
1	-1	-1	-1	-1	5	0	2	0.0125
2	-1	-1	-1	1	5	0	2	0.1
3	-1	-1	1	-1	5	3.5	32	0.0125
4	-1	-1	1	1	5	3.5	32	0.1
5	-1	1	-1	-1	5	0	2	0.0125
6	-1	1	-1	1	5	0	2	0.1
7	-1	1	1	-1	5	3.5	32	0.0125
8	-1	1	1	1	5	3.5	32	0.1

9	1	-1	-1	-1	20	0	2	0.0125
10	1	-1	-1	1	20	0	2	0.1
11	1	-1	1	-1	20	3.5	32	0.0125
12	1	-1	1	1	20	3.5	32	0.1
13	1	1	-1	-1	20	0	2	0.0125
14	1	1	-1	1	20	0	2	0.1
15	1	1	1	-1	20	3.5	32	0.0125
16	1	1	1	1	20	3.5	32	0.1

7.2.4 Biotoxicity test

Fresh green algae, *Chlamydomonas reinhardtii* CPCC 243, obtained from the Canadian Phycological Culture Center (CPCC, University of Waterloo, Canada), were selected as the testing species to analyze the biotoxicity of NaCas. The algae were cultured in Bold's Basal Medium (BBM) at 23 ℃ on a 12 h light/12 h dark cycle. The algae were exposed to 50 mg/L of oil and different NaCas concentrations (25 and 100 mg/L) at different exposure times (24, 48, and 72 h). Cell density was measured using a flow cytometer (BD, Accuri C6 Plus, Canada). The photosynthetic parameters of the algae were measured using a WATER-PAM fluorometer (WALZ Company, Germany).

7.2.5 Biodegradation experiments

The biodegradation experiments were conducted using real seawater with/without supplementary externally isolated marine bacteria. Seawater was collected from the Ocean Science Center (OSC) at the Memorial University of Newfoundland (about 10 m deep, 47.6248°N, 52.6627°W). For each

microcosm, a 250 mL flask was supplemented with 100 mL of seawater. The effluent precipitate (100 mg/L) and nutrients (4.67 mM NH_4Cl and 1.47 mM KH_2PO_4) were added to each microcosm (Murphy et al., 2021). The biodegradation experiment was conducted at room temperature (22–25 ℃) with shaking of 150 rpm for 12 days. *Exiguobacterium* sp. N4-1P isolated from North Atlantic Canada was used as the external bacteria (Cao et al., 2020c). The bacteria were enriched overnight using Marine Broth 2216 (Difco #279110). They were then washed three times with sterilized seawater and diluted until their optical density at 600 nm was 1 (Cao et al., 2022). The washed cells (1 mL) were then added to the microcosm and acted as the bioaugmentation cells.

The organic nitrogen content at each time point (0, 3, 7, and 12 days) and the initial seawater were evaluated. As the chemical was mainly composed of organic nitrogen, its biodegradation was evaluated using the Pierce BCA Protein Assay Kit (Thermo Scientific, #23225) following the modified manufacturer's procedures (Cao et al., 2022). Briefly, 200 μL of the medium was added to the synthesized reaction agents and incubated for 2 h at 60 ℃. After cooling to room temperature, the optical absorbance was measured at 562 nm to represent nitrogen abundance.

7.3 Results and discussion

7.3.1 Sodium caseinate-assisted oil separation of washing effluent

The amphiphilicity of NaCas makes it possible for NaCas to sorb hydrophobic oil from washing effluent via the strong hydrophobic-hydrophobic interaction between NaCas and oil. After sorbing oil, the NaCas/oil mixture can be rapidly precipitated by adjusting the effluent's pH where the zeta potential of that mixture can be brought to zero. The effect of the treatment time on the oil removal performance of NaCas is shown in Figure 7.1a. 75% of oil droplets can be rapidly removed by

NaCas within 5 min, with a remarkable decrease in turbidity from 21.4 to 6.00 NTU. When the sorption time was increased to 60 min, the oil removal efficiency increased gradually to 85.1%, and the turbidity declined stepwise to 2.52 NTU. An additional increase in treatment time from 60 to 80 min did not further enhance the oil removal, which indicated that the sorption sites on NaCas were saturated. Moreover, the average size of the oil droplets became increasingly small as the treatment time increased, decreasing from initially around 589.6 nm to 322.0 nm at 5 min, 154.5 nm at 10 min, 6.2 nm at 20 min, 5.7 nm at 40 min, and 3.94 nm at 60 min, and then remained unchanged at 80 min (Figure. 7.1e).

Oil removal in terms of the NaCas concentration is depicted in Figure 7.1b. The removal efficiency was 46.6%, and the turbidity of the effluent was 10.89 at NaCas loading of 0.0125 wt%. More oil droplets were captured as the NaCas concentration increased to 0.2 wt%, leading to high oil removal efficiency and low turbidity. This is because a high NaCas concentration provides abundant sorption sites to capture oil droplets. Interestingly, it was observed that oil removal decreased slightly at the NaCas concentration of 0.4 g/L. On one hand, at high NaCas concentrations, the interfacial activity of NaCas deteriorated (Srinivasan, 1998) due to the reduction of β-casein at the oil/water interface. This could weaken the interaction between NaCas and the oil droplets. On the other hand, it was found that the particle size of NaCas increases at high concentrations (Yue et al., 2022d), which might reduce the number of sorption sites on NaCas. A similar finding was reported by Mirshahghassemi and Lead (2015); the authors found that the oil removal efficiency decreased slightly, from 99.3% to 98.0%, when the Fe_3O_4 concentration increased to 35.2 mg/L.

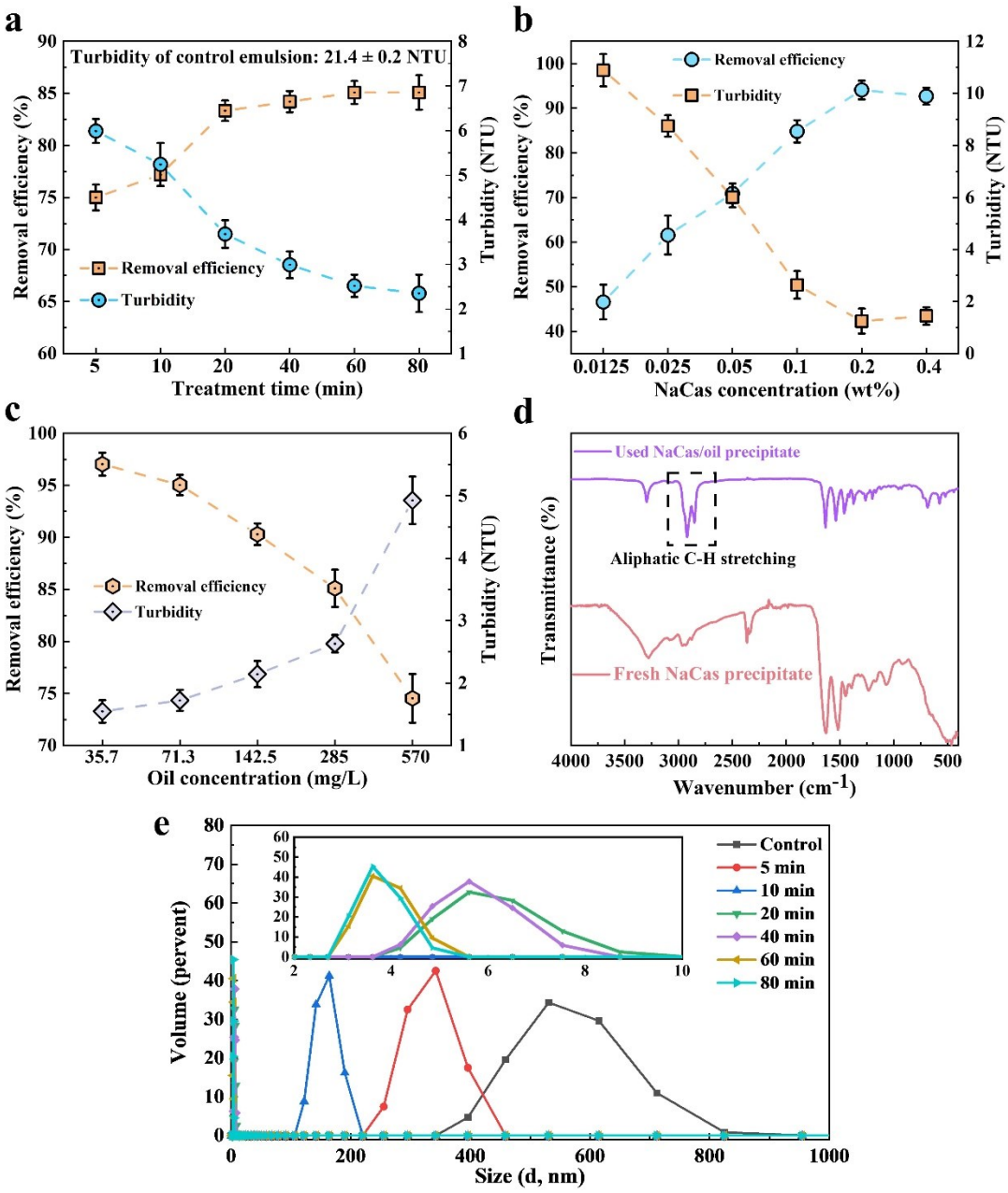

Figure 7.1 Effects of (a) treatment time, (b) NaCas concentration, and (c) oil concentration on oil removal efficiency and turbidity (treatment time = 60 min, oil concentration = 285 mg/L, NaCas concentration = 0.1 wt%). (d) ATR-FTIR of NaCas and NaCas/oil precipitates.

The oil treatment performance of NaCas at different oil concentrations is shown in Figure 7.1c. About 97.0% of the oil droplets were captured by NaCas, with turbidity as low as 1.54 NTU. The

oil removal performance of NaCas decreased when the oil content increased. The result of the decrease in the oil removal was a commensurate increase in effluent turbidity, with a dramatic increase to 4.9 NTU. ATR-FTIR of the NaCas/oil precipitate displayed the characteristic peaks of hydrocarbon (Figure 7.1d). The bands of NaCas at 2850–3000 cm^{-1} (2854, 2924, and 2954) and 1458 cm^{-1} were assigned to the aliphatic C–H stretching and C–H bend or scissoring of hydrocarbons, respectively (LiBreTests), which indicate the oil sorption on NaCas.

7.3.2 Effect of salinity

Pollution control can be affected by various environmental factors (Safaei et al., 2022; Song et al., 2021). Seawater is often used for shoreline washing processes and thus it is necessary to understand the roles of seawater characteristics in the NaCas-assisted oil separation of washing effluent. The salinity of the majority of the open ocean is 3.3 wt% to 3.5 wt%, but some areas are different, resulting from water evaporation and freshwater input by rivers and rain (Ocean-Salinity, 2022; Yue et al., 2022b). In this study, oil removal trended downward with the increasing salinity (Figure 7.2a), falling to 82.2%; turbidity rose to 4.05 NTU. Subsequently, a significant decrease in oil removal was observed in the salinity of 0.5–3.5 wt%, with the turbidity rising. To examine the mechanism behind this phenomenon, the IFT, and the zeta potential were investigated. It was observed that the interfacial activity of the NaCas/oil interface increasingly reduced as the salinity increased (Figure 7.2b).

Three possible reasons may explain this phenomenon. First, Jones and Ray (1941) proposed the Jones–Ray effect, the electrolytes behave as “capillary-inactive” and can increase the surface tension when higher than their dilute concentration (around 1 mM). Ghorbanizadeh and Rostami

(2017) investigated the behavior of the oil/water interface's IFT as a function of the salt concentration. It was observed that the IFT declined at a low NaCl concentration (< 0.25 M) and increased thereafter at a high ionic strength (> 0.25 M). This is because, at a low salt concentration, the surface-active component (e.g., dispersants as additives to improve the properties of engine oil) in the oil was ionized and sorbed at the oil/water interface owing to the interaction between that component and salt ions (Lashkarbolooki et al., 2014), which lowered the IFT. At high salt concentrations, the concentration of the surface-active component at the oil/water interface decreased as a result of the salting-out effect (Moeini et al., 2014); thus, the IFT increased. Second, the addition of a high salt concentration could give rise to dehydration and therefore cause the attraction force between NaCas particles (Thomar et al., 2014), as proved by the reduced surface charge shown in Figure 7.2b. The large NaCas particles could provide fewer oleophilic groups to sorb oil droplets. Third, the increased IFT has something to do with the formation of the reverse micelle (microdispersion). It has been recognized that polar ingredients in oil tend to generate microdispersion at the oil/brine interface (AlHammadi et al., 2018; Subramanian et al., 2017). Mehraban et al. (2021) examined the impact of salinity on the oil/water IFT. The results showed that microdispersion existed at the oil/brine interface, thus causing high IFT. Interestingly, they found that the microdispersion content decreased as the salinity increased, matching the decreased IFT of the oil/brine interface. Similar experimental findings can be viewed elsewhere (Gaonkar, 1992). In summary, the influence of salt on oil removal from washing effluent is complicated, in which the promotion and inhibition of oil removal are involved. In this study, salt-induced inhibition surpassed salt-induced promotion for oil removal.

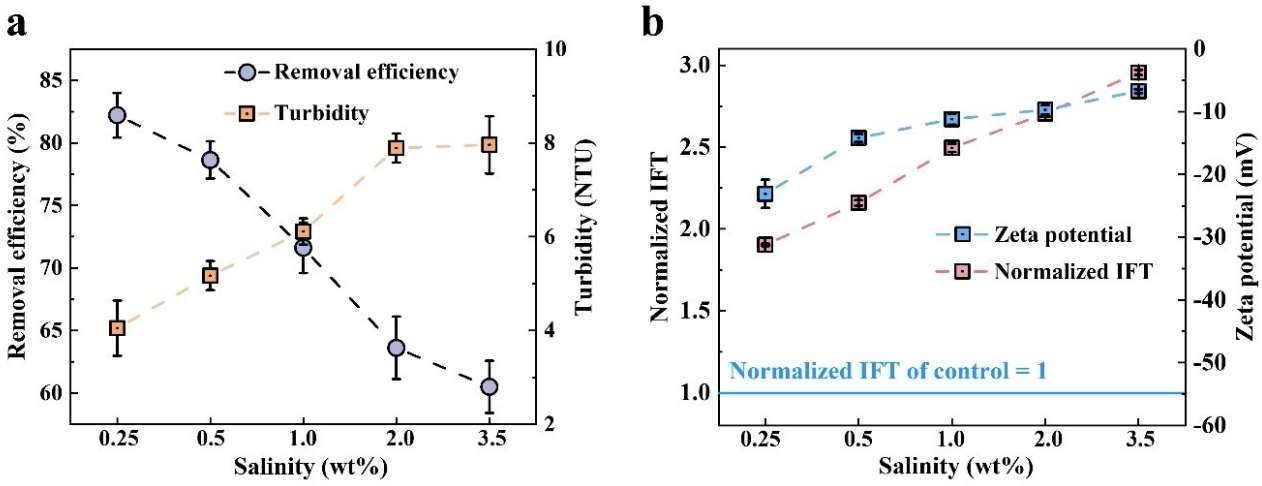

Figure 7.2 Effects of salinity on the (a) oil removal efficiency and turbidity and (b) IFT of the NaCas/oil interface and the zeta potential of the mixture (treatment time = 60 min, oil concentration = 285 mg/L, NaCas concentration = 0.1 wt%).

7.3.3 Effect of humic acid

Dissolved organic matter (DOM) is ubiquitous in the marine environment, and the DOM concentration varies greatly in the ocean (Dittmar et al., 2021). More than half of the DOM is composed of humic acid in a body of natural water (Findlay and Parr, 2017). The oil removal in terms of humic acid is depicted in Figure 7.3a. The oil removal gradually diminished from 80.4% to 60.8% as the humic acid concentration increased. The reduction in oil removal was matched by the rise in turbidity, which nearly doubled from 4.52 to 8.56 NTU. The addition of humic acid increases the surface charge of the system (Figure 7.3b), which could enhance the repulsion force between the oil and NaCas, thus constraining the oil removal. Another reason contributing to the decreased oil removal is the competitive sorption between humic acids and NaCas. As displayed in Figure 7.3c, the color of the precipitate became increasingly brown as the humic acid content increased, indicating that more and more humic acid molecules were sorbed on NaCas.

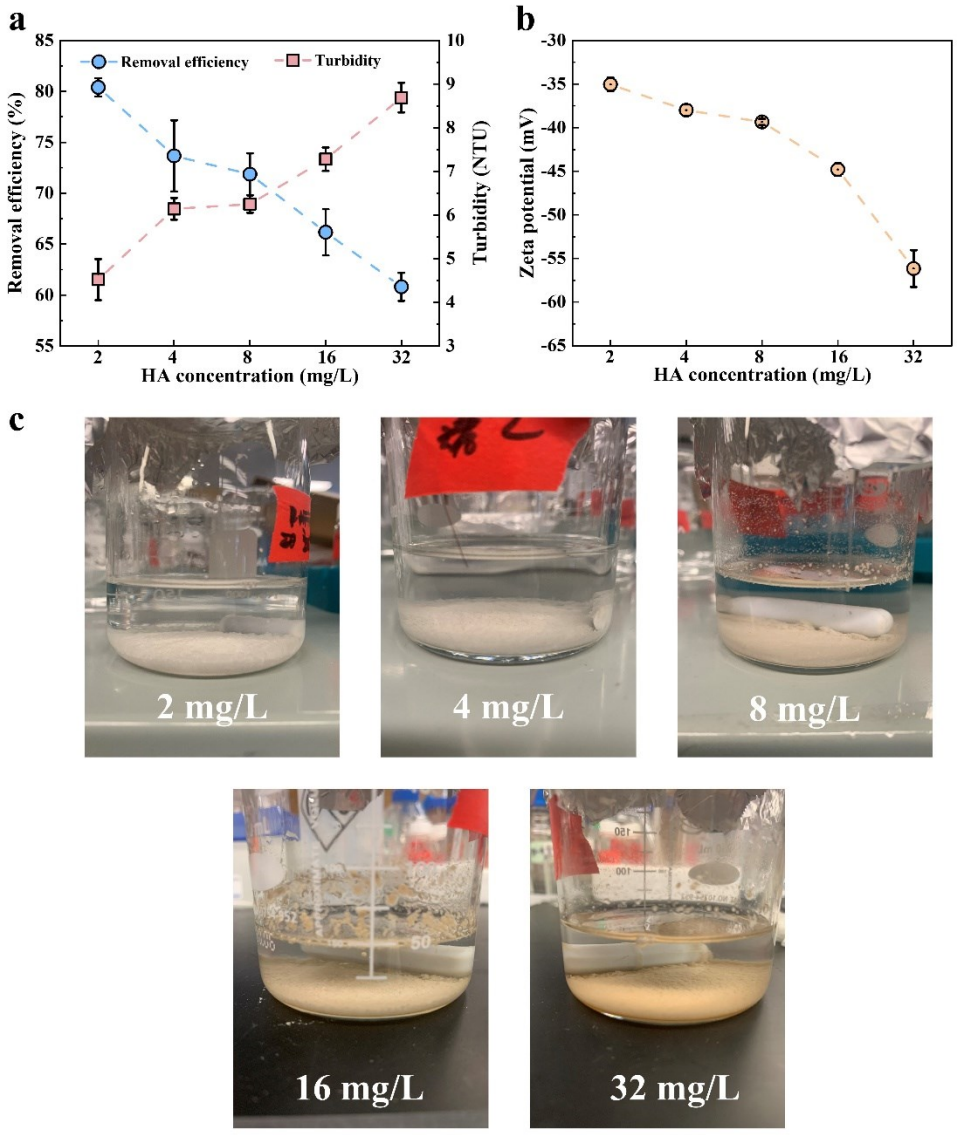

Figure 7.3 Effects of humic acid on (a) oil removal efficiency and turbidity, (b) zeta potential of the mixture (treatment time = 60 min, oil concentration = 285 mg/L, NaCas concentration = 0.1 wt%), and (c) photographs of NaCas precipitate at different HA concentrations.

Humic acid is amphiphilic and can form humic pseudomicelles, a structure similar to synthetic surfactants' micelles (Von Wandruszka, 2000). Humic acid can spontaneously move to the oil/water interface and self-aggregate through hydrogen bonding and π-π interaction. A study by Meng et al.

(2019) explored how humic acid affects the IFT at the oil/water interface. The experiments demonstrated that the addition of humic acid in a certain range (5 to 25 mg/L) decreased the IFT at the toluene/water and asphaltene/water interfaces. Although humic acid occupied the active site on NaCas, did it contribute to oil removal? It was proved that after coating the humic acid on the surface of K10 montmorillonite, the IFT of the asphaltene/K10 montmorillonite interface was almost unchanged (Meng et al., 2019). This could be explained by the fact that the structure of humic acid deforms once it is sorbed on a solid surface (Zhu et al., 2015b). Therefore, the humic acid sorbed on the surface of NaCas might have less contribution to oil capture.

7.3.4 Effect of temperature

Oil spills may occur in areas from tropical to subantarctic (Feng et al., 2021). Global warming and consequent sea ice melting are opening up the Arctic and other cold regions to oil exploration and transportation, making oil spills a horrible threat to the marine environment in cold regions. For example, in May 2020, around 21,000 tonnes of oil spilled into the subsoil and river in the Russian Arctic, with a possible risk of spreading into the Arctic Ocean. The oil removal from washing effluent at different temperatures is shown in Figure 7.4. As the temperature increased, the oil removal decreased. The oil removal increased gradually from 64.5% to 84.2% when the temperature climbed from 5 to 20 ℃, and the turbidity dropped from 7.25 to 2.62 NTU. On one hand, the IFT of NaCas declined stepwise as the temperature increased (Figure 4.3b). NaCas contains hydrophilic and lipophilic groups, thus acting as a surfactant. Ye et al. (2008) explored how temperature affected the IFT of oil/surfactant. The results showed that the increased temperature (< 70 ℃) led to a decreased IFT and shortened time to achieve a low and stable IFT. The facilitated IFT equilibrium process could favor NaCas in capturing more oil droplets during

the given time period. On the other hand, it has been reported that oil viscosity decreases as the temperature increases (Chen et al., 2021b). Oils with low viscosity are more easily captured by NaCas than those with high viscosity. Similar results were reported by Asadpour et al. (2014), who found that the oil sorption capacity was enhanced at high temperatures due to the decreased oil viscosity.

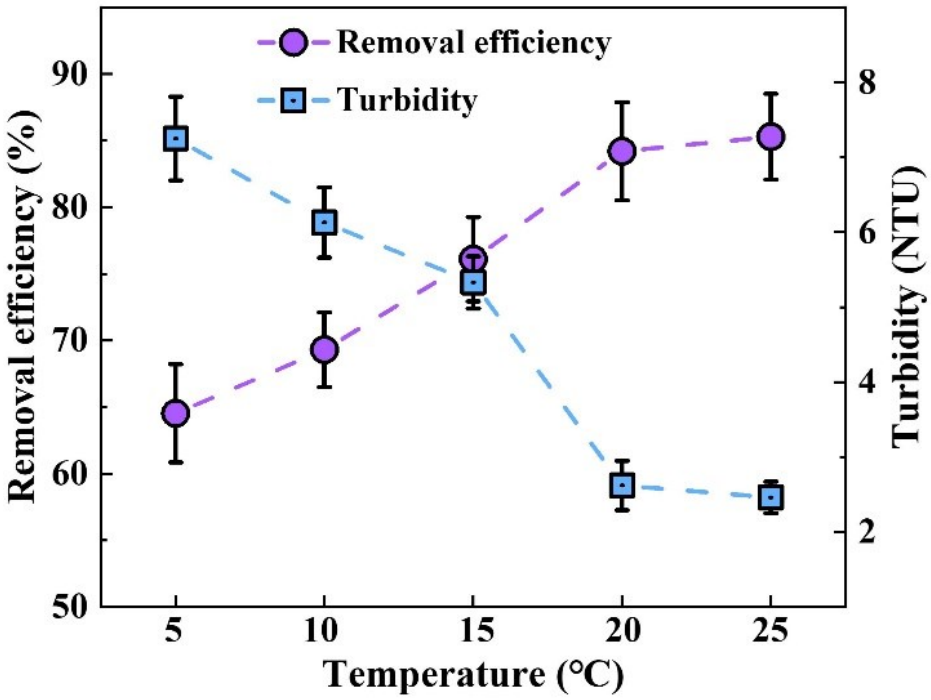

Figure 7.4 Effect of temperature on oil removal efficiency (treatment time = 60 min, oil concentration = 285 mg/L, NaCas concentration = 0.1 wt%).

The increase in temperature from 20 to 25 ℃ resulted in a further decrease in IFT but a slight change in oil removal and turbidity, with the former rising to 85.3% and the latter declining to 2.46 NTU, which was likely due to the saturated active sites of NaCas. This observation in part indicated that the number of sorption sites on NaCas is a key factor in oil removal at high temperatures. Some studies have reported different results. Asadpour et al. (2014) found that 40 ℃ was the optimal

temperature for oil uptake using mangrove bark fine powder, over which the oil sorption capacity declined gradually. This was because oil with low viscosity tends to be discharged from the interior structure of the sorbent. Coincidentally, Kumar (2019) also found that the highest oil sorption was achieved at a temperature of 40 ℃ and decreased stepwise beyond this point, owing to the variation of electrostatic interaction between oil and the sorbent.

7.3.5 Factorial analysis of interactive effects on oil removal

As discussed in the previous sections, the oil removal performance of NaCas was subjected to different individual factors. The interaction of these factors might have different effects on oil removal efficiency. It has been acknowledged that a system usually focuses on its primary effects and low-order interactions, while high-order interactions can be ignored (Wen et al., 2021). Thus, factorial analysis considering four individual factors (temperature, salinity, humic acid, and NaCas content) and two-factor interactions were conducted, with the results shown in Figure 7.5. The mean of oil removal efficiency can be described as a function of individual and two-factor interactors: the mean of removal efficiency = 19.63 + 0.253 Temperature – 0.59 Salinity – 0.380 Humic acid + 340.7 NaCas concentration – 0.1334 Temperature × Salinity + 0.00106 Temperature × Humic acid + 13.24 Temperature × NaCas concentration + 0.0460 Salinity × Humic acid – 49.56 Salinity × NaCas concentration – 2.99 Humic acid × NaCas concentration.

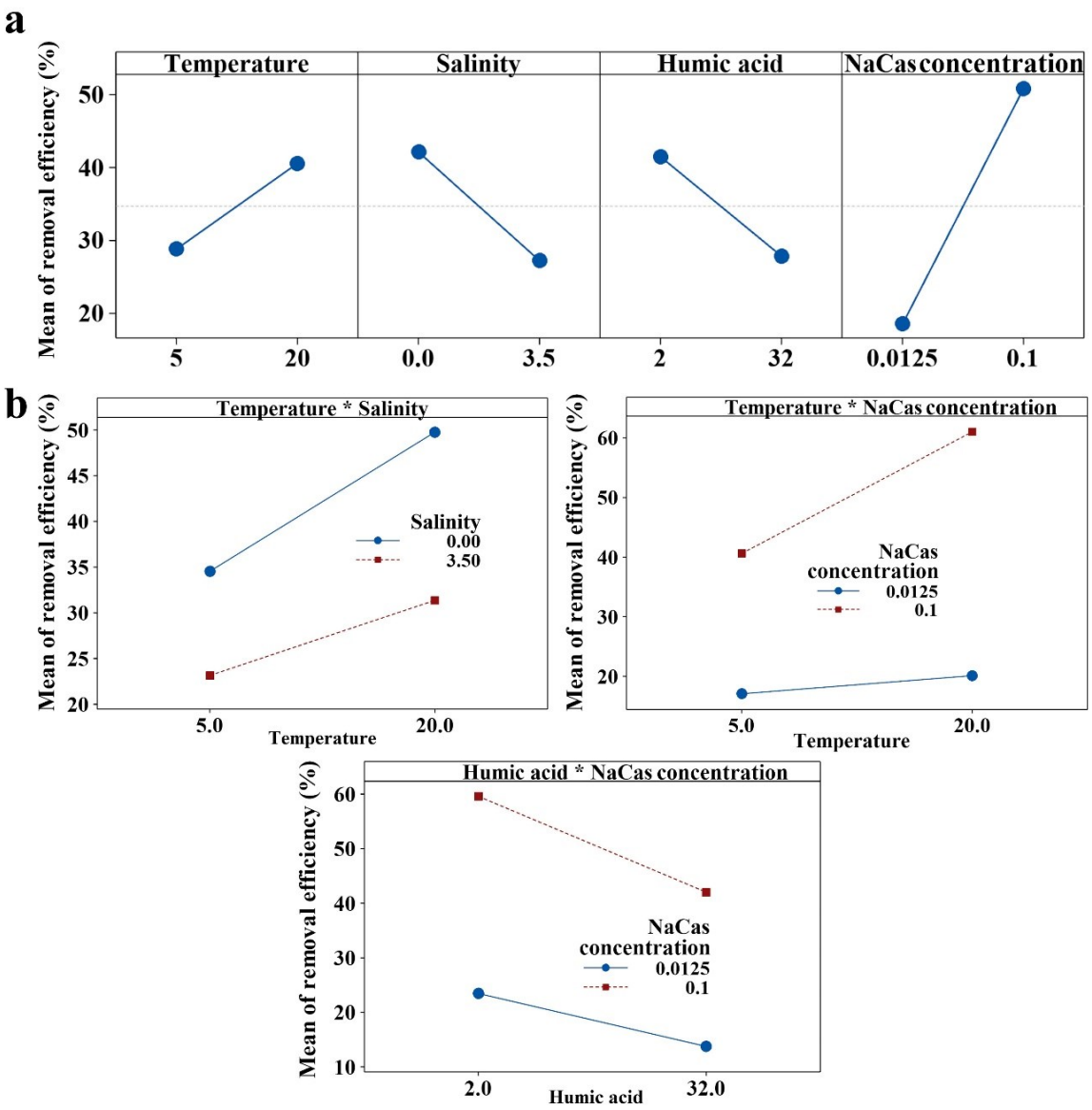

Figure 7.5 Factorial analysis of oil removal efficiency: (a) main effect plots and (b) interaction plots.

As plotted in Figure 7.5a, all four individual factors display significant effects on oil removal ($p < 0.05$). Ocean temperature varies in different areas of the planet with various solar energy, from as high as 30 ℃ in the tropical region to as low as –2 ℃ near the poles. In this study, 5 ℃ and 20 ℃

were chosen as the low and high levels, respectively. As plotted, the mean oil removal efficiency in terms of temperature climbed from 28.8% to 40.5% as the temperature rose from 5 to 20 ℃.

The salinity of the marine environment, especially at the ocean's surface, varies from region to region. The salinity of the majority of the ocean is between 3.4 wt% and 36 wt% (parts per thousand), but this range tends to be higher or lower in some places. For instance, the Mediterranean Sea, with more evaporation and limited freshwater addition, has a high salinity of no less than 3.8 wt%. The salinity of the cold ocean around the South Pole is slightly lower than 3.4 wt%; the salinity of the oceans close to the North Pole is no more than 3.0 wt%. In particular, the Baltic Sea has a very low salinity of approximately 1.0 wt%, due to the vast amount of freshwater added from other rivers. Thus, salinities of 0 and 3.5 wt% are low and high levels, respectively. In this study, the salinity increased to 3.5 wt%, the mean removal efficiency plummeted from 42.1% to 27.2%.

The humic acid concentration was also a significant factor affecting oil removal. The average DOM content in seawater is below 1 mg/L but is higher in productive seawater where phytoplankton enriches or in other areas of poor nourishment (e.g., in the subtropical cyclones or temperate regions in late summer) (Dittmar et al., 2021). Peatland acts as another major provider of DOM, depending on its degree of decomposition and humification. This type of DOM can enter the hydrosphere by flushing water flow or by wave erosion. The low and high levels of DOM content in this study were 2 and 32 mg/L, respectively. The mean removal efficiency decreased from 41.5% to 27.8% when the humic acid concentration was 32 mg/L. As another significant positive effect, the NaCas concentration is also of great importance to oil removal. The increase in the NaCas concentration from 0.00125 wt% to 0.1 wt% gave rise to an increase in oil removal efficiency from

18.5% to 50.8%. Due to the wide availability of the NaCas, it would be possible to use a large amount of NaCas to treat such washing effluents containing oil.

The effect of the two-factor interactions on oil removal is shown in Figure 7.5b. Temperature × salinity, temperature × NaCas concentration, and humic acid × NaCas content had significant effects on oil removal ($p < 0.05$). As temperature varied from low to high levels, the negative impact of salinity on oil separation was more remarkable. The NaCas concentration shifting from low to high levels exhibited a more positive effect on oil removal at high temperatures, as proved by the increased slope of the plot, which means that this effect was sensitive to temperature. This result also suggests that it would be not necessary to invest too much NaCas to treat oil-concentrated washing effluent at low temperatures. It was found that humic acid showed higher inhibition in oil removal at high NaCas concentrations than that at low NaCas concentrations, which demonstrated that this inhibitory impact might be caused by the humic acid sorbed on NaCas, rather than those dissolved and nomadic in the effluent. It suggested control of humic acid concentration in washing effluents can help NaCas to perform well.

7.3.6 Biotoxicity assessment

The biotoxic effect of the cleanup process is an important consideration for decision-making. Green treatment is preferred in oil pollution control (Chen et al., 2021c). The effect of NaCas on oil biotoxicity is shown in Figure 7.6. The cell density of algae under different environmental conditions is plotted in Figure 7.6a. The number of algae decreased in the presence of oil, indicating that oil had an inhibitory effect on algae growth. This effect became increasingly severe by prolonging the exposure time. The number of algae experienced almost no change within 24 h after

NaCas was added. The addition of 25 mg/L of NaCas can overcome oil toxicity and thus promote algae growth. The number of algae increased by 35.8% and 84.3% with the help of 25 mg/L of NaCas at 48 and 72 h, respectively. It was observed that the cell number at a high NaCas concentration (100 mg/L) increased by 46.2% and 93.0% at 48 and 72 h, respectively, which was less than that at a low NaCas concentration. This might be because the NaCas content was higher than a specific threshold; thus, algae could not uptake and make use of it.

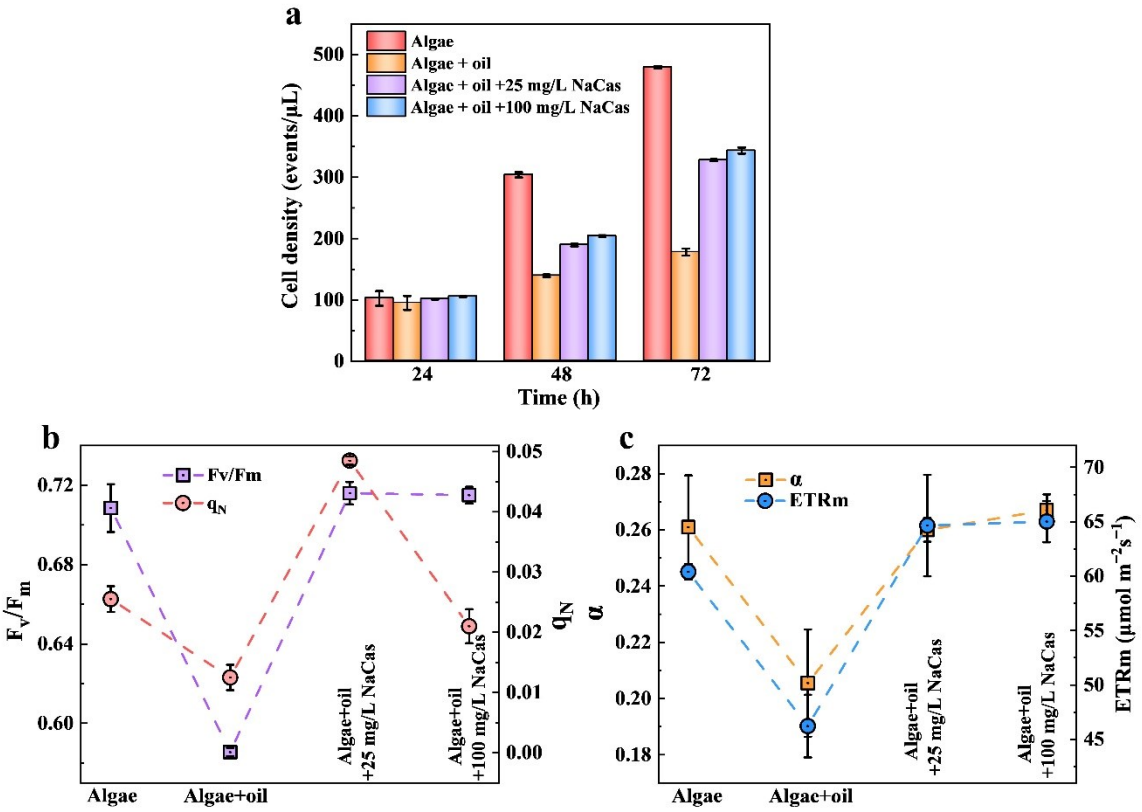

Figure 7.6 (a) Cell density, (b) Fv/Fm and qN, and (c) α and ETRm of algae under different conditions.

Algae are a diverse group of solar-driven organisms; thus, photosynthesis efficiency is of fundamental significance for their growth. To obtain an in-depth understanding of algae growth in the presence of oil and NaCas, photosynthesis parameters were measured. F_v/F_m, which refers to

photosystem II photochemical efficiency, signifies the efficiency of the conversion of absorbed solar light into photochemistry. q_N represents the value of non-photochemical quenching and is a mechanism employed by algae to protect themselves from the adverse effects of high light intensity (Xin et al., 2019). α, which is the slope of the rapid light curve that estimates the relative electronic transport rate as a function of photosynthesis-active radiation, describes the light use efficiency. The electron transport rate (ETRm) is the photosynthetic rate of algae (Chen et al., 2016). The variations of Fv/Fm and qN are plotted in Figure 7.6b. Fv/Fm declined remarkably from 0.709 to 0.585 when the algae were exposed to the oil and then experienced an uptrend to 0.715 with the help of 25 mg/L of NaCas. The Fv/Fm level was stable with 100 mg/L of NaCas. qN underwent a similar variation tendency, changing from 0.025 to 0.0125 and then to 0.049 in the algae, algae + oil, and algae + oil + 25 mg/L NaCas groups, respectively. However, the qN level fell off to 0.021 with high NaCas content, which was still higher than that in the algae + oil group. The effects of oil and NaCas on the α and ETRm can be observed in Figure 7.6c. The light utilization of the algae was inhibited due to the oil, with α declining from 0.261 to 0.205. Fortunately, NaCas completely offset this inhibitory effect and recovered the α value to 0.260 at 25 mg/L of NaCas and even to a higher threshold at 0.267 at 100 mg/L of NaCas. It was also observed that NaCas can fully surmount the adverse effect of oil on the ETRm by restoring the ETRm from 46.21 to 32.351 and finally to 65.02 μmol $m^{-2}s^{-1}$. NaCas was able to alleviate the biotoxicity of oil and to make the photosynthesis of the algae less vulnerable to oil. The remaining NaCas may exist in the liquid after oil separation. The biotoxicity results suggest that NaCas in the discharged effluent could further reduce the impact of pollutants on environmental microorganisms.

7.3.7 Post-treatment of precipitation residues

After oil removal and subsequent pH-responsive separation from wastewater, the precipitate containing NaCas and oil must be disposed of to relieve the further adverse effects on the environment. In this study, two methods, thermal decomposition, and biodegradation, were proposed. Burning is an effective oil spill treatment for removing relatively large amounts of oil (Wang et al., 2022d). Therefore, thermal decomposition was applied to dispose of the NaCas precipitates. The TGA curves of the fresh and used NaCas/oil precipitates are plotted in Figure 7.7a. For the fresh NaCas precipitate, weight loss below 200 ℃ was attributed to the evaporation of bound water. The additional weight loss at 200 to 500 ℃ corresponded to the destruction of peptide bonds and the release of NH_3 (Wang et al., 2022a). At temperatures higher than 500 ℃, the weight loss resulted from the carbonization and CO_2 release of the degradation products in the first two stages. The NaCas/oil precipitate used displayed an almost identical weight loss tendency as fresh NaCas but, notably, experienced more weight loss than its fresh NaCas counterpart at temperatures higher than 200 ℃. This is a result of the evaporation of oil sorbed on NaCas. The weight loss at 200 to 310 ℃ was a result of the evaporation of low-molecular-weight hydrocarbons; the additional loss at 310 to 400 ℃ was due to the evaporation of high-molecular-weight hydrocarbons (Singh and Khullar, 2019). As reported, engine oil can be almost fully burned when the temperature is 500 ℃ (Kozak, 2019), beyond which, therefore, the weight loss of the NaCas/oil precipitate largely reflects the pyrolysis of remnant NaCas.

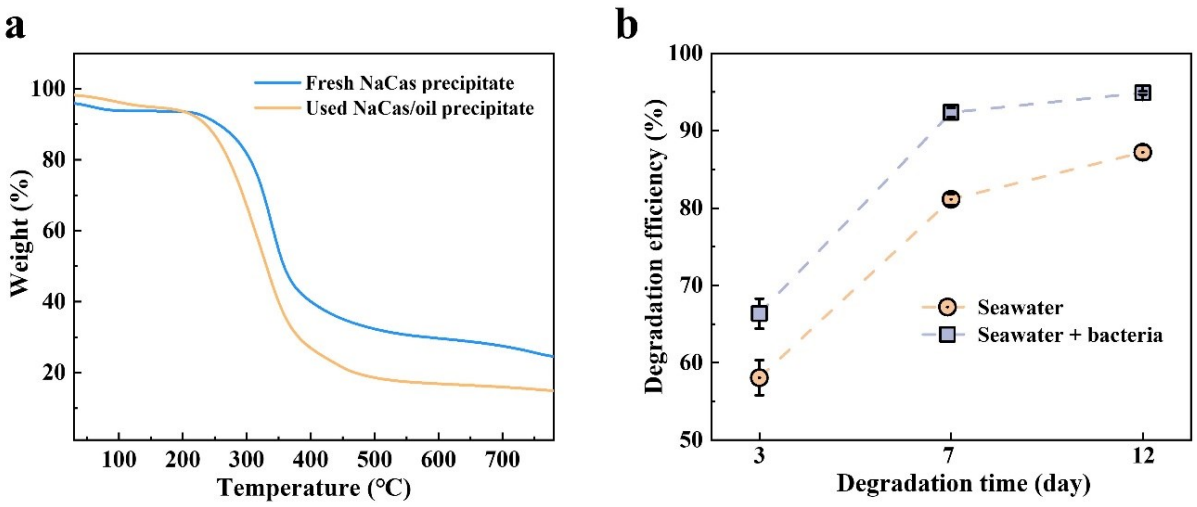

Figure 7.7 (a) TGA curves of fresh and used NaCas/oil precipitate and (b) biodegradation efficiency of the used NaCas/oil precipitate.

Biodegradation is a remediation approach in which microorganisms convert pollutants to biomass, CO_2, water, and innocuous oxygenated end products, providing energy and carbon for proliferation and growth. Many hydrocarbons and sodium caseinate are biodegradable under aerobic conditions (Kaminogawa et al., 1980; Lee et al., 2016). As depicted in Figure. 7.7b, the degradation efficiency of the NaCas/oil precipitate used in fresh seawater increased sharply from 58.1% on the third day to 81.1% on the seventh day and climbed moderately to 87.2% 5 days later. After the bacteria were added to the seawater, an increase in the degradation efficiency of the NaCas/oil precipitate was observed. The degradation efficiencies were 66.3%, 92.3%, and 94.9% on the 3rd, 7th, and 12th days, respectively. *Exiguobacterium* sp. N4-1P has salt tolerance (as high as 15 g/L of NaCl). In seawater, the high surface hydrophobicity of the bacteria drives them to attach to the oil accompanied by the production of bio-emulsifiers, which facilitates the formation of micelles to make hydrocarbons bioavailable (Cao et al., 2020c). Cao et al. (2020c) proved that *Exiguobacterium* sp. N4-1P can degrade 40% of n-alkanes and 24% of polycyclic aromatic

hydrocarbons at a salinity of 15 g/L within 30 days but can still degrade these oil products to a certain degree in the high salinity range of 0 to 70 g/L.

As stated above, burning and biological treatments are suitable pathways for disposing of the NaCas/oil precipitate used to minimize environmental threats. The implementation of these two methods should be considered with discretion and comprehensive evaluation. Combustion smoke in the burning process can generate fine particulate matter ($PM_{2.5}$) and carbon dioxide. Wang et al. (2022d) analyzed the distribution of $PM_{2.5}$ after in situ burning and evaluated the health risks in the northwest Arctic area of Canada. They concluded that the diffusion of the burning pollutants was affected by wind, and convection dispersion initiated by temperature inversion. In addition, the burning area should be sparsely populated. Compared to burning, biodegradation is more environmentally sustainable and cost-effective. However, it would take a long time for bioremediation to achieve great removal efficiency. Bioremediation performance relies on oil properties, nutrient provision, and shoreline geography. For example, it was observed that light oil is more susceptible to biodegradation in the upper intertidal zone than in the lower intertidal zone (Venosa et al., 1996). Moreover, biodegradation is difficult for heavy oils (Hoff et al., 1995; Pan et al., 2022). Another study found that saturated and aromatic hydrocarbons can be biodegraded more rapidly than polar fractions such as resin and asphaltenes (Head et al., 2006). In summary, the application of these two post-treatments should systematically consider oil characteristics, shoreline conditions, health impact, and other environmental backgrounds.

7.4 Summary

In this study, NaCas, an environmentally friendly, cost-effective, and biodegradable agent, was deployed to capture oil pollutants from the oily effluent generated from shoreline washing processes. Oil droplets can be effectively and rapidly captured by NaCas and subsequently removed after pH-triggered separation, producing a clean supernatant with low turbidity. NaCas performance was systematically examined under various conditions. The results show that with the increase in salinity came a decrease in oil removal efficiency because of the increase in IFT and reduced active sites. Humic acid inhibited NaCas performance by competing for active sites on the salt. More oil droplets were captured by NaCas at high temperatures due to the raised surface activity and shortened IFT equilibrium time. Factorial analysis showed that four individual factors (temperature, salinity, humic acid, and NaCas content) and three interactions (temperature × salinity, temperature × NaCas, and humic acid × NaCas) significantly affected the oil removal. Biotoxicity experiments revealed that NaCas could offset the inhibitory effect of oil on the photosynthesis of algae and thus promote algae growth. Notably, thermal treatment and biodegradation can be environmentally friendly methods for the post-treatment of the NaCas/oil precipitate. The use of NaCas-assisted responsive separation in the treatment of washing effluents can help achieve a sustainable shoreline oil spill response.

CHAPTER 8 A DUAL FUNCTIONAL AND SELF-POWERED WASHING FLUID FOR SHORELINE OIL SPILL RESPONSE

8.1 Background

The gigantic petroleum exploration and production are creating a huge marine environmental crisis, threatening the lives and well-being of people and other species (Sachs et al., 2019; Safaei et al., 2022; Yue et al., 2020). The spilled oil often reaches the shoreline, resulting from the push of winds and currents. Oil forms thick layers and covers beaches that serve as homes to a sea of wildlife and provide public recreation throughout the world (Bi et al., 2022). As a consequence, effective cleanup strategies for oiled shoreline cleanup are of fundamental significance.

Surface washing is an effective strategy to decontaminate oiled shorelines by enhancing the oil miscibility in surface washing fluid (Chen et al., 2021b; Yue et al., 2022a). Typically, surface washing agents (SWAs) are sprayed on stranded oil for a specific duration, followed by water flushing to remove the oil. However, the application of SWAs has been limited due to reasons such as the absence of operational guidelines and potential toxicity. Fortunately, environmentally friendly surface washing fluids have recently been developed and demonstrated as a promising alternative for protecting oiled shorelines. For instance, the Nanoclay/surfactant complex and magnetite dispersion were designed for treating oil-affected shorelines (Bi et al., 2021b; Yue et al., 2022b). Sodium caseinate, a food-grade material, has been successfully employed as a washing fluid for the effective decontamination of sand and peat moss (Yue et al., 2022d; Yue et al., 2022f). Although these findings are encouraging, it is expected to further improve the washing performance through the involvement of multiple oil removal mechanisms simultaneously.

Chemical oxidation methods, e.g. advanced oxidation process, electrocatalysis, and photocatalysis, are of power for wastewater remediation (Ma et al., 2022; Wang et al., 2022b; Yang et al., 2017; Yue et al., 2021a; Yue and Rahaman, 2021a), yet they heavily rely on the input of energy sources (e.g. light and electricity) and raise health concerns. For instance, SO_4^{2-}-based oxidation can produce toxic hydrogen sulfide (H_2S) after catalytic processes (Betterton and Hoffmann, 1990; Dong et al., 2021). Therefore, it is necessary to seek a self-powered and sustainable oxidation path that can harness energy from the environment to decontaminate oiled shorelines. Various energy sources can be collected from the natural environment, such as thermal, biological, and mechanical energy. Notably, surface washing with vigorous water motions can sustainably produce mechanical energy. This motivates the question of how to take further advantage of mechanical energy in surface washing. In other words, can the water motion be made use of both physically and chemically in oiled shoreline cleanup? Nanogenerator can convert mechanical energy into electricity and has been implemented in water splitting (Tang et al., 2015b), seawater desalination (Wang et al., 2019a), and water and air purification (Chen et al., 2015; Yang et al., 2013b). Piezoelectric is one of the types of nanogenerators, which is a recently emerging area that potentially enables green advances in catalytic processes independent of energy source investment (Jin et al., 2019; Kubota et al., 2019). The piezo-potential induced by external stress can generate an electric field that is effective for transferring electrons and holes and thus initiating reactive oxygen species (ROSs) generation (Bößl and Tudela, 2021; Tu et al., 2020). Therefore, pizeocatalysis is a bridge to transfer ceaseless mechanical energy to chemical energy and thus triggers redox reactions.

Research about piezocatalyst development has been in no small part steeped in two-dimensional sheets of molybdenum disulfide (MoS_2) (Huo et al., 2022; Ma et al., 2021a; Nie et al., 2022; Ren

et al., 2021). MoS_2 attracts great interest owing to its strong ferroelectricity, easy deformation, and its ability to tolerate remarkable pressure (Rahmatinejad et al., 2022; Wu et al., 2014; Zhu et al., 2015a). Significantly, MoS_2 has displayed good biocompatibility and low toxicity, which facilitate its application in the biomedical area (Liu and Liu, 2018; Liu et al., 2014; Yin et al., 2016). In this study, single- and few-layer MoS_2 was used as a piezoelectric surface washing fluid to clean up oiled sand. Unlike traditional chemical methods, this system harvested mechanical energy from water shaking to activate piezocatalytic treatment of oiled sand and to accomplish self-powered surface washing. Characterizations were conducted to investigate the property of MoS_2. The washing performance of MoS_2 fluid was studied under different environmental conditions. Importantly, the mechanism of surface washing was elucidated through various approaches, and degradation products were also analyzed. The present study provides new insights into the utilization of ambient water motion to achieve surface washing both physically and chemically.

8.2 Materials and methods

8.2.1 Materials

Engine oil (15W40) was used as the representative oil for testing. *n*-hexane, sodium molybdate dihydrate ($Na_2MoO_4 \cdot 2H_2O$), thiourea (CH_4N_2S), hydrochloric acid (HCl), NaCl, ethanol, p-benzoquinone (p-BQ), *tert*-butanol (TBA), triethanolamine (TEOA), and L-histidine (L-his) were purchased from Sigma Aldrich (Oakville, Canada). 5,5-dimethyl-1-pyrroline-n-oxide (DMPO) and 2,2,6,6-tetramethyl-4-piperidinol (TEMP) were obtained from Fisher Scientific (Canada). Standard calcinated sand was obtained from Sigma Aldrich (Oakville, Canada). Ultrapure (UP) water (18 MΩ) was used throughout the experiments.

8.2.2 Synthesis of MoS_2

MoS_2 was synthesized according to a "bottom-up" hydrothermal method (Su et al., 2018). Typically, $Na_2MoO_4 \cdot 2H_2O$ and CH_4N_2S, with a molar ratio of 1:5, were dissolved in UP water at room temperature (21 ± 1 ℃) under vigorous agitation. Subsequently, the solution was acidized using HCl until its pH was less than 1, followed by agitation for 60 min. The mixture was poured into a Teflon-lined stainless steel autoclave and was heated at 200 ℃ for 24 h. Once the autoclave naturally cooled to the ambient temperature, the slurry products were separated by centrifugation, followed by washing with UP water and ethanol three times and vacuum drying at 60 ℃ for 24 h.

8.2.3 Preparation of oil-contaminated sand

Oil-contaminated sand was prepared by mixing 0.2 g of engine oil with 1 kg of clean sand. Subsequently, *n*-hexane was added to the mixture to uniformly distribute engine oil. The oil-contaminated sand was obtained when the *n*-hexane was completely evaporated at room temperature.

8.2.4 Surface washing experiments

MoS_2 fluid was prepared by sonicating different amounts of MoS_2 in UP water to obtain mono- and few-layer of MoS_2. Vials each containing 1 g of oil-contaminated sand and 15 mL of MoS_2 washing fluid were shaken in a shaker (Innova 42R Incubator Shaker, USA) at 300 rpm and 20 ℃ for 24 h. The washing wastewater was decanted, followed by gentle rinsing using UP water and overnight drying at 60 ℃ to remove the remnant washing fluid. Then, the residual oil was extracted using 15 mL of *n*-hexane at 300 rpm and 20 ℃ for 24 h. The oil concentration was detected by using an Agilent Cary UV-Vis spectrophotometer (3500, USA) at a wavelength of 284 nm.

8.2.5 Quenching experiments

To avoid the impact of scavengers on oil removal in surface washing processes, quenching experiments of reactive species were conducted by measuring oil concentration in oil-in-water emulsions. The oil-in-water emulsion was prepared by vigorously stirring engine oil and UP water using a homogenizer (Ultra-Turrax T25, IKA, Germany) at 12,000 rpm for 30 min. Subsequently, a mixture containing emulsion (15 mL), MoS_2, and a scavenger was sealed in vials and shaken at 300 rpm and 20 ℃ for 24 h. Then, the oil in the mixture was extracted at 300 rpm and 20 ℃ for 24 h by adding the mixture (2 mL) and n-Hexane (15 mL) in vials. The oil concentration was detected using Gas Chromatography (GC 8890, Agilent Technologies Co., Ltd., USA) (Qu et al., 2022).

8.2.6 Analytical and characterization methods

The average particle size was measured by using a Zetasizer (Malvern, USA). Interfacial tension (IFT) was measured with a KRUSS force tensiometer (K100, Germany). Transmission electron microscopy (TEM) images were obtained on a Thermo Scientific Talos F200X G2 S/TEM). X-ray photoelectron spectroscopy (XPS) characterization was performed on a Thermo Scientific K-Alpha spectrometer, and attenuated total reflectance fourier transform infrared (ATR-FTIR) spectra were obtained on an ATR-FTIR spectrometer (INVENIO, Bruker, Germany). X-ray diffraction (XRD) measurements were conducted on a Bruker D4 X-ray diffractometer Electron paramagnetic resonance (EPR) and spectra were recorded on an Elexsys E580 spectrometer (Bruker, Germany). The composition of the degradation products was analyzed using Gas Chromatography–mass spectrometry (GC 7890/5977, Agilent Technologies Co., Ltd., USA) equipped with an HP−5MS capillary column (30 m × 250 μm × 0.25 μm). The oven temperature was at 50 ℃ for 5 min, then

ramped to 250 ℃ at 2 ℃/min for 15 min, and finally to 300 ℃ at 10 ℃/min for 10 min. The injection volume is 1.0 μL.

8.3 Results and discussion

8.3.1 Characterization of MoS_2

The XRD pattern of the MoS_2 (Figure 8.1a) exhibited three diffraction peaks at 13.2 °, 33.0 °, and 57.5 °, corresponding to the (002), (100), and (110) peaks, respectively (Xie et al., 2013). The low intensity of the (002) peak indicated the presence of few-layer structures of MoS_2 (Sathiyan et al., 2015; Wang et al., 2014). The ATR-FTIR result of MoS_2 is shown in Figure 8.1b. The bands at 673, 891, 1015, 1099, and 1398 cm^{-1} were characteristic bands of MoS_2 (Ali et al., 2020; Liu et al., 2014). The band at 494 and 928 cm^{-1} was attributed to the S-S bond (Lalithambika et al., 2019). XPS analysis was conducted to investigate the chemical states of Mo and S in the products (Figure 8.1c and d). The high-resolution XPS spectra of Mo 3d display two 1T phase peaks at 231.5 and 228.3 eV, and two 2H phase peaks at 232.7 and 229.6 eV (Lin et al., 2022; Rahmatinejad et al., 2023). Two peaks at 162.4 and 161.2 eV in S 2p spectra are the characteristics of spin-orbit S 2p1/2 and S 2p3/2 of 1T MoS2, respectively, and two peaks at 161.8 and 163.2 eV reveal 2H MoS_2 (Lin et al., 2022). All these results prove the 1T/2H mixed-phase MoS_2.

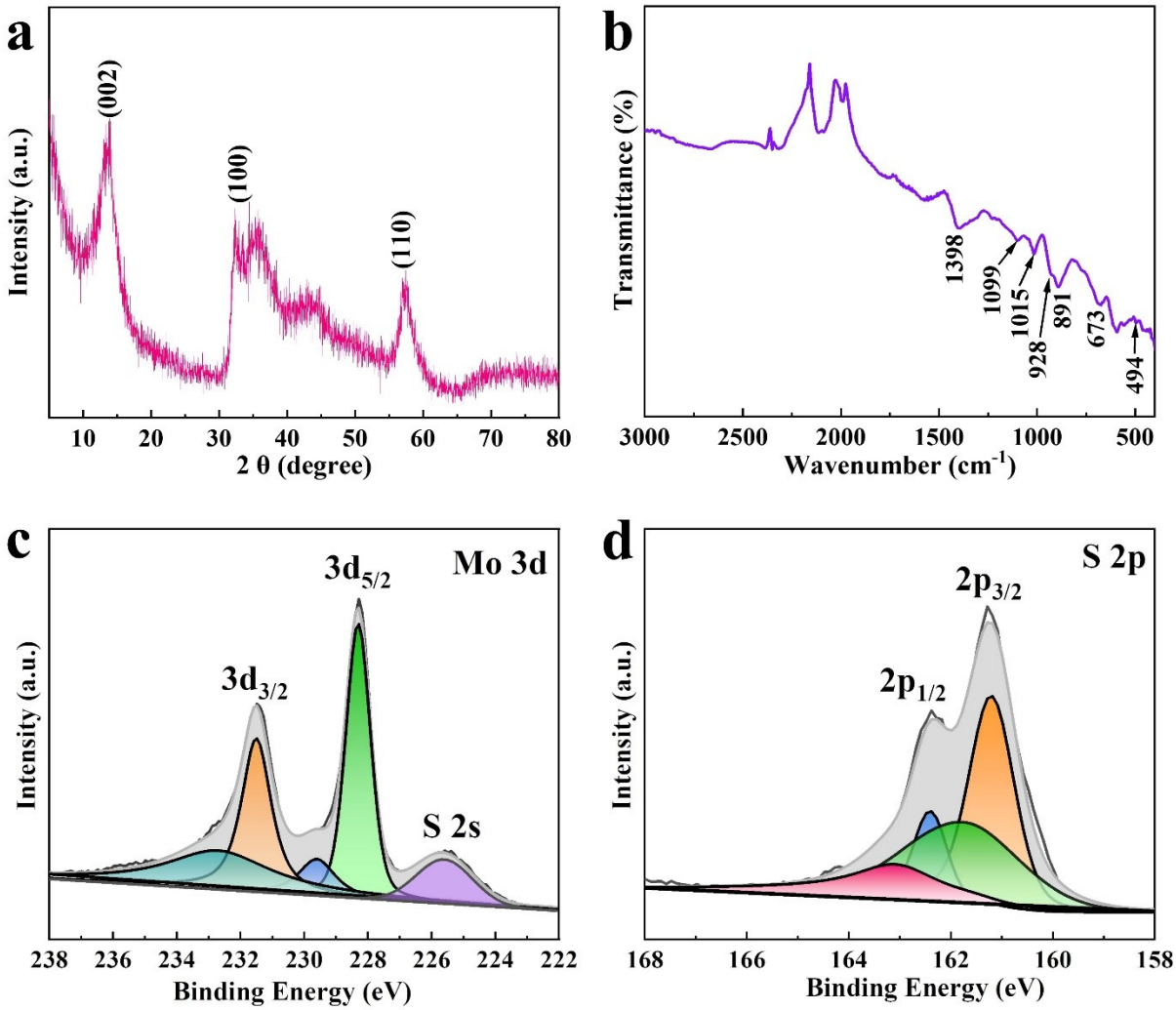

Figure 8.1 (a) XRD, (b) ATR-FTIR, (c) and (d) XPS results of the MoS_2.

TEM images show that MoS_2 has a layer structure, revealing lamellar and irregular edges (Figure 8.2). High-resolution TEM images further confirmed the presence of single-layer and few-layer structures of MoS_2 (Figures 8.2a-c). UV-Vis spectrum (Figure 8.2d) was also implemented to investigate the layer structure of MoS_2 dispersion. The adsorption peaks at 616 and 660 nm represented the direct transition at the K point of the Brillouin zone (Castellanos-Gomez et al., 2016; O'Neill et al., 2012). The absorption peaks at 396 and 486 nm reflect a direct excitonic transition from the deep valence to the conduction band (Gopalakrishnan et al., 2014; Su et al.,

2018). These adsorption peaks provide evidence for the existence of monolayer and few-layer MoS_2. The piezoelectricity of MoS_2 was studied by Zhu et al. (2015a), who found that MoS_2 had a thickness-dependent piezoelectric coefficient and observed a piezoelectric response for odd-layer MoS_2 nanosheets.

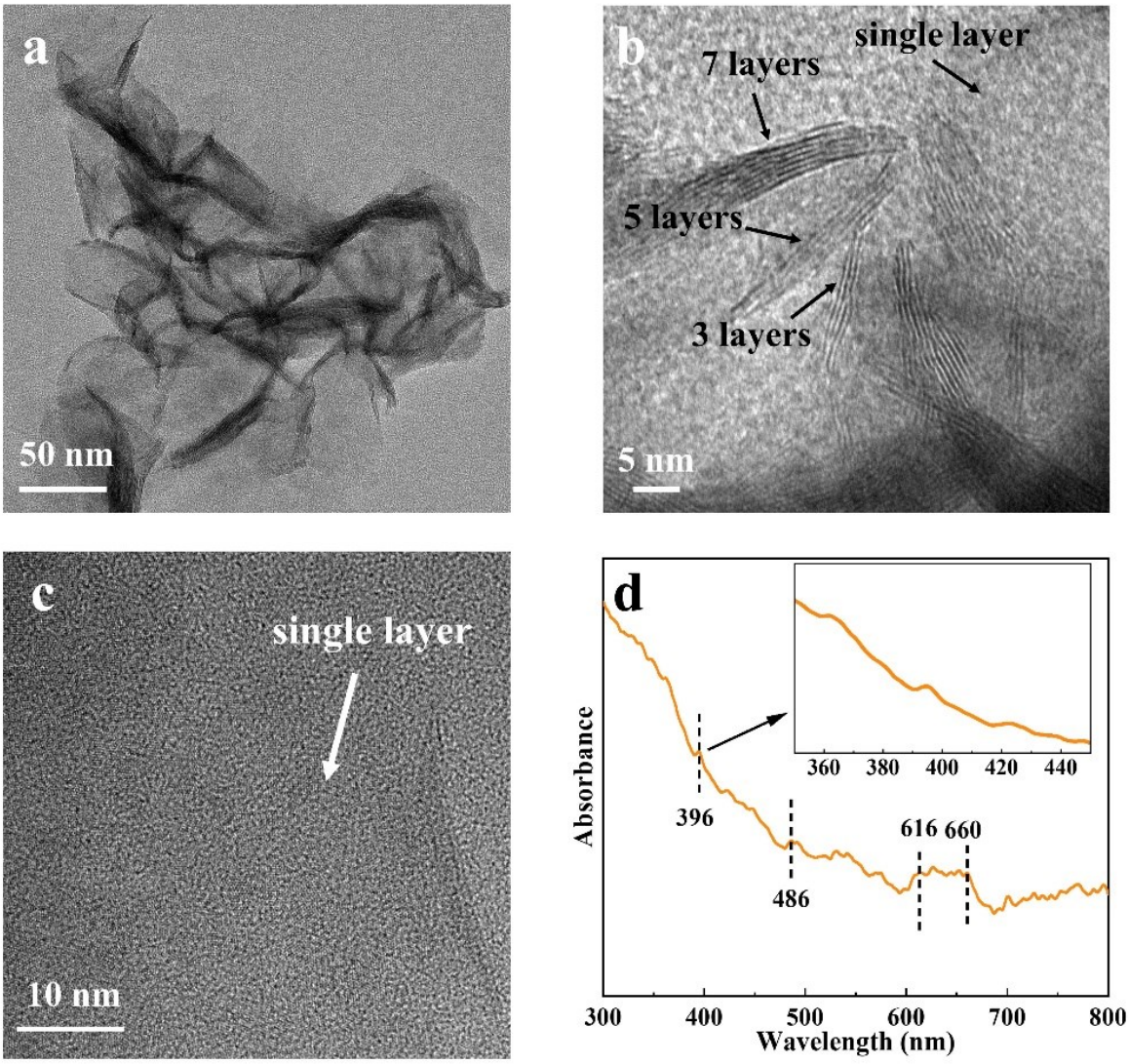

Figure 8.2 (a-c) TEM images and (d) UV-Vis spectrum of the MoS_2.

8.3.2 Effect of MoS2 concentration on oil removal

The oil removal efficiency in terms of MoS_2 concentration is shown in Figure 8.3a. The curve slopes upward with the increasing MoS_2 concentration, gradually rising from 63.5% at 0.02 g/L to 74.5% at 1.0 g/L. On the one hand, high MoS_2 concentration has high interfacial activity, as proved by the IFT-concentration curve in Figure 8.3a. Increased concentration led to lower IFT of the MoS_2 washing fluid. It might be due to the thickness-dependent wettability of MoS_2. Gaur et al. (2014) proved that the hydrophobicity of MoS_2 increased with decreasing its layer amounts. The mechanism, theoretically revealed by Guo et al. (2016) using density functional theory, was that the surface energy of MoS_2 declined with the decreasing number of layers. Hence, the hydrophobic-hydrophobic interaction between MoS_2 and oil facilitated the oil removal. On the other hand, high MoS_2 concentration can provide more active sites and thus generate more reactive species to attack oil pollutants.

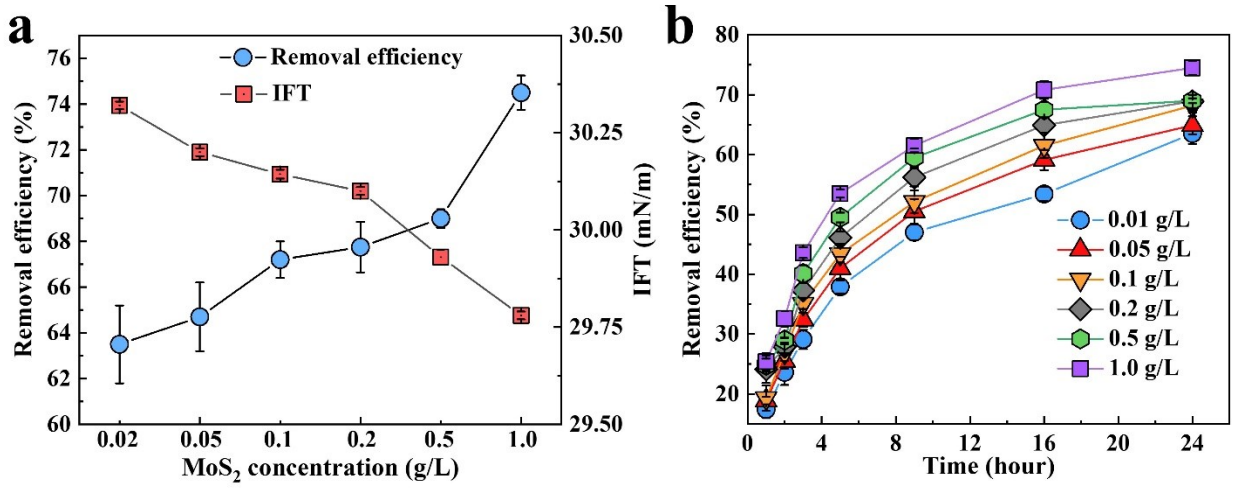

Figure 8.3 Effect of (a) MoS_2 concentration and (b) washing time on the oil removal.

8.3.3 Effect of washing time on oil removal

The washing performance was observed to be dependent on the washing time. Figure 8.3b displays the effect of washing time on oil removal efficiency at different MoS_2 concentrations in the washing fluid. Each curve slopes upward steeply in the initial stage of surface washing, indicating a high oil removal rate, followed by gradually reduced slopes with the increase of washing time. Taking 0.1 g/L of MoS_2 as an example, oil removal increased from 26.9% to 58.3% from 2 to 9 h, after which increased slowly to 68.2% in the following 15 h. These results demonstrated that the MoS_2 washing fluid became less efficient with increasing washing time. During the early stage, the abundant active sites on MoS_2 facilitated the rapid removal of oil from the sand surface. However, as more oil was removed, on the one hand, the oil in the washing fluid had the potential to reattach to the sand surface. On the other hand, oil might be adsorbed on the MoS_2, occupying its edge sites. When subjected to mechanical energy, mono- and few-layer MoS_2 created a piezoelectric polarization, leading to the separation of electrons and hole pairs, and subsequently migrating to an opposite direction (Wu et al., 2016). The polar water molecules reacted with positive and negative charges that were localized on the active edge sites to generate ROSs (Wu et al., 2018). When the edge sites were occupied by oil droplets, their strong hydrophobicity prevented water molecules from contacting the MoS_2, thus reducing the amount of ROSs. Additionally, it was also observed that high MoS_2 concentrations gave rise to a high removal rate during the initial stage of oil removal.

8.3.4 Effect of salinity on oil removal

The salinity of the surface of the marine environment varies from region to region, which is usually in the range of 3.3 wt% to 3.7 wt%. Some ocean environments have higher or lower salinity because

of the unique climate and hydrology conditions (Yue et al., 2023). In this study, a range of salinity was selected to test its impact on washing performance. The washing performance of MoS_2 fluid, as shown in Figure 8.4a, was affected by salinity. Overall, the salinity favored oil removal but displayed different extents at different salinities. Oil removal efficiency peaked at 80.1% at a salinity of 0.1 wt%, after which declined gradually and with increasing salinity. Two aspects might enhance the oil removal in the presence of salinity. Firstly, chlorine ions (Cl^-) can generate reactive chlorine species through eqs 1-6 (Guo et al., 2022; Khajouei et al., 2022; Sun et al., 2016), which further contributes to oil removal. Secondly, salinity facilitated the growth of oil-particle aggregates (OPA) that are stable over periods of weeks (Le Floch et al., 2002). Prior research has shown that OPA plays a beneficial role in expediting the removal of oil from shoreline sediments (Bragg and Yang, 1995). Consequently, in this study, the formation of OPA enhanced the dispersion of oil droplets within the washing fluids, effectively preventing their reattachment to the sand.

$$Cl^- + OH^- \rightarrow \bullet HClO^- \quad \text{(eq 1)}$$

$$Cl^- + \bullet OH^- \leftrightarrow \bullet HClO^- \quad \text{(eq 2)}$$

$$\bullet HClO^- + H^+ \rightarrow \bullet Cl + H_2O \quad \text{(eq 3)}$$

$$Cl^- + \bullet Cl \rightarrow \bullet Cl_2^- \quad \text{(eq 4)}$$

$$Cl_2^- + OH^- \leftrightarrow \bullet HClO^- + Cl^- \quad \text{(eq 5)}$$

$$Cl_2^- + H_2O \rightarrow \bullet HClO^- + H^+ \quad \text{(eq 6)}$$

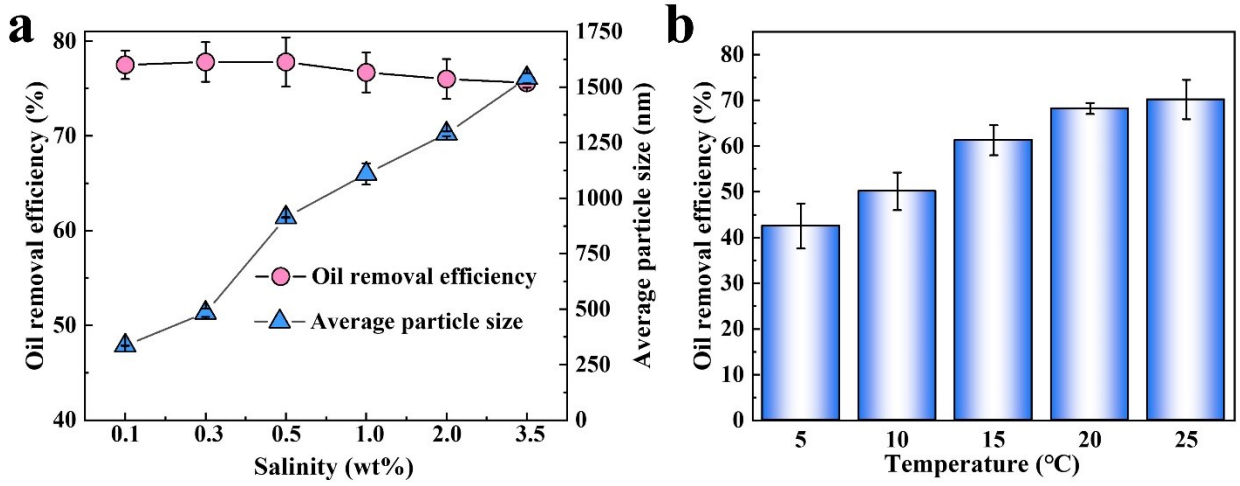

Figure 8.4 Effect of (a) salinity and (b) washing temperature on the oil removal.

With increasing salinity came the salinity-promoted enhancement in oil removal gradually attenuated. This can be attributed to the increasing aggregation of MoS_2 in high salinity conditions, as shown in Figure 8.4a which displays the size of MoS_2 in saline washing fluids. The average size of MoS_2 increased remarkably from 335.5 to 1540.5 nm in saline surface washing fluids. The aggregation of mono- and few-layers MoS_2 could inhibit its piezoelectricity owing to the opposite orientations of neighbored atomic layers (Wu et al., 2014). Wu et al. (2014) observed that the piezoelectricity of MoS_2 decreased with the increasing number of its odd layers and eventually disappeared in the bulk phase. These findings suggested that when it comes to the practical application of MoS_2, the use of seawater as an alternative for washing oiled sand holds promise. This approach can conserve water resources and alleviate water scarcity concerns.

8.3.5 Effect of temperature on oil removal

Temperature plays a key role in affecting the transport behavior of pollutants (An et al., 2010; Huang et al., 2022; Valikhan Anaraki et al., 2022). The washing performance of the MoS_2 fluid

regarding the temperatures is shown in Figure 8.4b. The MoS_2 fluid was more efficient for the cleanup of the oiled sands at higher temperatures, removing 42.5% of oil at 5 ℃ and 70.2% of oil at 25 ℃. As the washing temperature rose the oil viscosity decreased, leading to the lower energy required to break oil into small droplets and decreased adhesion force between sand and oil. This could facilitate the release of the attached oil. The small oil droplets also likely increased the contact area and collision with ROSs and thereby promoted the chemical oxidation of the oil. Moreover, it was reported that the increase in temperature increased the negative surface charge of silica, resulting in the greater electrostatic repulsion between oil and sand and thus inhibiting the re-attachment of oil.

The weak enhancement in oil removal at 25 ℃ was observed, increasing merely by 2.0% compared to 20 ℃. This might be a result of the inhibited piezoelectric potential caused by the "screening effect". Sohn et al. (2019) found that monolayer MoS_2 had a temperature-dependent piezoelectric effect. The generated piezoelectric charges were offset due to the plenty of thermally-existed electrons in the MoS_2 monolayer at high temperatures. Thus, the inhibited piezoelectric effect produced fewer ROSs to remove oil. A recent study by Wang et al. Wang et al. (2023) displayed similar results that the piezocatalysis performance of MoS_2 was enhanced from 10 to 25 ℃ but inhibited at 30 to 50 ℃.

8.3.6 Reusability and mechanism

Repetitive tests were carried out to evaluate the reusability of the MoS_2 washing fluid. After each cycle, MoS_2 was separated and re-dispersed in UP water. As depicted in Figure 8.5a, water rinsing for MoS_2 plays a positive role in maintaining the reusability of MoS_2. Specifically, the oil removal

efficiency decreased stepwise to around 58.0% after 5 cycles without water rinsing. The weakened washing performance might be due to the adsorption of oil on the active sites of MoS_2. After rinsing the used MoS_2 with UP water, it exhibited better surface-washing performance than its counterpart without UP water rinsing. Significantly, the ATR-FTIR spectrum of the used MoS_2 (Figure 8.5b) barely changed, underscoring the stability of chemical groups throughout the surface washing processes.

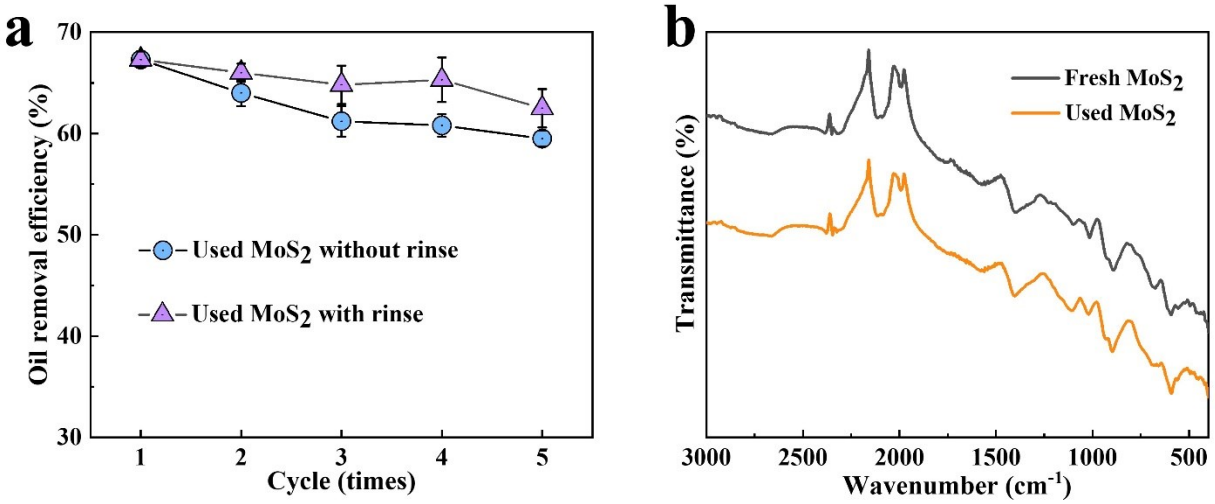

Figure 8.5 (a) reusability and (b) ATR-FTIR spectra of the MoS_2.

The addition of chemical scavengers is able to effectively eliminate the contribution of the corresponding radicals when the scavengers are used. The inhibition of pollutant degradation upon the existence of a scavenger indicates the crucial role of the matching radical in the degradation process. Hence, quenching experiments were implemented to identify the reactive species and their relative contributions to oil removal. p-BQ and L-his are effective for quenching superoxide anion radical ($O_2 \cdot^-$) and singlet oxygen ($^1O_2$), respectively (Du et al., 2020; Luo et al., 2019). TBA and TEOA were used as scavengers of hydroxyl radicals (•OH) and holes (h^+), respectively (Du et al., 2020; Yue et al., 2021a). Given the influence of scavengers on oil/water interfacial tension that

matters in surface washing, testing oil concentration in oil-in-water emulsions was used as an alternative approach to investigate the impact of different reactive species. As depicted in Fig. 6a, the normalized oil removal efficiency was reduced by 0.18 in the presence of TBA, implying a minor contribution of •OH in the piezocatalysis. When $•O_2^-$ and holes were captured by p-BQ and TEOA, respectively, the normalized removal moderately decreased to 0.659 and 0.442, proving that $•O_2^-$ and holes were contributors to oil removal. Oil removal was significantly inhibited when L-his was added, suggesting the dominant role of $^1O_2$ in oil removal. Overall, $^1O_2$ played a more crucial role in oil removal than $•O_2^-$, •OH, and holes.

EPR measurement was carried out to further investigate the generation of reactive species in the MoS_2-based surface washing process. The oxidation of TEMP by $^1O_2$ produces paramagnetic TEMPO, which displayed characteristic strong triplet signals on the EPR spectrum (Figure 8.6b), indicating its domination in reactive species. DMPO-$•O_2^-$ displayed relatively weak intensity, suggesting the existence of $•O_2^-$ (Figure 8.6c). The DMPO-•OH signal exhibited further weak intensity (Figure 8.6d), likely owing to either the limited number of •OH in the piezocatalytic surface washing or its transformation to other species (Pan et al., 2018). It is noteworthy that other peaks indicated by purple triangles were assigned to the carbon center radicals, due to the reaction between DMPO and $•O_2^-$ (Xu et al., 2018a). These results demonstrated that shaking is a necessary initiator to trigger the piezocatalytic process, and they align well with the quenching experiments.

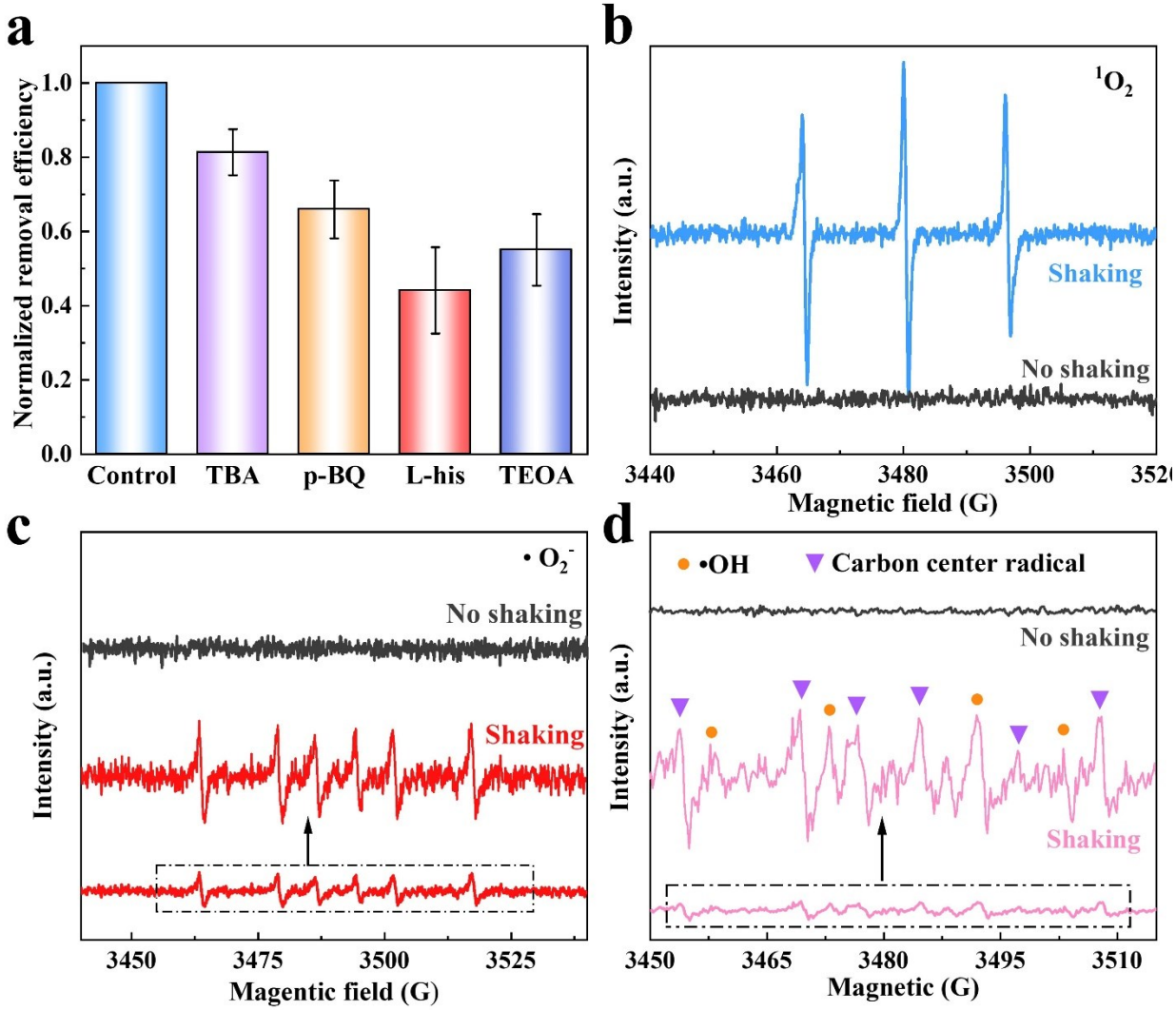

Figure 8.6 (a) oil removal at different quenching chemicals, EPR spectra of (b) 1O2, (c) •O2-, and (d) •OH.

Based on the above discussions, Figure 8.7 depicts the reaction mechanism involved in these experimental results. The electrons (e^-) and holes (h^+) are separated by piezoelectric under external water motion (eq 7). The electrons react with dissolved oxygen to form $•O_2^-$ (eq 8). Water molecules touched holes to generate •OH (eq 9). The $•O_2^-$ can produce $^1O_2$ via combining with H^+, •OH, or h^+ as in eqs 10-12 (Fotiou et al., 2016; Yue et al., 2021a). These highly reactive species

subsequently degrade oil pollutants, and the dissociation of hydrogen peroxide (H_2O_2) may occur rapidly according to eqs 13-14 (Mitchell et al., 2014).

MoS_2 + water agitation $\rightarrow$ $MoS_{2\ piezo}$ (e^- and h^+) (eq 7)

$O_2 + e^- \rightarrow \bullet O_2^-$ (eq 8)

$H_2O + h^+ \rightarrow \bullet OH + H^+$ (eq 9)

$\bullet O_2^- + \bullet OH \rightarrow {}^1O_2 + OH^-$ (eq 10)

$\bullet O_2^- + h^+ \rightarrow {}^1O_2$ (eq 11)

$2\bullet O_2^- + 2H^+ \rightarrow H_2O_2 + {}^1O_2$ (eq 12)

$H_2O_2 + \bullet OH \rightarrow \bullet HOO + H_2O$ (eq 13)

$\bullet HOO \rightarrow \bullet O_2^- + H^+$ (eq 14)

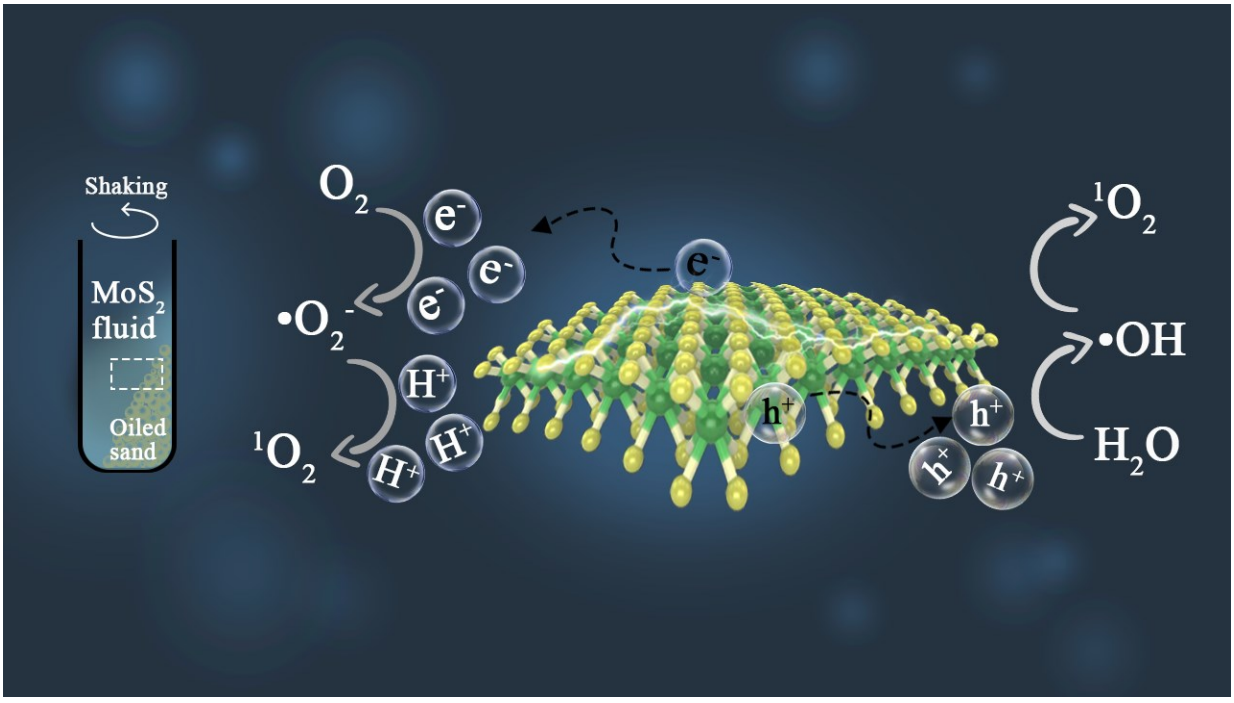

Figure 8.7 Schematic illustration of self-powered surface washing and reaction mechanism of MoS2 piezocatalysis.

The possible components of the piezocatalytic surface washing were investigated using GC-MS, as depicted in Figure 8.8, Tables 8.1, and 8.2. The raw engine oil primarily consists of high molecular weight hydrocarbons (HMWHs) along with some low molecular weight hydrocarbons (LMWHs). After undergoing catalytic surface washing, the relative proportions of different hydrocarbons were altered. There was a significant decrease in peak abundance within the retention time range of 80-125 min, with several peaks disappearing altogether. Notably, the GC-MS results revealed that the percentage of LMWHs increased, indicating the cracking of HMWHs compounds such as nonadecane, tricosane, and tetracosane into LMWHs and thus leading to a narrower carbon distribution. These findings provide evidence that chemical oxidation played a role in the MoS_2 fluid-assisted surface washing process.

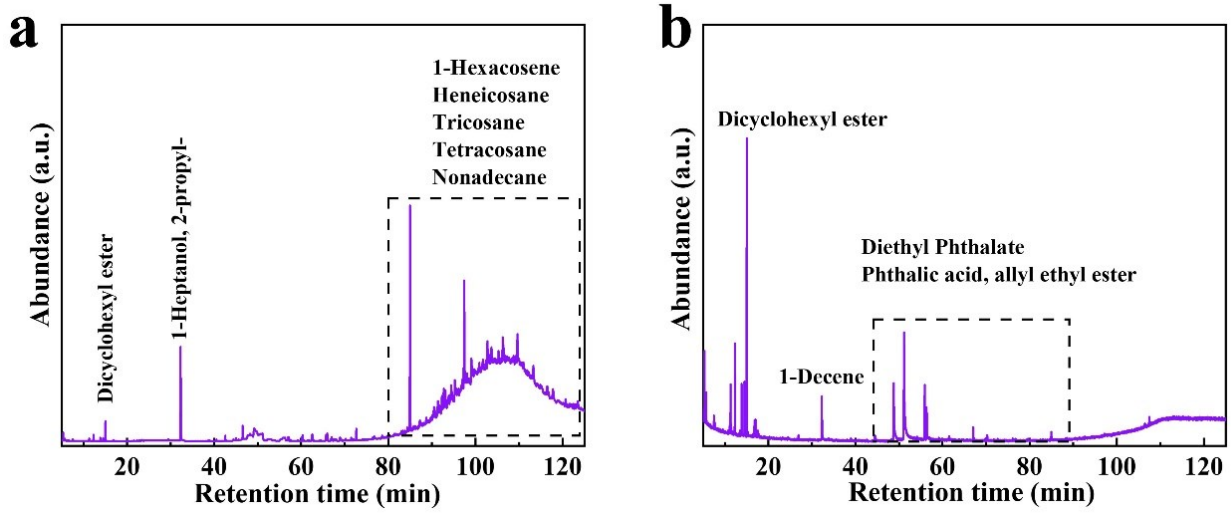

Figure 8.8 GC-MS chromatography and possible components of (a) raw engine oil and (b) products after surface washing.

Table 8.1 Possible components of raw engine oil

Retention time (min)	Name
15.034	Oxalic acid
	Dicyclohexyl ester
	Cyclohexyl octyl ester
32.318	1-Heptanol, 2-propyl-
	Oxalic acid
	cyclobutyl dodecyl ester
46.562	Phenol
	2 4-bis(1 1-dimethyl ethyl)-phenol
	4'-Diethylaminoacetanilide
72.641	7,9-Di-tert-butyl-1-oxaspiro(4,5)deca-6,9-diene-2,8-dione
	2,5-Cyclohexadien-1-one
85.006	1,1'-Biphenyl
	1,3-Diphenyl-2-aza fluorene
	(4-benzyl-1-piperidyl)(2-phenylcyclopropyl)-Methanone
	5-(1-Naphthyloxymethyl)-3-phenyl-2-oxazolidone
90.471-117.8	1-Hexacosene
	1-Nonadecene
	1-Iodo-2-methyl-undecane
	11-butyl- Docosane
	1,54-dibromo- Tetrapentacontane
	2-methyl-1-Hexadecanol
	Heneicosane

3,5,3',5'-Tetramethylbiphenyl

4,4'-(1,2-ethenediyl)bis- Benzenamine

2,2'-Bithiophene-5-carboxylic acid

Benzo[c]cinnoline-2-carboxylic acid

9H-Carbazol-3-amine, 9-ethyl-

Thiophene-2-carboxylic acid

(1-methyl piperidine-4-yl)amide

(E)-3-Octadecene

(E)-5-Octadecene

Tricosane

Imidazo[4,5-e][1,4]diazepin-5(1H)-one

1-Bromodocosane

Z-14-Nonacosane

Cyclohexanol, 2-[2-pyridyl]-

Tetracosane

Hexacosane

Nonadecane

Bacchotricuneatin c

Table 8.2 Possible components of the products after surface washing

Retention time (min)	Name
15.05	Propanedinitrile, dicyclohexyl-
	2-Heptene, 5-ethyl-2,4-dimethyl-
	Dicyclohexyl ester
32.302	Oxalic acid
	1-Decene
56.898	Diethyl Phthalate
	Phthalic acid, allyl ethyl ester
	Phthalic acid, ethyl pentadecyl ester
	1-Methyl-3-methyl adamantane
	Benzothiazole, 2-methyl-

8.4 Summary

This study presents a self-powered piezocatalytic washing process that achieves both physical and chemical decontamination of oiled sand. MoS_2 exhibited single- and few-layer structures, which helped initiate piezocatalysis. MoS_2 washing fluid can physically remove the oil by decreasing the IFT of the fluid. During the surface washing, the water motion triggered MoS_2 to generate piezoelectric potential, thus driving the migration of free charges. Those charges reacted with dissolved oxygen and water to produce ROSs including $^1O_2$, $\bullet O_2^-$, and •OH, which played a crucial role in the degradation process, leading to the conversion of HMWHs to low LMWHs. The washing performance of the MoS_2 fluid depended on the operational conditions. The oil removal efficiency was increased with MoS_2 concentration, washing temperature, and time. Low salinity was found

to enhance washing performance more than that of high salinity. The MoS_2 showcased high stability after five reuse cycles. This study presents an innovative approach to surface washing by harnessing green energy, thereby revealing the untapped potential of piezoelectric materials for the cleanup of oiled shorelines.

CHAPTER 9 CONTRIBUTIONS AND SIGNIFICANCE OF THESIS RESEARCH, AND SUGGESTIONS FOR FUTURE WORK

9.1 Contributions and significance of thesis research

Surface washing is a powerful technique to remove hazardous pollutants from shorelines. However, the toxicity and reuse of the SWAs and disposal of wastewater treatment are a matter of concern. To address these concerns, eco-friendly nanomaterials were used to prepare stimuli-responsive surface washing fluids for advancing shoreline oil spill response.

The contributions and significance of this thesis research lie in the following aspects: (1) synthesizing environmentally sustainable surface washing materials, such as nanoclay/sodium alginate, NaCas, Fe_3O_4, and MoS_2; (2) systematically evaluating the efficacy of surface washing fluids across various environmental conditions, stimuli-responsive behavior of the washing effluent and the biotoxicity of the surface washing fluid, examining of post-treatment procedures for washing sludge, encompassing both biodegradation and incineration methodologies; and (3) designing a self-powered and sustainable piezocatalytic surface washing fluid to remove oil.

(1) Synthesis of eco-friendly nanomaterials

A range of surface washing fluids have been effectively synthesized and characterized, each demonstrating high oil removal capabilities (60% – 80%) and significant potential for real-world applications. For instance, the carboxyl-functionalized Fe_3O_4, synthesized through a straightforward solvothermal method, offers abundant active sites for efficient oil removal, while also exhibiting good reusability after 5 cycles and cost-effectiveness (0.486 CAD/oil g).

Furthermore, the amphiphilic nature of NaCas renders it highly effective in washing oiled sand (approximately 65%), underscoring its practical utility.

(2) Performance evaluation, biotoxicity analysis, and posttreatment.

The effectiveness of the surface washing materials has been methodically examined across pertinent environmental conditions, such as salinity and temperature. Utilizing stimuli-responsive behavior offers a promising avenue for the pretreatment of washing effluent, yielding a clear supernatant characterized by low oil concentrations (20 mg/L) and turbidity (0.08 NTU). For instance, through pH adjustment of the washing effluent to approximately 4.4, NaCas swiftly segregates from the mixture, effectively capturing oil and other organic constituents. This process results in a clean supernatant with reduced COD (from 458.9 to 193.2 mg/L) and TOC (from 70 to 28.9 mg/L) levels. Toxicity analysis further corroborates that these fluids possess the capability to mitigate oil-induced toxicity among algae and select species. Moreover, the post-treatment of washing sludge, encompassing biodegradation and incineration, represents a suitable pathway for disposing of used washing sludge, thereby minimizing potential environmental hazards. MD simulations have additionally provided insights into the mechanism underlying oil removal.

(3) Sustainable catalytic washing fluid.

An innovative self-powered and sustainable piezocatalytic washing fluid has been effectively developed, and its efficacy in surface washing has been extensively investigated. The perpetual mechanical energy generated by water motion triggers the initiation of piezocatalytic processes, resulting in the generation of ROSs such as $\bullet O_2^-$, •OH. These ROSs play a pivotal role in breaking down oil into LMWH fragments with decreased toxicity.

9.2 Outlook for future work

Building upon the insights garnered from this thesis research, the following recommendations are put forth for future research in the realm of shoreline oil spill response:

(1) Subsequent research endeavors will concentrate on synthesizing responsive washing nanomaterials capable of releasing oil after responsive separation. Through adjustment of the oil/nanomaterial mixture parameters, the employed washing nanomaterials can undergo oil release, thereby enabling their reutilization across multiple cycles.

(2) A prospective avenue for exploration involves engineering piezocatalysts with heightened resistance to chlorine ions, which are pervasive in seawater. Given that seawater is readily available and cost-effective, its potential utilization as a solvent for formulating surface washing fluids could reduce operational expenses.

(3) In the coming phases, emphasis will be placed on devising piezocatalysts with enhanced amphiphilic properties, thereby augmenting their role in physical oil removal. Facilitating the detachment of oil from sand surfaces and dispersing it within the liquid phase as oil droplets is anticipated to accelerate the degradation rate.

JOURNAL PUBLICATIONS

[1] **R. Yue,** Z. Ye, B. Zhang, C. An, Z. Qu, S. Wan. Two birds with one stone: a dual-functional washing fluid for shoreline oil spill response. *ACS ES&T Engineering*. (Accepted)

[2] **R. Yue,** Z. Ye, S. Gao, Y. Cao, K. Lee, C. An, Z. Qu, S. Wan. Exploring the use of sodium caseinate-assisted responsive separation for the treatment of washing effluents in shoreline oil spill response. *Science of the Total Environment*. 2023, 873: 162363.

[3] **R. Yue,** C. An, Z. Ye, X Li, Q. Li; P. Zhang, Z. Qu; S. Wan. A pH-responsive phosphoprotein washing fluid for the removal of phenanthrene from contaminated peat moss in the cold region. *Chemosphere*, 2023, 313: 137389.

[4] **R. Yue,** C. An, Z Ye. X. Chen, K. Lee, K. Zhang, S. Wan, Z. Qu. Exploring the characteristics, performance, and mechanisms of a magnetic-mediated washing fluid for the cleanup of oiled beach sand. *Journal of Hazardous Materials*. 2022, 438: 129447.

[5] **R. Yue,** C. An, Z Ye. S. Gao, X. Chen, B. Zhang, K. Lee, H. Bi. A pH-responsive phosphoprotein surface washing fluid for cleaning oiled shoreline: Performance evaluation, biotoxicity analysis, and molecular dynamic simulation. *Chemical Engineering Journal*, 2022, 437: 135336.

[6] **R. Yue,** C. An, Z. Ye, E. Owens, E. Taylor, S. Zhao. Green biomass-derived materials for oil spill response: Recent advancements and future perspectives. *Current Opinion in Chemical Engineering*, 2022, 36: 100767.

[7] **R. Yue,** C. An, Z. Ye, H. Bi, Z. Chen, X. Liu, X. Zhang, K. Lee. A dual responsive nanoclay/sodium alginate surface washing agent for effective shoreline cleanup. *Environmental Research*, 2022, 205: 112531.

[8] **R. Yue,** MS. Rahaman. Hydrophilic and underwater superoleophobic porous graphitic carbon nitride (g-C_3N_4) membranes with photo-Fenton self-cleaning ability for efficient oil/water separation. *Journal of Colloid and Interface Science*, 2022, 608: 1960-1972.

[9] **R. Yue,** T. Chen, Z. Ye, B. Barbeau, MS. Rahaman**.** A photo-Fenton graphene oxide membrane with improved perm-selectivity and self-cleaning ability for efficient dye removal under visible light irradiation. *Journal of Water Process Engineering*, 2021, 44: 102443.

[10] **R. Yue,** B. Raisi, J. Rahmatinejad, Z. Ye, B. Barbeau, MS. Rahaman. A photo-Fenton nanocomposite ultrafiltration membrane for enhanced dye removal with self-cleaning properties. *Journal of Colloid and Interface Science*, 2021, 604: 458-468. [IF: 9.9]

[11] Z. Qu, C. An, **R. Yue**, H. Bi, S, Zhao. Assessment of the infiltration of water-in-oil emulsion into soil after spill incidents. *Science of the Total Environment.* 2023, 896: 165325.

[12] Z. Qu, C. An, Z. Mei, **R. Yue,** S. Zhao, Q. Feng, M. Cai, J. Wen. An experimental and modeling study on the penetration of spilled oil into thawing frozen soil. *Environmental Science: Processes & Impacts*, 2022, 24: 2398–2408.

[13] X. Chen, B. Hui, **R. Yue,** Z. Chen, C. An. Effects of Oil Characteristics on the Performance of Shoreline Response Operations: A Review. *Frontiers in Environmental Science*, 2022. 10: 1033909.

[14] Z.K. Chen, Q. Feng; **R. Yue,** Z. Chen, O. Moselhi, A. Soliman, A. Hammad, C. An. Construction, Renovation, and Demolition Waste in Landfill: A Review of Waste Characteristics, Environmental Impacts, and Mitigation Measures. *Environmental Science and Pollution Research*, 2022: 1-18.

[15] H. Bi, C. N. Mulligan, C. An, E. Owens, E. Taylor, J. McCourt, J. Yin, Q. Feng, X. Chen, and **R. Yue.** Development of a calcium alginate-cellulose nanocrystal-based coating to reduce the impact of oil spills on shorelines, *Journal of Hazardous Materials*, 2022,436 129228.

[16] H. Bi, C. An, C. Mulligan, K. Zhang, K. Lee, **R Yue.** Treatment of oiled beach sand using a green and responsive washing fluid with nonionic surfactant-modified nanoclay. *Journal of Cleaner Production*, 2021: 130122.

REFERENCES

Abbasi, A., Sohail, M., Minhas, M. U., Khaliq, T., Kousar, M., Khan, S., Hussain, Z., Munir, A., 2020. Bioinspired sodium alginate based thermosensitive hydrogel membranes for accelerated wound healing. Int. J. Biol. Macromol. 155, 751-765.

Afzal, M. Z., Yue, R. Y., Sun, X. F., Song, C., Wang, S. G., 2019. Enhanced removal of ciprofloxacin using humic acid modified hydrogel beads. J. Colloid Interface Sci. 543, 76-83.

Akmanova, A., Nurlan, N., Han, S., Lee, W., 2021. Advances in the enhanced removal of aqueous Hg (II) by metallic catalysts: a review. Curr. Opin. Chem. Eng. 33, 100704.

AlHammadi, M., Mahzari, P., Sohrabi, M., 2018. Fundamental investigation of underlying mechanisms behind improved oil recovery by low salinity water injection in carbonate rocks. Fuel 220, 345-357.

Ali, G. A., Thalji, M. R., Soh, W. C., Algarni, H., Chong, K. F., 2020. One-step electrochemical synthesis of MoS_2/graphene composite for supercapacitor application. J. Solid State Electrochem. 24, 25-34.

An, C., He, Y.-l., Huang, G.-h., Liu, Y.-h., 2010. Performance of mesophilic anaerobic granules for removal of octahydro-1, 3, 5, 7-tetranitro-1, 3, 5, 7-tetrazocine (HMX) from aqueous solution. J. Hazard. Mater. 179, 526-532.

An, C., Huang, G.-h., Wei, J., Yu, H., 2011. Effect of short-chain organic acids on the enhanced desorption of phenanthrene by rhamnolipid biosurfactant in soil–water environment. Water Res. 45, 5501-5510.

An, C., Huang, G., Yao, Y., Zhao, S., 2017. Emerging usage of electrocoagulation technology for oil removal from wastewater: A review. Sci. Total Environ. 579, 537-556.

Ancheyta, J., 2016. Deactivation of heavy oil hydroprocessing catalysts: fundamentals and modeling. John Wiley & Sons.

Asadpour, R., Sapari, N. B., Isa, M. H., Orji, K. U., 2014. Enhancing the hydrophobicity of mangrove bark by esterification for oil adsorption. Water Sci. Technol. 70, 1220-1228.

Asgari, M., Miri, T., Soleymani, M., Barati, A., 2021. A novel method for in situ encapsulation of curcumin in magnetite-silica core-shell nanocomposites: a multifunctional platform for controlled drug delivery and magnetic hyperthermia therapy. J. Mol. Liq. 324, 114731.

ASTM, Use of chemical shoreline cleaning agents: Environmental and operational considerations. American Society for Testing and Materials, West Conshohocken, PA, 2017.

Aveyard, R., Binks, B. P., Clint, J. H., 2003. Emulsions stabilised solely by colloidal particles. Adv. Colloid Interface Sci. 100, 503-546.

Babamiri, O., Vanaei, A., Guo, X., Wu, P., Richter, A., Ng, K., 2021. Numerical Simulation of Water Quality and Self-Purification in a Mountainous River Using QUAL2KW. J. Environ. Inform. 37, 26-35.

Babincova, M., Sourivong, P., Leszczynska, D., Babinec, P., 2000. Blood-specific whole-body electromagnetic hyperthermia. Medical Hypotheses 55, 459-460.

Bai, X., Wang, Y., Zheng, X., Zhu, K., Long, A., Wu, X., Zhang, H., 2019. Remediation of phenanthrene contaminated soil by coupling soil washing with Tween 80, oxidation using the UV/$S_2O8_2^-$ process and recycling of the surfactant. Chem. Eng. J. 369, 1014-1023.

Barreca, S., Orecchio, S., Pace, A., 2014. The effect of montmorillonite clay in alginate gel beads for polychlorinated biphenyl adsorption: Isothermal and kinetic studies. Appl. Clay Sci. 99, 220-228.

Barron, M., Bejarano, A. C., Conmy, R. N., Sundaravadivelu, D., Meyer, P., 2020. Toxicity of oil spill response agents and crude oils to five aquatic test species. Mar. Pollut. Bull. 153, 110954-110962.
Befkadu, A. A., Quanyuan, C., 2018. Surfactant-enhanced soil washing for removal of petroleum hydrocarbons from contaminated soils: a review. Pedosphere 28, 383-410.
Berglund, L. A., Burgert, I., 2018. Bioinspired wood nanotechnology for functional materials. Adv. Mater. 30, 1704285.
Betterton, E. A., Hoffmann, M. R., 1990. Kinetics and mechanism of the oxidation of aqueous hydrogen sulfide by peroxymonosulfate. Environ. Sci. Technol. 24, 1819-1824.
Bhagat, J., Sarkar, A., Ingole, B., 2016. DNA damage and oxidative stress in marine gastropod Morula granulata exposed to phenanthrene. Water, Air, Soil Pollut.. 227, 1-12.
Bi, H., An, C., Chen, X., Owens, E., Lee, K., 2020. Investigation into the oil removal from sand using a surface washing agent under different environmental conditions. J. Environ. Manage. 275, 111232-111241.
Bi, H., An, C., Mulligan, C. N., Wang, Z., Zhang, B., Lee, K., 2021a. Exploring the use of alginate hydrogel coating as a new initiative for emergent shoreline oiling prevention. Sci. Total Environ., 149234.
Bi, H., An, C., Mulligan, C. N., Zhang, K., Lee, K., Yue, R., 2021b. Treatment of oiled beach sand using a green and responsive washing fluid with nonionic surfactant-modified nanoclay. J. Cleaner Prod., 130122.
Bi, H., An, C., Owens, E., Lee, K., Chen, Z., Mulligan, C., Taylor, E., Boufadel, M., 2021c. A framework for the evaluation and selection of shoreline surface washing agents in oil spill response. J. Environ. Manage. 287, 112346.
Bi, H., Mulligan, C. N., An, C., Owens, E., Taylor, E., McCourt, J., Yin, J., Feng, Q., Chen, X., Yue, R., 2022. Development of a calcium alginate-cellulose nanocrystal-based coating to reduce the impact of oil spills on shorelines. J. Hazard. Mater. 436, 129228.
Binks, B., Liu, W., Rodrigues, J. A., 2008. Novel stabilization of emulsions via the heteroaggregation of nanoparticles. Langmuir 24, 4443-4446.
Birben, E., Sahiner, U. M., Sackesen, C., Erzurum, S., Kalayci, O., 2012. Oxidative stress and antioxidant defense. World Allergy Organ. J. 5, 9-19.
Bonal, N., Paramkusam, B. R., Basudhar, P. K., 2018. Enhancement of surfactant efficacy during the cleanup of engine oil contaminated soil using salt and multi-walled carbon nanotubes. J. Hazard. Mater. 351, 54-62.
Bößl, F., Tudela, I., 2021. Piezocatalysis: Can catalysts really dance? Curr. Opin. Green Sustainable Chem. 32, 100537.
Boufadel, M., Geng, X. L., An, C., Owens, E., Chen, Z., Lee, K. N., Taylor, E., Prince, R. C., 2019. A review on the factors affecting the deposition, retention, and riodegradation of oil stranded on beaches and guidelines for designing laboratory experiments. Curr. Pollut. Rep. 5, 407-423.
Bragg, J. R., Yang, S. H., 1995. Clay-oil flocculation and its role in natural cleansing in Prince William Sound following the Exxon Valdez oil spill. ASTM Spec. Tech. Publ. 1219, 178-214.
Cai, G., Yang, X., Lai, Q., Yu, X., Zhang, H., Li, Y., Chen, Z., Lei, X., Zheng, W., Xu, H., 2016a. Lysing bloom-causing alga phaeocystis globosa with microbial algicide: an efficient process that decreases the toxicity of algal exudates. Sci. Rep. 6, 1-11.
Cai, Q., Zhang, B., Chen, B., Cao, T., Lv, Z., 2016b. Biosurfactant produced by a Rhodococcus erythropolis mutant as an oil spill response agent. Water Qual. Res. J. 51, 97-105.
Cai, Q., Zhu, Z., Chen, B., Zhang, B., 2019. Oil-in-water emulsion breaking marine bacteria for demulsifying oily wastewater. Water Res. 149, 292-301.

Cai, Z., Fu, J., Liu, W., Fu, K. M., O'Reilly, S. E., Zhao, D. Y., 2017. Effects of oil dispersants on settling of marine sediment particles and particle-facilitated distribution and transport of oil components. Mar. Pollut. Bull. 114, 408-418.
Cao, F., Xia, Y., Chen, D., Xu, N., Hemar, Y., Li, N., Sun, Y., 2020a. Insights on the structure of caseinate particles based on surfactants-induced dissociation. Food Hydrocolloids 104, 105766.
Cao, Y., Kang, Q., Zhang, B., Zhu, Z., Dong, G., Cai, Q., Lee, K., Chen, B., 2022. Machine learning-aided causal inference for unraveling chemical dispersant and salinity effects on crude oil biodegradation. Bioresour. Technol. 345, 126468.
Cao, Y., Zhang, B., Zhu, Z., Song, X., Cai, Q., Chen, B., Dong, G., Ye, X., 2020b. Microbial eco-physiological strategies for salinity-mediated crude oil biodegradation. Sci. Total Environ. 727, 138723-138730.
Cao, Y., Zhang, B., Zhu, Z., Song, X., Cai, Q., Chen, B., Dong, G., Ye, X., 2020c. Microbial eco-physiological strategies for salinity-mediated crude oil biodegradation. Sci. Total Environ. 727, 138723.
Carugo, O., Djinović-Carugo, K., 2013. A proteomic Ramachandran plot (PRplot). Amino Acids 44, 781-790.
Castellanos-Gomez, A., Quereda, J., van der Meulen, H. P., Agraït, N., Rubio-Bollinger, G., 2016. Spatially resolved optical absorption spectroscopy of single-and few-layer MoS_2 by hyperspectral imaging. Nanotechnology 27, 115705.
Chang, C., Wang, T., Hu, Q., Zhou, M., Xue, J., Luo, Y., 2017. Pectin coating improves physicochemical properties of caseinate/zein nanoparticles as oral delivery vehicles for curcumin. Food Hydrocolloids 70, 143-151.
Chao, W., Wang, S., Li, Y., Cao, G., Zhao, Y., Sun, X., Wang, C., Ho, S.-H., 2020a. Natural sponge-like wood-derived aerogel for solar-assisted adsorption and recovery of high-viscous crude oil. Chem. Eng. J. 400, 125865.
Chao, W. X., Wang, S. B., Li, Y. D., Cao, G. L., Zhao, Y. S., Sun, X. H., Wang, C. Y., Ho, S. H., 2020b. Natural sponge-like wood-derived aerogel for solar-assisted adsorption and recovery of high-viscous crude oil. Chem. Eng. J. 400, 125865.
Chen, J., Cao, T., Zhang, X., Xi, Y., Ni, L., Jeppesen, E., 2016. Differential photosynthetic and morphological adaptations to low light affect depth distribution of two submersed macrophytes in lakes. Sci. Rep. 6, 1-9.
Chen, S., Gao, C., Tang, W., Zhu, H., Han, Y., Jiang, Q., Li, T., Cao, X., Wang, Z., 2015. Self-powered cleaning of air pollution by wind driven triboelectric nanogenerator. Nano Energy 14, 217-225.
Chen, W., Zhang, H., Zhang, M., Shen, X., Zhang, X., Wu, F., Hu, J., Wang, B., Wang, X., 2021a. Removal of PAHs at high concentrations in a soil washing solution containing TX-100 via simultaneous sorption and biodegradation processes by immobilized degrading bacteria in PVA-SA hydrogel beads. J. Hazard. Mater. 410, 124533.
Chen, X., Huang, G., An, C., Feng, R., Wu, Y., Huang, C., 2019. Plasma-induced PAA-ZnO coated PVDF membrane for oily wastewater treatment: preparation, optimization, and characterization through Taguchi OA design and synchrotron-based X-ray analysis. J. Membr. Sci. 582, 70-82.
Chen, X., Huang, G., An, C., Feng, R., Wu, Y., Huang, C., 2022a. Superwetting polyethersulfone membrane functionalized with ZrO_2 nanoparticles for polycyclic aromatic hydrocarbon removal. J. Mater. Sci. Technol. 98, 14-25.

Chen, X. J., Huang, G. H., An, C., Feng, R. F., Wu, Y. H., Huang, C., 2022b. Superwetting polyethersulfone membrane functionalized with ZrO_2 nanoparticles for polycyclic aromatic hydrocarbon removal. J. Mater. Sci. Technol. 98, 14-25.
Chen, Z., An, C., Boufadel, M., Owens, E., Chen, Z., Lee, K., Cao, Y. T., Cai, M. F., 2020a. Use of surface-washing agents for the treatment of oiled shorelines: research advancements, technical applications and future challenges. Chem. Eng. J. 391, 123565-123584.
Chen, Z., An, C., Fang, H. X., Zhang, Y. L., Zhou, Z. G., Zhou, Y., Zhao, S., 2020b. Assessment of regional greenhouse gas emission from beef cattle production: A case study of Saskatchewan in Canada. J. Environ. Manage. 264, 110443-110454.
Chen, Z., An, C., Wang, Y. X., Zhang, B. Y., Tian, X. L., Lee, K., 2021b. A green initiative for oiled sand cleanup using chitosan/rhamnolipid complex dispersion with pH-stimulus response. Chemosphere 288, 132628.
Chen, Z., An, C., Yin, J. N., Owens, E., Lee, K., Zhang, K. Q., Tian, X. L., 2021c. Exploring the use of cellulose nanocrystal as surface-washing agent for oiled shoreline cleanup. J. Hazard. Mater. 402, 123464-123473.
Cho, H., Choi, J. Y., Goltz, M. N., Park, J. W., 2002. Combined effect of natural organic matter and surfactants on the apparent solubility of polycyclic aromatic hydrocarbons. J. Environ. Qual. 31, 275-280.
Chu, W., 2003. Remediation of contaminated soils by surfactant-aided soil washing. Pract. Period. Hazard. Toxic, Radioact. Waste Manage. 7, 19-24.
Churchman, G., Gates, W., Theng, B., Yuan, G., 2006. Clays and clay minerals for pollution control. Dev. Clay Sci. 1, 625-675.
Cocozza, C., D'orazio, V., Miano, T., Shotyk, W., 2003. Characterization of solid and aqueous phases of a peat bog profile using molecular fluorescence spectroscopy, ESR and FT-IR, and comparison with physical properties. Org. Geochem. 34, 49-60.
Corpuz, A. G., Pal, P., Banat, F., 2019. Effect of temperature and use of regenerated surfactants on the removal of oil from water using colloidal gas aphrons. Sep. Purif. Technol. 227, 115678.
CSPMA, 2022. https://peatmoss.com/.
D'Ugo, E., Bertuccini, L., Spadaro, F., Giuseppetti, R., Iosi, F., Santavenere, F., Giuliani, F., Gricia, M., Rodomonte, A., Lovecchio, N., 2021. Electrogenic and hydrocarbonoclastic biofilm at the oil-water interface as microbial responses to oil spill. Water Res. 197, 117092.
Dai, Q., Chung, K. H., 1995. Bitumen—sand interaction in oil sand processing. Fuel 74, 1858-1864.
Dauphas, S., Mouhous-Riou, N., Metro, B., Mackie, A., Wilde, P. J., Anton, M., Riaublanc, A., 2005. The supramolecular organisation of β-casein: Effect on interfacial properties. Food Hydrocolloids 19, 387-393.
De Kruif, C. G., Huppertz, T., Urban, V. S., Petukhov, A. V., 2012. Casein micelles and their internal structure. Adv. Colloid Interface Sci. 171, 36-52.
Debs, K. B., Cardona, D. S., da Silva, H. D., Nassar, N. N., Carrilho, E. N., Haddad, P. S., Labuto, G., 2019. Oil spill cleanup employing magnetite nanoparticles and yeast-based magnetic bionanocomposite. J. Environ. Manage. 230, 405-412.
Deng, Y., Qi, D., Deng, C., Zhang, X., Zhao, D., 2008. Superparamagnetic high-magnetization microspheres with an Fe3O4@ SiO2 core and perpendicularly aligned mesoporous SiO2 shell for removal of microcystins. J. Am. Chem. Soc. 130, 28-29.
Dethier, M., Ruesink, J., Berry, H., Sprenger, A. G., 2012. Decoupling of recruitment from adult clam assemblages along an estuarine shoreline. J. Exp. Mar. Biol. Ecol. 422, 48-54.

Ding, F., Gao, M., 2021. Pore wettability for enhanced oil recovery, contaminant adsorption and oil/water separation: A review. Adv. Colloid Interface Sci. 289, 102377.
Dittmar, T., Lennartz, S. T., Buck-Wiese, H., Hansell, D. A., Santinelli, C., Vanni, C., Blasius, B., Hehemann, J.-H., 2021. Enigmatic persistence of dissolved organic matter in the ocean. Nat. Rev. Earth Environ. 2, 570-583.
Divandari, H., Hemmati-Sarapardeh, A., Schaffie, M., Ranjbar, M., 2019. Integrating synthesized citric acid-coated magnetite nanoparticles with magnetic fields for enhanced oil recovery: Experimental study and mechanistic understanding. J. Petrol. Sci. Eng. 174, 425-436.
Djellabi, R., Giannantonio, R., Falletta, E., Bianchi, C. L., 2021. SWOT analysis of photocatalytic materials towards large scale environmental remediation. Curr. Opin. Chem. Eng. 33, 100696.
Dong, C., Wang, Z., Ye, Z., He, J., Zheng, Z., Gong, X., Zhang, J., Lo, I. M., 2021. Superoxide radicals dominated visible light driven peroxymonosulfate activation using molybdenum selenide ($MoSe_2$) for boosting catalytic degradation of pharmaceuticals and personal care products. Appl. Catal. B Environ. 296, 120223.
Dong, J., Worthen, A. J., Foster, L. M., Chen, Y. S., Cornell, K. A., Bryant, S. L., Truskett, T. M., Bielawski, C. W., Johnston, K. P., 2014. Modified montmorillonite clay microparticles for stable oil-in-seawater emulsions. ACS Appl. Mater. Interfaces 6, 11502-11513.
Dos Santos, E. V., Sáez, C., Martínez-Huitle, C. A., Cañizares, P., Rodrigo, M. A., 2015. Combined soil washing and CDEO for the removal of atrazine from soils. J. Hazard. Mater. 300, 129-134.
Du, W., Zhang, Q., Shang, Y., Wang, W., Li, Q., Yue, Q., Gao, B., Xu, X., 2020. Sulfate saturated biosorbent-derived Co-S@ NC nanoarchitecture as an efficient catalyst for peroxymonosulfate activation. Appl. Catal. B Environ. 262, 118302.
Elanchezhiyan, S. S., Meenakshi, S., 2016. Facile synthesis of metal incorporated chitin for the recovery of oil from oil-in-water emulsion using adsorptive method. J. Cleaner Prod. 139, 1339-1350.
Elmobarak, W., Almomani, F., 2021a. A new insight into the separation of oil from oil/water emulsion by Fe_3O_4–SiO_2 nanoparticles. Environ. Res. 202, 111645-111655.
Elmobarak, W. F., Almomani, F., 2021b. Application of Fe_3O_4 magnetite nanoparticles grafted in silica (SiO_2) for oil recovery from oil in water emulsions. Chemosphere 265, 129054.
Etcheverry, M., Cappa, V., Trelles, J., Zanini, G., 2017. Montmorillonite-alginate beads: natural mineral and biopolymers based sorbent of paraquat herbicides. J. Environ. Chem. Eng. 5, 5868-5875.
Farshchi, A., Ettelaie, R., Holmes, M., 2013. Influence of pH value and locust bean gum concentration on the stability of sodium caseinate-stabilized emulsions. Food Hydrocolloids 32, 402-411.
Félix, M.-A., Braendle, C., 2010. The natural history of Caenorhabditis elegans. Curr. Biol. 20, R965-R969.
Feng, Q., An, C., Cao, Y., Chen, Z., Owens, E., Taylor, E., Wang, Z., Saad, E., 2021. An analysis of selected oil spill case studies on the shorelines of Canada. J. Environ. Inform. Lett. 5, 39-47.
Feng, Y. M., Lee, Y. S., 2016. Surface modification of zein colloidal particles with sodium caseinate to stabilize oil-in-water pickering emulsion. Food Hydrocolloids 56, 292-302.
Findlay, S. E., Parr, T. B., Dissolved organic matter. Methods in Stream Ecology. Elsevier, 2017, pp. 21-36.
Fingas, M., 2002. The basics of oil spill cleanup. CRC Press.
Flory, P. J., 1942. Thermodynamics of high polymer solutions. The Journal of chemical physics 10, 51-61.

Fotiou, T., Triantis, T. M., Kaloudis, T., O'Shea, K. E., Dionysiou, D. D., Hiskia, A., 2016. Assessment of the roles of reactive oxygen species in the UV and visible light photocatalytic degradation of cyanotoxins and water taste and odor compounds using C–TiO_2. Water Res. 90, 52-61.

Gao, S., Jing, M., Xu, M., Han, D., Niu, Q., Liu, R., 2020. Cytotoxicity of perfluorodecanoic acid on mouse primary nephrocytes through oxidative stress: Combined analysis at cellular and molecular levels. J. Hazard. Mater. 393, 122444.

Gaonkar, A. G., 1992. Effects of salt, temperature, and surfactants on the interfacial tension behavior of a vegetable oil/water system. J. Colloid Interface Sci. 149, 256-260.

Gaur, A. P., Sahoo, S., Ahmadi, M., Dash, S. P., Guinel, M. J.-F., Katiyar, R. S., 2014. Surface energy engineering for tunable wettability through controlled synthesis of MoS_2. Nano Lett. 14, 4314-4321.

Ge, J., Hu, Y., Biasini, M., Beyermann, W. P., Yin, Y., 2007. Superparamagnetic magnetite colloidal nanocrystal clusters. Angew. Chem. Int. Ed. 46, 4342-4345.

Ge, J., Shi, L. A., Wang, Y. C., Zhao, H. Y., Yao, H. B., Zhu, Y. B., Zhang, Y., Zhu, H. W., Wu, H. A., Yu, S. H., 2017. Joule-heated graphene-wrapped sponge enables fast clean-up of viscous crude-oil spill. Nat. Nanotechnol. 12, 434-440.

Geng, X., Boufadel, M. C., Rajaram, H., Cui, F. D., Lee, K., An, C., 2020. Numerical study of solute transport in heterogeneous beach aquifers subjected to tides. Water Resour. Res. 56, e2019WR026430.

Ghorbanizadeh, S., Rostami, B., 2017. Surface and interfacial tension behavior of salt water containing dissolved amphiphilic compounds of crude oil: the role of single-salt ionic composition. Energy Fuels 31, 9117-9124.

Gomes, T., Xie, L., Brede, D., Lind, O.-C., Solhaug, K. A., Salbu, B., Tollefsen, K. E., 2017. Sensitivity of the green algae chlamydomonas reinhardtii to gamma radiation: photosynthetic performance and ROS formation. Aquat. Toxicol. 183, 1-10.

Gopalakrishnan, D., Damien, D., Shaijumon, M. M., 2014. MoS_2 quantum dot-interspersed exfoliated MoS_2 nanosheets. ACS Nano 8, 5297-5303.

Gopi, S., Kargl, R., Kleinschek, K. S., Pius, A., Thomas, S., 2018. Chitin nanowhisker–Inspired electrospun PVDF membrane for enhanced oil-water separation. J. Environ. Manage. 228, 249-259.

Gu, H. B., Zhou, X. M., Lyu, S. Y., Pan, D., Dong, M. Y., Wu, S. D., Ding, T., Wei, X., Seok, I., Wei, S. Y., 2020a. Magnetic nanocellulose-magnetite aerogel for easy oil adsorption. J. Colloid Interface Sci. 560, 849-856.

Gu, W., Li, X., Du, M., Ren, Z., Li, Q., Li, Y., 2021. Identification and regulation of ecotoxicity of polychlorinated naphthalenes to aquatic food Chain (green algae-Daphnia magna-fish). Aquat. Toxicol. 233, 105774.

Gu, W., Zhao, Y., Li, Q., Li, Y., 2020b. Plant-microorganism combined remediation of polychlorinated naphthalenes contaminated soils based on molecular directed transformation and Taguchi experimental design-assisted dynamics simulation. J. Hazard. Mater. 396, 122753.

Guan, H., Cheng, Z. Y., Wang, X. Q., 2018. Highly compressible wood sponges with a spring-like lamellar structure as effective and reusable oil absorbents. ACS Nano 12, 10365-10373.

Guo, K., Wu, Z., Chen, C., Fang, J., 2022. UV/Chlorine process: an efficient advanced oxidation process with multiple radicals and functions in water treatment. Acc. Chem. Res. 55, 286-297.

Guo, Y., Wang, Z., Zhang, L., Shen, X., Liu, F., 2016. Thickness dependence of surface energy and contact angle of water droplets on ultrathin MoS_2 films. Phys. Chem. Chem. Phys. 18, 14449-14453.

Gupta, R. K., Dunderdale, G. J., England, M. W., Hozumi, A., 2017. Oil/water separation techniques: a review of recent progresses and future directions. J. Mater. Chem. A 5, 16025-16058.
He, S., Zhang, N., Jing, P., 2019. Insights into interaction of chlorophylls with sodium caseinate in aqueous nanometre-scale dispersion: color stability, spectroscopic, electrostatic, and morphological properties. RSC Adv. 9, 4530-4538.
He, Y., Huang, G. H., An, C., Huang, J., Zhang, P., Chen, X. J., Xin, X. Y., 2018. Reduction of escherichia coli using ceramic disk filter decorated by nano-TiO_2: a low-cost solution for household water purification. Sci. Total Environ. 616, 1628-1637.
Head, I. M., Jones, D. M., Röling, W. F., 2006. Marine microorganisms make a meal of oil. Nat. Rev. Microbiol. 4, 173-182.
Henry, I., Netzer, R., Davies, E. J., Brakstad, O. G., 2020. Formation and fate of oil-related aggregates (ORAs) in seawater at different temperatures. Mar. Pollut. Bull. 159, 111483-111496.
Hirata, Y., Ryu, M., Oda, Y., Igarashi, K., Nagatsuka, A., Furuta, T., Sugiura, M., 2009. Novel characteristics of sophorolipids, yeast glycolipid biosurfactants, as biodegradable low-foaming surfactants. J. Biosci. Bioeng. 108, 142-146.
Hoff, R., Blenkinsopp, S., Sergy, G., Wang, Z., Henry, C., Roberts, P., Foght, J., Westlake, D., 1995. Evaluating biodegradation potential of various oils.
Holloway, M., 1991. Soiled shores. Sci. Am. 265, 102-117.
Hong, S., Chon, T., Joo, G., 2021. Spatial distribution patterns of eurasian otter (Lutra Lutra) in association with environmental factors unravelled by machine learning and diffusion kernel method. J. Environ. Inform. 37, 130-141.
Hong, Y., Huang, G., An, C., Song, P., Xin, X., Chen, X., Zhang, P., Zhao, Y., Zheng, R., 2019. Enhanced nitrogen removal in the treatment of rural domestic sewage using vertical-flow multi-soil-layering systems: experimental and modeling insights. J. Environ. Manage. 240, 273-284.
Hosseini, H., Shirani, H., Hamidpour, M., Ranjbar Karimi, R., Hossein Shamshiri, M., Sadegh Hosseini, M., Dashti, H., 2013. Effects of natural and modified montmorillonite on plant availability of Cd (II) and Pb (II) in polluted soils. Environ. Eng. Manag. J. 12, 2079-2085.
Hu, J., Zhan, Y., Zhang, G., Feng, Q., Yang, W., Chiao, Y.-H., Zhang, S., Sun, A., 2021. Durable and super-hydrophilic/underwater super-oleophobic two-dimensional MXene composite lamellar membrane with photocatalytic self-cleaning property for efficient oil/water separation in harsh environments. J. Membr. Sci. 637, 119627.
Hua, F., Tsang, Y. F., Wang, Y., Chan, S., Chua, H., Sin, S., 2007. Performance study of ceramic microfiltration membrane for oily wastewater treatment. Chem. Eng. J. 128, 169-175.
Huang, W., Chen, X., Fan, Y., Li, Y., 2022. Management of drinking water source in rural communities under climate change. J. Environ. Inform. 39, 136-151.
Huang, X., Yan, X., Xia, L., Wang, P., Wang, Q., Zhang, X., Zhong, B., Zhao, H., Wen, G., 2016. A three-dimensional graphene/Fe_3O_4/carbon microtube of sandwich-type architecture with improved wave absorbing performance. Scr. Mater. 120, 107-111.
Huang, Y.-X., Wang, Z., Jin, J., Lin, S., 2017. Novel Janus membrane for membrane distillation with simultaneous fouling and wetting resistance. Environ. Sci. Technol. 51, 13304-13310.
Huang, Y. N., Zhan, H., Li, D., Tian, H. F., Chang, C. Y., 2019. Tunicate cellulose nanocrystals modified commercial filter paper for efficient oil/water separation. J. Membr. Sci. 591.
Huggins, M. L., 1942. Some properties of solutions of long-chain compounds. The Journal of Physical Chemistry 46, 151-158.

Huo, B., Meng, F., Yang, J., Wang, Y., Qi, J., Ma, W., Wang, Z., Wang, J., Wang, Z., 2022. High efficiently piezocatalysis degradation of tetracycline by few-layered MoS_2/GDY: mechanism and toxicity evaluation. Chem. Eng. J. 436, 135173.

Inglingstad, R. A., Devold, T. G., Eriksen, E. K., Holm, H., Jacobsen, M., Liland, K. H., Rukke, E. O., Vegarud, G. E., 2010. Comparison of the digestion of caseins and whey proteins in equine, bovine, caprine and human milks by human gastrointestinal enzymes. Dairy Sci. Technol. 90, 549-563.

ITOPF, I., 2017. Oil tanker spill statistics 2016. https://www.itopf.org/knowledge-resources/data-statistics/statistics/.

Izadi, N., Koochi, M. M., Amrollahi, A., Pourkhalil, M., 2019. Investigation of functionalized polyelectrolyte polymer-coated Fe_3O_4 nanoparticles stabilized in high salinity brine at high temperatures as an EOR agent. J. Petrol. Sci. Eng. 178, 1079-1091.

Jiang, J., Yu, S. J., Zhang, W. Q., Zhang, H. J., Cui, Z. G., Xia, W. S., Binks, B. P., 2021. Charge-reversible surfactant-induced transformation between oil-in-dispersion emulsions and Pickering emulsions. Angew. Chem. Int. Ed. 60, 11793-11798.

Jiang, R., Wu, D., Lu, G., Yan, Z., Liu, J., Zhou, R., Nkoom, M., 2019. Fabrication of Fe_3O_4 quantum dots modified BiOCl/$BiVO_4$ pn heterojunction to enhance photocatalytic activity for removing broad-spectrum antibiotics under visible light. J Taiwan Inst Chem E 96, 681-690.

Jin, C., Liu, D., Hu, J., Wang, Y., Zhang, Q., Lv, L., Zhuge, F., 2019. The role of microstructure in piezocatalytic degradation of organic dye pollutants in wastewater. Nano Energy 59, 372-379.

Jin, X., Teng, D., Fang, J., Liu, Y., Jiang, Z., Song, Y., Zhang, T., Siyal, A. A., Dai, J., Fu, J., 2021. Petroleum oil and products recovery from oily sludge: Characterization and analysis of pyrolysis products. Environ. Res. 202, 111675-111687.

Jones, G., Ray, W. A., 1941. The surface tension of solutions of electrolytes as a function of the concentration. III. Sodium chloride. J. Am. Chem. Soc. 63, 3262-3263.

Jones, K. D., Tiller, C. L., 1999. Effect of solution chemistry on the extent of binding of phenanthrene by a soil humic acid: a comparison of dissolved and clay bound humic. Environ. Sci. Technol. 33, 580-587.

Joseph-Ezra, H., Nasser, A., Ben-Ari, J., Mingelgrin, U., 2014. Mechanochemically enhanced degradation of pyrene and phenanthrene loaded on magnetite. Environ. Sci. Technol. 48, 5876-5882.

Kaminogawa, S., Yamauchi, K., Miyazawa, S., Koga, Y., 1980. Degradation of casein components by acid protease of bovine milk. J. Dairy Sci. 63, 701-704.

Karatum, O., Steiner III, S. A., Griffin, J. S., Shi, W., Plata, D. L., 2016. Flexible, mechanically durable aerogel composites for oil capture and recovery. ACS Appl. Mater. Interfaces 8, 215-224.

Kavalenka, M. N., Vüllers, F., Lischker, S., Zeiger, C., Hopf, A., Röhrig, M., Rapp, B. E., Worgull, M., Hölscher, H., 2015. Bioinspired air-retaining nanofur for drag reduction. ACS Appl. Mater. Interfaces 7, 10651-10655.

Khajouei, G., Finklea, H. O., Lin, L., 2022. UV/chlorine advanced oxidation processes for degradation of contaminants in water and wastewater: A comprehensive review. J. Environ. Chem. Eng., 107508.

Kim, J., Tran, V. T., Oh, S., Kim, C.-S., Hong, J. C., Kim, S., Joo, Y.-S., Mun, S., Kim, M.-H., Jung, J.-W., 2018. Scalable solvothermal synthesis of superparamagnetic Fe_3O_4 nanoclusters for bioseparation and theragnostic probes. ACS Appl. Mater. Interfaces 10, 41935-41946.

Kim, N., Kwon, K., Park, J., Kim, J., Choi, J.-W., 2019. Ex situ soil washing of highly contaminated silt loam soil using core-crosslinked amphiphilic polymer nanoparticles. Chemosphere 224, 212-219.
Kozak, M., 2019. A comparison of thermogravimetric characteristics of fresh and used engine oils. Combust. Engines 58.
Kubota, K., Pang, Y., Miura, A., Ito, H., 2019. Redox reactions of small organic molecules using ball milling and piezoelectric materials. Science 366, 1500-1504.
Kumar, V., 2019. Separation of crude oil from water using chitosan based hydrogel. Cellulose 26, 6229-6239.
Kumura, H., Takagaki, K., Sone, T., Tsukahara, M., Tanaka, T., Shimazaki, K.-i., 2002. Casein digestion by Debaryomyces hansenii isolated from cheese. Biosci. Biotechnol. Biochem. 66, 1370-1373.
La, Z., Chai, L., 2021. Comprehensive study of evolution of global environmental quality research using informetric co-word network. J. Environ. Inform. 38, 116-130.
Lalithambika, K., Shanmugapriya, K., Sriram, S., 2019. Photocatalytic activity of MoS_2 nanoparticles: an experimental and DFT analysis. Appl. Phys. A 125, 1-8.
Lashkarbolooki, M., Ayatollahi, S., Riazi, M., 2014. The impacts of aqueous ions on interfacial tension and wettability of an asphaltenic–acidic crude oil reservoir during smart water injection. J. Chem. Eng. Data 59, 3624-3634.
Lavoine, N., Bergström, L., 2017. Nanocellulose-based foams and aerogels: processing, properties, and applications. J. Mater. Chem. A 5, 16105-16117.
Le Floch, S., Guyomarch, J., Merlin, F. X., Stoffyn-Egli, P., Dixon, J., Lee, K., 2002. The influence of salinity on oil-mineral aggregate formation. Spill Sci. Technol. Bull. 8, 65-71.
Le, H. V., Bui, Q. T., Bui, D. T., Tran, H. H., Hoang, N. D., 2020. A Hybrid Intelligence System Based on Relevance Vector Machines and Imperialist Competitive Optimization for Modelling Forest Fire Danger Using GIS. J. Environ. Inform. 36, 43-57.
Lee, K., 2000. In situ bioremediation of oiled shoreline environments. Opportunities for Environmental Applications of Marine Biotechnology, 44-60.
Lee, K., Chen, B., Boufadel, M., Swanson, S. M., Hodson, P. V., Foght, J., Venosa, A. D., 2016. Behaviour and environmental impacts of crude oil released into aqueous environments.
Lee, K., Wells, P. G., Gordon, D. C., 2020. Reflecting on an anniversary. The 1970 SS Arrow oil spill in Chedabucto Bay, Nova Scotia, Canada. Mar. Pollut. Bull. 157, 111332.
Li, A., Lin, R. J., Lin, C., He, B. Y., Zheng, T. T., Lu, L. B., Cao, Y., 2016. An environment-friendly and multi-functional absorbent from chitosan for organic pollutants and heavy metal ion. Carbohydr. Polym. 148, 272-280.
Li, L. X., Hu, T., Sun, H. X., Zhang, J. P., Wang, A. Q., 2017. Pressure-sensitive and conductive carbon aerogels from poplars catkins for selective oil absorption and oil/water separation. ACS Appl. Mater. Interfaces 9, 18001-18007.
Li, R. J., Li, J. Y., Rao, L. H., Lin, H. J., Shen, L. G., Xu, Y. C., Chen, J. R., Liao, B. Q., 2021a. Inkjet printing of dopamine followed by UV light irradiation to modify mussel-inspired PVDF membrane for efficient oil-water separation. J. Membr. Sci. 619, 118790.
Li, X., Gu, W., Chen, B., Zhu, Z., Zhang, B., 2021b. Functional modification of HHCB: Strategy for obtaining environmentally friendly derivatives. J. Hazard. Mater. 416, 126116.
Li, X., He, W., Zhao, Y., Chen, B., Zhu, Z., Kang, Q., Zhang, B., 2022. Dermal exposure to synthetic musks: Human health risk assessment, mechanism, and control strategy. Ecotoxicol. Environ. Saf. 236, 113463.

Li, Z., Li, J., Shi, X., 2020. A Two-Stage Multisite and Multivariate Weather Generator. J. Environ. Inform. 35, 94-102.
Liang, S., Fang, T., Xiong, W., Ding, B., Yan, Y., Zhang, J., 2019. Oil detachment by modified nanoparticles: a molecular dynamics simulation study. Comp. Mater. Sci. 170, 109177.
Liang, X. C., Wang, X. L., Xu, Q., Lu, Y., Zhang, Y., Xia, H., Lu, A., Zhang, L. N., 2018. Rubbery chitosan/carrageenan hydrogels constructed through an electroneutrality system and their potential application as cartilage scaffolds. Biomacromolecules 19, 340-352.
LiBreTests, https://chem.libretexts.org/Bookshelves/Organic_Chemistry/Organic_Chemistry_(McMurry)/12%3A_Structure_Determination_-_Mass_Spectrometry_and_Infrared_Spectroscopy/12.08%3A_Infrared_Spectra_of_Some_Common_Functional_Groups.
Lin, H.-Y., Le, K. T., Chen, P.-H., Wu, J. M., 2022. Systematic investigation of the piezocatalysis–adsorption duality of polymorphic MoS_2 nanoflowers. Appl. Catal. B Environ. 317, 121717.
Lin, X., Xie, Y., Lu, H., Xin, Y., Altaf, R., Zhu, S., Liu, D., 2021. Facile preparation of dual La-Zr modified magnetite adsorbents for efficient and selective phosphorus recovery. Chem. Eng. J. 413, 127530.
Liu, J.-W., Wei, K.-H., Xu, S.-W., Cui, J., Ma, J., Xiao, X.-L., Xi, B.-D., He, X.-S., 2021a. Surfactant-enhanced remediation of oil-contaminated soil and groundwater: a review. Sci. Total Environ. 756, 144142.
Liu, J., Sun, Z., Deng, Y., Zou, Y., Li, C., Guo, X., Xiong, L., Gao, Y., Li, F., Zhao, D., 2009. Highly water-dispersible biocompatible magnetite particles with low cytotoxicity stabilized by citrate groups. Angew. Chem. Int. Ed. 48, 5875-5879.
Liu, S., Jing, B., Nie, C., Ao, Z., Duan, X., Lai, B., Shao, Y., Wang, S., An, T., 2021b. Piezoelectric activation of peroxymonosulfate by MoS_2 nanoflowers for the enhanced degradation of aqueous organic pollutants. Environ. Sci.: Nano. 8, 784-794.
Liu, S., Yao, K., Fu, L.-H., Ma, M.-G., 2016. Selective synthesis of Fe_3O_4, γ-Fe_2O_3, and α-Fe_2O_3 using cellulose-based composites as precursors. RSC Adv. 6, 2135-2140.
Liu, T., Liu, Z., 2018. 2D MoS_2 nanostructures for biomedical applications. Adv. Healthcare Mater. 7, 1701158.
Liu, T., Wang, C., Gu, X., Gong, H., Cheng, L., Shi, X., Feng, L., Sun, B., Liu, Z., 2014. Drug delivery with PEGylated MoS_2 nano-sheets for combined photothermal and chemotherapy of cancer. Adv. Mater. 26, 3433-3440.
Liu, Y., Guo, R., 2008. pH-dependent structures and properties of casein micelles. Biophys. Chem. 136, 67-73.
Liu, Y. Q., Huang, G., An, C., Chen, X. J., Zhang, P., Feng, R. F., Xiong, W. H., 2020. Use of Nano-TiO2 self-assembled flax fiber as a new initiative for immiscible oil/water separation. J. Cleaner Prod. 249, 119352.
Low, L., Siva, S. P., Ho, Y. K., Chan, E. S., Tey, B. T., 2020. Recent advances of characterization techniques for the formation, physical properties and stability of Pickering emulsion. Adv. Colloid Interface Sci. 277, 102117-102139.
Lowry, E., Sedghi, M., Goual, L., 2016. Molecular simulations of NAPL removal from mineral surfaces using microemulsions and surfactants. Colloids Surf., A 506, 485-494.
Luo, C., Zheng, H., Wang, L., Fang, H., Hu, J., Fan, C., Cao, Y., Wang, J., 2010. Direct three-dimensional imaging of the buried interfaces between water and superhydrophobic surfaces. Angew. Chem. Int. Ed. 122, 9331-9334.

Luo, R., Li, M., Wang, C., Zhang, M., Khan, M. A. N., Sun, X., Shen, J., Han, W., Wang, L., Li, J., 2019. Singlet oxygen-dominated non-radical oxidation process for efficient degradation of bisphenol A under high salinity condition. Water Res. 148, 416-424.
Ma, H., Forssell, P., Partanen, R., Seppanen, R., Buchert, J., Boer, H., 2009. Sodium caseinates with an altered isoelectric point as emulsifiers in oil/water systems. J. Agric. Food Chem. 57, 3800-3807.
Ma, Q. L., Cheng, H. F., Fane, A. G., Wang, R., Zhang, H., 2016. Recent development of advanced materials with special wettability for selective oil/water separation. Small 12, 2186-2202.
Ma, W., Sun, M., Huang, D., Chu, C., Hedtke, T., Wang, X., Zhao, Y., Kim, J.-H., Elimelech, M., 2022. Catalytic membrane with copper single-atom catalysts for effective hydrogen peroxide activation and pollutant destruction. Environ. Sci. Technol. 56, 8733-8745.
Ma, W., Yao, B., Zhang, W., He, Y., Yu, Y., Niu, J., 2021a. Fabrication of PVDF-based piezocatalytic active membrane with enhanced oxytetracycline degradation efficiency through embedding few-layer E-MoS_2 nanosheets. Chem. Eng. J. 415, 129000.
Ma, X., Zhang, C., Gnanasekar, P., Xiao, P., Luo, Q., Li, S., Qin, D., Chen, T., Chen, J., Zhu, J., 2021b. Mechanically robust, solar-driven, and degradable lignin-based polyurethane adsorbent for efficient crude oil spill remediation. Chem. Eng. J. 415, 128956-128966.
Machado, J., de Freitas, R. A., Wypych, F., 2019. Layered clay minerals, synthetic layered double hydroxides and hydroxide salts applied as pickering emulsifiers. Appl. Clay Sci. 169, 10-20.
Manheim, J., Wehde, K., Zhang, W. T. J., Vozka, P., Romanczyk, M., Kilaz, G., Kenttämaa, H. I., 2019. Identification and quantitation of linear alkanes in lubricant base oils by using GC×GC/EI TOF mass spectrometry. J. Am. Soc. Mass. Spectrom. 30, 2670-2677.
Markande, A. R., Patel, D., Varjani, S., 2021. A review on biosurfactants: properties, applications and current developments. Bioresour. Technol. 330, 124963.
Marvin, C. H., Berthiaume, A., Burniston, D. A., Chibwe, L., Dove, A., Evans, M., Hewitt, L. M., Hodson, P. V., Muir, D. C., Parrott, J., 2021. Polycyclic aromatic compounds in the Canadian Environment: Aquatic and terrestrial environments. Environ. Pollut. 285, 117442.
McGlashan, M. L., 2007. Chemical Thermodynamics: Volume 2. Royal Society of Chemistry.
McHale, G., Newton, M. I., Shirtcliffe, N. J., 2010. Immersed superhydrophobic surfaces: Gas exchange, slip and drag reduction properties. Soft Matter 6, 714-719.
Mehraban, M. F., Farzaneh, S. A., Sohrabi, M., 2021. Debunking the impact of salinity on crude oil/water interfacial tension. Energy Fuels 35, 3766-3779.
Meng, Q., Sun, L., Chen, D., Wu, G., 2019. Adsorption of asphaltenes at oil–water and oil–clay interfaces in the presence of humic acids. Langmuir 35, 16718-16725.
Merlin, F., Zhu, Z., Yang, M., Chen, B., Lee, K., Boufadel, M. C., Isaacman, L., Zhang, B., 2021. Dispersants as marine oil spill treating agents: a review on mesoscale tests and field trials. Environmental Systems Research 10, 1-19.
Michalet, X., 2010. Mean square displacement analysis of single-particle trajectories with localization error: brownian motion in an isotropic medium. Phys. Rev. E 82, 041914.
Mirshahghassemi, S., Cai, B., Lead, J. R., 2019. A comparison between the oil removal capacity of polymer-coated magnetic nanoparticles in natural and synthetic environmental samples. Environ. Sci. Technol. 53, 4426-4432.
Mirshahghassemi, S., Lead, J. R., 2015. Oil recovery from water under environmentally relevant conditions using magnetic nanoparticles. Environ. Sci. Technol. 49, 11729-11736.
Mitchell, S. M., Ahmad, M., Teel, A. L., Watts, R. J., 2014. Degradation of perfluorooctanoic acid by reactive species generated through catalyzed H2O2 propagation reactions. Environ. Sci. Tech. Let. 1, 117-121.

Moeini, F., Hemmati-Sarapardeh, A., Ghazanfari, M.-H., Masihi, M., Ayatollahi, S., 2014. Toward mechanistic understanding of heavy crude oil/brine interfacial tension: The roles of salinity, temperature and pressure. Fluid Phase Equilib. 375, 191-200.
Molnes, S., Torrijos, I. P., Strand, S., Paso, K. G., Syverud, K., 2016. Sandstone injectivity and salt stability of cellulose nanocrystals (CNC) dispersions-premises for use of CNC in enhanced oil recovery. Ind. Crops Prod. 93, 152-160.
Morris, R. V., Vaniman, D. T., Blake, D. F., Gellert, R., Chipera, S. J., Rampe, E. B., Ming, D. W., Morrison, S. M., Downs, R. T., Treiman, A. H., 2016. Silicic volcanism on Mars evidenced by tridymite in high-SiO_2 sedimentary rock at Gale crater. Proc. Natl. Acad. Sci. U. S. A. 113, 7071-7076.
Mousset, E., Huguenot, D., van Hullebusch, E. D., Oturan, N., Guibaud, G., Esposito, G., Oturan, M. A., 2016. Impact of electrochemical treatment of soil washing solution on PAH degradation efficiency and soil respirometry. Environ. Pollut. 211, 354-362.
Mulligan, C. N., Yong, R., Gibbs, B., 2001. Surfactant-enhanced remediation of contaminated soil: a review. Engineering geology 60, 371-380.
Muñoz-Sandoval, E., Cortes-López, A. J., Flores-Gómez, B., Fajardo-Díaz, J. L., Sánchez-Salas, R., López-Urías, F., 2017. Carbon sponge-type nanostructures based on coaxial nitrogen-doped multiwalled carbon nanotubes grown by CVD using benzylamine as precursor. Carbon 115, 409-421.
Murphy, S. M., Bautista, M. A., Cramm, M. A., Hubert, C. R., 2021. Diesel and crude oil biodegradation by cold-adapted microbial communities in the Labrador Sea. Applied and environmental microbiology 87, e00800-00821.
Naselli Flores, L., Barone, R., 2009. Green algae.
Nguyen, D. D., Tai, N.-H., Lee, S.-B., Kuo, W.-S., 2012. Superhydrophobic and superoleophilic properties of graphene-based sponges fabricated using a facile dip coating method. Energ. Environ. Sci. 5, 7908-7912.
Nguyen, T. T., Youssef, N. H., McInerney, M. J., Sabatini, D. A., 2008. Rhamnolipid biosurfactant mixtures for environmental remediation. Water Res. 42, 1735-1743.
Nie, G., Xiao, L., Bi, J., Wang, S., Duan, X., 2022. New insight to piezocatalytic peroxymonosulfate activation: The critical role of dissolved oxygen in mediating radical and nonradical pathways. Appl. Catal. B Environ. 315, 121584.
Nosonovsky, M., Bhushan, B., 2006. Stochastic model for metastable wetting of roughness-induced superhydrophobic surfaces. Microsystem Technologies 12, 231-237.
O'Connell, J., Grinberg, V. Y., De Kruif, C., 2003. Association behavior of β-casein. J. Colloid Interface Sci. 258, 33-39.
O'Neill, A., Khan, U., Coleman, J. N., 2012. Preparation of high concentration dispersions of exfoliated MoS_2 with increased flake size. Chem. Mater. 24, 2414-2421.
Observations, N., 2020. MODIS Sea Surface Temperature.
Ocean-Salinity, https://www.sciencelearn.org.nz/resources/686-ocean-salinity. 2022.
Offiong, N., Fatunla, O. K., Essien, J. P., Yang, C., Dong, J., 2021. Soil washing of total petroleum and polycyclic aromatic hydrocarbons from crude oil-contaminated ultisol using aqueous extracts of waterleaf. Environ. Technol. 43, 1-10.
Oh, S., Wang, Q., Shin, W. S., Song, D.-I., 2013. Effect of salting out on the desorption-resistance of polycyclic aromatic hydrocarbons (PAHs) in coastal sediment. Chem. Eng. J. 225, 84-92.
Ou, X. F., Yang, X. H., Zheng, J. Q., Liu, M. X., 2019. Free-standing graphene oxide–chitin nanocrystal composite membrane for dye adsorption and oil/water separation. ACS Sustain. Chem. Eng. 7, 13379-13390.

Owens, E., Taylor, E., Parker, H. A., Spill site characterization in environmental forensic investigations. Standard Handbook Oil Spill Environmental Forensics. Elsevier, 2016, pp. 1-24.

Pan, Y., Su, H., Zhu, Y., Molamahmood, H. V., Long, M., 2018. CaO_2 based Fenton-like reaction at neutral pH: accelerated reduction of ferric species and production of superoxide radicals. Water Res. 145, 731-740.

Pan, Y., Zeng, X., Gao, X., Xu, H., Sun, Y., Wang, D., Wu, J., 2022. Assessing human health hisk to DNAPLs exposure in bayesian uncertainty analysis. J. Environ. Inform. 39, 67-80.

Peatlands, N., 2022. https://storymaps.arcgis.com/stories/19d24f59487b46f6a011dba140eddbe7.

Perugini, L., Cinelli, G., Cofelice, M., Ceglie, A., Lopez, F., Cuomo, F., 2018. Effect of the coexistence of sodium caseinate and Tween 20 as stabilizers of food emulsions at acidic pH. Colloids Surf., B 168, 163-168.

Phanthong, P., Reubroycharoen, P., Kongparakul, S., Samart, C., Wang, Z. D., Hao, X. G., Abudula, A., Guan, G. Q., 2018. Fabrication and evaluation of nanocellulose sponge for oil/water separation. Carbohydr. Polym. 190, 184-189.

Pitois, A., Abrahamsen, L. G., Ivanov, P. I., Bryan, N. D., 2008. Humic acid sorption onto a quartz sand surface: A kinetic study and insight into fractionation. J. Colloid Interface Sci. 325, 93-100.

Portnaya, I., Cogan, U., Livney, Y. D., Ramon, O., Shimoni, K., Rosenberg, M., Danino, D., 2006. Micellization of bovine β-casein studied by isothermal titration microcalorimetry and cryogenic transmission electron microscopy. J. Agric. Food Chem. 54, 5555-5561.

Post, A., Arnold, B., Weiss, J., Hinrichs, J., 2012. Effect of temperature and pH on the solubility of caseins: Environmental influences on the dissociation of αS-and β-casein. J. Dairy Sci. 95, 1603-1616.

Pu, Q., Han, Z., Li, X., Li, Q., Li, Y., 2022. Designing and screening of fluoroquinolone substitutes using combined in silico approaches: biological metabolism–bioconcentration bilateral selection and their mechanism analyses. Green Chemistry 24, 3778-3793.

Qiu, Y., Xu, M., Sun, Z., Li, H., 2019. Remediation of PAH-contaminated soil by combining surfactant enhanced soil washing and iron-activated persulfate oxidation process. Int. J. Environ. Res. Public Health 16, 441.

Qu, Z., An, C., Mei, Z., Yue, R., Zhao, S., Feng, Q., Cai, M., Wen, J., 2022. An experimental and modeling study on the penetration of spilled oil into thawing frozen soil. Environ. Sci. Processes Impacts 24, 2398-2408.

Rahmatinejad, J., Liu, X., Zhang, X., Raisi, B., Ye, Z., 2022. Embedding amorphous MoSx within hierarchical porous carbon by facile one-pot synthesis for superior sodium ion storage. J. Energy Chem. 75, 240-249.

Rahmatinejad, J., Raisi, B., Liu, X., Zhang, X., Sadeghi Chevinli, A., Yang, L., Ye, Z., 2023. 1T-2H mixed-phase moS_2 stabilized with a hyperbranched polyethylene ionomer for Mg^{2+}/Li^{+} co-Intercalation toward high-capacity dual-salt batteries. Small, 2304878.

Ramachandran, V., Shriram, M., Mathew, E. R., Ramkumar, K., Prakash, D. G., Venkatachalam, C. D., 2021. Oil spill remediation and valorization of oil-soaked peat sorbent to biofuel by hydrothermal liquefaction. Biomass Convers. Biorefin., 1-13.

Ramadass, K., Megharaj, M., Venkateswarlu, K., Naidu, R., 2015. Toxicity and oxidative stress induced by used and unused motor oil on freshwater microalga, pseudokirchneriella subcapitata. Environ. Sci. Pollut. Res. 22, 8890-8901.

Ramil, A., Vázquez-Nion, D., Pozo-Antonio, J., Sanmartín, P., Prieto, B., 2020. Using hyperspectral imaging to quantify phototrophic biofilms on granite. J. Environ. Inform. 35, 34-44.
Ren, T., Tian, W., Shen, Q., Yuan, Z., Chen, D., Li, N., Lu, J., 2021. Enhanced piezocatalysis of polymorphic few-layered MoS_2 nanosheets by phase engineering. Nano Energy 90, 106527.
Rezaeian, M. S., Mousavi, S. M., Saljoughi, E., Amiri, H. A. A., 2020. Evaluation of thin film composite membrane in production of ionically modified water applied for enhanced oil recovery. Desalination 474, 114194.
Rose, G. D., 2019. Ramachandran maps for side chains in globular proteins. Proteins: Structure, Function, and Bioinformatics 87, 357-364.
Roy, C., Tim, J., Marine geochemistry. Hoboken, NJ: John Wiley & Sons, 2012.
Sachs, J. D., Schmidt-Traub, G., Mazzucato, M., Messner, D., Nakicenovic, N., Rockström, J., 2019. Six transformations to achieve the sustainable development goals. Nat. Sustain. 2, 805-814.
Safaei, S. H., Young, S., Samimi, Z., Parvizi, F., Shokrollahi, A., Baniamer, M., 2022. Technology development for the removal of covid-19 pharmaceutical active compounds from water and wastewater: a review. J. Environ. Inform 40, 141-156.
Santos, D., Viante, M., Pochapski, D., Downs, A., Almeida, C., 2018. Enhanced removal of p-nitrophenol from aqueous media by montmorillonite clay modified with a cationic surfactant. J. Hazard. Mater. 355, 136-144.
Sathiyan, S., Ahmad, H., Chong, W., Lee, S., Sivabalan, S., 2015. Evolution of the Polarizing Effect of MoS_2. IEEE Photonics J. 7, 1-10.
Sayed, A. M., Olesen, K. B., Alkahala, A. S., Sølling, T. I., Alyafei, N., 2019. The effect of organic acids and salinity on the interfacial tension of n-decane/water systems. J. Petrol. Sci. Eng. 173, 1047-1052.
Shan, S., Zhang, T., Wang, W., Liu, D., Shi, W., Cui, F., 2021. Magnetite/hydrated cerium (III) carbonate for efficient phosphate elimination from aqueous solutions and the mechanistic investigation. Chem. Eng. J. 425, 128894.
Shang, Y., Xu, X., Yue, Q. Y., Gao, B. Y., Li, Y. W., 2020. Nitrogen-doped carbon nanotubes encapsulating Fe/Zn nanoparticles as a persulfate activator for sulfamethoxazole degradation: role of encapsulated bimetallic nanoparticles and nonradical reaction. Environ. Sci.: Nano. 7, 1444-1453.
Shasha, C., Krishnan, K. M., 2021. Nonequilibrium dynamics of magnetic nanoparticles with applications in biomedicine. Adv. Mater. 33, 1904131.
Shen, J., Huang, G., An, C., Zhao, S., Rosendahl, S., 2017. Immobilization of tetrabromobisphenol A by pinecone-derived biochars at solid-liquid interface: synchrotron-assisted analysis and role of inorganic fertilizer ions. Chem. Eng. J. 321, 346-357.
Shrestha, N., Wang, J., 2020a. Water quality management of a cold climate region watershed in changing climate. J. Environ. Inform. 35, 56-80.
Shrestha, N. K., Wang, J., 2020b. Water Quality Management of a Cold Climate Region Watershed in Changing Climate. J. Environ. Inform. 35, 56-80.
Singh, N., Khullar, V., 2019. Efficient volumetric absorption solar thermal platforms employing thermally stable-solar selective nanofluids engineered from used engine oil. Sci. Rep. 9, 1-12.
Soares, S. F., Rodrigues, M. I., Trindade, T., Daniel-da-Silva, A. L., 2017. Chitosan-silica hybrid nanosorbents for oil removal from water. Colloids Surf., A 532, 305-313.
Sohn, A., Choi, S., Han, S. A., Kim, T.-H., Kim, J. H., Kim, Y., Kim, S.-W., 2019. Temperature-dependent piezotronic effect of MoS_2 monolayer. Nano Energy 58, 811-816.

Song, J. W., Chen, C. J., Yang, Z., Kuang, Y. D., Li, T., Li, Y. J., Huang, H., Kierzewski, I., Liu, B. Y., He, S. M., 2018. Highly compressible, anisotropic aerogel with aligned cellulose nanofibers. ACS Nano 12, 140-147.

Song, P., Huang, G., An, C., Xin, X., Zhang, P., Chen, X., Ren, S., Xu, Z., Yang, X., 2021. Exploring the decentralized treatment of sulfamethoxazole-contained poultry wastewater through vertical-flow multi-soil-layering systems in rural communities. Water Res. 188, 116480.

Sordello, F., Zeb, G., Hu, K., Calza, P., Minero, C., Szkopek, T., Cerruti, M., 2014. Tuning TiO_2 nanoparticle morphology in graphene-TiO_2 hybrids by graphene surface modification. Nanoscale 6, 6710-6719.

Sørensen, L., Melbye, A. G., Booth, A. M., 2014. Oil droplet interaction with suspended sediment in the seawater column: Influence of physical parameters and chemical dispersants. Mar. Pollut. Bull. 78, 146-152.

Springsteen, G., Yerabolu, J. R., Nelson, J., Rhea, C. J., Krishnamurthy, R., 2018. Linked cycles of oxidative decarboxylation of glyoxylate as protometabolic analogs of the citric acid cycle. Nat Commun 9, 1-8.

Srinivasan, M., Formation and stability of oil-in-water caseinate emulsions. Vol. Doctor of Philosophy. Massey University, 1998, pp. 301.

Srinivasan, M., Singh, H., Munro, P., 2000. The effect of sodium chloride on the formation and stability of sodium caseinate emulsions. Food Hydrocolloids 14, 497-507.

Stevenson, F., 1994. Humus chemistry: genesis, composition, reactions. John Wiley & Sons.

Stoffyn-Egli, P., Lee, K., 2002. Formation and characterization of oil–mineral aggregates. Spill Sci. Technol. Bull. 8, 31-44.

Su, C., Horseman, T., Cao, H., Christie, K., Li, Y., Lin, S., 2019. Robust superhydrophobic membrane for membrane distillation with excellent scaling resistance. Environ. Sci. Technol. 53, 11801-11809.

Su, Y., Zhang, L., Wang, W., Li, X., Zhang, Y., Shao, D., 2018. Enhanced H_2 evolution based on ultrasound-assisted piezo-catalysis of modified MoS_2. J. Mater. Chem. A 6, 11909-11915.

Subramanian, D., May, N., Firoozabadi, A., 2017. Functional molecules and the stability of water-in-crude oil emulsions. Energy Fuels 31, 8967-8977.

Sun, F. F., Liu, W., Dong, Z. X., Deng, Y. L., 2017. Underwater superoleophobicity cellulose nanofibril aerogel through regioselective sulfonation for oil/water separation. Chem. Eng. J. 330, 774-782.

Sun, H., Liu, H., Wang, S. Y., Liu, Y., 2019. Remediation of oil spill-contaminated sands by chemical-free microbubbles generated in tap and saline water. J. Hazard. Mater. 366, 124-129.

Sun, P., Lee, W.-N., Zhang, R., Huang, C.-H., 2016. Degradation of DEET and caffeine under UV/chlorine and simulated sunlight/chlorine conditions. Environ. Sci. Technol. 50, 13265-13273.

Sun, R. K., He, L., Shang, Q. T., Jiang, S. Q., Zhou, C. X., Hong, P. Z., Zhao, H., Sun, S. L., Li, C. Y., 2020. Hydrophobic magnetic porous material of Eichhornia crassipes for highly efficient oil adsorption and separation. ACS Omega 5, 9920-9928.

Sun, Y., Tai, Z., Yan, T., Dai, Y., Hemar, Y., Li, N., 2021. Unveiling the structure of the primary caseinate particle using small-angle X-ray scattering and simulation methodologies. Food Res. Int., 110653.

Sun, Y., Yu, H., Zhang, J., Yin, Y., Shi, H., Wang, X., 2006. Bioaccumulation, depuration and oxidative stress in fish Carassius auratus under phenanthrene exposure. Chemosphere 63, 1319-1327.

Sundar, S., Mishra, A., Shukla, J., 2021. Effects of mitigation options on the control of methane emissions caused by rice paddies and livestock populations to reduce global warming: a modeling study and comparison with environmental data. J. Environ. Inform.
Tang, J., Quinlan, P. J., Tam, K. C., 2015a. Stimuli-responsive Pickering emulsions: recent advances and potential applications. Soft Matter 11, 3512-3529.
Tang, W., Han, Y., Han, C. B., Gao, C. Z., Cao, X., Wang, Z. L., 2015b. Self-powered water splitting using flowing kinetic energy. Adv. Mater. 27, 272-276.
Tang, Y., Gao, C., Zhang, Y., Tang, X., 2021. The microstructure and physiochemical stability of Pickering emulsions stabilized by chitosan particles coating with sodium alginate: Influence of the ratio between chitosan and sodium alginate. Int. J. Biol. Macromol. 183, 1402-1409.
Thomar, P., Benyahia, L., Durand, D., Nicolai, T., 2014. The influence of adding monovalent salt on the rheology of concentrated sodium caseinate suspensions and the solubility of calcium caseinate. International Dairy Journal 37, 48-54.
Tong, M., He, L., Rong, H., Li, M., Kim, H., 2020. Transport behaviors of plastic particles in saturated quartz sand without and with biochar/Fe_3O_4-biochar amendment. Water Res. 169, 115284.
Trellu, C., Pechaud, Y., Oturan, N., Mousset, E., van Hullebusch, E. D., Huguenot, D., Oturan, M. A., 2021. Remediation of soils contaminated by hydrophobic organic compounds: how to recover extracting agents from soil washing solutions? J. Hazard. Mater. 404, 124137.
Tu, S., Guo, Y., Zhang, Y., Hu, C., Zhang, T., Ma, T., Huang, H., 2020. Piezocatalysis and piezo-photocatalysis: catalysts classification and modification strategy, reaction mechanism, and practical application. Adv. Funct. Mater. 30, 2005158.
U.S.EPA, 2021. https://www.epa.gov/system/files/documents/2021-09/ps_sept21.pdf.
Urum, K., Pekdemir, T., 2004. Evaluation of biosurfactants for crude oil contaminated soil washing. Chemosphere 57, 1139-1150.
Vahabisani, A., An, C., Xin, X. Y., Owens, E., Lee, K., 2021. Exploring the effects of microalgal biomass on the oil behavior in a sand-water system. Environ. Sci. Pollut. Res. 28, 32985-32994.
Valikhan Anaraki, M., Mahmoudian, F., Nabizadeh Chianeh, F., Farzin, S., 2022. Dye pollutant removal from synthetic wastewater: A new modeling and predicting approach based on experimental data analysis, kriging interpolation method, and computational intelligence techniques. J. Environ. Inform. 40, 84-94.
Venosa, A. D., Suidan, M. T., Wrenn, B. A., Strohmeier, K. L., Haines, J. R., Eberhart, B. L., King, D., Holder, E., 1996. Bioremediation of an experimental oil spill on the shoreline of Delaware Bay. Environ. Sci. Technol. 30, 1764-1775.
Von Wandruszka, R., 2000. Humic acids: Their detergent qualities and potential uses in pollution remediation. Geochem. Trans. 1, 1-6.
Wang, E., Wen, H., Guo, P., Luo, Y., Wang, C., He, Z., Pan, J., Chen, X., Cao, B., Wang, Y., 2022a. Fabrication of methacrylated casein/alginate microspheres crosslinked by UV light coupled with Ca^{2+} chelation for pH-sensitive drug delivery. Colloid. Polym. Sci. 300, 553-567.
Wang, G., Xiao, H., Zhu, J., Zhao, H., Liu, K., Ma, S., Zhang, S., Komarneni, S., 2021a. Simultaneous removal of Zn^{2+} and p-nitrophenol from wastewater using nanocomposites of montmorillonite with alkyl-ammonium and complexant. Environ. Res. 201, 111496-111508.
Wang, H., Zhu, Q., Ding, Z., Li, Z., Zheng, H., Fu, J., Diao, C., Zhang, X., Tian, J., Zi, Y., 2019a. A fully-packaged ship-shaped hybrid nanogenerator for blue energy harvesting toward seawater self-desalination and self-powered positioning. Nano Energy 57, 616-624.

Wang, J., Deng, H., Sun, Y., Yang, C., 2020a. Montmorillonite and alginate co-stabilized biocompatible Pickering emulsions with multiple-stimulus tunable rheology. J. Colloid Interface Sci. 562, 529-539.
Wang, J., Liang, Y., Wang, Z., Huo, B., Liu, C., Chen, X., Xu, H., Li, D., Zhu, Z., Wang, Y., 2023. High efficiently degradation of organic pollutants via low-speed water flow activation of Cu_2O@ MoS_2/PVDF modified pipeline with piezocatalysis performance. Chem. Eng. J., 141409.
Wang, L., Xiao, L., Jin, Q., Chang, Q., 2022b. In-Situ construction of La-B Co-doped g-C_3N_4 for highly efficient photocatalytic H_2 production and RhB degradation. J. Environ. Inform. 40, 30-40.
Wang, M., Peng, M., Zhu, J., Li, Y. D., Zeng, J. B., 2020b. Mussel-inspired chitosan modified superhydrophilic and underwater superoleophobic cotton fabric for efficient oil/water separation. Carbohydr. Polym. 244, 116449.
Wang, M., Zhang, B., Li, G., Wu, T., Sun, D., 2019b. Efficient remediation of crude oil-contaminated soil using a solvent/surfactant system. RSC Adv. 9, 2402-2411.
Wang, N. N., Wang, H., Wang, Y. Y., Wei, Y. H., Si, J. Y., Yuen, A. C. Y., Xie, J. S., Yu, B., Zhu, S. E., Lu, H. D., 2019c. Robust, lightweight, hydrophobic, and fire-retarded polyimide/MXene aerogels for effective oil/water separation. ACS Appl. Mater. Interfaces 11, 40512-40523.
Wang, P. p., Sun, H., Ji, Y., Li, W., Wang, X., 2014. Three-dimensional assembly of single-layered MoS_2. Adv. Mater. 26, 964-969.
Wang, S. D., Shen, Y. M., Zheng, Y. H., 2005. Two-dimensional numerical simulation for transport and fate of oil spills in seas. Ocean Eng. 32, 1556-1571.
Wang, T., Chen, X., Zhong, Q., Chen, Z., Wang, R., Patel, A. R., 2019d. Facile and efficient construction of water-soluble biomaterials with tunable mesoscopic structures using all-natural edible proteins. Adv. Funct. Mater. 29, 1901830.
Wang, Z., An, C., Chen, X., Lee, K., Zhang, B., Feng, Q., 2021b. Disposable masks release microplastics to the aqueous environment with exacerbation by natural weathering. J. Hazard. Mater. 417, 126036-126045.
Wang, Z., An, C., Lee, K., Chen, X., Zhang, B., Yin, J., Feng, Q., 2022c. Physicochemical change and microparticle release from disposable gloves in the aqueous environment impacted by accelerated weathering. Sci. Total Environ. 832, 154986.
Wang, Z., An, C., Lee, K., Owens, E., Boufadel, M., Feng, Q., 2022d. Dispersion modeling of particulate matter from the in-situ burning of spilled oil in the northwest Arctic area of Canada. J. Environ. Manage. 301, 113913.
Wang, Z., An, C., Lee, K., Owens, E., Chen, Z., Boufadel, M., Taylor, E., Feng, Q., 2020c. Factors influencing the fate of oil spilled on shorelines: a review. Environ. Chem. Lett., 1-18.
Wang, Z., An, C., Lee, K., Owens, E., Chen, Z., Boufadel, M., Taylor, E., Feng, Q., 2021c. Factors influencing the fate of oil spilled on shorelines: a review. Environ. Chem. Lett. 19, 1611-1628.
Wang, Z., Lin, S., 2017. Membrane fouling and wetting in membrane distillation and their mitigation by novel membranes with special wettability. Water Res. 112, 38-47.
Wen, B., Zhang, J.-j., Zhang, S.-z., Shan, X.-q., Khan, S. U., Xing, B., 2007. Phenanthrene sorption to soil humic acid and different humin fractions. Environ. Sci. Technol. 41, 3165-3171.
Wen, X., Lei, X., Lei, X., Tan, Q., Fang, G., Wang, X., Wang, C., Liu, Z., 2021. Incorporation of optimal limited ecological curves into the operation chart of cascade hydropower systems to alleviate ecological damages in hydrological extremes. J. Environ. Inform. 37, 153-166.

Wu, J., Ma, G. H., 2016. Recent studies of Pickering emulsions: particles make the difference. Small 12, 4633-4648.
Wu, J. M., Chang, W. E., Chang, Y. T., Chang, C. K., 2016. Piezo-catalytic effect on the enhancement of the ultra-high degradation activity in the dark by single-and few-layers MoS_2 nanoflowers. Adv. Mater. 28, 3718-3725.
Wu, J. M., Sun, Y.-G., Chang, W.-E., Lee, J.-T., 2018. Piezoelectricity induced water splitting and formation of hydroxyl radical from active edge sites of MoS_2 nanoflowers. Nano Energy 46, 372-382.
Wu, W., Sun, H., 2010. Sorption–desorption hysteresis of phenanthrene–effect of nanopores, solute concentration, and salinity. Chemosphere 81, 961-967.
Wu, W., Wang, L., Li, Y., Zhang, F., Lin, L., Niu, S., Chenet, D., Zhang, X., Hao, Y., Heinz, T. F., 2014. Piezoelectricity of single-atomic-layer MoS_2 for energy conversion and piezotronics. Nature 514, 470-474.
Xi, Y., Liu, B., Jiang, H., Yin, S., Ngai, T., Yang, X., 2020. Sodium caseinate as a particulate emulsifier for making indefinitely recycled pH-responsive emulsions. Chem. Sci. 11, 3797-3803.
Xiao, J., Li, Y., Huang, Q., 2016. Recent advances on food-grade particles stabilized Pickering emulsions: fabrication, characterization and research trends. Trends Food Sci. Tech. 55, 48-60.
Xie, J., Zhang, H., Li, S., Wang, R., Sun, X., Zhou, M., Zhou, J., Lou, X. W., Xie, Y., 2013. Defect-rich MoS_2 ultrathin nanosheets with additional active edge sites for enhanced electrocatalytic hydrogen evolution. Adv. Mater. 25, 5807-5813.
Xin, X., Huang, G., An, C., Raina-Fulton, R., Weger, H., 2019. Insights into long-term toxicity of triclosan to freshwater green algae in Lake Erie. Environ. Sci. Technol. 53, 2189-2198.
Xin, X., Huang, G., Zhang, B., Zhou, Y., 2021. Trophic transfer potential of $nTiO_2$, nZnO, and triclosan in an algae-algae eating fish food chain. Aquat. Toxicol. 235, 105824.
Xu, S., Zhu, H., Cao, W., Wen, Z., Wang, J., François-Xavier, C. P., Wintgens, T., 2018a. Cu-Al_2O_3-g-C_3N_4 and Cu-Al_2O_3-C-dots with dual-reaction centres for simultaneous enhancement of Fenton-like catalytic activity and selective H_2O_2 conversion to hydroxyl radicals. Appl. Catal. B Environ. 234, 223-233.
Xu, W., Xiong, Y., Li, Z., Luo, D., Wang, Z., Sun, Y., Shah, B. R., 2020. Stability, microstructural and rheological properties of complex prebiotic emulsion stabilized by sodium caseinate with inulin and konjac glucomannan. Food Hydrocolloids 105, 105772.
Xu, Y., Zhang, Y., Liu, X., Chen, H., Fang, Y., 2018b. Retrieving oil and recycling surfactant in surfactant-enhanced soil washing. ACS Sustain. Chem. Eng. 6, 4981-4986.
Yagoub, H., Zhu, L. P., Shibraen, M. H., Xu, X. W., Babiker, D. M., Xu, J., Yang, S. G., 2019. Complex membrane of cellulose and chitin nanocrystals with cationic guar gum for oil/water separation. J. Appl. Polym. Sci. 136, 47947.
Yan, L. Y., Li, P. Y., Zhou, W. K., Wang, Z. G., Fan, X. M., Chen, M. F., Fang, Y., Liu, H. Q., 2018. Shrimp shell-inspired antifouling chitin nanofibrous membrane for efficient oil/water emulsion separation with in situ removal of heavy metal ions. ACS Sustain. Chem. Eng. 7, 2064-2072.
Yang, H., Zhou, T., Zhang, W., 2013a. A strategy for separating and recycling solid catalysts based on the pH-triggered Pickering-emulsion inversion. Angew. Chem. Int. Ed. 52, 7455-7459.
Yang, K., Zhu, L., Xing, B., 2006. Enhanced soil washing of phenanthrene by mixed solutions of TX100 and SDBS. Environ. Sci. Technol. 40, 4274-4280.
Yang, S., Wang, J., Wang, Y., Ding, Y., Zhang, W., Liu, F., 2021. Interfacial polymerized polyamide nanofiltration membrane by demulsification of hexane-in-water droplets through hydrophobic

PTFE membrane: membrane performance and formation mechanism. Sep. Purif. Technol. 275, 119227.
Yang, Y., Ok, Y. S., Kim, K.-H., Kwon, E. E., Tsang, Y. F., 2017. Occurrences and removal of pharmaceuticals and personal care products (PPCPs) in drinking water and water/sewage treatment plants: A review. Sci. Total Environ. 596, 303-320.
Yang, Y., Zhang, H., Liu, Y., Lin, Z.-H., Lee, S., Lin, Z., Wong, C. P., Wang, Z. L., 2013b. Silicon-based hybrid energy cell for self-powered electrodegradation and personal electronics. ACS Nano 7, 2808-2813.
Ye, Z., Zhang, F., Han, L., Luo, P., Yang, J., Chen, H., 2008. The effect of temperature on the interfacial tension between crude oil and gemini surfactant solution. Colloids Surf., A 322, 138-141.
Yi, L. F., Yang, J. Y., Fang, X., Xia, Y., Zhao, L. J., Wu, H., Guo, S. Y., 2020. Facile fabrication of wood-inspired aerogel from chitosan for efficient removal of oil from Water. J. Hazard. Mater. 385, 121507.
Yin, J., Huang, G., An, C., Zhang, P., Xin, X., Feng, R., 2021a. Exploration of nanocellulose washing agent for the green remediation of phenanthrene-contaminated soil. J. Hazard. Mater. 403, 123861.
Yin, J. N., Huang, G. h., An, C., Zhang, P., Xin, X. Y., Feng, R. F., 2021b. Exploration of nanocellulose washing agent for the green remediation of phenanthrene-contaminated soil. J. Hazard. Mater. 403, 123861.
Yin, W., Yu, J., Lv, F., Yan, L., Zheng, L. R., Gu, Z., Zhao, Y., 2016. Functionalized nano-MoS_2 with peroxidase catalytic and near-infrared photothermal activities for safe and synergetic wound antibacterial applications. ACS Nano 10, 11000-11011.
Yoo, Y., Park, H., Choi, Y., Jung, J., Song, H., Kim, J., Cho, H., 2021. Method for determining optimum operational conditions of microbubble scrubber using image processing. J. Environ. Inform. 38, 83-92.
Yu, B., Wu, P., Sui, J., Ni, J., Whitcombe, T., 2020. Variation of runoff and sediment transport in the Huai River–A case study. J. Environ. Inform. 35, 94-102.
Yu, H., Huang, G., Wei, J., An, C., 2011. Solubilization of mixed polycyclic aromatic hydrocarbons through a rhamnolipid biosurfactant. J. Environ. Qual. 40, 477-483.
Yu, H., Liu, H. L., Yuan, X., Ding, W. J., Li, Y., Wang, J. K., 2019a. Separation of oil-water emulsion and adsorption of Cu(II) on a chitosan-cellulose acetate-TiO_2 based membrane. Chemosphere 235, 239-247.
Yu, L., Li, S., Stubbs, L. P., Lau, H. C., 2021. Rheological investigation of clay-stabilized oil-in-water Pickering emulsions for potential reservoir applications. J. Petrol. Sci. Eng. 204, 108722-108736.
Yu, Y., Qi, Z., Li, W., Fu, S., Yu, X., Xiong, D., 2019b. Effects of physical parameters and chemical dispersant on the formation of oil-particle aggregates (OPAs) in marine environments. Mar. Pollut. Bull. 148, 66-74.
Yuan, D. S., Zhang, T., Guo, Q., Qiu, F. X., Yang, D. Y., Ou, Z. P., 2018. Recyclable biomass carbon@ SiO_2@ MnO_2 aerogel with hierarchical structures for fast and selective oil-water separation. Chem. Eng. J. 351, 622-630.
Yue, R., An, C., Ye, Z., Bi, H., Chen, Z., Liu, X., Zhang, X., Lee, K., 2022a. Cleanup of oiled shorelines using a dual responsive nanoclay/sodium alginate surface washing agent. Environ. Res. 205, 112531.

Yue, R., An, C., Ye, Z., Chen, X., Lee, K., Zhang, K., Wan, S., Qu, Z., 2022b. Exploring the characteristics, performance, and mechanisms of a magnetic-mediated washing fluid for the cleanup of oiled beach sand. J. Hazard. Mater. 438, 129447.
Yue, R., An, C., Ye, Z., Chen, X., Lee, K., Zhang, K., Wan, S., Qu, Z., 2022c. Exploring the Characteristics, Performance, and Mechanisms of a Magnetic-mediated Washing Fluid for the Cleanup of Oiled Beach Sand. J. Hazard. Mater., 129447.
Yue, R., An, C., Ye, Z., Gao, S., Chen, X., Zhang, B., Lee, K., Bi, H., 2022d. A pH-responsive phosphoprotein surface washing fluid for cleaning oiled shoreline: performance evaluation, biotoxicity analysis, and molecular dynamic simulation. Chem. Eng. J., 135336.
Yue, R., An, C., Ye, Z., Gao, S., Chen, X., Zhang, B., Lee, K., Bi, H., 2022e. A pH-responsive phosphoprotein surface washing fluid for cleaning oiled shoreline: performance evaluation, biotoxicity analysis, and molecular dynamic simulation. Chem. Eng. J. 437, 135336.
Yue, R., An, C., Ye, Z., Li, X., Li, Q., Zhang, P., Qu, Z., Wan, S., 2022f. A pH-responsive phosphoprotein washing fluid for the removal of phenanthrene from contaminated peat moss in the cold region. Chemosphere 313, 137389.
Yue, R., An, C., Ye, Z., Owens, E., Taylor, E., Zhao, S., 2022g. Green biomass-derived materials for oil spill response: recent advancements and future perspectives. Curr. Opin. Chem. Eng. 36, 100767.
Yue, R., Chen, T., Ye, Z., Barbeau, B., Rahaman, M. S., 2021a. A photo-Fenton graphene oxide membrane with improved perm-selectivity and self-cleaning ability for efficient dye removal under visible light irradiation. J. Water Process Eng. 44, 102443.
Yue, R., Guan, J., Zhang, C., Yuan, P., Liu, L., Afzal, M. Z., Wang, S., Sun, X., 2020. Photoinduced superwetting membranes for separation of oil-in-water emulsions. Sep. Purif. Technol. 241, 116536-116541.
Yue, R., Rahaman, M. S., 2021a. Hydrophilic and underwater superoleophobic porous graphitic carbon nitride (g-C_3N_4) membranes with photo-Fenton self-cleaning ability for efficient oil/water separation. J. Colloid Interface Sci. 608, 1960-1972.
Yue, R., Raisi, B., Rahamtinejad, J., Ye, Z. B., Barbeau, B., Rahaman, M. S., 2021b. A photo-Fenton nanocomposite ultrafiltration membrane for enhanced dye removal with self-cleaning properties. J. Colloid Interface Sci. 604, 458-468.
Yue, R., Ye, Z., Gao, S., Cao, Y., Lee, K., An, C., Qu, Z., Wan, S., 2023. Exploring the use of sodium caseinate-assisted responsive separation for the treatment of washing effluents in shoreline oil spill response. Sci. Total Environ. 873, 162363.
Yue, R. Y., Rahaman, M. S., 2021b. Hydrophilic and Underwater Superoleophobic Porous Graphitic Carbon Nitride (g-C3N4) Membranes with Photo-Fenton Self-cleaning Ability for Efficient Oil/Water Separation. J. Colloid Interface Sci. 608, 1960-1972.
Zaccone, C., Miano, T., Shotyk, W., 2007. Qualitative comparison between raw peat and related humic acids in an ombrotrophic bog profile. Org. Geochem. 38, 151-160.
Zamani Kouhpanji, M. R., Nemati, Z., Mahmoodi, M. M., Um, J., Modiano, J., Franklin, R., Stadler, B., 2021. Selective detection of cancer cells using magnetic nanowires. ACS Appl. Mater. Interfaces 13, 21060-21066.
Zeng, Y., Zhang, M., Lin, D., Yang, K., 2020. Selective removal of phenanthrene from SDBS or TX100 solution by sorption of resin SP850. Chem. Eng. J. 388, 124191.
Zhai, A., Ding, X., Zhao, Y., Xiao, W., Lu, B., 2020. Improvement of instantaneous point source model for simulating radionuclide diffusion in oceans under nuclear power plant accidents. J. Environ. Inform. 36, 133-145.

Zhang, C., Lu, J., Wu, J., Luo, Y., 2017. Removal of phenanthrene from coastal waters by green tide algae Ulva prolifera. Sci. Total Environ. 609, 1322-1328.
Zhang, H., Li, Y., Shi, R. H., Chen, L. H., Fan, M., 2018a. A robust salt-tolerant superoleophobic chitosan/nanofibrillated cellulose aerogel for highly efficient oil/water separation. Carbohydr. Polym. 200, 611-615.
Zhang, H., Pan, L., Tao, Y., 2014a. Toxicity assessment of environmental pollutant phenanthrene in clam Venerupis philippinarum using oxidative stress biomarkers. Environ. Toxicol. Pharmacol. 37, 697-704.
Zhang, J., Ji, Y., Wang, P., Shao, Q., Li, Y., Huang, X., 2020. Adsorbing and activating N_2 on heterogeneous Au–Fe_3O_4 nanoparticles for N_2 fixation. Adv. Funct. Mater. 30, 1906579.
Zhang, J., Li, L., Xu, J., Sun, D., 2014b. Effect of cetyltrimethylammonium bromide addition on the emulsions stabilized by montmorillonite. Colloid. Polym. Sci. 292, 441-447.
Zhang, K., Jia, N., Li, S., Liu, L., 2018b. How surfactant-decorated nanoparticles contribute to thermodynamic miscibility. Nanotechnology 29, 475701.
Zhang, M., Jiang, S., Han, F., Li, M., Wang, N., Liu, L., 2021a. Anisotropic cellulose nanofiber/chitosan aerogel with thermal management and oil absorption properties. Carbohydr. Polym. 264, 118033.
Zhang, W., Zheng, J., Zheng, P., Tsang, D. C., Qiu, R., 2015. The roles of humic substances in the interactions of phenanthrene and heavy metals on the bentonite surface. Journal of Soils and Sediments 15, 1463-1472.
Zhang, X., Wang, X., Yan, B., 2021b. Single and combined effects of phenanthrene and polystyrene microplastics on oxidative stress of the clam (Mactra veneriformis). Sci. Total Environ. 771, 144728.
Zhao, C., Zhou, J., Yan, Y., Yang, L., Xing, G., Li, H., Wu, P., Wang, M., Zheng, H., 2021. Application of coagulation/flocculation in oily wastewater treatment: A review. Sci. Total Environ. 765, 142795.
Zhao, L., Bian, J., Zhang, Y., Zhu, L., Liu, Z., 2014. Comparison of the sorption behaviors and mechanisms of perfluorosulfonates and perfluorocarboxylic acids on three kinds of clay minerals. Chemosphere 114, 51-58.
Zhao, S., Huang, G., An, C., Wei, J., Yao, Y., 2015. Enhancement of soil retention for phenanthrene in binary cationic gemini and nonionic surfactant mixtures: Characterizing two-step adsorption and partition processes through experimental and modeling approaches. J. Hazard. Mater. 286, 144-151.
Zhao, S., Huang, W., Wang, X., Fan, Y., An, C., 2019a. Sorption of phenanthrene onto diatomite under the influences of solution chemistry: A study of linear sorption based on maximal information coefficient. J. Environ. Inform. 34, 35-44.
Zhao, X., Cheng, L., Jia, N., Wang, R., Liu, L., Gao, C., 2020. Polyphenol-metal manipulated nanohybridization of CNT membranes with FeOOH nanorods for high-flux, antifouling and self-cleaning oil/water separation. J. Membr. Sci. 600, 117857.
Zhao, Y., Sun, T. B., Liao, W. D., Wang, Y. Q., Yu, J., Zhang, M., Yu, Z. Q., Yang, B., Gui, D. Y., Zhu, C. Z., 2019b. Amphiphilic graphene aerogel with high oil and water adsorption capacity and high contact area for interface reaction. ACS Appl. Mater. Interfaces 11, 22794-22800.
Zhong, L., Fu, S. Y., Peng, X. W., Zhan, H. Y., Sun, R. C., 2012. Colloidal stability of negatively charged cellulose nanocrystalline in aqueous systems. Carbohydr. Polym. 90, 644-649.
Zhou, W. K., Fang, Y., Li, P. Y., Yan, L. Y., Fan, X. M., Wang, Z. G., Zhang, W., Liu, H. Q., 2019. Ampholytic chitosan/alginate composite nanofibrous membranes with super anti-crude oil-

fouling behavior and multifunctional oil/water separation properties. ACS Sustain. Chem. Eng. 7, 15463-15470.
Zhu, H., Wang, Y., Xiao, J., Liu, M., Xiong, S., Wong, Z. J., Ye, Z., Ye, Y., Yin, X., Zhang, X., 2015a. Observation of piezoelectricity in free-standing monolayer MoS_2. Nat. Nanotechnol. 10, 151-155.
Zhu, K., Ju, Y., Xu, J., Yang, Z., Gao, S., Hou, Y., 2018. Magnetic nanomaterials: chemical design, synthesis, and potential applications. Acc. Chem. Res. 51, 404-413.
Zhu, X., Chen, D., Wu, G., 2015b. Molecular dynamic simulation of asphaltene co-aggregation with humic acid during oil spill. Chemosphere 138, 412-421.
Zhu, Z., Zhang, B., Cai, Q., Cao, Y., Ling, J., Lee, K., Chen, B., 2021. A critical review on the environmental application of lipopeptide micelles. Bioresour. Technol., 125602.